REVERSE TRANSPORT OF THE DOPAMINE TRANSPORTER IN NEUROPSYCHIATRIC DISEASE: MECHANISMS OF REGULATION AND DYSFUNCTION

By
Andrea N. Belovich

Dissertation
Submitted to the Faculty of the
Graduate School of Vanderbilt University
in partial fulfillment of the requirements
for the degree of

DOCTOR OF PHILOSOPHY
in
Pharmacology

May, 2017
Nashville, Tennessee

Approved:

Eugenia Gurevich, Ph.D.

Hassane Mchaourab, Ph.D.

Brad Grueter, Ph.D.

Seth Bordenstein, Ph.D.

Aurelio Galli, Ph.D.

Dedicated to my parents, Richard and Laura, and to my brother, Reisto.

You have *always* believed in me.

ACKNOWLEDGMENTS

One of the most inspiring discoveries I have made during my doctoral education is the joy that comes from working as part of a community of passionate, dedicated, and visionary scientists and educators. When I imagine what my life would have been like for the past few years without the support of this community, I can only conclude that my pre-doctoral training would have been decidedly more challenging and infinitely less rewarding. There are too many members of this community (past and present) to list and thank individually, but the following people deserve special recognition for their role in guiding me through the process of becoming a Ph.D.

I would first like to thank my thesis committee, Eugenia Gurevich, Brad Grueter, Seth Bordenstein, Jeremy Veenstra-VanderWeele, and Hassane Mchaourab, for helping to shape my professional growth and development. Their encouragement has meant the world to me. I also wish to acknowledge the wonderfully unique collection of talent that is the Galli lab, especially Heinrich Matthies, Kevin Erreger, and Christine Saunders. Heiner, Kevin, and Christine are respected colleagues and role models who have provided me with generous scientific and professional training. Nicole Bibus Christianson and Amanda Poe have selflessly given me both their technical and personal guidance, and I am indebted to them for their endless support. I am also immensely grateful to my mentor Aurelio Galli, who has provided me with opportunities to be challenged, to grow, and to develop the confidence necessary to succeed in any challenge that may present itself in the future.

Finally, I wish to thank my parents, Richard and Laura Belovich, and my brother Reisto Belovich, who have all been a wellspring of patience, love, and support. No matter how deeply nor how frequently I have drawn from this well, I have never found it to be dry.

TABLE OF CONTENTS

LIST OF TABLES

LIST OF FIGURES

LIST OF ABBREVIATIONS

5-HT	**Serotonin**
AADC	**Aromatic amino acid decarboxylase**
ACh	**Acetylcholine**
ADE	**Anomalous DAT-mediated DA efflux**
ADIR	**Autism Diagnostic Interview Revised**
ADOS	**Autism Diagnostic Observational Session**
ADHD	**Attention-deficit hyperactivity disorder**
AMPH	**Amphetamine**
ANOVA	**Analysis of variance**
AS	**Angelman Syndrome**
ASD	**Autism spectrum disorder**
BAD	**Bipolar Affective Disorder**
BoNT/C	**Botulinum toxin serotype C**
CaMKII	**Calcium/calmodulin-dependent kinase II**
CHO	**Chinese hamster ovary**
CK2	**Casein kinase 2**
CK2α	**Casein kinase 2 α**
CNS	**Central nervous system**
CNV	**Copy number variation**
COC	**Cocaine**
COMT	**Catechol-O-methyltransferase**
CTR	**Control**
DA	**Dopamine**
DAG	**Diacylglycerol**

DAT	**Dopamine transporter**
dDAT	***Drosophila melanogaster* dopamine transporter**
DEER	**Double electron electron resonance**
DR	**Dopamine receptor**
DN	**Dominant negative**
EL	**Extracellular loop**
EPI	**Electrostatic potential isosurfaces**
EPR	**Electron paramagnetic resonance**
FMRP	**Fragile X mental retardation protein**
FXRS	**Fragile X mental retardation syndrome**
GAT	**γ-aminobutyric acid transporter**
GFP	**Green fluorescent protein**
GLYT	**Glycine transporter**
GPCR	**G protein-coupled receptor**
GST	**Glutathione S-transferase**
hDAT	**Human dopamine transporter**
HVA	**Homovanillic acid**
hM1R	**Human muscarinic acetylcholine receptor M1**
IL	**Intracellular loop**
IB	**Immunoblot**
IP	**Immunoprecipitate**
IP_3	**Inositol trisphosphate**
KO	**Knock out**
LeuT	**Leucine transporter**
L-DOPA	**L-3,4-dihydroxyphenylalanine**
MAO	**Monoamine oxidase**

MD	**Molecular dynamics**
MPH	**Methylphenidate**
MPP^+	**1-methyl-4-phenylpyridinium**
NET	**Norepinephrine transporter**
NSS	**Neurotransmitter:sodium symporters**
NAc	**Nucleus Accumbens**
PET	**Positron emission tomography**
PD	**Parkinson's Disease**
PFC	**Prefrontal cortex**
PH	**Pleckstrin homology**
PIP_2	**Phosphatidylinositol (4,5)-bisphosphate**
PIP_3	**Phosphatidylinositol (3,4,5)-trisphosphate**
PKA	**Protein kinase A**
PKC	**Protein kinase C**
PKCβ	**Protein kinase C β**
PLC_δ	**Phospholipase C_δ**
PMA	**Phorbyl-12-myristate-13-acetate**
POPC	**Phosphatidylcholine**
POPE	**Phosphatidylethanolamine**
RFP	**Red fluorescent protein**
SCG	**Superior cervical ganglion**
SCMFM	**Self-consistent mean-field model**
SERT	**Serotonin transporter**
SLC	**Solute-linked carrier**
SNARE	**Soluble NSF attachment receptor**
SNP	**Single nucleotide polymorphism**

SNV	**Single nucleotide variation**
SRS	**Social Responsiveness Scale**
STX1	**Syntaxin 1**
TBB	**4,5,6,7-tetrabromobenzotriazole**
TH	**Tyrosine hydroxylase**
TM	**Transmembrane domain**
TI	**Tuberoinfundibular**
VMAT	**Vesicular monoamine transporter**
VTA	**Ventral tegmental area**
WES	**Whole exome sequencing**
WPPSI	**Wechsler Preschool and Primary Scale of Intelligence**
WT	**Wild type**

CHAPTER 1

INTRODUCTION

Dopaminergic circuits

The catecholamine neurotransmitter dopamine (3,4-Dihydroxyphenethylamine; DA) plays a key role in regulating the functions of the central nervous system (CNS) and the brain. Dopaminergic neurotransmission is known to play an important role in mediating locomotion, cognition, mood, motivation, salience, and reward. Dopaminergic innervation of the brain can be classified into four major pathways: the mesocortical pathway, the nigrostriatal pathway, the tuberoinfundibular pathway, and the mesolimbic pathway (**Fig. 1**). The tuberoinfundibular (TI) pathway plays a role in regulating neuroendocrine function and is a collection of hypothalamic DA neurons that project from the hypothalamic arcuate nucleus to the pituitary gland. Signaling from tuberoinfundibular DA (TIDA) neurons is known to have an inhibitory effect on the pituitary gland's release of prolactin, a hormone that regulates lactation, libido, fertility, and body weight (Fitzgerald and Dinan, 2008, Lyons *et al.*, 2012). The nigrostriatal pathway is essential for movement and locomotion and consists of DA neurons whose cell bodies originate in the substantia nigra and project to the dorsal striatum. Degeneration of DA neurons in the nigrostriatal pathway is a hallmark of Parkinson's Disease (PD), and results in impaired motor function, including resting tremor and loss of coordinated movement. The mesocortical dopaminergic pathway consists of projections from the midbrain (specifically the Ventral Tegmental Area; VTA) to the prefrontal cortex (PFC). The mesocortical pathway is involved in regulating emotion and cognition, as well as learning and working memory (Brozoski *et al.,* 1979, Surmeier, 2007*).* The DA neurons of the mesolimbic pathway also originate in the VTA, but project to the Nucleus Accumbens (NAc) in the ventral striatum. DA release in the NAc has been implicated in reward and pleasure. Direct electrical or chemical stimulation of the NAc results in DA release and elicits behaviors similar to

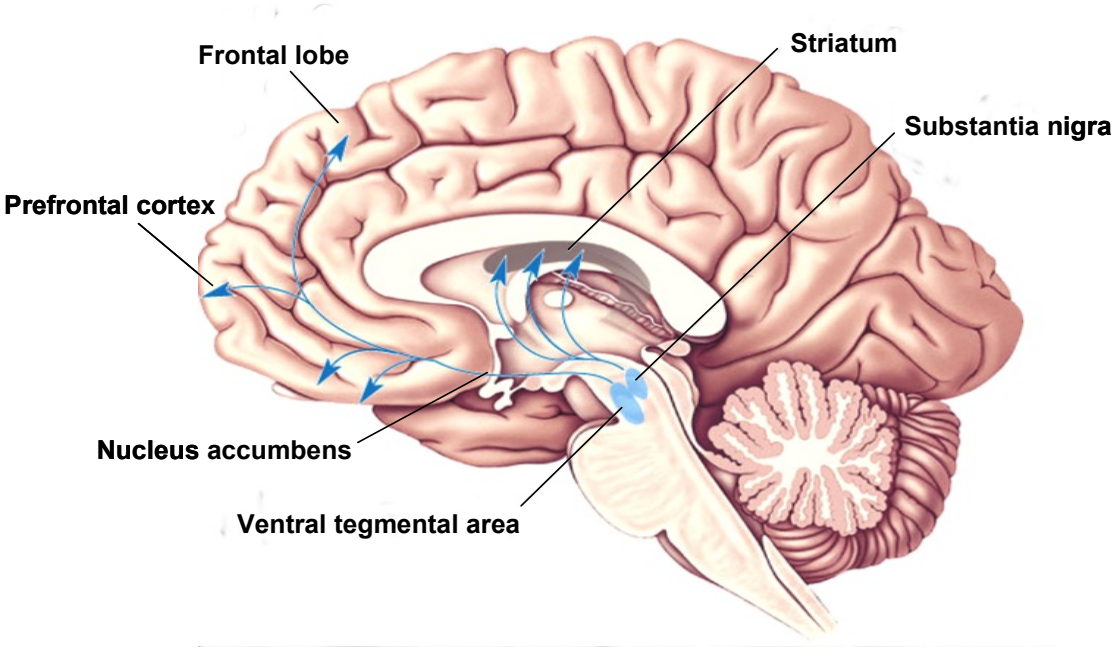

Figure 1. Schematic of dopaminergic projections in the brain. Dopaminergic neurons originating in the ventral tegmental area (VTA) and substantia nigra (Snr) project to other regions of the brain to form four major pathways: mesocortical (VTA neurons project to prefrontal cortex), mesolimbic (VTA neurons project to nucleus accumbens), nigrostriatal (Snr neurons project to striatum). Tuberoinfundibular pathway is not depicted. Image adapted from Bear *et al.* (2006).

those that occur in response to natural rewards (Wise, 1998). In particular, the reward-potentiating effects of drugs of abuse, including the psychostimulants amphetamine (AMPH) and cocaine (COC), result from elevation of DA levels in the NAc (Carboni *et al.,* 1989, Wise, 1998).

Dopaminergic signaling is thought to play an important role in regulating the response of neurons to other neurotransmitters. This gives DA a complex role in integrating several different inputs (Surmeier *et al*., 2007), so it is unsurprising that perturbations of the signaling process can have drastic effects on brain function. In addition to being altered in Parkinson's Disease and drug abuse, DA homeostasis abnormalities are associated with several other neuropsychiatric disorders, including Major Depressive Disorder, schizophrenia, Bipolar Affective Disorder (BAD), Attention Deficit Hyperactivity Disorder (ADHD), and Autism Spectrum Disorder (ASD). Furthermore, drugs whose mechanisms of action are known to alter dopaminergic neurotransmission are the standard course of treatment for several of these disorders, such as methylphenidate (MPH) and AMPH (ADHD; targets DA transporter (DAT)), risperidone (ASD; targets DA receptor D2R), L-DOPA (Parkinson's Disease; DA precursor), and haloperidol (schizophrenia; targets DA receptor D1R).

The dopaminergic synapse

DA homeostasis is controlled at the synaptic level at four main stages: DA synthesis, vesicular release of DA, the sensitivity and expression levels of the pre- and post-synaptic DA receptors, and the degradation and clearance of extracellular DA from the synaptic space. DA is synthesized in the cytosol of presynaptic terminals of DA neurons, where tyrosine hydroxylase (TH) hydrates the amino acid tyrosine (Tyr) to dihydroxyphenylalanine (DOPA), which is then decarboxlyated by the enzyme aromatic amino acid decarboxylase (AADC) into DA (**Fig. 2**). TH hydration of Tyr is the rate limiting step of the DA synthetic pathway, so the amount of DA that is

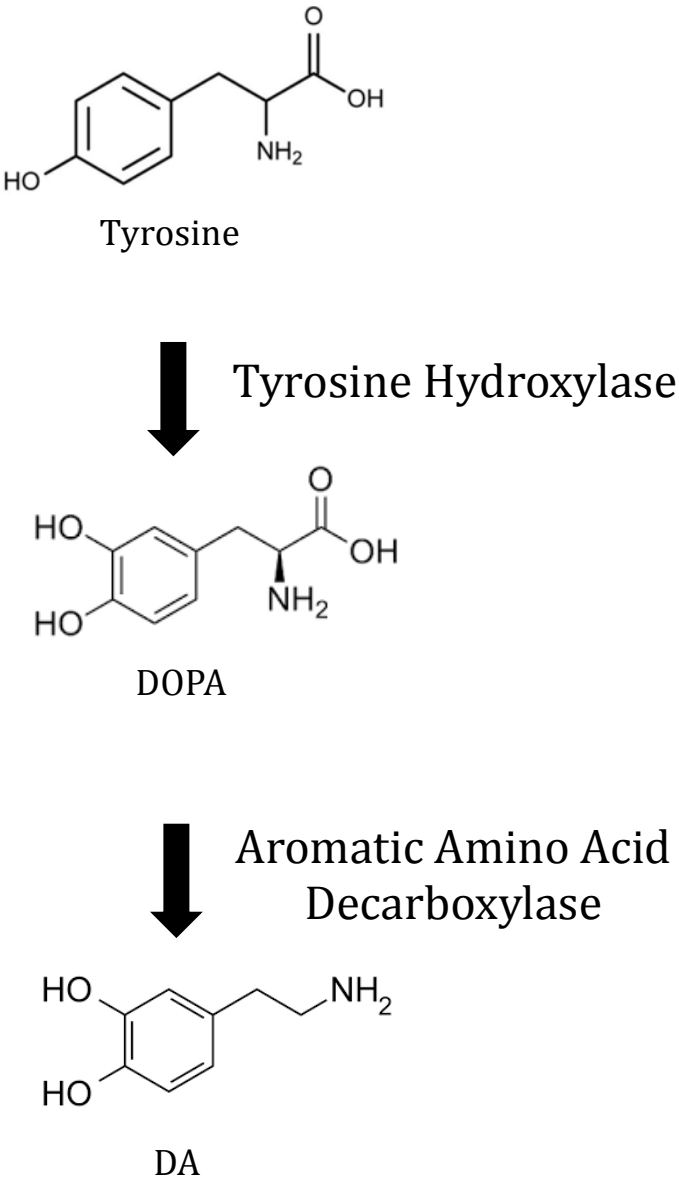

Figure 2. Dopamine Synthesis. Dopamine (DA) is synthesized from the amino acid tyrosine, which is taken up into the presynaptic neuron and hydroxylated by Tyrosine Hydroxylase (TH) to dihydroxyphenylalanine (DOPA). DOPA is then decarboxylated by aromatic amino acid decarbolxylase (AADC) into DA.

synthesized can be regulated by the level of expression of TH. After synthesis, DA is then loaded into synaptic vesicles by the vesicular monoamine transporter (VMAT, encoded by gene *SCL18*). VMAT is an amine/proton antiporter, which uses the proton gradient generated inside the vesicle by V-ATPase to load DA against its concentration gradient into the synaptic vesicles. Given enough L-DOPA precursor, dopaminergic neurons can load DA inside vesicles at concentrations approaching 1 M (Staal *et al.*, 2004, Sulzer *et al.*, 2005). DA-containing vesicles fuse with the plasma membrane in response to increased levels of Ca^{2+}, which occurs when voltage-gated Ca^{2+} channels are activated by the arrival of an action potential. DA is then released into the synaptic cleft, and activates DA receptors (DRs) in the synapse.

DRs are G-protein coupled receptors (GPCR) that couple to either $G_{\alpha s}$ or $G_{\alpha i/o}$. There are five types of DRs: D1, D2, D3, D4, and D5, which are further divided into two subgroups, D1-like receptors, which consist of D1 and D5, and the D2-like receptors, which consist of D2, D3, and D4. The D1-like receptors couple to $G_{\alpha s}$, and upon activation, stimulate the production of cAMP by adenylyl cyclase, which activates protein kinase A and has a stimulatory effect on the cell. In contrast, the D2-like receptors couple to $G_{\alpha i/o}$, which dampens cell activity by suppressing adenylyl activity, resulting in a decrease in cAMP. D2 receptors can be expressed on post-synaptic as well as pre-synaptic neurons, where they function as autoreceptors, dampening pre-synaptic activity when activated (**Fig. 3**). DA transmission can be regulated by the expression of DRs, the activity of autoreceptors on the presynaptic neuron, and by the internalization of DRs from the plasma membrane.

Termination of the DA signal is achieved by removing DA from the synaptic space. This occurs by diffusion of DA away from the synaptic cleft, enzymatic degradation of DA by monoamine oxidases (MAO's) and catechol-*O*-methyltransferase (COMT) to the major metabolite, homovanillic acid (HVA) (**Fig. 4**), or by the active reuptake of DA into the

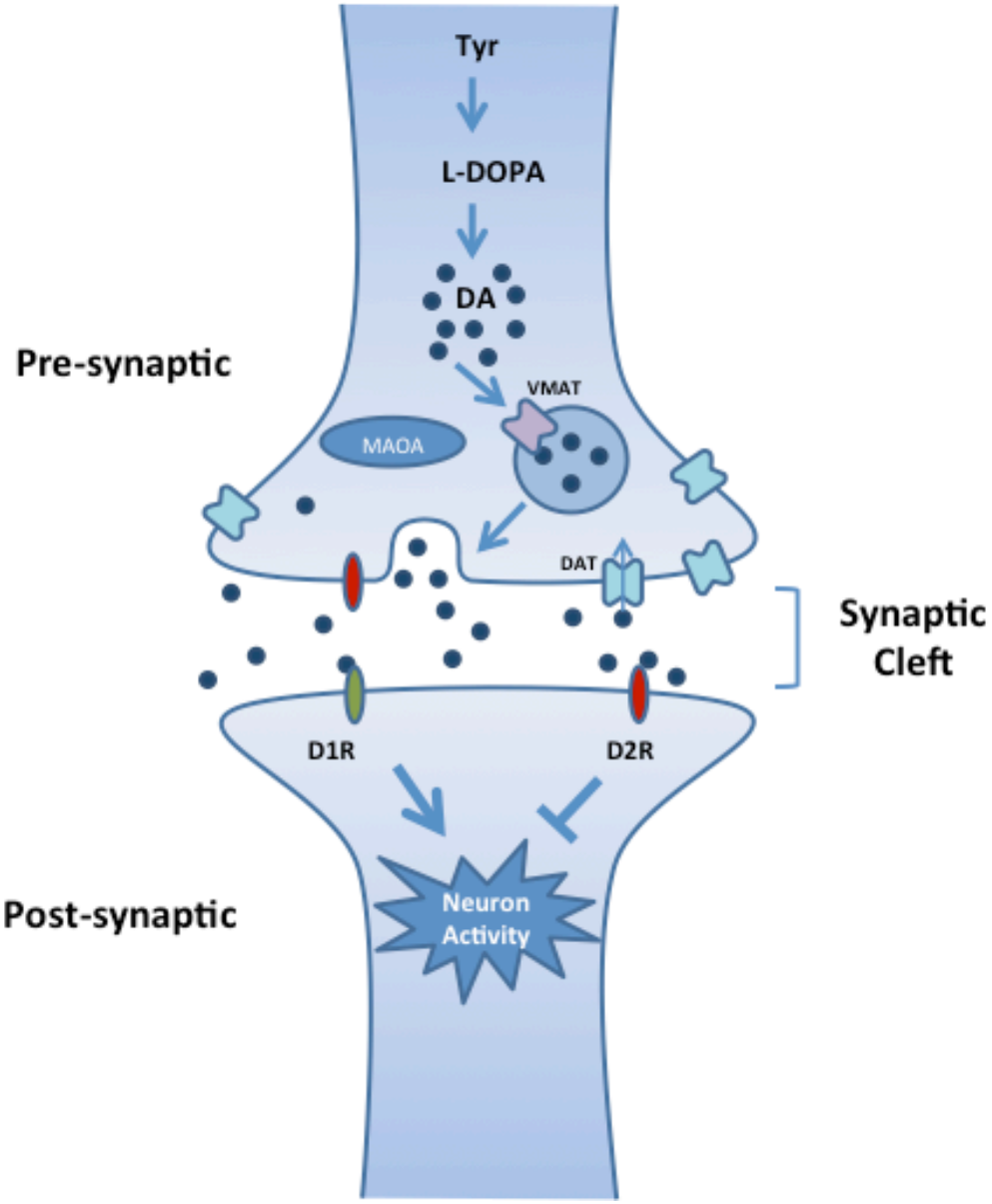

Figure 3. Overview of the dopaminergic synapse. DA is synthesized in the presynaptic neuron (top), and is packaged into secretory vesicles by the vesicular monoamine transporter (VMAT). Upon arrival of an action potential, the vesicles fuse with the plasma membrane and release DA into the synaptic cleft. DA activates dopamine receptors (D1R: D1-like receptors; D2R: D2-like receptors) on both the post-synaptic and pre-synaptic densities, controlling intracellular signaling. DA is then cleared from the synapse by active reuptake into the presynaptic neuron via the dopamine transporter (DAT), enzymatic degradation, or diffusion. Tyr: tyrosine; L-DOPA: L-3,4-dihydroxyphenylalanine; TH: tyrosine hydroxylase; AADC: aromatic amino acid decarboxylase; MAOA: monoamine oxidase A.

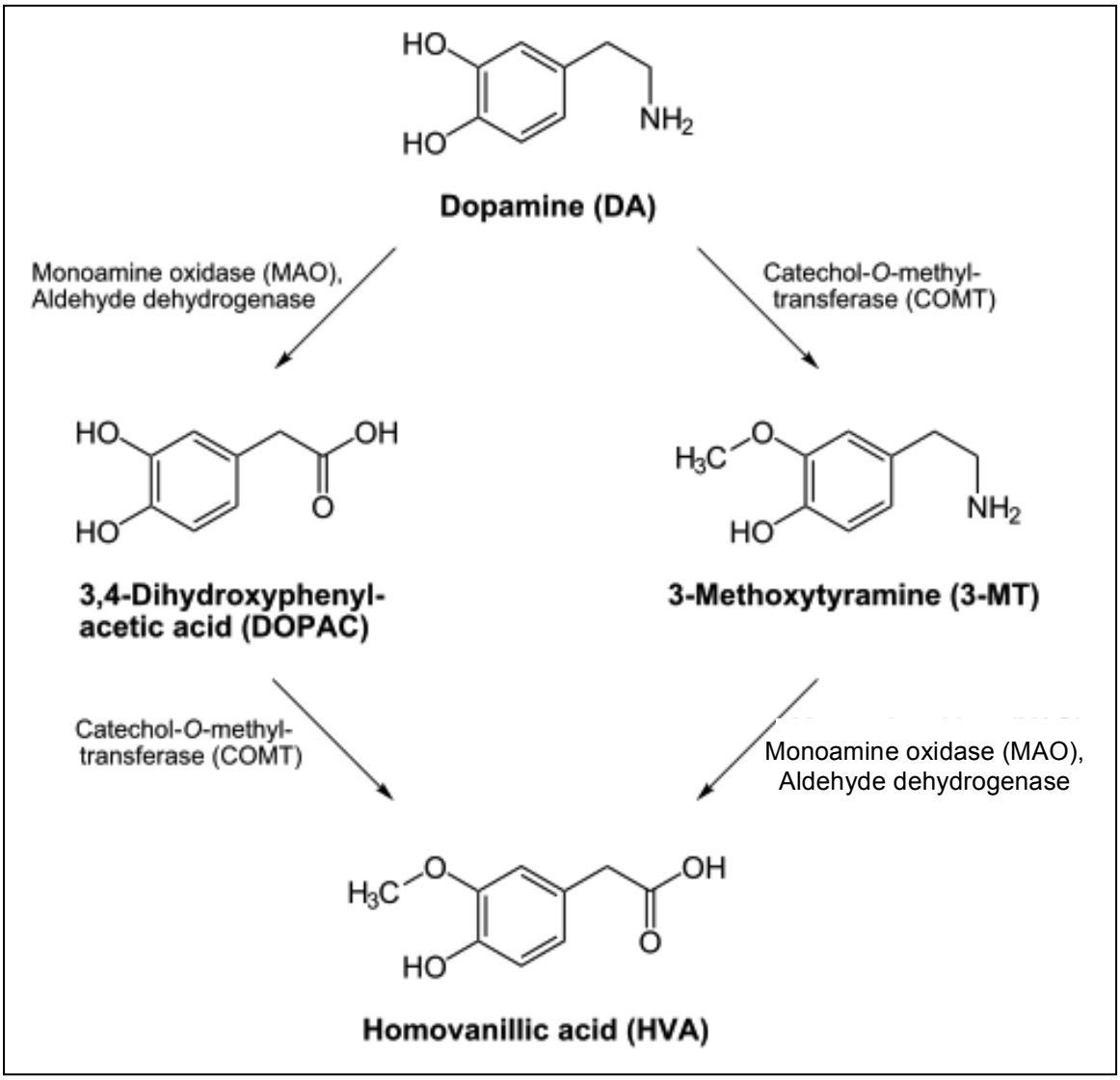

Figure 4. Enzymatic degradation of DA. The enzymes Catechol-*O*-methyl transferase (COMT) and Monoamine oxidase (MAO)/aldehyde dehydrogenase remove DA from the synapse by converting it into the metabolite homovanillic acid (HVA).

presynaptic terminal by the DAT (**Fig. 3**). Once inside the presynaptic terminal, DA can then be reloaded into vesicles by VMAT for re-release.

Dopamine transporter structure

The DAT is a solute-dependent carrier (SLC) transporter, and in particular, is part of the SLC6 family, which includes other neurotransmitter and amino acid transporters such as the 5-HT transporter (SERT), the norepinephrine transporter (NET), the glycine transporter (GLYT), and the GABA transporter (GAT), among others. The SLC6 transporters are secondary active transporters, as they use the electrochemical gradients generated by Na^+/K^+ ATPase pumps in the plasma membrane to symport substrate against the substrate's concentration gradient into the cytosol (Torres *et al.*, 2003). The DAT requires both Na^+ and Cl^- ions to cotransport DA, with a predicted stoichiometry of two Na^+ ions and one Cl^- ion per molecule of substrate (Giros and Caron, 1993, Sonders and Amara, 1996).

Topology and overall structure

In humans, the DAT (hDAT) is encoded by the gene *SLC6A3*. The hDAT cDNA was cloned in the early 90's, and consists of 620 amino acids (Giros *et al.,* 1992). The number of transmembrane (TM) domains, intracellular loops (ILs), extracellular loops (ELs), and locations of the N- and C-termini were predicted using hydrophobicity analysis (Giros *et al.,* 1992), allowing for generation of topology maps similar to that shown in **Figure 5.** From this model, it was predicted that the DAT would have 12 transmembrane (TM) domains. Furthermore, it was predicted to have 6 ILs and 6 ELs, with glycosylation sites located on EL2 between TM3 and TM4, and both N- and C-termini located in the cytosol. High-resolution crystal structures of the bacterial homolog for SLC6 transporters, the LeuT, have been used to confirm this general topology (Yamashita *et al.*, 2005). Finally, the recent crystallization of the *Drosophila*

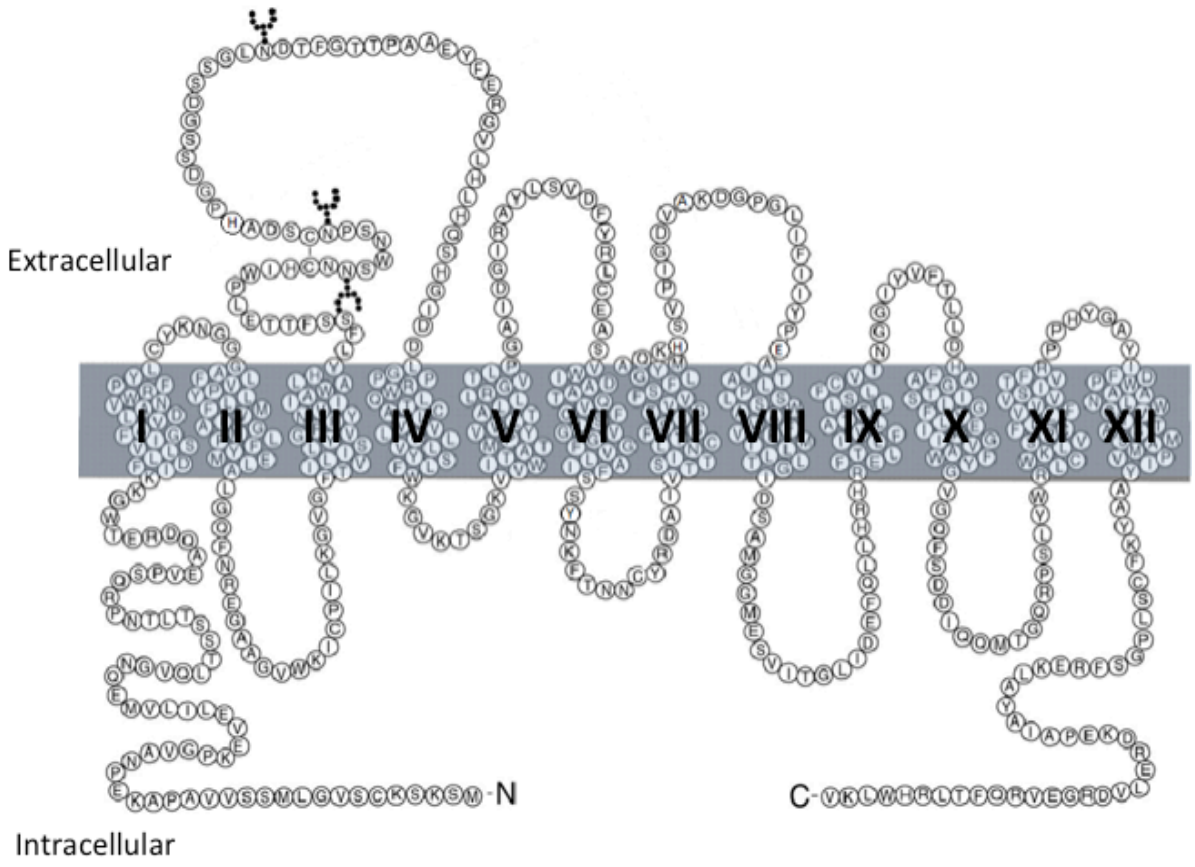

Figure 5. hDAT topology map. Sequence analysis of the hDAT predicts the DAT is a membrane protein consisting of 12 transmembrane domains. The DAT is predicted to have both N- and C-termini located on the intracellular face, with the extracellular loop between the third and fourth transmembrane domains containing a disulfide bond and N-linked glycosylation sites. Image adapted from Loland *et al.,* 2002.

melanogaster DAT (DAT_{cryst}) (**Fig. 6**) further confirmed structural predictions based on the topology maps and LeuT structure (Penmatsa *et al.*, 2013)**.**

Substrate and ion binding sites

Both the LeuT and the DAT_{cryst} confirm that the substrate and the two sodium binding sites are composed of the unwound regions of TM1 and TM6 (oriented antiparallel to each other), in addition to TM3 and TM8 (Yamashita *et al.*, 2005, Penmatsa *et al.*, 2013). While the two Na^+ binding sites translated exactly between the LeuT and the DAT_{cryst}, the LeuT (as a Cl^- independent transporter) lacks a Cl^- binding site. However, the location of a Cl^- binding site was predicted from studies with a Cl^- dependent variant of the LeuT (LeuT E290S) to consist of a coordination between TM2, TM6, and TM7, near the Na1 site (Kantcheva, *et al.*, 2013). This was confirmed in the DAT_{cryst} (Penmatsa *et al.*, 2013).

N- and C-termini

Limited structural data is available regarding the N- and C-termini of the LeuT and the neurotransmitter:sodium symporters (NSSs), with the exception of the DAT_{cryst} structure resolved in 2013 (Penmatsa *et al.,* 2013). The DAT_{cryst} structure showed that the C-terminus contains an alpha helix itself, and appears to act as a "latch" covering the cytoplasmic gate (Penmatsa *et al.*, 2013). However, to date, only computational and physiological data exist to model the hDAT N-terminus. Both the N- and C-termini contain several phosphorylation sites, including consensus sequences for calcium/calmodulin-dependent kinase II (CaMKII), protein kinase A (PKA), and protein kinase C (PKC) (Giros and Caron, 1993). In fact, interaction between the C-terminus and CaMKII has been suggested to be necessary for CaMKII-mediated phosphorylation of the N-terminus (Fog *et al.*, 2006). Phosphorylation of the N-terminus is vital for regulating certain functions of the hDAT, namely reverse transport of DA (Khoshbouei *et al.*, 2004). In particular, the putative phosphorylation sites at Ser residues, 2, 4, 7, 12, and 13, are

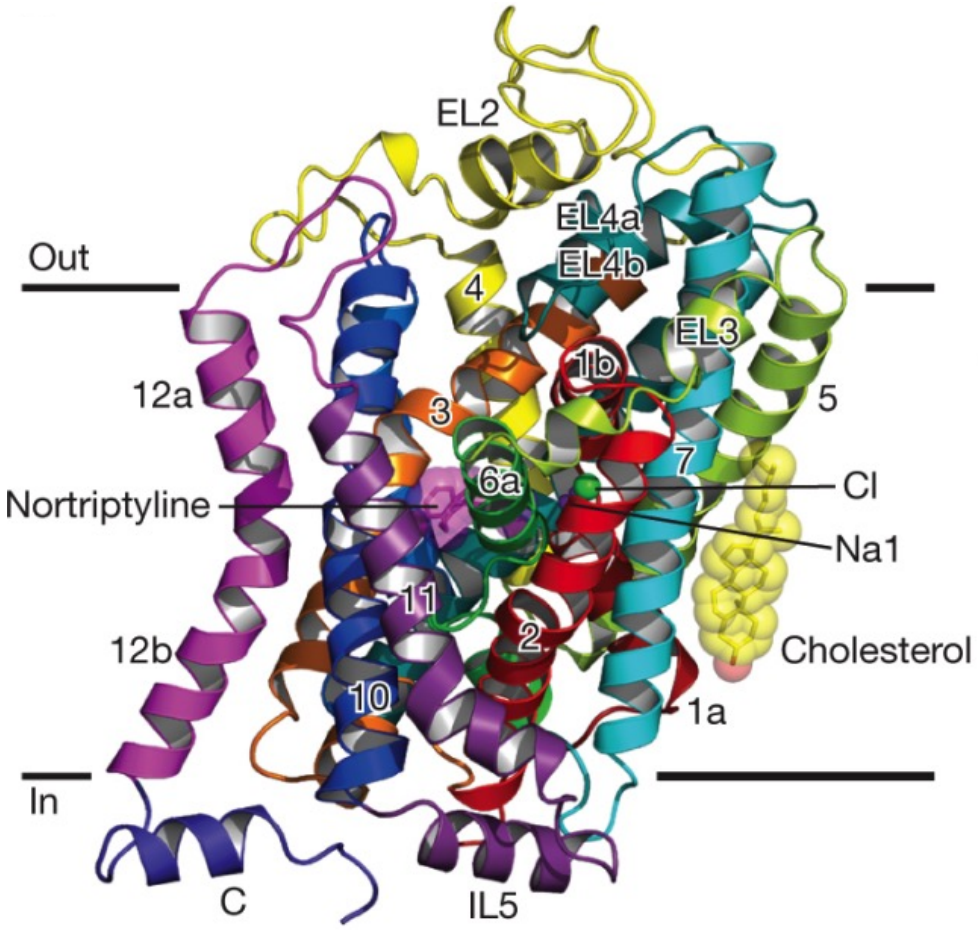

Figure 6. ***Drosophila*** **dopamine transporter (DAT_{cryst}) structure.** DAT_{cryst} was co-crystalized with the tricyclic antidepressant nortriptyline, two sodium ions, a chloride ion, and one molecule of cholesterol (represented by magenta, purple, green, and yellow spheres, respectively). DAT_{cryst} structure viewed parallel to plasma membrane. Image adapted from Penmatsa *et al.,* 2013.

thought to be especially important for reverse transport of DA (Khoshbouei *et al.*, 2004, Bowton *et al.*, 2010).

Oligomerization

The LeuT has been crystallized as a dimer (Yamashita *et al.*, 2005), with TM12 and TM9 important for this dimer interface. However, the DAT_{cryst} structure suggests that TM12 is kinked in the dDAT due to the presence of a proline residue at position 572 and unlikely to form dimers like the LeuT does (Penmatsa *et al.*, 2013). Furthermore, the DAT_{cryst} did not form dimers or oligomers in the micelles used to crystallize it (Penmatsa *et al.*, 2013). Contrary to the crystal structure of DAT_{cryst}, there is physiological data that suggests the hDAT does in fact form oligomers (Hastrup *et al.*, 2001, Torres *et al.*, 2003, Hastrup *et al.*, 2003, Sorkina *et al.*, 2003, Chen and Reith, 2008) and that this oligomerization influences transporter function (Torres *et al.*, 2003, Chen and Reith, 2008). However, it has been suggested that instead of TM9 and TM12 being the interface of dimerization, as occurs in the LeuT, DAT dimerization interface actually occurs with TM4 and TM6, and possibly TM2 (Hastrup *et al.*, 2001, Hastrup *et al.*, 2003, Torres *et al.*, 2003).

Dopamine transporter function

One of the most celebrated models of substrate transport is the alternating-access model, as proposed by Patlak in 1957 and later popularized by Jardetzky in 1966 (Patlak, 1957, Jardetzky, 1966). This model proposes that the transporter, which spans the cell membrane, is open to either the extracellular environment ("outward-facing" conformation) or the intracellular environment ("inward-facing" conformation), and alternates between the two conformations to transport substrate. When the transporter substrate interacts with its binding site, the transporter changes its conformation and opens to the other side of the membrane, releasing the substrate. There are mechanistic variations of the alternating access model, including the

rocker-switch model (**Fig. 7a**), of which the prokaryotic proton-coupled lactose transporter LacY is an example (Abramson *et al.*, 2003), and the gated-pore mechanism, or the occluded model of alternating access (**Fig. 7b**), which is used to model SLC6 transporters and the SLC6 bacterial homolog, the LeuT (Forrest and Rudnick, 2009).

The rocker-switch model can be characterized by an equilibrium between two conformational states: inward-facing and outward-facing. Transport occurs by binding of the substrate and ion(s) to their respective sites while the transporter is in an outward-facing conformation. The transporter then "rocks" around the substrate binding region and opens to the cytosol in an inward-facing conformation, releasing substrate and ions. Unlike the rocker-switch model, the occluded access model is characterized by an equilibrium between three conformational states: outward-facing, occluded, and inward-facing. The occluded state occurs because of the presence of two gates, an extracellular gate and an intracellular gate. When the transporter is in the outward-facing conformation, the substrate and ions can bind to their respective sites; then, the extracellular gate closes and the transporter adopts the occluded state, with both intracellular and extracellular gates closed, trapping the substrate within. The transporter must then adopt the inward-facing conformation and the intracellular gate must open for the substrate and ions to be released into the cytosol.

Altering the conformational equilibrium in which the DAT exists can influence transporter function. An example of this principle in practice is the functional regulation of the DAT by zinc (Zn^{2+}). In ELs 2 and 4, there are three amino acid residues that have been demonstrated to coordinate Zn^{2+} binding: His193 (EL2), His375 (EL4), and Gln396 (EL4) (**Fig. 8**) (Norregaard *et al.*, 1998, Loland *et al.*, 2002). When Zn^{2+} interacts with this binding site, the DAT shows impaired DA uptake, but retains normal substrate binding (Norregaard *et al.,* 1998). This suggests that by "pinning" together EL2 and EL4, Zn^{2+} impairs the ability of the transporter to

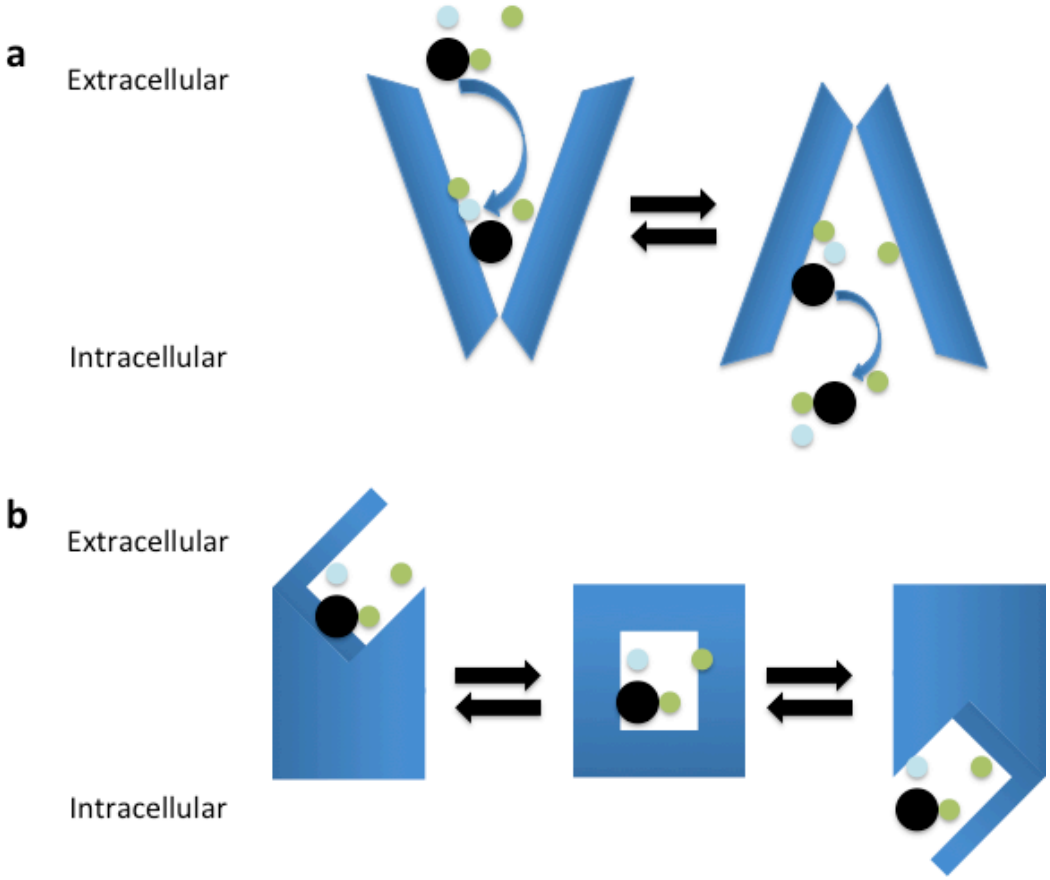

Figure 7. Models of alternating access. (a) Rocker-switch mechanism. Substrate (black sphere) and ion(s) (blue/green spheres) enter when the transporter is in outward facing conformation (left). After substrate binds, the transporter changes conformation by rotating around the substrate/ions, adopting an inward facing conformation (right) and releases substrate/ions into the cytosol. **(b)** Occluded State Mechanism. Substrate and ion(s) enter when the transporter is in outward facing conformation with the extracellular gate open (left). Upon substrate binding, the extracellular gate closes and the transporter adopts an intermediate occluded state (middle). The transporter changes conformation to the inward facing state and the intracellular gate opens (right), releasing substrate/ions into the cytoplasm.

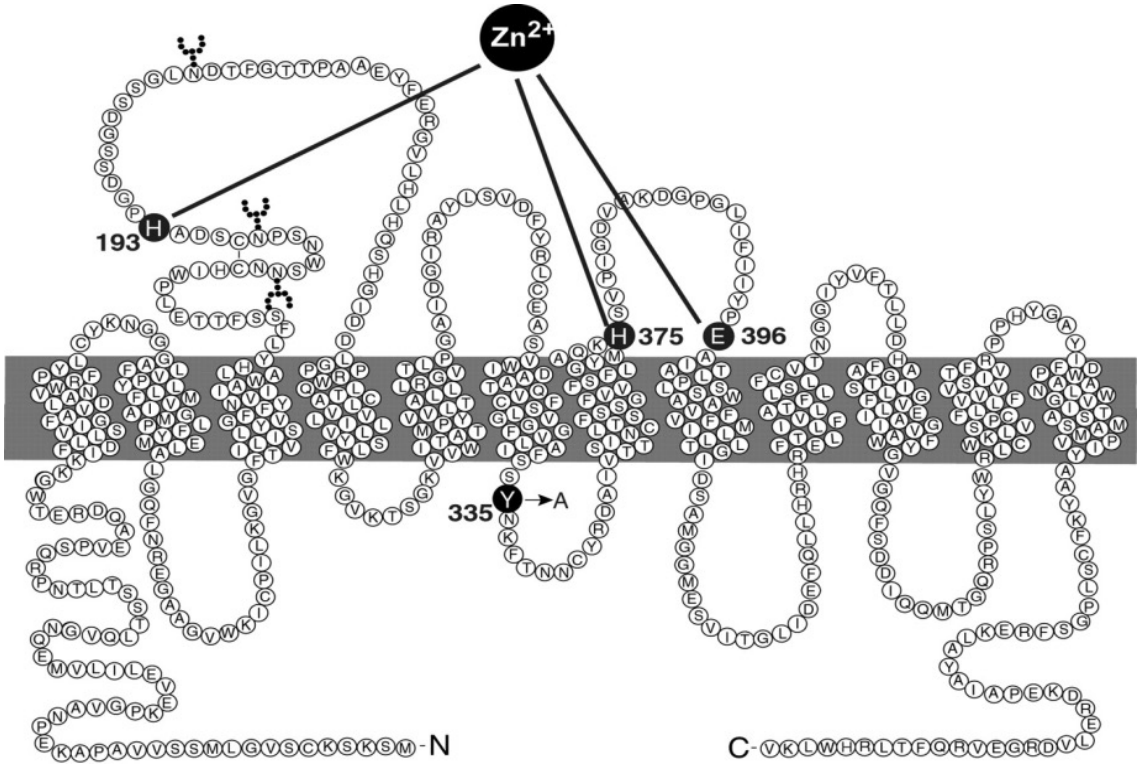

Figure 8. Endogenous zinc binding sites in the hDAT and hDAT Y335A. Residues in extracellular loops 2 (His193) and 4 (His375, E396) coordinate the binding of zinc with the hDAT. Mutation of Y335A (highlighted) results in uptake-deficient transporter, partially rescued by addition of zinc. Image from Loland *et al.*, 2002.

change conformation and disallows the translocation of substrate. Further investigations into the relationship between the outward and inward face were conducted by mutating a residue located in IL3 (a region known to be part of the intracellular gating mechanism), Tyr335 to Ala (hDAT Y335A) (Loland *et al.*, 2002). The hDAT Y335A displays an impaired ability to uptake DA, as well as decreased surface expression, though substrate affinity is normal (Loland *et al.,* 2002). Addition of Zn^{2+} partially rescues this phenotype, restoring some uptake function of the hDAT Y335A (Loland *et al.*, 2002). This suggests that hDAT Y335A is unable to shift towards an inward-facing conformation without EL2 and EL4 being brought into close proximity (in this case, by Zn^{2+}).

While the alternating access model of transport provides a useful construct for thinking about DAT uptake dynamics, the actual DAT transport process appears to be more nuanced, as there is evidence that the DAT does not uptake substrate and ions in a stoichiometric manner. The process of transporting substrate across the plasma membrane is electrogenic, and induces a measurable current: since DA carries a positive charge at physiological pH, based on the $2Na^{+}/1Cl^{-}/1$ substrate^{+} stoichiometry, the inward current should reflect a transference of two positive charges per transport cycle. Indeed, as seen when DAT is expressed in mammalian cells or in *Xenopus* oocytes, the transport of substrate, including DA, AMPH, and (1-methyl-4-phenylpryidium) MPP^{+} into the cytosol generates an inward current (Sonders *et al.,* 1997, Sitte *et al.,* 1998, Khoshbouei *et al.,* 2003). However, it has been observed that the inward current passed is greater than that predicted by stoichiometry (Sonders and Amara, 1996, Kahlig *et al.*, 2004). This suggests that the DAT does not always abide by the alternating access model, and instead may exhibit channel-like activity in passing currents (**Fig. 9**). Another complication in assessing DAT-mediated transport is that the DAT exhibits a second, constitutive leak current that can be blocked by uptake inhibitors like COC and by substrates (Sonders *et al.,* 1997,

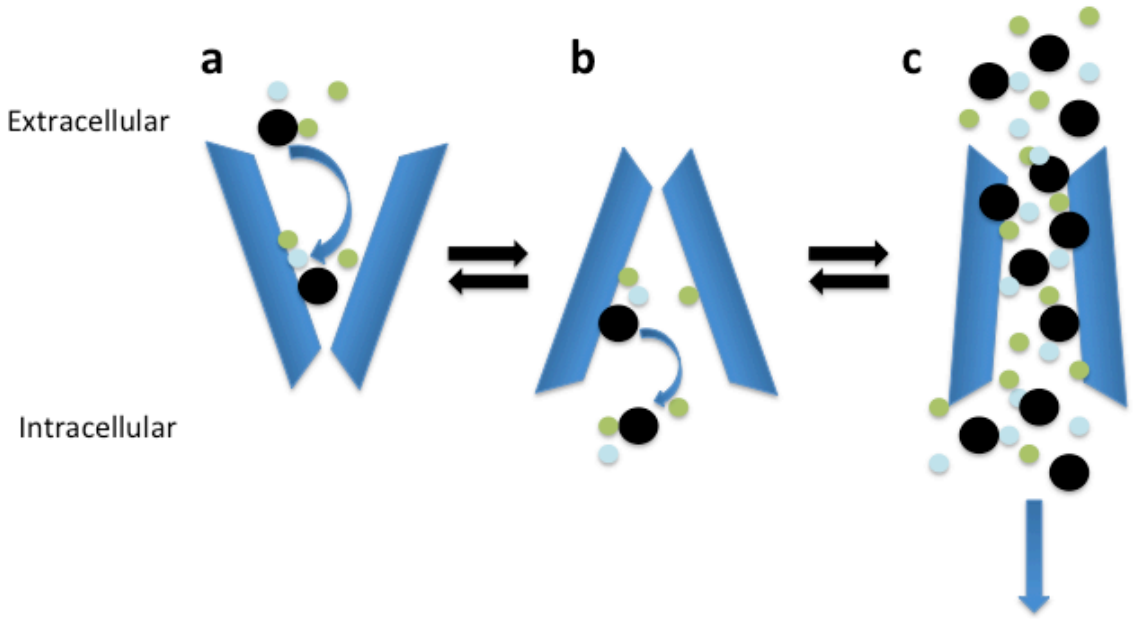

Figure 9. Model of DAT uptake activity. The DAT exhibits behavior consistent with the alternating access model **(a, b)**, but also shows channel-like activity, behaving as a pore for substrates (black spheres) and ions (blue/green spheres; **c**).

Kahlig *et al.*, 2004). Interestingly, this "leak" activity can vary based upon intracellular conditions and dynamics (Ingram *et al.*, 2002, Carvelli *et al.*, 2004).

Reverse transport: amphetamine-induced dopamine efflux

The DAT also is capable of reversing the direction of substrate transport, resulting in the translocation of substrate from the intracellular to the extracellular side. The most dramatic example of this function involves the mechanism of action of the psychostimulant AMPH. The historical study of reverse transport of substrate function has been well summarized by Roberston and colleagues in 2009 (Roberston *et al.*, 2009), though the physiological role of this mechanism remains an enigma (Leviel, 2011).

Amphetamine

AMPH and its derivatives are structurally similar to DA (**Fig. 10**), and are able to act as substrates for the DAT. AMPH can affect DAT function by acting as a competitive inhibitor of the DAT, preventing the DAT from transporting DA into the cell, thereby increasing extracellular DA levels, having a similar effect as cocaine, a DAT inhibitor that blocks DA transport. However, AMPH also induces the DAT to reverse the transport of DA into the extracellular space (a DA efflux event), further enhancing the levels of extracellular DA and contributing to the rewarding effects and abuse potential of AMPH. A summary of the differences between the mechanism of DAT blockers (like COC) and the mechanism of AMPH is seen in **Figure 11**. The behavioral effects of AMPH are thought to be mediated by the DAT, since mice and *Drosophila melanogaster* lacking the DAT do not show any locomotor response to AMPH, although they do exhibit constitutively elevated DA levels as well as hyperlocomotion (Giros *et al.*, 1996, Pizzo *et al.*, 2013).

The mechanism by which AMPH induces the reverse transport of DA has been studied for several decades, and the understanding of the mechanism has seen much evolution. The first

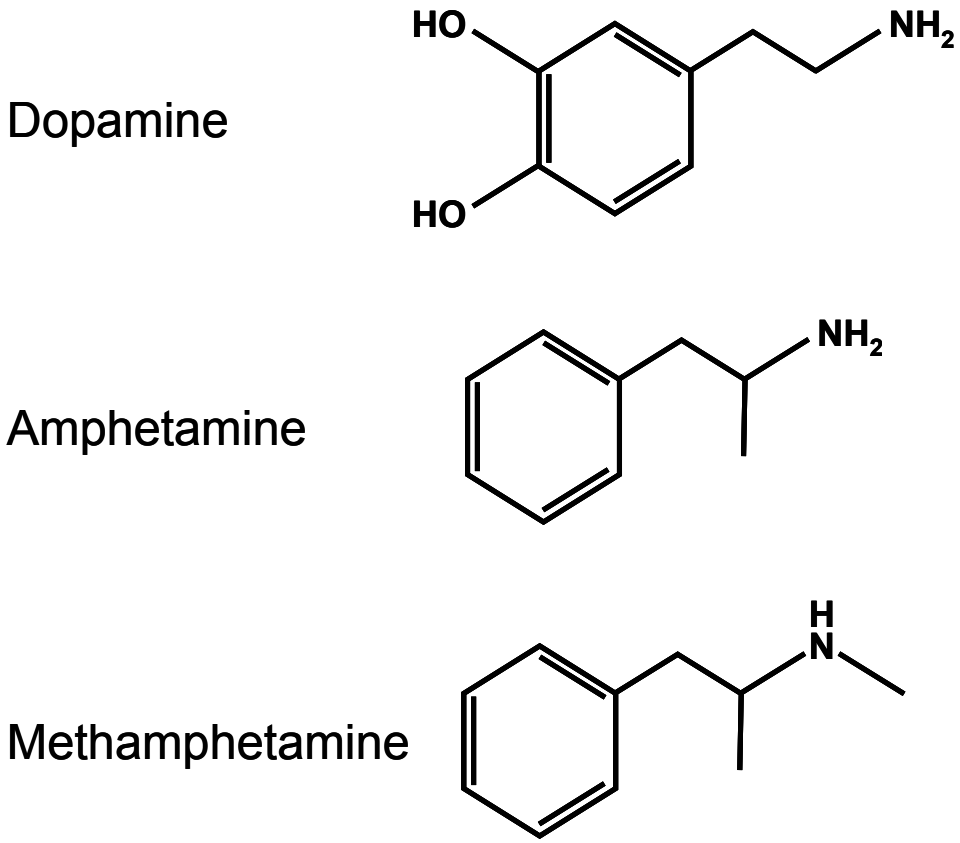

Figure 10. Chemical structures of DAT substrates. The psychostimulants amphetamine and methamphetamine share structural similarities with the endogenous substrate dopamine, and are recognized as substrates by the DAT.

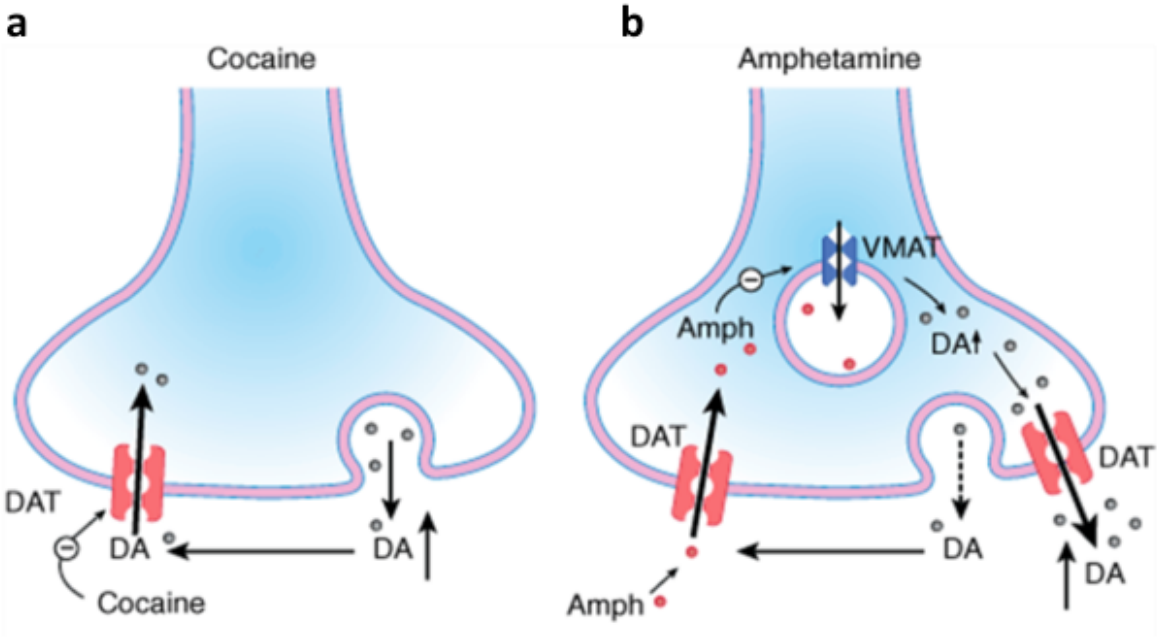

Figure 11. Mechanism of action of psychostimulants. (a) Cocaine (COC) is an inhibitor of the DAT, contributing to the elevation of extracellular dopamine by preventing the reuptake of dopamine released through vesicular fusion. **(b)** Amphetamine (AMPH) is a substrate for the DAT, and is transported into the presynaptic neuron. AMPH prevents the loading of dopamine into synaptic vesicles, increasing the intracellular dopamine concentration. AMPH then induces the DAT to adopt an efflux-willing conformation, which releases DA into the extracellular space through the DAT itself. Image from Katzung *et al.,* (2009).

mechanism introduced, the facilitated exchange diffusion model, was suggested in 1979 by Fischer and Cho (Fischer and Cho, 1979) (**Fig. 12**). Consistent with the alternating access model of transport, the facilitated exchange diffusion model suggests the exchange of extracellular AMPH for intracellular DA: as AMPH interacts with the outward-facing conformation of the DAT, it is transported into the neuron and the DAT changes its conformation to an inward-facing state to release the substrate. Once AMPH is released into the cell, the DAT is left in an inward-facing conformation, available to bind to intracellular DA. As the transporter returns to its outward-facing conformation, it then releases DA into the extracellular environment (Fischer and Cho, 1979).

Once AMPH has been transported into the presynaptic bouton, it interferes with the loading of DA into vesicles, raising the intracellular concentration of unsequestered DA. AMPH is a substrate for the VMAT as well and is transported into secretory vesicles. The weak-base hypothesis, (discussed in more detail in a review by Sulzer *et al.*, 2005), suggests that, as a weak base, AMPH sequesters protons inside the secretory vesicle, destroying the proton gradient necessary for VMAT to load DA into the vesicle. Another hypothesis proposes that AMPH competes with DA for transport by VMAT, and would cause depletion of DA from the vesicles *via* the facilitated exchange diffusion model (Sulzer *et al.*, 2005). Regardless, AMPH causes the elevation of DA inside the cell, which can trigger the reverse transport of DA (Fischer and Cho, 1979).

However, in 2005, the DAT was also discovered to adopt a channel-like state in response to AMPH, resulting in the rapid release of DA (DA efflux) (Kahlig *et al*., 2005) (**Fig. 13**). This mechanism is radically different from the facilitated exchange diffusion model in that there is no known stoichiometry between ions and substrate, and occurs on the order of milliseconds rather than slower diffusion. Additionally, such an efflux event can be considered within the range of a DA quantum from vesicular release, a release of approximately 2,000-14,000 molecules of DA, which can influence high-affinity DA receptors in 20-100 nearby dopaminergic synapses (Sulzer and

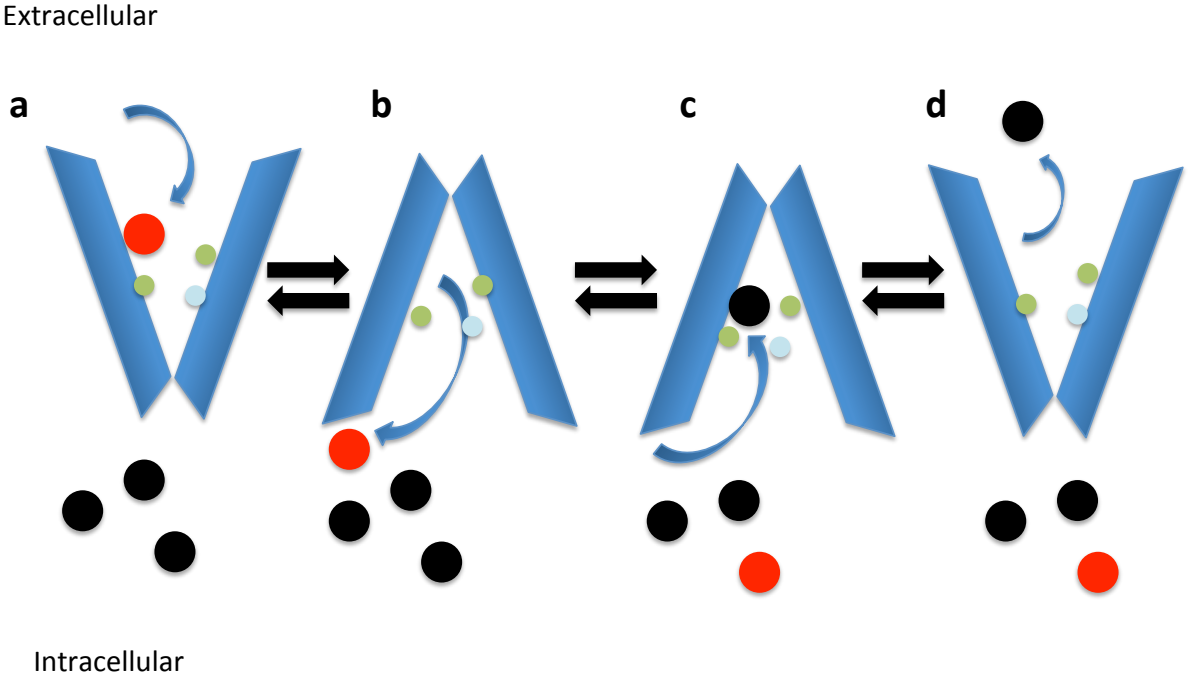

Figure 12. Alternating access model of AMPH-induced DA efflux. AMPH (red sphere) and ions (blue/green spheres) bind to outward facing DAT **(a)**, and DAT changes conformation to inward facing, releasing AMPH into cytosol **(b)**. Intracellular DA (black sphere) binds to inward facing DAT **(c),** and DAT changes conformation to outward facing to release DA into the extracellular space **(d).**

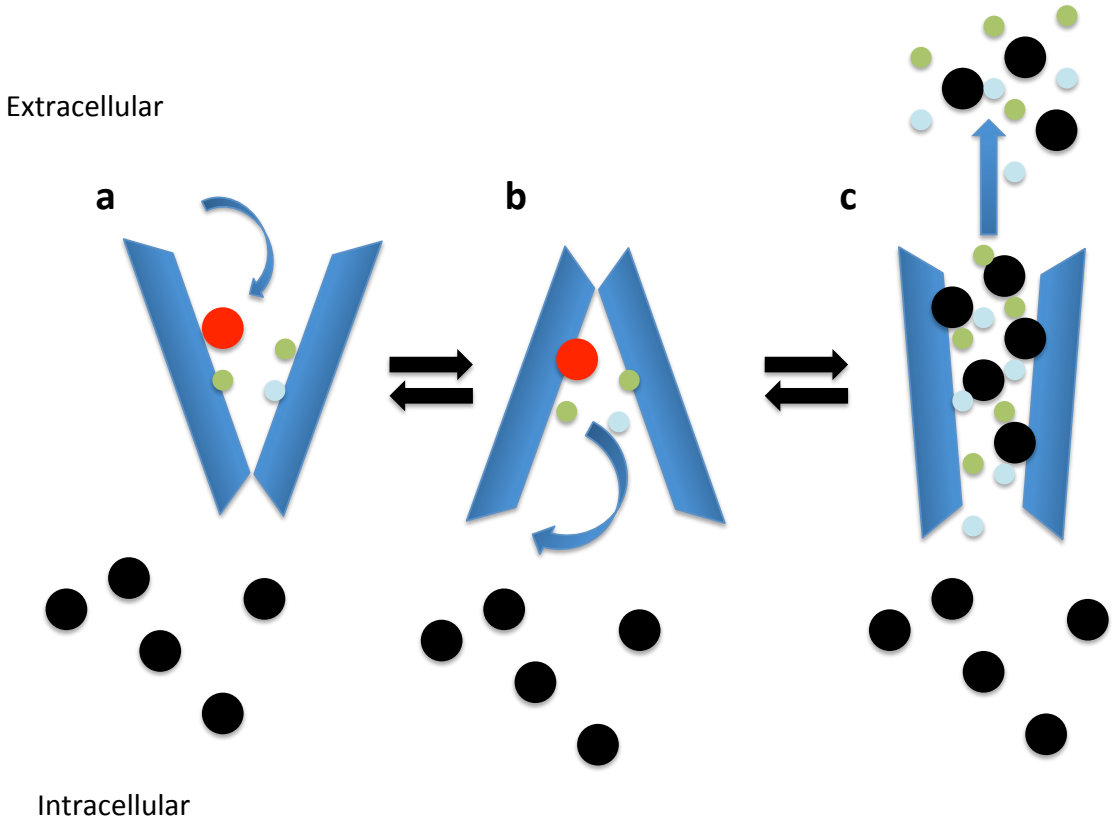

Figure 13. Model of AMPH-induced DA efflux mechanism: channel-like activity. AMPH (red sphere) and ions (blue/green spheres) bind to outward facing DAT (**a**), and DAT changes conformation to inward facing, releasing AMPH into cytosol (**b**). AMPH induces transporter to adopt channel-like state (**c**), allowing DA (black sphere) to pass through transporter, resulting in DA efflux event.

Pothos, 2000, Cragg and Rice, 2004, Kahlig *et al.,* 2005). This DA quantum release also suggests that this coordinated burst of DA release may have a discernable impact on dopaminergic signaling, and may contribute to AMPH's effects (Kahlig *et al.*, 2005).

Interacting proteins and reverse transport of DA

The ability of AMPH to cause the DAT to undergo the conformational changes required for DA efflux is likely to depend, at least in part, upon alterations to the DAT via phosphorylation and/or changes in interactions with other intracellular proteins/entities. The N-terminus of the DAT in particular possesses several consensus sequences for phosphorylation sites by kinases such as CaMKII and PKC. When phosphorylation of the DAT N-terminus is prevented either by truncation or targeted mutation of Ser residues to Ala, the ability of AMPH to induce DA efflux is dramatically inhibited (Khoshbouei *et al.*, 2004). Furthermore, phosphomimetic mutations (Ser to Asp) of the N-terminus promote AMPH-induced DA efflux (Khoshbouei *et al.*, 2004). Although the phosphorylation state of the N-terminus of the DAT is important for AMPH-induced DA efflux, it appears to have no effect on the ability of the DAT to uptake substrate (Khoshbouei *et al.*, 2004), indicating that this mechanism regulates DAT functions in an asymmetric manner.

AMPH has been observed to cause the activation of CaMKII, in synaptosomal preparations (Iwata *et al.,* 1997, Choe and Wang, 2002, Wei *et al.,* 2007). Consistent with the idea that AMPH acts as a substrate for the DAT and enters the neuron via DAT uptake, when DAT expressing synaptosomes were exposed to a DAT inhibitor, AMPH failed to activate CaMKII (Iwata *et al.*, 1997). AMPH has also been shown to increase the intracellular concentration of Ca^{2+} in DAT expressing cells (Gnegy *et al.*, 2004), an increase dependent upon the activation of L-type and N-type Ca^{2+} channels, both of which are voltage-gated channels (Kantor *et al.*, 2004). Furthermore, in the absence of extracellular Ca^{2+}, the ability of AMPH to activate CaMKII in synaptosomal

preparations is also diminished (Iwata *et al.*, 1997). As elevated Ca^{2+} levels activate CaMKII, AMPH likely activates CaMKII and other Ca^{2+} dependent intracellular signaling pathways by increasing the concentrations of Ca^{2+} inside DAT-expressing cells. Once activated, CaMKII associates with and phosphorylates the distal DAT N-terminus serine residues, promoting DA efflux (Fog *et al.*, 2006, Bowton *et al.*, 2010). Inhibition of CaMKII impairs the ability of AMPH to induce DA efflux both *in vitro* and *in vivo*, as does the prevention of CaMKII/DAT interactions (Fog *et al.*, 2006).

PKC has also been shown to be activated *in vivo* by the addition of AMPH to brain slices, which then also phosphorylates serine residues of the DAT N-terminus (Giambalvo, 1992, Foster *et al.,* 2002, Giambalvo, 2004, Johnson *et al.*, 2005). Inhibition of PKC in rat striatal slices prevents AMPH-induced DA efflux (Kantor and Gnegy, 1998, Johnson *et al.,* 2005). While PKC does phosphorylate the N-terminus, AMPH-induced PKC activation also results in the internalization of the DAT (Zhu *et al.*, 1997), which requires the C-terminus of the DAT (Holton *et al.,* 2005). PKC can also be activated by the addition of phorbol esters such as PMA, which causes internalization and ubiquitination/degradation of the DAT (Hong and Amara, 2013). However, transporters internalized in response to AMPH-activation of PKC usually undergo recycling and eventually are trafficked back to the surface in neurons (Hong and Amara, 2013).

Interaction partners for the DAT are not limited to kinases, as evidenced by the growing body of evidence supporting the role of Syntaxin 1 (STX1), a member of the soluble N-ethylmaleimide-sensitive factor attachment protein receptor (SNARE) protein complex, in the AMPH-induced DA efflux mechanism. STX1 is required for the docking and fusion of synaptic vesicles with the plasma membrane, and therefore plays an essential role in the exocytotic release of neurotransmitters (Sudhof, 2004). There is evidence suggesting that STX1 directly interacts with the N-terminus of several different SLC6 neurotransmitter transporters (Deken *et al.*, 2000, Quick, 2003, Lee *et al.*, 2004), and alters their electrophysiological properties (Quick,

2003, Carvelli *et al.,* 2008). For STX1 interactions with the DAT, glutathione-S-transferase (GST) pulldowns show that the first 33 residues of the DAT N-terminus are important for this interaction (Binda *et al.*, 2008), the same region of the DAT N-terminus necessary for AMPH-induced DA efflux. Furthermore, this DAT/STX1 interaction is mediated by AMPH-activated CaMKII and supports AMPH-induced DA efflux (Binda *et al.*, 2008).

Dopamine transporter variants and neuropsychiatric disease

While the mechanism by which the reverse transport of DA affects physiology remains mysterious (Leviel, 2011), the information available about the role of dysregulated reverse transport in psychiatric disease is growing as more neuropsychiatric disease-associated hDAT variants are being identified and characterized. These neuropsychiatric disorders include ADHD, ASD, BAD, and early-onset PD. While dopaminergic signaling has been implicated in each of these disorders individually, several cases of comorbidity occur between these conditions. ADHD and BAD are documented to share symptoms and can occur simultaneously with pediatric onset of BAD (Geller *et al.*, 2002, Faraone and Tsuang, 2003), while patients with ASD often display symptoms of ADHD as well. Since hyperactivity is a shared trait in each of these disorders, it can be suggested that these individual neuropsychiatric disorders share at least some common pathological dysregulation of neuropathways.

Due to the prevalence of functionally altered DAT variants found in these disorders, as discussed later in this chapter, DAT dysfunction appears to be a promising mechanism or paradigm in the underlying dysregulation of the putative common neuropathway(s) in these disorders. In fact, the most well-known mouse model of a hyperactive state, like that observed in human ADHD, is the DAT knockout mouse (KO) (Giros *et al.*, 1996), although in humans lacking function DAT, infantile dystonia and juvenile Parkinson's Disease occur (Kurian *et al.*, 2009, Kurian *et al.*, 2011). Furthermore, a specific hDAT variant (hDAT A559V) has been identified in five individuals, each

presenting with either BAD, ADHD, or ASD (Grunhage *et al.*, 2000, Mazei-Robison *et al.*, 2005, Bowton *et al.*, 2014). Intriguingly, the individuals who share a common disorder are siblings (*i.e.,* ADHD siblings, ASD siblings). This raises the question of whether the interplay between different environments and the same genetic variants can result in the manifestation of different disorders. On the other hand, perhaps particular disorders can arise from interactions between the hDAT variant and other distinct, though as yet unidentified, variants in the probands' genetic backgrounds.

The hDAT variants discussed both in this section and in the original work of this thesis possess a functional commonality: an impaired or altered ability to reverse transport DA. To date, there are two (often overlapping) kinds of disease-associated impairments in reverse transport: (1) anomalous DA efflux (ADE), characterized by a mutant DAT constitutively leaking DA into the extracellular space and (2) impaired or altered ability of the hDAT to respond to AMPH in a coordinated manner. While the effects of these dysfunctions are still not immediately translatable to physiology, the growing body of evidence suggests that this mechanism is physiologically relevant to the etiology of neuropsychiatric disorders. **Table 1** summarizes the functional phenotypes of the hDAT variants characterized to date, as well as their associated disease and the number of individuals with the variant.

hDAT A559V

The hDAT A559V variant is the most well-studied functional variant of the hDAT and was first identified in a patient with bipolar disorder (Grunhage *et al.*, 2000), then in two patients (siblings) with attention deficit hyperactivity disorder (ADHD) (Mazei-Robison *et al.*, 2005), and in two unrelated patients with autism spectrum disorder (Bowton *et al.*, 2014). The hDAT A559V variant was first functionally characterized *in vitro* in 2008, and was shown to have unchanged DA uptake from type (WT) hDAT, but exhibited anomalous DA efflux, as revealed by blocking DA leak with the DAT inhibitor COC, and abnormal response to AMPH (Mazei-Robison *et al.*, 2008). The

Variant	# Affected Individuals	Disease(s) associated	Surface Expression	Uptake	Anomalous DA efflux	AMPH response
A559V[1]	5	Bipolar, ADHD, ASD	Normal	Normal	Yes	Impaired
T356M[2]	1	ASD	Normal	Impaired	Yes	Impaired
D421N[2]	1	ADHD, PD[3]	Normal	Impaired	Yes	Impaired
R615C	1	ADHD	Impaired	Impaired	N/A[4]	Normal[4]
R51W	1	ASD	Normal	Normal	N/A	Impaired
STX1 R26Q[5]	1	ASD	Normal	Increased	N/A	Impaired
R445C	1	Infantile Dystonia	Impaired[6]	Impaired	No[7]	Impaired[8]

Table 1. Disease-associated variants and their respective functional phenotypes. [1]1 Individual with bipolar disorder, 2 individuals (siblings) with ADHD, and 2 individuals (siblings) with ASD. [2]*De novo* mutation. [3]Individual had both ADHD and PD, as well as heritable I312F variant (impaired uptake only, present in non-symptomatic sibling (Hansen *et al.*, 2014). [4]R615C has increased basal phosphorylation levels and interaction with CaMKII, may affect ADE/AMPH response, but not tested. [5]Syntaxin1 (STX1) is an interacting protein with the hDAT, involved in the AMPH-induced DA efflux mechanism (Binda *et al.*, 2008). Functional phenotypes are for WT hDAT when coexpressed with STX1 R26Q. [6]hDAT variant displays decreased glycosylation. [7]hDAT variant was tested for ADE. [8]Cells heterologously expressing hDAT R445C were patch pipette loaded with DA, bypassing impairments in uptake.

hDAT A559V is unable to uptake AMPH, and therefore does not respond to AMPH treatment with the DA efflux phenotype typical of WT hDAT (Mazei-Robison *et al.*, 2008, Bowton *et al.*, 2014). Instead, ADE by hDAT A559V is blocked by application of AMPH (Mazei-Robison *et al.*, 2008). The mechanism behind this ADE was further explored in 2010, and was discovered to be supported by D2-autoreceptor activation of CaMKII, which mediates phosphorylation of the hDAT N-terminus (Bowton *et al.*, 2010). It did not go unnoticed that this mechanism is similar to that which occurs during the AMPH-induced mechanism of DA efflux, and in fact, pseudophosphorylation of the N-terminus of hDAT A559V (mimicking AMPH-mediated phosphorylation) supports channel-like activity of the DAT, possibly leading to DA efflux or ADE (Bowton *et al.*, 2010). It is intriguing that despite the hDAT A559V's inability to respond to AMPH, a phosphorylation pathway normally stimulated by AMPH is dysregulated in the hDAT A559V.

The relationship between the intracellular machinery susceptible to subversion by AMPH and the hDAT A559V's functional phenotype was also investigated in the context of AMPH-induced trafficking of the hDAT (Bowton *et al*., 2014). AMPH is known to induce redistribution of the transporter at and away from the plasma membrane (Saunders *et al.*, 2000, Kahlig *et al.*, 2004, Johnson *et al.,* 2005, Kahlig *et al*., 2006, Boudanova *et al.*, 2008). However, in the case of hDAT A559V, AMPH does not induce internalization *in vitro* unless it is perfused into the intracellular environment *via* whole-cell patch clamp or PKCßII is inhibited (Bowton *et al.*, 2014). PKCßII is an isoform of PKCß that is required for D2R-mediated regulation of DAT surface expression and has also been shown to interact with the hDAT to promote DA efflux (Johnson *et al.*, 2005). hDAT A559V cells show increased basal levels of activated PKCßII at the plasma membrane compared to cells expressing WT hDAT, perhaps due to the increased activity of D2Rs (Bowton *et al.*, 2010, Bowton *et al.*, 2014). Additionally, inhibition of PKCßII rescues the impaired ability of AMPH to induce DA efflux in hDAT A559V cells (Bowton *et al.*, 2014). It is possible that elevated activity of PKCßII contributes to the constitutively elevated phosphorylation of the hDAT A559V N-terminus,

which has been suggested to not only support constitutive ADE, but also promote an inward-facing conformation (Bowton *et al.*, 2010, Bowton *et al.*, 2014). Since DA uptake is unaffected, but AMPH uptake is, it is tempting to suggest that perhaps the A559V mutation results in an increased affinity for AMPH, preventing AMPH from being released into the cytosol in high enough amounts to evoke cellular responses.

Finally, hDAT A559V has been developed as a behavioral model (Mergy *et al.*, 2014). Mice expressing the hDAT A559V show elevated extracellular DA levels in the brain, as well as an increase in basal locomotion (Mergy *et al.*, 2014). However, as predicted by *in vitro* characterizations, hDAT A559V shows normal uptake. Additionally, as expected, mice with the hDAT A559V variant show a decreased locomotor response to AMPH, as well as an impaired ability to depolarize DA neurons (Mergy *et al.*, 2014). It is tempting to speculate that ADE, and/or the underlying AMPH-susceptible machinery, plays a role in depolarization of DA neurons. The hDAT A559V mouse model is now being used as a model for studying the impact of DAT dysfunction in neuropsychiatric disease.

hDAT R615C

Another ADHD-associated hDAT variant, the hDAT R615C, was characterized in 2012 (Sakrikar *et al.,* 2012). Although this variant was not tested for ADE, it displays altered functional characteristics that may impact ADE. Unlike the hDAT A559V or hDAT D421N variants, hDAT R615C shows no impairment in AMPH-induced DA efflux as measured by amperometric current *in vitro*, although it does have impaired DA uptake. Furthermore, the R615C hDAT was shown to have increased levels of endocytosis and turnover, with decreased overall total and surface expression compared to WT hDAT. Impaired surface expression of the DAT results in elevated DA levels and hyperlocomotion (Giros *et al.,* 1996), so it is possible that the hDAT R615C might

contribute to ADHD pathology *via* a concomitant impairment in DA uptake and surface expression.

However, Sakrikar *et al* also found that hDAT R615C showed a 2-fold increase in association with CaMKII, as well as an increase in phosphorylation of the hDAT R615C (Sakrikar *et al.*, 2014). Importantly, CaMKII phosphorylates the N-terminus of the hDAT during the AMPH-induced DA efflux mechanism, so these data led researchers to believe that the hDAT R615C was able to compensate for lack of surface expression, and still show similar AMPH-induced DA efflux. This would suggest that neurons expressing hDAT R615C would have abnormal regulation of phosphorylation of the N-terminus, which has been shown to result in spontaneous DA efflux in the hDAT A559V variant (Bowton *et al.*, 2010). Although to date the hDAT R615C has not yet been tested for ADE, it bears the hallmarks of an ADE hDAT variant and merits further investigation. It is also tempting to speculate that, due to its elevated basal phosphorylation, the hDAT R615C may have altered sensitivity to AMPH under differing cellular conditions.

hDAT D421N

Recently, an adult individual with both early-onset Parkinson's Disease and ADHD was identified out of a cohort of patients with Parkinson's-like movement disorders (Hansen *et al.*, 2014). This individual is the first documented case of being compound heterozygous for variants in the hDAT, possessing a heritable variant, hDAT I312F and a *de novo* variant, hDAT D421N. The hDAT I312F showed an impairment in DA uptake *in vitro*, but was also present in an unaffected sibling. However, the *de novo* hDAT D421N demonstrated a functional phenotype similar to the ASD *de novo* variant, hDAT T356M (Hamilton and Campbell *et al.*, 2013; discussed in detail in the body of this thesis), impaired DA uptake, impaired DA efflux response to AMPH, and ADE (Hansen *et al.*, 2014). Another similarity with the hDAT T356M is that the D421N mutation also perturbs affinity for

Na^+ by interfering with the second Na^+ binding site (Hansen *et al.*, 2014). As is the case for hDAT T356M, there have not yet been any published investigations on the intracellular mechanisms surrounding the observed ADE of hDAT D421N, nor whether the AMPH-susceptible phosphorylation pathways are dysregulated in these variants, as is the case with the hDAT A559V.

hDAT R445C

Another hDAT variant found in an individual with Parkinson's-like symptoms (Infantile Dystonia) is the hDAT R445C (Ng *et al.*, 2014). While this variant showed decreased formation of the mature hDAT when expressed in a heterologous cell line and decreased surface expression, enough was expressed to allow functional assessment. This transporter was shown to have ablated AMPH-induced DA efflux, did not present any evidence of ADE, nor did this transporter variant possess the ability to uptake substrate (Ng *et al.*, 2014). The absence of virtually all function of the hDAT R445C variant is an intriguing puzzle, but unfortunately does not allow for any conclusive remarks regarding the role of reverse transport of DA in infantile dystonia, except to note that this is an additional case of impaired/absent reverse DA transport capability.

While the hDAT R445C is, thus far, the only infantile dystonia-associated hDAT variant to be tested for AMPH response or ADE, it is only one of 13 different hDAT variants discovered to be present in this disorder (Kurian *et al.*, 2009, Kurian *et al.,* 2011, Ng *et al.*, 2014). A striking commonality is that, when expressed heterologously, all 13 of these variant hDAT constructs show decreased maturation and glycosylation, as well as decreased trafficking and surface expression (**Table 2**). However, since the heterologous expression systems differ between the studies and manifest differing levels of surface expression, it is uncertain whether this impaired glycosylation is a disease-relevant characteristic of these variants or merely an artifact. The relationship between impaired hDAT glycosylation and Infantile Dystonia is unclear, although all 7 of the hDAT variants tested for uptake function *in vitro* (predictably) showed decreased ability to transport substrate.

Variant	# Affected Individuals	Surface Expression	Uptake	Mature Glycosylation
R85L**	1	Impaired	Impaired	Impaired
V158F*	1*	Impaired	N/A	Impaired
L224P	1	Impaired	N/A	Impaired
G327R#	1#	Impaired	N/A	Impaired
A314V	3	Impaired	Impaired	Impaired
L368Q	2	Impaired	Impaired	Impaired
G386R***	1***	Impaired	Impaired	Impaired
P395L	1	Impaired	Impaired	Impaired
R445C**	1	Impaired	Impaired	Impaired
Y470S***	1***	Impaired	Impaired	Impaired
R521W	1	Impaired	N/A	Impaired
P529L#	1#	Impaired	N/A	Impaired
P554L*	1*	Impaired	N/A	Impaired

Table 2. Infantile Dystonia-associated hDAT mutations and respective *in vitro* functional phenotypes. *Same individual, **Same individual, ***Same individual, #Same individual. Total unique individuals: 12

Impaired DA uptake has been identified in other disorders (ADHD, ASD) that lack the devastating neurodegeneration of infantile dystonia, so the possibility that impaired trafficking is a disease-relevant characteristic of these variants cannot simply be dismissed. More data will need to be collected on this subject, which may be illuminated if another hDAT variant could be found and shown to have the same phenotypical profile as hDAT R445C (functionally "dead") but with normal surface expression and glycosylation.

Angelman syndrome

Although the body of work is very limited, Angelman syndrome (AS) has also been investigated in the context of AMPH-induced reverse transport of DA. AS is a neurogenetic disorder caused by a defective ubiquitin ligase Ube3A allele inherited maternally (Mabb *et al.*, 2011), and its symptomology includes ASD and movement disorders. Mice lacking the maternally inherited Ube3A allele have been used to model AS, and were shown to have autoinihibted αCaMKII in the brain (Weeber *et al.*, 2003). The important role played by αCaMKII in AMPH-induced DA efflux led Steinkellner and colleagues to explore whether this mechanism was impaired in the mouse model of AS (Steinkellner *et al.*, 2012). When AMPH was applied to brain slices from AS mice, it was found that DA efflux was reduced compared to WT mice, while DA uptake was unchanged. This shows an example of AMPH-induced DAT reverse transport being impaired in a disorder in which ASD symptoms present.

Fragile X mental retardation syndrome

Fragile X mental retardation protein (FMRP) is an RNA-binding protein, and the gene that, when missing, contributes to Fragile X mental retardation syndrome (FXRS). Knockout models of the gene encoding FMRP (*Fmr1*), are a well-validated model of FXRS. FMRP was found to interact with 78 ASD candidate genes (Darnell *et al.,* 2014), including PKC-ß. Although no evidence was found to suggest a direct interaction between FMRP and the hDAT, behavioral studies performed

on the *Fmr1* KO mouse model have shown attenuated AMPH-induced DA release in the dorsal striatum, corresponding to a decreased stereotypic behavioral response to high doses (10 uM) of AMPH (Fulks *et al.*, 2010). However, there is limited information available about the mechanism by which this impaired AMPH response occurs, and could be due to the observed decrease in the number of presynaptic afferents in the Nac in *Fmr1* KO mice compared to WT mice (Smith *et al.*, 2014). However, AMPH administration in the prefrontal cortex, a brain region largely lacking DAT expression, improved cognitive symptoms and enhanced object recognition (Ventura *et al.*, 2004). Although there is as yet no solid connection between DA reverse transport and FXRS, a clinical study showed that treatment with either MPH or Adderall (AMPH) improved attention deficit and motor symptoms of some individuals with FXRS, while other individuals reported worsening symptoms in response to treatment with stimulants (Berry-Kravis and Potanos, 2004). As these treatments are commonly recognized as ADHD treatments and are known to target the DAT, it may be worth investigating a link between the ADHD/DAT mechanism and FXRS.

Studying hDAT mediated reverse transport of DA

The central issue that complicates studying the role of the DAT in disease is that any inhibitor or previous genetic KO targets both the uptake and efflux functions of the DAT. For example, commonly used inhibitors of the DAT, like COC block the transporter in an un-competitive manner. COC can block both the outward constitutive DA leak, and prevents AMPH-induced DA efflux. KO of the DAT results in a hyperactive state in mice as well as in *Drosophila melanogaster* (Giros *et al.*, 1996, Pizzo *et al.*, 2013), and in compensations in the other monoamine systems, like 5-HT. DAT KO animals are of limited use in understanding the role of the DAT in humans, since there are several cases of human DAT-deficiency syndrome, which have much more devastating results in humans, such as infantile parkinsonism. Therefore, understanding the mechanism underlying the reverse transport of DA and creating new genetic models that allow this mechanism to be asymmetrically manipulated are vitally important.

Chapters 2 and 3 of this thesis address the question of asymmetric manipulation of AMPH-induced DA efflux, through the direct interaction between the hDAT N-terminus and the membrane lipid phosphatidylinositol (4,5)-bisphosphate (PIP_2) (Chapter 2), and possibly through the intracellular gating regions (Chapter 3). As a result of the data generated in this part of my dissertation, an animal model of impaired AMPH-induced DA efflux has been discovered and produced (*Drosophila melanogaster*), which will help to inform the physiology of AMPH-induced DA efflux in future studies. The study in Chapter 2 is available in its entirety in *Nature Chemical Biology* (Hamilton and Belovich *et al.*, 2014), while the data in Chapter 3 are as yet unpublished.

Chapter 4 establishes the ASD-associated hDAT variant, hDAT T356M, as a functionally impaired protein, with the presence of ADE and impaired AMPH-induced efflux. Furthermore, this work marks the first instance of a *Drosophila melanogaster* behavioral model of ASD symptomology, namely hyperlocomotion. This can be found in full in *Molecular Psychiatry* (Hamilton and Campbell *et al.,* 2013). Chapter 5 demonstrates how hDAT T356M function can be partially restored by the addition of Zn^{2+} (reduction of ADE, improvement of AMPH-induced DA efflux), and the study therein can be found in *Molecular Autism* (Hamilton and Shekar *et al.*, 2015). Taken together, Chapters 4 and 5 establish hDAT T356M as a behaviorally relevant, functionally impaired ASD-associated coding variant, as well as contribute to the mechanistic understanding of how Zn^{2+}-susceptible conformational states of the hDAT influence the hDAT's ability to respond to AMPH.

Chapter 6 underscores the importance of the AMPH-induced DA efflux mechanism in ASD, and reports the identification and characterization of two independently occurring variants, one in the hDAT itself (hDAT R51W) and another in an interacting protein, Syntaxin 1 (STX1 R26Q). hDAT R51W is shown to have an asymmetric impairment in function, where only the AMPH-induced DA efflux mechanism is affected while substrate uptake and surface expression remain unaffected.

STX1 is known to interact with the N-terminus of the hDAT, and is important for AMPH-induced DA efflux (Binda *et al.*, 2008). When co-expressed with WT hDAT, this ASD-associated variant, STX1 R26Q, impairs the hDAT's efflux response to AMPH. Finally, this study shows that the STX1/hDAT interaction necessary for AMPH-induced efflux is mediated by Casein Kinase 2 (CK2), for which an inhibitor is currently undergoing clinical trials. These data are published in *EBioMedicine* (Lancet) (Cartier and Hamilton *et al.*, 2015), and emphasize the importance of the DAT reverse transport mechanism in ASD.

CHAPTER 2

PHOSPHATIDYLINOSITOL (4,5)-BISPHOSPHATE REGULATES PSYCHOSTIMULANT BEHAVIORS THROUGH ITS INTERACTION WITH THE DOPAMINE TRANSPORTER N-TERMINUS[1]

Abstract

Phosphatidylinositol (4,5)-bisphosphate (PIP_2) regulates the function of ion channels and transporters. Here, we demonstrate that PIP_2 directly binds the human dopamine (DA) transporter (hDAT), a key regulator of DA homeostasis and a target of the psychostimulant amphetamine (AMPH). This binding occurs through electrostatic interactions with positively charged hDAT N-terminal residues and is shown to facilitate AMPH-induced, DAT-mediated DA efflux and the psychomotor properties of AMPH. Substitution of these residues with uncharged amino acids reduces hDAT-PIP_2 interactions and AMPH-induced DA efflux without altering the hDAT physiological function of DA uptake. We evaluated the significance of this interaction *in vivo* using locomotion as a behavioral assay in *Drosophila melanogaster*. Expression of mutated hDAT with reduced PIP_2 interaction in *Drosophila* DA neurons impairs AMPH-induced locomotion without altering basal locomotion. We present what is to our knowledge the first demonstration of how PIP_2 interactions with a membrane protein can regulate the behaviors of complex organisms.

[1] The work presented in this chapter is *in press* as Hamilton P. J.[*], A. N. Belovich[*], G. Khelashvili, C. Saunders, K. Erreger, J. A. Javitch, H. H. Sitte, H. Weinstein, H. J. G. Matthies[**] and A. Galli[**] (2014). "PIP2 regulates psychostimulant behaviors through its interaction with a membrane protein." *Nature Chemical Biology* 10(7):582-9. * and ** denote equal contribution.

Introduction

The functional regulation of plasma membrane proteins by lipid molecules is an integral component of cell function and metabolism (McLaughlin and Murray, 2005, Suh and Hille, 2008). Phosphatidylinositol (4,5)-bisphosphate (PIP_2) is the phospholipid precursor of the second messengers inositol trisphosphate (IP_3), diacylglycerol (DAG), and phosphatidylinositol (3,4,5)-trisphosphate (PIP_3), and is, itself, capable of acting as a second messenger and cofactor for regulating protein function (Czech, 2000, Suh and Hille, 2008, Whorton and MacKinnon, 2011, Ben-Aissa *et al.*, 2012, Kadamur and Ross, 2013). Additionally, PIP_2 has been shown to modulate, through electrostatic interactions, the *in vitro* function of ion channels and transporters, including the serotonin transporter (SERT) (Suh and Hille, 2008, Buchmayer *et al.*, 2013). A sizeable research effort has been dedicated to determining the diversity of cellular roles for PIP_2 and defining the ubiquity of its electrostatic interactions with various plasma membrane proteins, but how these interactions might modulate the behaviors of complex organisms *in vivo* has never been studied.

The plasma membrane dopamine (DA) transporter (DAT) is a presynaptic protein that plays a pivotal role in regulating DA neurotransmission by mediating the high-affinity reuptake of synaptically-released DA. Gene knockout experiments in multiple organisms, including *Drosophila melanogaster* (Hamilton and Campbell *et al.*, 2013, Pizzo *et al.*, 2013), point to the DAT as the main target for the locomotor stimulatory effects of amphetamine (AMPH) (Giros *et al.*, 1996). AMPH's addictive properties are mediated, at least in part, through elevation of extracellular DA by inducing DA efflux through the DAT (Sulzer *et al.*, 2005, Robertson *et al.*, 2009). Thus, in order to target and limit AMPH actions pharmacologically, it is essential to understand how to precisely manipulate the DAT to prevent DA efflux without altering its physiological function of DA uptake.

The DAT N-terminus is a structural domain of functional significance. AMPH targets the N-terminus to cause posttranslational modifications (e.g. phosphorylation (Cervinski *et al.*, 2005)), which are essential for AMPH to cause DA efflux (Khoshbouei *et al.*, 2004, Fog *et al.*, 2006) and behaviors (Pizzo *et al.*, 2013). Notably, DAT localization to plasma membrane lipid rafts is also vital for DA efflux (Cremona *et al.,* 2011) and AMPH-induced behaviors (Pizzo *et al.*, 2013). In this study, we elucidate how plasma membrane PIP_2, which is enriched in lipid rafts (Hope and Pike, 1996, Wang and Richards, 2012), dictates specific aspects of the transport cycle through its interactions with the N-terminus of the DAT. In terms of AMPH-induced DA efflux, our experimental and computational data demonstrate that the regulatory effect of PIP_2 stems from its electrostatic association with the N-terminus. Here, we introduce the first animal model (*Drosophila melanogaster*) in which we evaluate the behavioral consequences of altered PIP_2 interactions with a plasma membrane protein. We reveal that DAT-PIP_2 interactions are required for AMPH-induced behaviors, thereby presenting PIP_2 and its synthetic pathway as novel regulators of AMPH abuse.

Results

DAT associates with PIP_2

In this study, we aimed to determine the modalities of the regulatory function of PIP_2 in terms of DA homeostasis and AMPH actions. We hypothesized that this regulatory function may be mediated through a physical association between DAT and PIP_2. Using live confocal imaging, we show that in hDAT cells, green fluorescent protein(GFP)-tagged hDAT (GFP-hDAT; green) co-localized (yellow) with a red fluorescent protein(RFP)-tagged plasma membrane PIP_2 sensor (red) (**Fig. 14a**). As a PIP_2 sensor, we used the pleckstrin homology (PH) domain from phospholipase C_δ ($PHPLC_\delta$-mRFP) that binds specifically to PIP_2 at the plasma membrane and has been used to monitor pools of PIP_2 (Varnai and Balla, 1998). In these cells, we further probed the association of hDAT with PIP_2 by immunoprecipitating (IP) PIP_2 with an anti-PIP_2

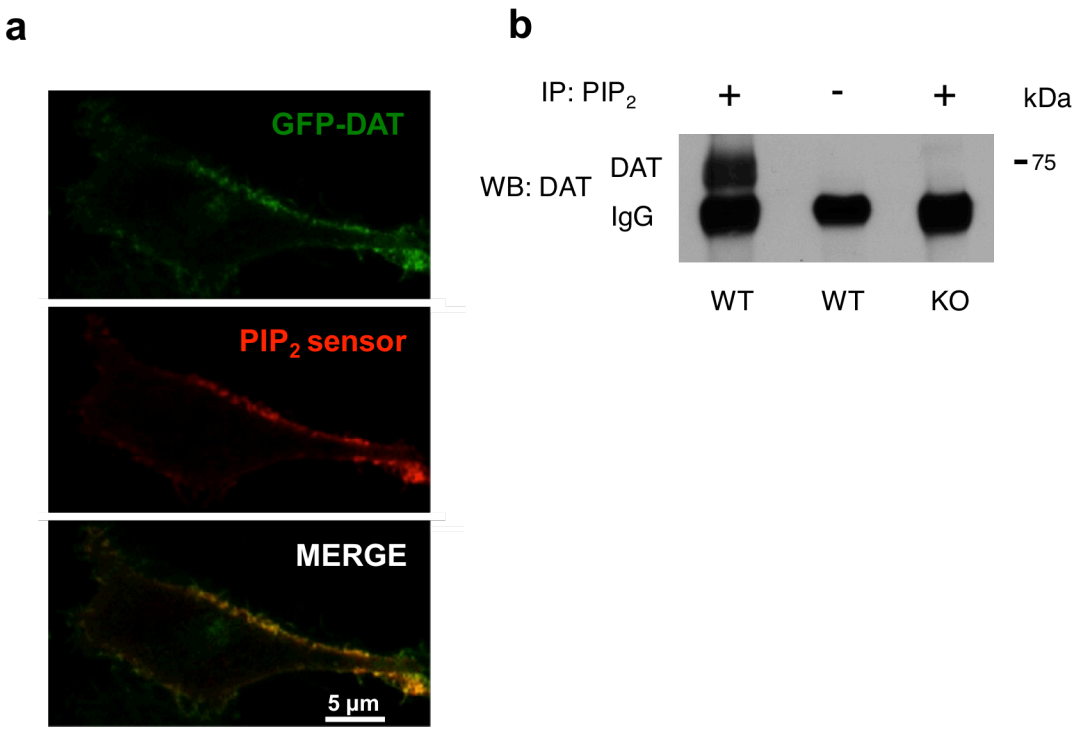

Figure 14. Phosphatidylinositol (4,5)-bisphosphate (PIP_2) interacts with hDAT. **(a)** hDAT and PIP_2 colocalize at the plasma membrane. In hDAT expressing cells, GFP-hDAT (green) colocalizes (yellow) at the plasma membrane with the PIP_2 sensor $PHPLC_{\delta}$-mRFP (red; representative image from three live experiments with 10-15 cells imaged per experiment) Scale bar, 5 µm. **(b)** PIP_2 associates with endogenous mouse DAT in striatal tissue. In striatal lysate, DAT was detected in PIP_2 immunoprecipitates using an anti-DAT antibody (+). DAT immunoreactivity was absent in the beads fraction (-) and in PIP_2 immunoprecipitates from DAT knock out (KO) animals (endogenous mouse IgG is observed) (representative of n = 3).

antibody and immunoblotting the immunoprecipitates for DAT (IB) with an anti-DAT antibody (see below). These data strongly suggest that PIP_2 associates with hDAT in this cell line. To reveal the association between PIP_2 and DAT in brain tissue, immunoprecipitations were performed from the striatal tissue of wild-type mice (WT; in presence (+) or absence (-) of the anti-PIP_2 antibody) or DAT knock out (KO) mice (Giros *et al.*, 1996) (**Fig. 14b**). In contrast to WT mice, DAT-PIP_2 association was lacking in DAT KO mice. Moreover, in the absence (-) of the PIP_2 antibody, no immunoreactivity was detected. These data demonstrate that PIP_2 associates with the DAT both in cell culture and *ex vivo*.

The DAT N-terminus interacts directly with PIP_2

PIP_2 is negatively charged at physiological pH (McLaughlin and Murray, 2005). Electrostatic interactions between PIP_2 and target proteins are thought to lead to changes in protein conformation and, subsequently, their activity (Hilgemann and Ball, 1996, McLaughlin *et al.*, 2002). It is recognized that PIP_2 binds positively charged (basic) residues, such as Arg and Lys, possibly in proximity to one or more hydrophobic amino acids (Suh and Hille, 2008). Recently, residues K352 and K460 of the SERT (a DAT homolog) have been identified *in vitro* as possible sites that mediate SERT-PIP_2 association (Buchmayer *et al.*, 2013). In the DAT, the homologous amino acids to K352 and K460 are Lys at position 337 (K337) and Arg at position 443 (R443). We reasoned that these two DAT residues represent possible PIP_2 binding sites of functional significance. However, charge-neutralizing substitution of K337 and R443 to Ala (hDAT K337A-R443A), to prevent the interaction of these residues with PIP_2, caused substantial trafficking of the DAT away from the plasma membrane, as assessed by cell surface biotinylation. The amount of hDAT K337A-R443A at the cell surface was reduced by 82.6 ± 5.2% ($p \leq 0.01$ by Student's t-test; $n = 7$) with respect to hDAT. Therefore, in DAT, in contrast to SERT, these two residues support DAT surface expression, preventing us from determining

whether their possible interaction with PIP_2 regulates any mechanistic aspect of the transport cycle.

The N-terminus of the DAT is a structural domain that has been shown to regulate specific aspects of DAT transport cycle, without altering DAT surface expression (Khoshbouei *et al.*, 2004, Fog *et al.*, 2006, Bowton *et al.*, 2010). It also contains several Lys and Arg residues (**Fig. 15**). We therefore sought to determine whether the N-terminus of the DAT directly interacts with PIP_2 *in vitro*. To this end, we generated a purified recombinant GST-fused N-terminal DAT fragment comprising the first 64 N-terminal amino acids of hDAT (GST-64 hDAT) (Binda *et al.*, 2008). The lipid binding analysis of the GST-fusion proteins was conducted using liposomes composed of mixed lipids (phosphatidylcholine, either with or without PIP_2) as previously described (Varnai *et al.*, 2002). The GST fusion proteins bound to liposomes were pelleted (liposome-pull down) and the binding was assessed by immunoblotting (anti-GST antibody). **Figure 16a** (top) shows the pull down of GST fusion proteins (GST and GST-64 hDAT) by liposomes containing (**+**) PIP_2, as compared to liposomes lacking (**-**) PIP_2. The presence (**+**) or absence (**-**) of PIP_2 did not alter pull down of GST alone (GST control). As an additional control, we "sequestered" PIP_2 by preincubating the liposomes with a basic peptide consisting of the sequence of the putative PIP_2 binding domain of the Kv7.2 channel fused to the fatty acid moiety, palmitic acid (Robbins *et al.*, 2006) (pal-HRQKHFEKRR; positively charged at physiological pH) (Robbins *et al.*, 2006). This peptide is known to interact electrostatically with the polar head groups of PIP_2 to hinder its interaction with plasma membrane proteins (Robbins *et al.*, 2006). Preincubation of PIP_2-containing liposomes with 3 μM of the basic peptide (pal-HRQKHFEKRR) inhibited pull down of GST-64 hDAT. **Figure 16a** (bottom) shows quantitation of immunoblots obtained from multiple experiments. Comassie stain was utilized to verify equal loading. These *in vitro* data provide the first evidence of a direct interaction between PIP_2 and a specific region of a neurotransmitter transporter, the DAT N-terminus.

hDAT

^{1}MSKSKCSVGLMSSVVAPAKEPNAVGPKEVELILVKEQNGVQLTSSTLTNPRQSPVEAQ^{58}

hSERT

^{1}METTPLNSQKQLSACEDGEDCQENGVLQKVVPTPGDKVESGQISNGYSAVPSPGAGDDTRHSIPATTT^{68}

hNET

^{1}MLLARMNPQVQPENNGADTGPEQPLRARKTAELLVVKERNGVQCLLAPRDGDAQ^{54}

hVMAT2

^{1}MALSELALVRWLQESRRSRKLILFIVFLAL^{30}

Figure 15. Sequences of the N-terminal regions of various transporters. The N-terminal regions of the human dopamine transporter (hDAT), serotonin transporter (hSERT), norepinephrine transporter (hNET), and vesicular monoamine transporter 2 (hVMAT2) are shown; positively charged residues are represented in red.

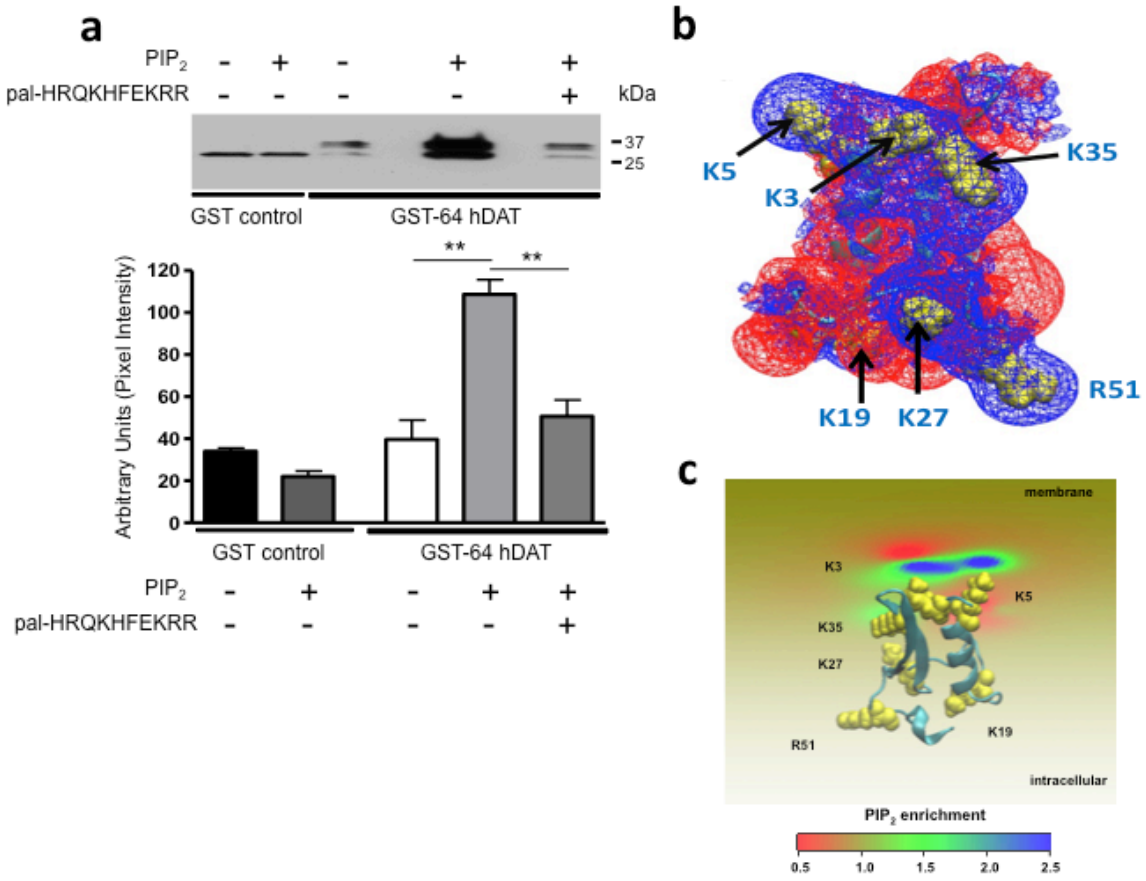

Figure 16. hDAT-PIP_2 electrostatic interactions are mediated by the hDAT N-terminus. (a) hDAT N-terminus binds directly to PIP_2. GST-64 hDAT is enriched in liposome-pull downs with liposomes containing PIP_2 (+) as compared to liposomes lacking PIP_2 (-) (** = $p \leq 0.01$ by one-way ANOVA followed by Bonferroni post-hoc test; n = 3; mean ± s.e.m.). Pull down of GST control was not altered by the presence (+) of absence (-) of PIP_2 in the liposomes ($p \geq 0.05$ by one-way ANOVA followed by Bonferroni post-hoc test; n = 3; mean ± s.e.m.). Preincubation of liposome containing PIP_2 with 3 μM of pal-HRQKHFEKRR (+) inhibited the pull down of GST-64 hDAT with liposomes containing PIP_2 (** = $p \leq 0.01$ by one-way ANOVA followed by Bonferroni post-hoc test; n = 3). Full blot is in Supplementary Figure 8. **(b)** Electrostatic potential (EP) isosurfaces (+1kT/e (+ charge)) shown as *blue wireframes* and (-1kT/e (- charge)) as *red wireframes* calculated for the predicted structure of the wild type N-terminus. **(c)** View from the intracellular side of the N-terminus (model) adsorbing on the lipid membrane. For clarity, the orientation of the N-terminus in panel (c) was obtained by a 180° rotation of the N-terminus configuration shown in panel (b). The level of the PIP_2 segregation by the N-terminus is expressed as the ratio of local and ambient lipid fraction values, and illustrated in color code (cold colors represent an enrichment of PIP_2). The positive residues in the N-terminus (yellow) that attract PIP_2 electrostatically are highlighted.

Computational modeling of hDAT interaction with PIP_2

To obtain molecular level structural insights into hDAT N-terminal interactions with PIP_2-containing membranes, we generated a structural context using a previously described homology model of the hDAT (Beuming *et al.*, 2008, Kniazeff *et al.*, 2008, Bisgaard *et al.*, 2011). To this we have added a recently constructed model of the DAT N-terminus obtained with a combination of structure-prediction methods (Rosetta, Modeller) and atomistic molecular dynamics (MD) simulations (see Methods). These *in silico* modeling steps enabled the prediction of 3-dimensional folds of the N-terminal loop segment composed of hDAT residues 1-59, in the context of the complete transmembrane domain. The resulting hDAT model was used in mean-field-level calculations (SCMFM; see Methods) to quantify the electrostatic interaction of the N-terminus with PIP_2-enriched lipid membranes.

The dominant role of the electrostatic component of the interaction energy between the hDAT N-terminus and PIP_2-containing membranes was substantiated by the shape and the values of the electrostatic potential isosurfaces (EPIs) surrounding the molecular model of the hDAT N-terminal segment shown in **Figure 16b**. The belt-like arrangement of the Lys/Arg residues generates a region of strong positive electrostatic potential (in blue) that favors strong interaction with the negatively charged PIP_2 lipids. Energy-guided docking of this face of the N-terminus to the membrane model and solving for the steady state distributions of the charged lipid species (PIP_2) under the influence of the electrostatic forces it generates (Khelashvili *et al.*, 2008, Khelashvili *et al.*, 2009, Khelashvili *et al.*, 2012) produces a quantitative estimate of the electrostatic component of the interaction energy. Thus, the rearrangement of the PIP_2 lipids in the electrostatic field of the N-terminal segment is predicted to result in a significantly increased concentration of PIP_2 near the Lys/Arg belt (**Fig. 16c**, color coding on the membrane shows the segregation of PIP_2 (blue) to be 2.5 times larger than the PIP_2 ambient concentration (yellow/green)). Particularly notable is the strength of the PIP_2 interaction mediated by DAT

residues Lys3 and Lys5. Together, these *in silico* studies suggest that the interactions between the hDAT N-terminus and PIP_2 lipids are driven by electrostatic forces.

Disrupting DAT-PIP_2 interaction inhibits reverse transport

We hypothesized that the functional consequence of DAT-PIP_2 interaction is to support reverse transport of DA. Thus, we disrupted DAT-PIP_2 associations in hDAT cells while recording AMPH-induced DA efflux with amperometry. The amperometric electrode, a carbon fiber electrode juxtaposed to the cell membrane, measures DA efflux by oxidation/reduction reactions, with DA efflux represented as a positive current. To simultaneously record DA efflux while delivering compounds to the intracellular milieu, we combined amperometry with the whole cell patch clamp (APC) technique (Khoshbouei *et al.*, 2004, Hamilton *et al.*, 2013). The whole cell patch electrode controls the intracellular ionic composition, which includes DA (Khoshbouei *et al.*, 2004) (see Methods).

First, we perfused hDAT cells through the whole cell electrode with DA and the basic peptide pal-HRQKHFEKRR (positively charged at physiological pH and tethered to the plasma membrane through the fatty acid moiety, palmitic acid (Robbins *et al.*, 2006)) while recording DA efflux with the amperometric electrode (**Fig. 17a**). We used this peptide to compete against the DAT N-terminus for PIP_2 interactions as determined in **Fig. 16a**. Pal-HRQKHFEKRR (3 μM, 10 minutes of intracellular perfusion) was effective in reducing AMPH-induced DA efflux with respect to the efflux obtained with the control peptide pal-HAQKHFEAAA, in which four positive residues were substituted with Ala (**Fig. 17a**, top). Quantitation of the peak amperometric currents demonstrates that intracellular perfusion of pal-HRQKHFEKRR significantly reduced DA efflux (**Fig. 17a**, bottom). These data underscore the importance of DAT-PIP_2 interactions in the regulation of DA efflux and point to the type of interactions as electrostatic in nature. We next assessed whether DAT-PIP_2 association regulates other DAT functions (e.g. DAT-

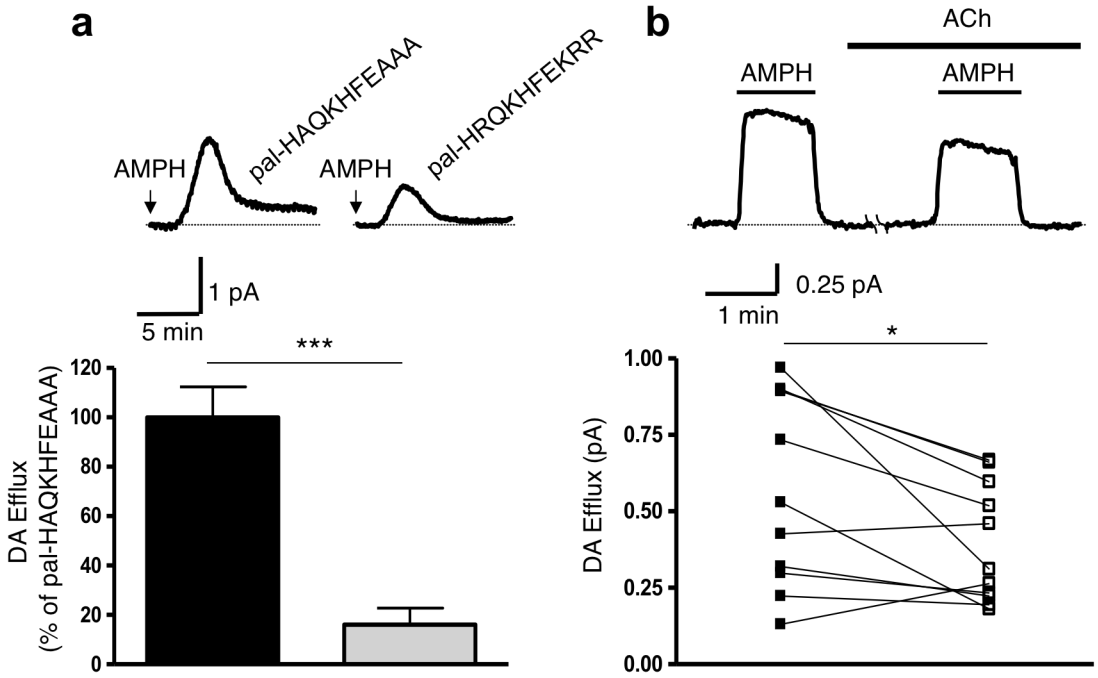

Figure 17. Sequestration or depletion of PIP_2 inhibits AMPH-induced DA efflux. **(a)** Sequestering PIP_2 with pal-HRQKHFEKRR decreases AMPH-induced DA efflux. Top: representative traces from stably transfected hDAT cells after patch delivery of 3 μM control peptide (pal-HAQKHFEAAA) or PIP_2 sequestering peptide (pal-HRQKHFEKRR) to the cytoplasm of the cell. Arrows indicate the application of 10 μM AMPH. Bottom: quantitation of amperometric peak currents for the two different treatments. Data are expressed as percentage of vehicle control (*** = $p \leq 0.0001$ by Student's t-test; n = 7; mean ± s.e.m.). **(b)** Depleting PIP_2 levels reduces AMPH-induced DA efflux. Top: representative trace of responses to 1 μM AMPH in stably transfected hDAT cells, co-expressing the human muscarinic acetylcholine receptor 1 (hM1R), before and after exposure to 100 μM acetylcholine (ACh). Bottom: quantitation of the amperometric peak currents representing AMPH-induced DA efflux before and after ACh-dependent PIP_2 depletion (* = $p \leq 0.05$ by Student's t-test; n = 11).

mediated inward currents). We recorded hDAT-mediated inward currents from hDAT cells voltage clamped at -60 mV with a whole-cell electrode containing either pal-HRQKHFEKRR or the control peptide pal-HAQKHFEAAA (3 μM, 10 minutes of intracellular perfusion). We stimulated the hDAT-mediated currents by perfusion of either 10 μM AMPH or DA, respectively. In contrast to DA efflux, pal-HRQKHFEKRR failed to inhibit hDAT-mediated inward currents, with respect to the control peptide, either for AMPH (109 ± 4.9% of control; $p \geq 0.8$ by Student's t-test; n = 4) or for DA (98 ± 16% of control; $p \geq 0.9$ by Student's t-test; n = 4).

To further investigate the role of DAT-PIP_2 interactions in AMPH regulation of DAT function, we transfected hDAT cells with the human muscarinic acetylcholine (ACh) receptor M1 (hM1R), a Gαq coupled receptor. Activation of hM1R activates phospholipase C (PLC), stimulating hydrolysis of PIP_2 and effectively depleting PIP_2 stores (Kadamur and Ross, 2013). Live imaging was adopted utilizing mRFP tagged PLC-δ1 PH domain (see **Fig. 14a**) to detect changes of PIP_2 levels at the plasma membrane induced by ACh, a potent hM1R agonist (Balla *et al.*, 2009). In hDAT cells, 5 minutes of ACh (100 μM) decreased surface RFP tagged PLC-δ1 PH domain levels to 64 ± 9% of vehicle control ($p \leq 0.009$ by Student's t-test comparing ACh to vehicle; n = 16). In cells loaded with DA (see Methods), we next quantified the magnitude of AMPH-induced DA efflux before and after bath perfusion of ACh (5 minutes, 100 μM) (**Fig. 17b**, top). Quantitation of the change in AMPH-induced DA efflux induced by PIP_2 depletion within the same cell (**Fig. 17b**, bottom) demonstrates that ACh exposure significantly decreased DA efflux. This decrease was not due to a trafficking phenomenon, since exposure of ACh (5 minutes, 100 μM) in hM1R-expressing hDAT cells did not cause significant trafficking of hDAT away from the plasma membrane as compared to vehicle-treated control (**Fig. 18**). We next determined whether providing an excess of intracellular PIP_2 reduces the ability of hM1R agonism to decrease DA efflux. For this, we adopted the APC technique (Khoshbouei *et al.*, 2004, Hamilton *et al.*, 2013). Inclusion of PIP_2 (50 μM) in the whole cell patch pipette solution

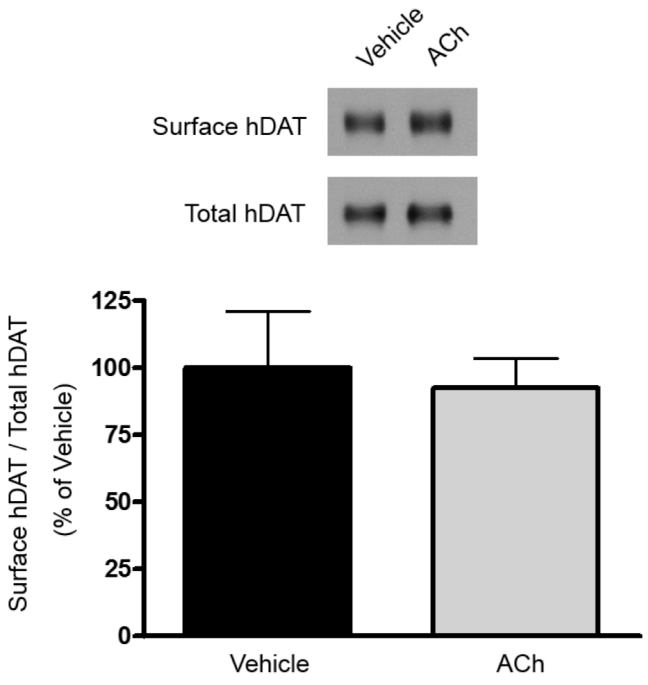

Figure 18. ACh treatment does not affect hDAT surface expression. Representative immunoblots for biotinylated (surface) and total hDAT protein fractions from stably transfected hDAT cells, co-expressing the human muscarinic acetylcholine receptor 1 (hM1R), treated either with vehicle or 100 μM ACh for 5 min. Surface fractions were quantitated, normalized to total hDAT, and expressed as a percent of vehicle treated hDAT cells ($p \geq 0.7$ by Student's t-test; $n = 3$ in duplicate; mean ± s.e.m.).

(10 minutes of intracellular perfusion) impaired the ability of ACh (5 minutes, 100 μM) to significantly decrease AMPH-induced DA efflux with respect to vehicle control (**Fig. 19**). Collectively, these data demonstrate that impairing the electrostatic interaction between PIP_2 and DAT selectively inhibits the ability of AMPH to cause DA efflux.

N-terminal lysine residues mediate DAT-PIP_2 association

Since our *in silico* modeling of the hDAT N-terminus indicated residues Lys3 and Lys5 to be essential in facilitating the electrostatic interaction of PIP_2 with DAT (**Fig. 16c**), we hypothesized that substitution of these residues with uncharged amino acids (e.g. alanine or asparagine) would disrupt DAT-PIP_2 associations. To probe this inference *in silico*, Lys3 and Lys5 were both substituted computationally with either Ala (hDAT K/A) or with Asn (hDAT K/N), and the resulting constructs (N-terminus of hDAT K/A and hDAT K/N) were evaluated for any conformational rearrangements due to the mutations. The constructs were used in the same computational protocols described for the hDAT model. The results for the mutant constructs show significantly reduced electrostatic interactions with PIP_2-containing membranes for both hDAT K/A (**Fig. 20a**, compare to **Fig. 16c**) and hDAT K/N (**Fig. 21**, compare to **Fig. 16c**).

The inferences from the computational evaluation of the N-terminus association with PIP_2 lipids *in silico* were probed biochemically by determining the effect of charge neutralizing mutations of Lys3 and Lys5. In hDAT K/A cells, we immunoprecipitated PIP_2 and immunoblotted the immunoprecipitates for DAT (IB: anti-DAT). The amount of DAT recovered in the PIP_2 immunoprecipitates was reduced in the hDAT K/A cells compared to the hDAT cells (**Fig. 20b**, top lane). In the absence of antibody against PIP_2, no signal was detected for DAT in the immunoprecipitates (**Fig. 20b**, middle lane, IP: beads). The total DAT in the hDAT K/A cells was not decreased with respect to hDAT cells (**Fig. 20b**, bottom lane; Total DAT). These data demonstrate that substitution of Lys3 and Lys5 decreases DAT-PIP_2 interaction, as predicted

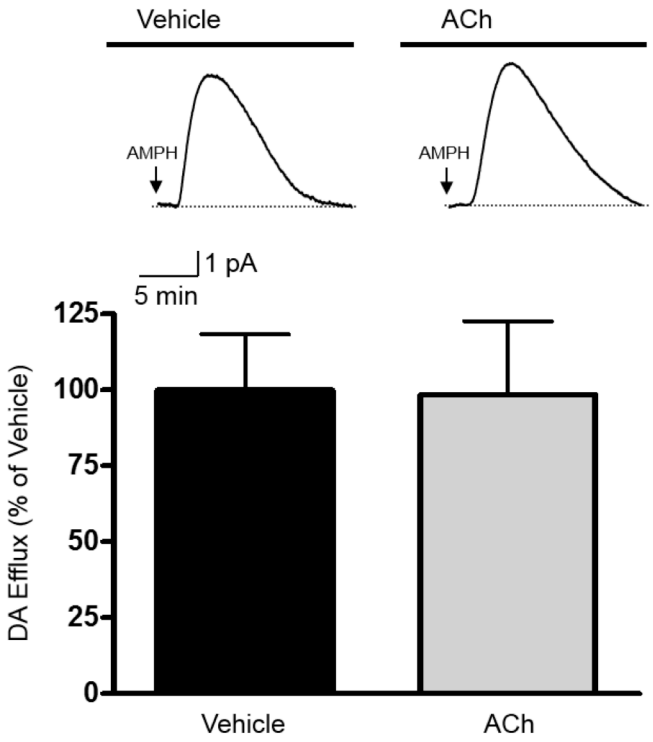

Figure 19. Excess intracellular PIP_2 levels prevents the ability of ACh to decrease AMPH-induced DA efflux. Top: representative traces of AMPH responses obtained with the APC technique in stably transfected hDAT cells, co-expressing hM1R, perfused intracellularly with 50 µM PIP_2. Cells were pre-exposed to either 100 µM ACh or vehicle for 5 minutes and DA effluxes induced by 10 µM AMPH were recorded in the continuous presence of ACh or vehicle. Bottom: quantitation of the amperometric peak currents normalized to vehicle control, and expressed as a percent of vehicle treated hDAT cells ($p \geq 0.9$ by Student's t-test; $n = 4$; mean ± s.e.m.).

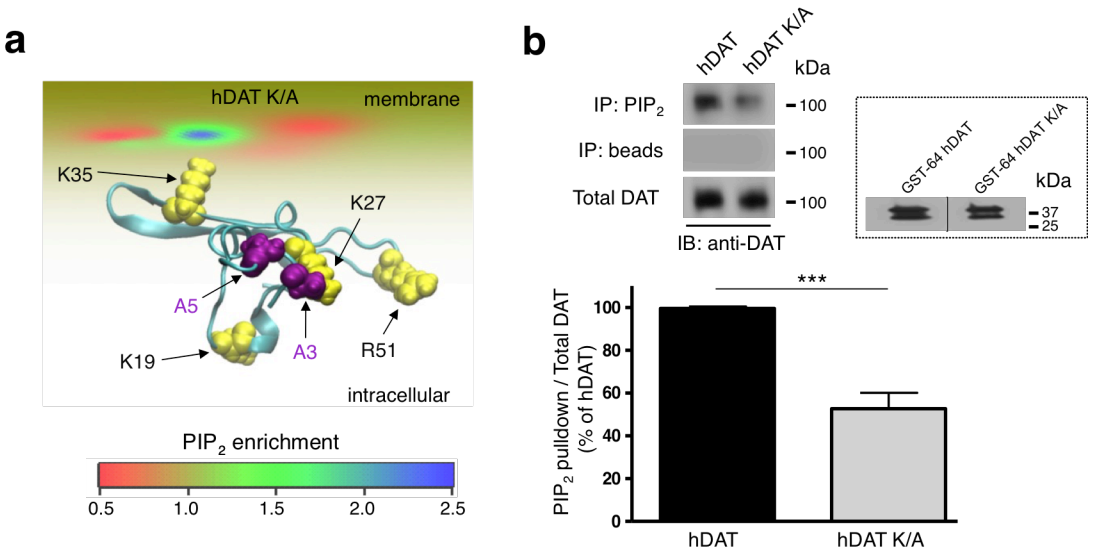

Figure 20. hDAT N-terminal Lys regulate DAT-PIP_2 interaction. (a) Mutating hDAT N-terminal residues Lys3 and Lys5 to uncharged Ala (hDAT K/A) disrupts PIP_2 segregation to the N-terminus. View from the intracellular side of the N-terminus of hDAT K/A adsorbing on the lipid membrane. The level of PIP_2 segregation by the N-terminus residues is expressed as the ratio of local and ambient lipid fraction values and illustrated in color code, with cold colors representing an enrichment of PIP_2. **(b)** N-terminal Lys residues mediate hDAT-PIP_2 interaction. Top: PIP_2 immunoprecipitates from hDAT and hDAT K/A cells were immunoblotted for DAT (top lane). The beads fraction supports absence of non-specific binding (middle lane). Bottom lane shows total DAT proteins. Full blot is in Supplementary Figure 9. Bottom: quantitation of PIP_2 pulldown band intensities normalized to the respective total DAT and expressed as a percentage hDAT (*** = $p \leq 0.001$ by Student's t-test; n = 4; mean ± s.e.m.). *Inset:* Representative blot for GST-64 hDAT and GST-64 hDAT K/A in pull downs with liposomes containing PIP_2.

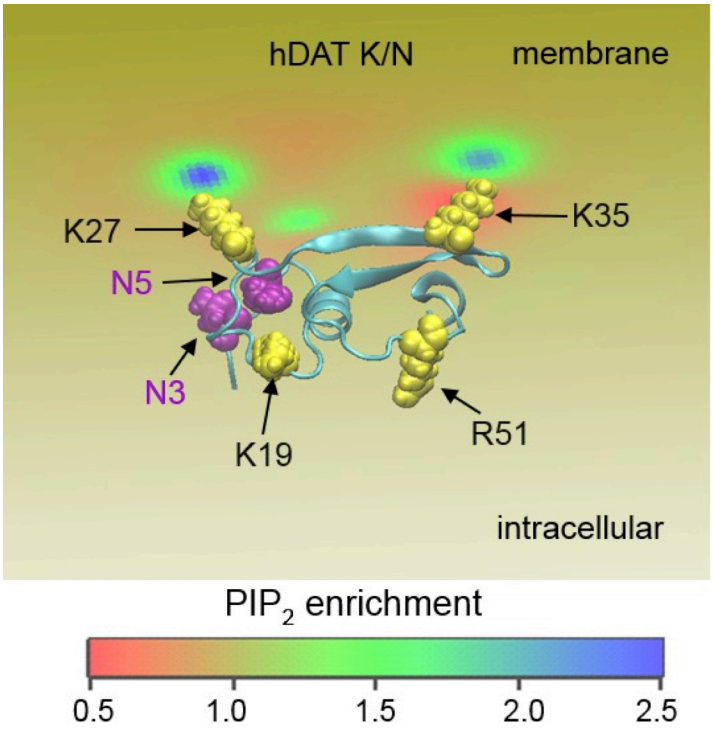

Figure 21. Mutation of hDAT N-terminal residues Lys3 and Lys5 to uncharged Asn (hDAT K/N) disrupts PIP_2 segregation to the N-terminus. View from the intracellular side of the N-terminus of hDAT K/N adsorbing on the lipid membrane. The level of PIP_2 segregation by the N-terminus is expressed as the ratio of local and ambient lipid fraction values, and illustrated in color code with cold colors representing an enrichment of PIP_2.

from the computational modeling. Quantitation of multiple experiments (n = 4) is shown in figure 20b (bottom). Next, we determined whether substitution N-terminal Lys3 and Lys5 to Ala impairs the direct interaction of DAT with PIP_2 *in vitro*. We generated a purified recombinant GST-fused N-terminal DAT fragment comprising the first 64 N-terminal amino acids of hDAT with Lys3 and Lys5 substituted to Ala (GST-64 hDAT K/A). The lipid binding analysis of the GST-fusion proteins (either GST-64 hDAT or GST-64 hDAT K/A) was conducted utilizing liposome-pull down as in figure 16. The inset in figure 20b shows the pull down of the GST fusion proteins by liposomes containing PIP_2. Quantitation of immunoblots obtained from multiple experiments demonstrated that pull down of GST-64 hDAT was significantly inhibited by Lys to Ala substitution (GST-64 hDAT K/A was 45 ± 20% of GST-64 hDAT; $p \leq 0.037$ by Student's t-test; n = 4).

In order to assess whether DAT physiological function is altered by disrupting DAT-PIP_2 association, we examined radioactive [^{3}H]DA uptake in both hDAT and hDAT K/A cells. In hDAT K/A cells, the maximal velocity of DA influx (V_{max}) and the apparent DA affinity (K_m) were not significantly different from those of hDAT (**Fig. 22a**, top). A representative plot of DA uptake kinetics (in triplicate) for hDAT and hDAT K/A is shown in **Figure 22a** (bottom), demonstrating that the uptake of substrate is not regulated by the interaction with PIP_2. Consistent with the uptake data, no significant difference was found in the whole-cell DAT-mediated inward current (recorded at -60 mV) between hDAT and hDAT K/A cells upon stimulation with 10 μM DA. The hDAT K/A inward currents were expressed as a percent of hDAT-mediated currents (103 ± 20% of hDAT; $p \geq 0.97$ by Student's t-test; n = 4).

Our pharmacological manipulations (**Fig. 17**) indicate that disrupting DAT-PIP_2 association has no effect on DAT-mediated DA uptake or DA-induced inward currents but inhibits the ability of AMPH to cause DA efflux. Consistent with this, hDAT K/A cells were found

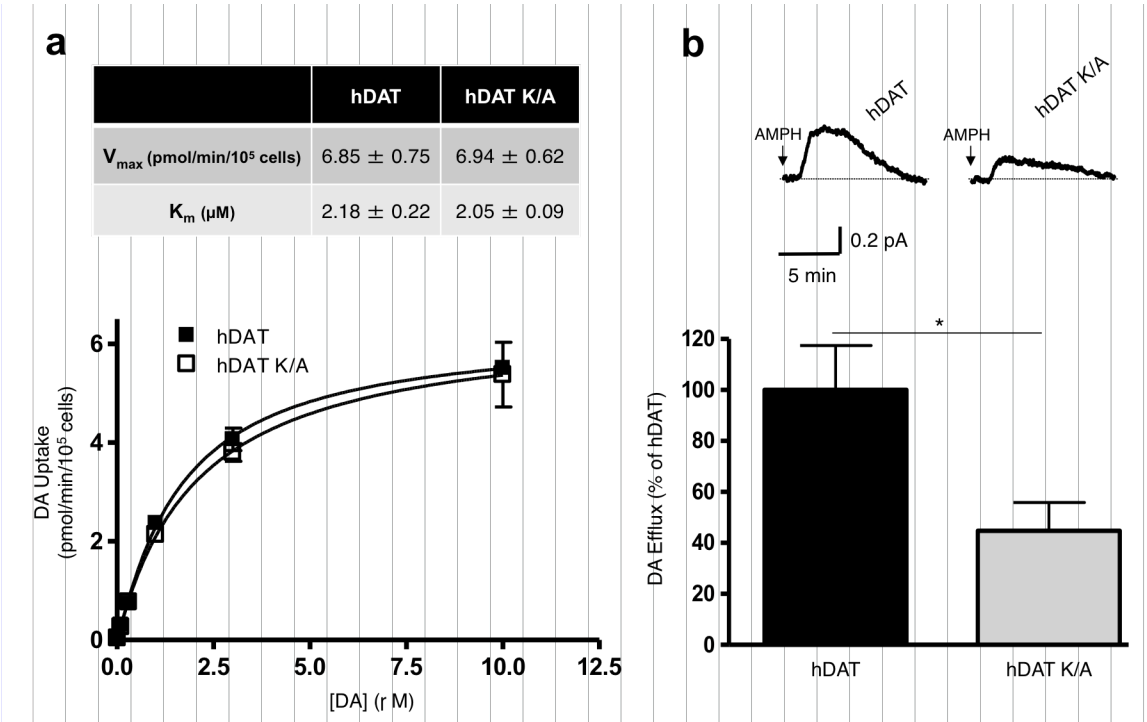

Figure 22. N-terminal Lys3 and Lys5 regulate specific modalities of hDAT function. (a) hDAT K/A exhibits normal DA uptake function. Top: kinetic parameters (V_{max} and K_m) for hDAT and hDAT K/A (V_{max}: $p \geq 0.92$ by Student's t-test; n = 3, in triplicate; K_m: $p \geq 0.62$ by Student's t-test; n = 3, in triplicate; mean ± s.e.m.). Bottom: representative plot of [^{3}H]DA uptake kinetics in hDAT (filled squares) and hDAT K/A (empty squares) cells ($p \geq 0.05$, by two-way ANOVA followed by Bonferroni post-test; in triplicate; mean ± s.e.m.). **(b)** hDAT K/A has reduced AMPH-induced DA efflux. Top: representative AMPH-induced amperometric currents recorded from hDAT and hDAT K/A cells. Arrows indicate application of 10 μM AMPH. Bottom: quantitation of AMPH-induced DA efflux. Data are represented as maximal DA efflux expressed as percent of the DA efflux recorded in hDAT controls (* = $p \leq 0.05$ by Student's t-test; n = 7-8; mean ± s.e.m.).

to display strikingly reduced AMPH-induced DA efflux (**Fig. 22b**, top). Quantitation of the amperometric recordings demonstrate that the Lys to Ala substitution not only decreased DAT-PIP_2 association (**Fig. 20**), but also decreased the ability of AMPH to cause DA efflux (**Fig. 22b**, bottom). The reduced AMPH-induced DA efflux was not associated with a reduction in either total or DAT surface expression as assessed by measuring changes in DAT proteins in the total and biotinylated fraction, respectively. Surface fractions were quantitated, normalized to total DAT, and expressed as a percent of hDAT (hDAT K/A was 122 ± 31% of hDAT; $p \geq 0.53$ by Student's t-test; n = 7-8). The findings in the hDAT K/A cells were mirrored by those obtained in the hDAT K/N cells in terms of both DAT-PIP_2 association and hDAT cell surface expression (**Fig. 23a** and **23b**). The hDAT K/N also displayed normal uptake (**Fig. 23c**) and, like the hDAT K/A, had a significant reduction in AMPH-induced DA efflux (**Fig. 23d**). Furthermore, AMPH uptake assays revealed that hDAT, hDAT K/A, and hDAT K/N cells displayed comparable AMPH transport (see Methods) (hDAT K/A: 101 ± 4.9% and hDAT K/N: 93.9 ± 17% relative to hDAT; $p \geq 0.88$ by one-way ANOVA; n = 3, in triplicate). These results demonstrate that the reduced ability of AMPH to cause DA efflux promoted by the Lys to Ala substitutions does not involve changes in the surface expression or changes in ability of the DAT mutants to transport AMPH. Another possibility for this decrease in DA efflux is that the N-terminal Lys substitution (hDAT K/A) perturbs the potential AMPH-induced phosphorylation of the Ser2 and Ser4 adjacent to these Lys residues by altering primary sequence requirements for phosphorylation. To explore this, we substituted Ser2 and Ser4 with Asp (to mimic phosphorylation) in the hDAT K/A background (hDAT K/A-S/D). Cells expressing hDAT K/A-S/D exhibited significantly reduced AMPH-induced DA efflux, similar to hDAT K/A cells (**Fig. 24a**, top). Quantitation of the amperometric recordings demonstrated that Ser to Asp substitution at positions 2 and 4 in the hDAT K/A background did not rescue the ability of AMPH to cause DA efflux (**Fig. 24a**, bottom). The reduced AMPH-induced DA efflux was not associated with a reduction in DA uptake (**Fig. 24b**). These data demonstrate that the reduction in DA efflux caused by substitution of Lys3 and

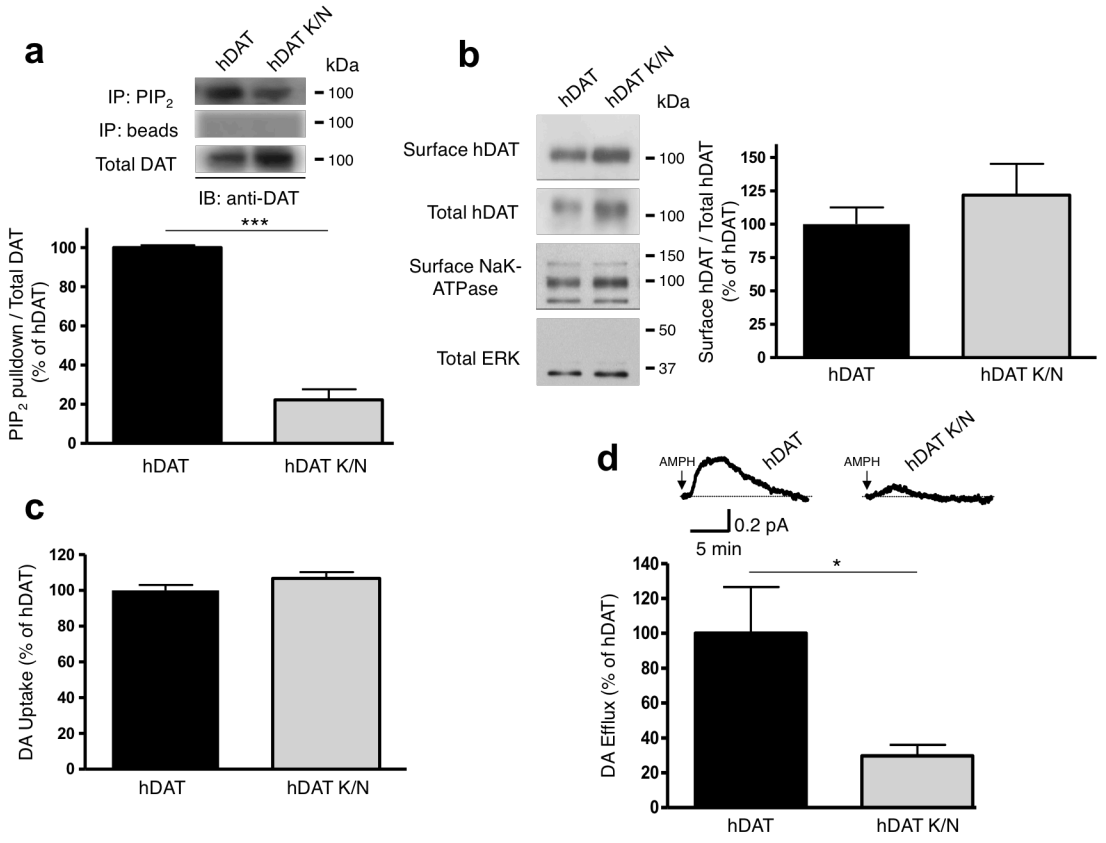

Figure 23. hDAT K/A findings mirrored in hDAT K/N. (a) Top: PIP_2 immunoprecipitates from hDAT and hDAT K/N cells were immunoblotted for DAT (top lane). The beads fraction supports absence of non-specific binding (middle lane). Bottom lane shows total DAT proteins. Bottom: quantitation of PIP_2 pull down band intensities normalized to the respective total DAT and expressed as a percentage hDAT (*** = $p \leq 0.0001$ by Student's t-test; n = 3; mean ± s.e.m.). **(b)** Representative immunoblots for biotinylated (surface) and total protein fractions from hDAT and hDAT K/N cells. Immunoblots for surface NaK-ATPase and total ERK are shown as well. Surface fractions were quantitated, normalized to total DAT, and expressed as a percentage of hDAT ($p \geq 0.41$ by Student's t-test; n = 4-5; mean ± s.e.m.). **(c)** [^{3}H]DA uptake (50 nM) in hDAT and hDAT K/N cells was expressed as a percent of uptake in hDAT cells ($p \geq 0.16$ by Student's t-test; n = 3, in quadruplicate; mean ± s.e.m.). **(d)** Representative AMPH-induced amperometric currents recorded from hDAT and hDAT K/N cells. Arrows indicate application of 10 µM AMPH. Bottom: quantitation of AMPH-induced DA efflux. Data are represented as maximal DA efflux expressed as a percent of the DA efflux recorded in hDAT cells (* = $p \leq 0.02$ by Student's t-test; n = 6-7; mean ± s.e.m.).

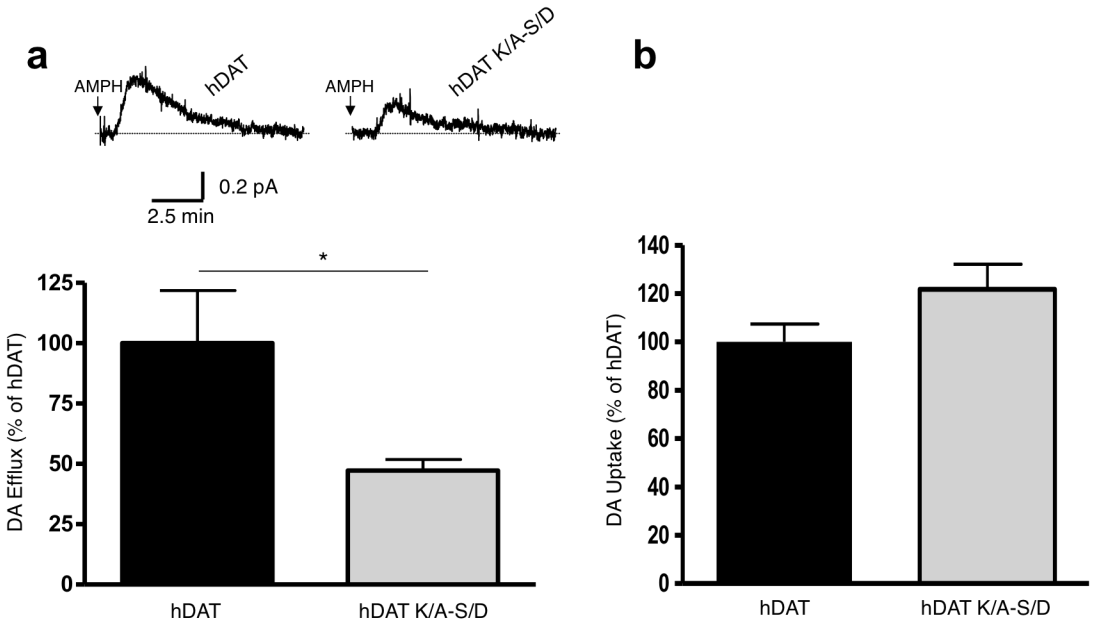

Figure 24. hDAT K/A-S/D displays reduced DA efflux and normal DA uptake. (a) hDAT K/A-S/D has reduced AMPH-induced DA efflux. Top: representative AMPH-induced amperometric currents recorded from hDAT and hDAT K/A-S/D cells. Arrows indicate application of 10 μM AMPH. Bottom: quantitation of AMPH-induced DA efflux. Data are represented as maximal DA efflux expressed as a percent of DA efflux recorded in hDAT cells (* = $p \leq 0.03$ by Student's t-test; n = 5-6; mean ± s.e.m.). **(b)** hDAT K/A-S/D exhibits normal [^{3}H]DA uptake (50 nM) function. Data expressed as a percent of the uptake measured in hDAT cells ($p \geq 0.2$ by Student's t-test; n = 4-8; mean ± s.e.m.).

Lys5 with uncharged amino acids cannot be attributed to impaired phosphorylation of adjacent Ser residues.

Reduced DAT-PIP_2 interaction impairs psychomotor behavior

Locomotion is an elemental behavior regulated by DA across species, including *Drosophila melanogaster* (Pendleton *et al.*, 2002, Wicker-Thomas and Hamann, 2008, Hamilton *et al.*, 2013, Pizzo *et al.*, 2013). Recently, locomotion in flies has been adopted to evaluate molecular discoveries of AMPH actions mechanistically *in vivo* (Hamilton *et al.*, 2013, Pizzo *et al.,* 2013). Thus, *Drosophila* offer a powerful model for elucidating the impact of altered DAT-PIP_2 interactions on locomotion and on the psychomotor stimulant effects of AMPH.

To generate fly lines expressing either hDAT or hDAT K/A selectively in DA neurons, we used the Gal4/UAS system to express a single copy of either hDAT or hDAT K/A in flies with a *Drosophila* DAT (dDAT) null background (dDAT KO; flies are homozygous for the dDAT null allele, DAT^{fmn}) (Kume *et al.*, 2005). Using phiC31-based integration, we generated transgenic flies expressing comparable mRNA levels for hDAT or hDAT K/A. Locomotion of flies was quantified by beam crossing detection over a >24 hour period (data binned in 15 minute intervals) including both the light (horizontal white bar) and the dark (horizontal black bar) cycle. While dDAT KO flies were hyperactive (Kume *et al.*, 2005), dDAT KO flies expressing hDAT in DA neurons displayed reduced basal locomotion in comparison to dDAT KO (**Fig. 25a**, compare hDAT to dDAT KO). These data demonstrate the validity of expressing hDAT in *Drosophila* for behavioral studies.

We hypothesized that flies harboring the hDAT K/A would demonstrate comparable locomotion with respect to hDAT expressing flies, since no difference in DA uptake was observed. Figure 25a demonstrates that *Drosophila* expressing hDAT and hDAT K/A displayed

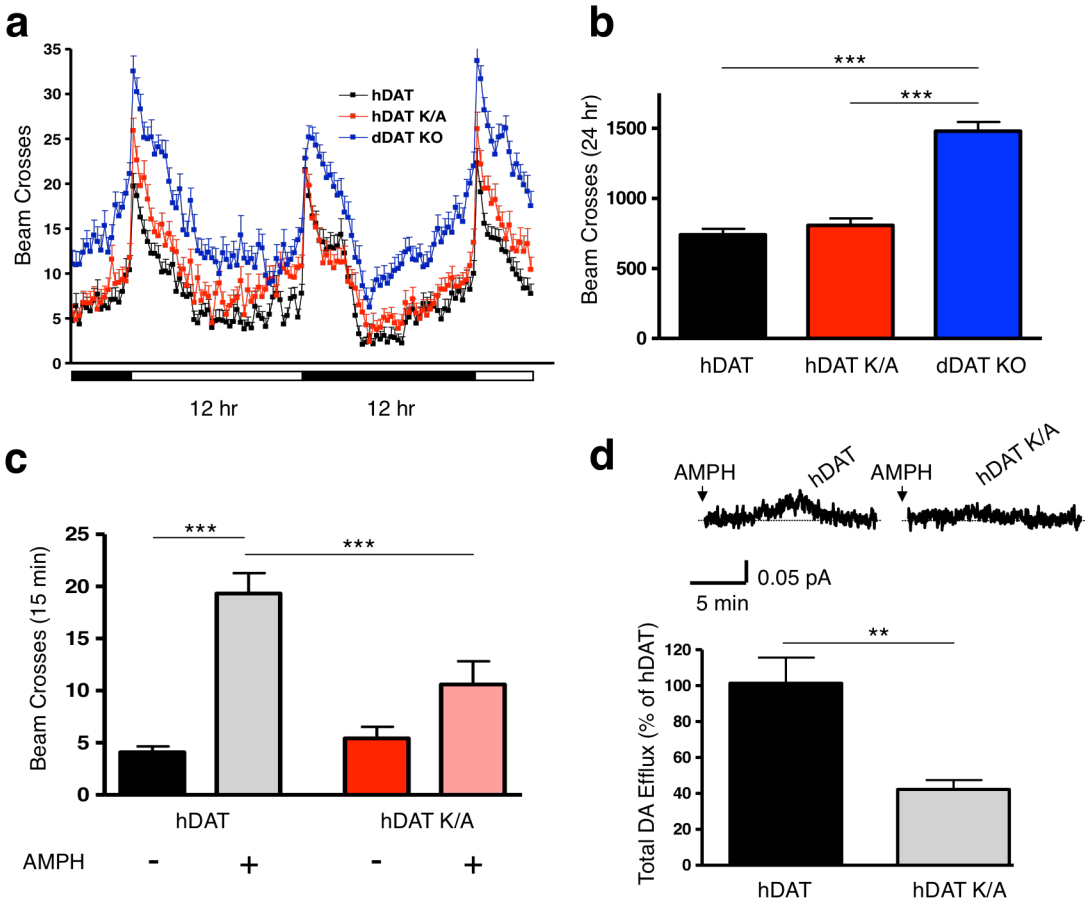

Figure 25. Expression of hDAT K/A in *Drosophila* dopaminergic neurons does not affect circadian locomotor activity yet impairs AMPH-induced locomotion and neuronal DA efflux. hDAT or hDAT K/A was expressed in DA neurons of dDAT KO flies. **(a)** Locomotion was assayed over 32 hours during the light (horizontal white bars) or dark (horizontal black bars) cycle. Flies expressing dDAT KO (blue squares) were hyperactive with respect to flies expressing wild type hDAT (black squares) and flies expressing hDAT K/A (red squares) (beam breaks binned in 15 minute intervals; n = 31-42; mean ± s.e.m.). **(b)** Quantitation of total beam crosses over 24 hours for hDAT, hDAT K/A, and dDAT KO flies (*** = $p \leq 0.001$ by one-way ANOVA followed by Bonferroni post-test; n = 31-42; mean ± s.e.m.). **(c)** AMPH did not cause a significant increase in locomotion in hDAT K/A flies compared to vehicle control ($p \geq 0.05$ by one-way ANOVA followed by Bonferroni post-test; n = 25-49; mean ± s.e.m.). In hDAT flies, AMPH induced a significant increase in locomotion compared to vehicle control (*** = $p \leq 0.001$ by one-way ANOVA followed by Bonferroni post-test; n= 25-60; mean ± s.e.m.). **(d)** hDAT K/A *Drosophila* DA neurons show reduced AMPH-induced DA efflux. Dopaminergic neurons were selected by fluorescence microscopy since the expression of mCherry was driven by TH-GAL4. Top: representative amperometric currents from hDAT and hDAT K/A neurons. Arrows indicate application of 1 μM AMPH. Bottom: quantitation of total AMPH-induced DA efflux. Data represented as cumulative DA efflux expressed as percent of DA efflux from hDAT neurons (** = $p \leq 0.01$ by Student's t-test; n = 4-5; mean ± s.e.m.).

comparable basal locomotion, whereas dDAT KO flies exhibited chronically elevated locomotion. Total circadian locomotor activities (24 hour) of hDAT and hDAT K/A flies were not significantly different, while total locomotor activity of dDAT KO flies was significantly higher than hDAT and hDAT K/A (**Fig. 25b**).

Encouraged by the lack of hyperactivity of hDAT K/A flies under basal conditions, we hypothesized that these flies would have blunted AMPH-induced locomotive behaviors resulting from reduced ability of AMPH to stimulate DA efflux. While AMPH caused a significant increase in locomotion in flies expressing hDAT, this increase was significantly reduced in flies expressing hDAT K/A (**Fig. 25c**). These data demonstrate, for the first time, the behavioral importance of the interaction of PIP_2 with a plasma membrane protein. This discovery is further enhanced by our ability to associate blunted AMPH-induced behaviors with a decreased ability of AMPH to cause DA efflux in isolated DA neurons from flies expressing hDAT K/A. *Ex vivo* cultures of *Drosophila* DA neurons were investigated with amperometry to quantify the magnitude of the AMPH-induced DA efflux in the different fly lines. The DA efflux recorded from hDAT K/A expressing neurons was significantly reduced compared to hDAT expressing neurons (**Fig. 25d**), suggesting that the reduced AMPH-induced locomotion in flies expressing hDAT K/A is due to diminished DA efflux in response to AMPH.

It is possible that this PIP_2 regulation of DA efflux is an evolutionarily conserved mechanism that controls DAT function across phylogeny. To test this possibility, we utilized the APC technique in Chinese hamster ovary (CHO) cells expressing the dDAT (dDAT cells). In dDAT cells, intracellular perfusion of pal-HRQKHFEKRR (3 μM, 10 minutes) was effective in reducing AMPH-induced DA efflux with respect to the efflux obtained with the control peptide pal-HAQKHFEAAA (34.9 ± 12.9% of control peptide; $p \leq 0.01$ by Student's t-test; $n = 3$). These results parallel those obtained in hDAT cells (**Fig. 17**). In this study, we provide the first

behavioral evidence for the relevance of the interaction of PIP_2 with a plasma membrane protein, associating AMPH behaviors to altered neuronal DAT function within the same organism.

Discussion

We recently demonstrated that disrupting the localization of DAT in lipid rafts impairs the ability of AMPH to cause both DA efflux (without altering DA uptake) (Cremona *et al.*, 2011), and associated behaviors (Pizzo *et al.*, 2013). This led us to hypothesize that the molecular underpinnings required for AMPH actions reside in lipid rafts. Raft microdomains are considered scaffolds for PIP_2 signaling, enabling PIP_2 to selectively regulate different cellular processes (Pendleton *et al.*, 2002, van Rheenen *et al.*, 2005). Yet, partitioning of PIP_2 into lipid rafts has been criticized as energetically improbable, since PIP_2 consists of a polyunsaturated acyl side chain (arachidonic acid) that is unlikely to spontaneously partition into cholesterol-rich rafts (McLaughlin and Murray, 2005). Therefore, it is theorized that the partitioning of PIP_2 into rafts is facilitated by interactions with raft-localized proteins (McLaughlin and Murray, 2005). Here we demonstrate that PIP_2 directly interacts with hDAT, a protein that localizes to the rafts (Cremona *et al.*, 2011, Gabriel *et al.*, 2013, Sorkina *et al.*, 2013).

We found that the DAT N-terminus (a domain of functional importance) (Khoshbouei *et al.*, 2004, Fog *et al.*, 2006) is engaged in direct electrostatic interactions with PIP_2, described by both computational and biochemical analysis. We demonstrate that this interaction is direct and distinct from the recently described association of PIP_2 with SERT (Buchmayer *et al.*, 2013). This DAT-PIP_2 interaction, which occurs in brain tissue, involves the two most distal N-terminal Lys (Lys3 and Lys5). These data, combined with the regulatory nature of DAT localization to PIP_2 enriched lipid rafts, led us to hypothesize that PIP_2 participates in coordinating the complex molecular events underlying *specific* DAT activities. This includes AMPH-induced DA efflux.

Notably, this interaction does not regulate the physiological function of DAT (DA uptake), DAT surface expression, and AMPH uptake. Other functions of the DAT include AMPH- or DA-stimulated inward currents that represent inward movements of ions associated with the transport of substrate. Therefore, we expected that substrate-induced inward currents would not be affected by disruption of DAT-PIP_2 interaction, in the same way that DA or AMPH uptake is not affected. We show that disrupting DAT-PIP_2 interaction by substitution of Lys3 and Lys5 with Ala did not impair the ability of hDAT to sustain electrical inward currents stimulated by either DA or AMPH. The regulatory nature of the direct DAT-PIP_2 interaction on DAT-mediated DA efflux is underscored by our results demonstrating that "sequestering" PIP_2, with our palmitoyl-positively charged peptide, or depleting PIP_2, by stimulating PLC activity, results in diminished reverse transport of DA. Consistent with these findings is the notable result that intracellular perfusion of the palmitoyl-positively charged peptide did not impair hDAT-mediated inward currents stimulated by either AMPH or DA relative to control peptide. These data underscore the interaction between DAT and PIP_2 as a key regulator of the specific DAT function of DA efflux.

N-terminal phosphorylation is a requirement for the ability of AMPH to cause a robust DA efflux (Khoshbouei *et al.*, 2004). The results of our specific molecular manipulations support the notion that Lys to Ala substitution did not impair DA efflux by altering primary sequence requirements for phosphorylation of Ser2 and Ser4. Indeed, pseudophosphorylation of these Ser residues in the hDAT K/A background failed to rescue DA efflux. Consistent with this notion, palmitoyl-positively charged peptide (which does not alter the N-terminus primary sequence) disrupts both the direct interaction of the N-terminus with PIP_2 as well as DA efflux. However, the computational modeling reveals the possibility that the strength of the association of Lys3 and Lys5 with PIP_2 regulates the proper conformation of the DAT N-terminus and affects the transporter N-terminus as a whole. Therefore, we cannot exclude the possibility that the observed DAT-PIP_2 association regulates N-terminal phosphorylation of non-adjacent Ser by

coordinating suitable conformations. Nevertheless, this possibility does not diminish the importance of the discovery that DAT-interaction with PIP_2 is a key determinant of AMPH-induced DA efflux and behaviors. On the contrary, it highlights an opportunity, in future studies, to understand whether the DAT N-terminal interaction with PIP_2 supports N-terminal phosphorylation and/or the importance of phosphorylation for N-terminal conformations and DAT-PIP_2 association.

The Ser-Lys-Ser-Lys N-terminal sequence of the DAT is conserved across several species, including *Drosophila*, suggesting that the DAT-PIP_2 association is a possible evolutionarily conserved mechanism that regulates specific DAT functions. Our data demonstrate that disruption of the dDAT-PIP_2 interaction impairs DA efflux, which parallels our results in the hDAT. It is tempting to speculate that this mechanism of N-terminal regulation of transporter function through electrostatic interactions with PIP_2 is a potential mode of regulation for other neurotransmitter transporters as well. Examination of sequences of the N-terminal regions of four major neurotransmitter transporters (hDAT, hSERT, hNET, and hVMAT2) reveals that the positively charged residues are not only abundant in this region, but are also often clustered. In the hDAT, we revealed the consequences of this clustering in a structural context, where one of these clusters contains Lys3 and Lys5, which enables this region to attract PIP_2 lipids. Therefore, a mechanism of PIP_2 regulation, similar to the one outlined here for DAT function, may apply to other neurotransmitter transporters with charged clusters in their N-terminal sequences.

Recently we discovered that the AMPH-induced 5-HT efflux mediated by SERT also relies on PIP_2 interactions with positively-charged residues (Buchmayer *et al.*, 2013). However, these residues are not localized to the N-terminus of SERT. These data do not exclude a possible role of SERT N-terminus basic residues in SERT-PIP_2 interaction and AMPH-induced

5-HT efflux. In contrast, in DAT, mutation (to Ala) of the corresponding SERT-PIP_2 binding sites causes substantial trafficking of DAT away from the plasma membrane, disrupting its membrane expression. Thus, this trafficking phenomenon prevents our ability to determine the significance of these residues in the mechanistic aspects of the DAT transport cycle. However, it is clear that they do not functionally replace Lys3 and Lys5 in terms of DA efflux.

Prior to this work, it was unclear whether the association and/or dissociation of plasma membrane proteins with PIP_2 played a role in the regulation of behaviors of complex organisms. Here, we took advantage of an animal model (*Drosophila melanogaster*) to determine the behavioral consequences of disrupting direct interactions of DAT with PIP_2. *Drosophila* expressing hDAT K/A solely in DA neurons did not display altered circadian locomotor activity. This is not surprising, since the cells expressing hDAT K/A have both normal DA uptake and DA affinity. However, hDAT K/A flies exhibit significant reductions in the behavioral psychomotor responses to AMPH. These data convey the significance of the interaction between PIP_2 and plasma membrane proteins (i.e. DAT) in fundamental organismal behaviors, such as locomotion. The discovery of this PIP_2 regulation of the psychomotor actions of AMPH is further enhanced by our ability to record DA efflux (for the first time) directly from DA neurons cultured from the same *Drosophila* lines utilized in our behavioral assays. DA neurons expressing hDAT K/A have a significant reduction in DA efflux with respect to neurons expressing hDAT. This enhances our molecular discoveries outlining the DAT-PIP_2 interaction as required for DA efflux and obligatory in the ability of AMPH to cause psychomotor behaviors. These data promote PIP_2 and its synthetic pathway from its canonical role as a modulator of cell function and metabolism to a new role as a regulatory agent of both elemental behaviors, such as locomotion, and maladaptive behaviors, such as psychostimulant abuse.

Materials and methods

Cell culture and transfection

The GFP-hDAT-pCIHygro expression vectors containing hDAT, hDAT K/A (Lys3 and Lys5 to Ala), hDAT K/N (Lys3 and Lys5 to Asn), or hDAT K/A-S/D (Lys3 and Lys5 to Ala and Ser2 and Ser4 to Asp) sequence were generated, confirmed and transiently transfected into Chinese hamster ovary (CHO) cells. The *Drosophila* DAT cDNA was generously provided by the laboratory of Dr. Satinder Singh (Yale University). In some experiments (noted in figure legend), stably transfected hDAT CHO cells were used. These cells were generated as previously described (Bowton *et al.*, 2010). Cells were maintained in a 5% CO_2 incubator at 37°C and maintained in Ham's F-12 medium supplemented with 10% fetal bovine serum (FBS), 1 mM L-glutamine, 100 U/mL penicillin, and 100 µg/mL streptomycin. Stably transfected hDAT CHO cells were kept under selection with 250 µg/mL hygromycin B (Corning Cellgro). Fugene-6 (Roche Molecular Biochemicals) in serum-free media was used to transfect cells using a 6:1 transfection reagent:DNA ratio. Assays were conducted 24-48 hours post transfection.

Drosophila neuron culture

Drosophila neurons were cultured from 1-3 day old males. Brains were dissected in Schneider's medium with 1.5% bovine serum albumen (BSA) and optic lobes were removed. Brains were washed with Schneider's medium and incubated for 40 minutes in collagenase (0.3%) and trypsin (0.125%). They were washed in Schneider's medium supplemented with 10% heat inactivated FBS. Dissociated cells were obtained by brain trituration in medium. Cells from each brain were plated on one poly-D-lysine coated MatTek® dish treated with collagen (type IV). Assays were performed the next day.

Cell imaging

We used the pleckstrin homology (PH) domain from phospholipase C_δ (PHPLC$_\delta$-mRFP) that binds to PIP_2 at the plasma membrane and has been used to monitor pools of PIP_2 at the plasma membrane(Varnai and Balla, 1998). Cells on poly-D-lysine coated MatTek® dishes were co-transfected with GFP-DAT and PHPLCδ-mRFP and, after 48 hours, were deprived of serum overnight. Single confocal image sections were generated by using a LSM 510 inverted confocal microscope (Zeiss) by sequential imaging of live cells.

Co-immunoprecipitations

Cells were grown to confluence in 25 cm^2 culture flasks and serum deprived overnight prior to assay. On the day of the assay, cells were washed three times with 4˚C phosphate-buffered saline (Gibco) containing 1 mM EGTA and 1 mM EDTA and lysed in RIPA buffer (100 mM NaCl, 1.0% IGEPAL CA-630 (NP-40), 0.5% sodium deoxycholate, 0.1% SDS, 50 mM Tris, pH = 8.0, supplemented with a protease inhibitor cocktail (Sigma Aldrich)). Lysates were passed twice through a 27.5 gauge needle and centrifuged at 15,000 x g for 30 minutes. With a portion of the total cell lysate (TCL) collected to run as the totals, 1 mL of the remaining supernatant was incubated at 4°C for 4 hours with Sepharose-G beads (Fisher Scientific), previously washed with 1% BSA in RIPA buffer and preincubated with 2.5 µg PIP_2 antibody (mouse monoclonal, Enzo Life Sciences). For the negative control, TCL supernatant was incubated with BSA-blocked Sepharose-G beads alone. Beads were spun down, washed with cold RIPA buffer, and samples eluted with Laemmli sample buffer at 95˚C for 5 minutes. TCL and eluates were analyzed by SDS-PAGE and immunoblotting (see below for antibody details). Band intensity was quantified using ImageJ software (National Institutes of Health). The association between PIP_2 and hDAT variants was represented as the ratio of eluate:TCL band intensity, normalized to the eluate:TCL ratio observed in hDAT and expressed as a percent. For the mouse DAT-PIP_2 co-immunoprecipitations from striatum, the same protocol was used with the

following modifications: striatum was dissected from either wild-type or DAT KO mice, solubilized in RIPA buffer (1:10 weight/volume), homogenized, lysed on ice for 30 minutes and then centrifuged. The remaining protocol was performed as described above. The mice used for these experiments were handled in compliance with IACUC protocols.

Cell surface biotinylation and protein immunoblot

Cells were cultured in 6-well plates. For cell surface biotinylation assays, cells were labeled with sulfo-NHS-SS-biotin (1.0 mg/ml; Pierce) before purification and analysis via SDS-PAGE/immunoblots (Mazei-Robison *et al.*, 2008). hDAT was detected using a rat monoclonal primary antibody to the N-terminus of hDAT (1:1000) (Millipore Bioscience Research Reagents) and a goat-anti-rat-HRP-conjugated secondary antibody (1:5000; Jackson ImmunoResearch).

Gluthathione transferase (GST) fusion proteins

GST and GST fused to the first 64 N-terminal amino acids of hDAT were purified as described previously (Binda *et al.*, 2008) with some modifications. Briefly, GST and the GST fusion proteins were produced in *Escherichia coli* BL21 DE3 LysS. The culture was grown at 30°C, expression induced by the addition of 1 mM isopropylβ-d-1-thiogalactopyranoside at 18°C, and the culture was harvested 8 hours after induction. The frozen pelleted bacteria was thawed in Tris-buffered saline (TBS) containing 10% glycerol and a Bacterial Protease inhibitor cocktail (Roche Diagnostics)(pH 7.4) and treated with 1 mg/mL lysozyme followed by 15 mM CHAPS. It was then sonicated and cleared by centrifugation. The lysate was passed over glutathione Sepharose 4B beads (GE Healthcare) and washed several times with TBS, followed by 10 mM Tris containing 10% glycerol and eluted with TBS containing 10 mM gluthathione. The quality, size, and amount (relative to BSA) of GST fusions were determined by SDS-PAGE and Bio-Safe Coomassie G-250 Stain. The amount was determined by analysis of imaged gels using ImageQuantTL.

Liposome binding

GST and GST fusion proteins where incubated with or without liposomes for 10 minutes at room temperature, centrifuged at 100,000 x g for 20 minutes at 4°C, and analyzed by immunoblot analysis using anti-GST antibodies (The Vanderbilt Antibody and Protein Resource Core). Liposomes were formed by extrusion of synthetic lipids at a final concentration of 1 mM. Liposomes were formed in 10 mM HEPES/TRIS, 100 mM NaCl with 95% phosphatidylcholine (DOPC; Echelon) and 5% PIP_2 (Phosphatidylinositol 4,5-bisphosphate diC16) at a pH of 7.4.

Amperometry and patch clamp electrophysiology

Cells were plated at a density of ~20,000 per 35-mm culture dish. To preload cells with DA, dishes were washed with KRH assay buffer (130 mM NaCl, 1.3 mM KCl, 1.2 mM KH_2PO_4, 10 mM HEPES, and 2.2 mM $CaCl_2$, pH 7.4) containing 10 mM dextrose, 100 µM pargyline, 1 mM tropolone, and 100 µM ascorbic acid, and incubated with 1 µM DA in KRH assay buffer for 20 minutes at 37°C. To preload *Drosophila* neurons, dishes were washed with KRH assay buffer (as above) containing 100 nM raclopride, and incubated with 1 µM DA in KRH assay buffer for 20 minutes at 26°C. All dishes were washed three times with the external bath solution (130 mM NaCl, 10 mM HEPES, 34 mM dextrose, 1.5 mM $CaCl_2$, 0.5 mM $MgSO_4$, 1.3 mM KH_2PO_4, adjusted pH to 7.35, and 300 mOsm).

To deliver DA (2 mM, Sigma Aldrich), PIP_2 inhibitory/control peptides (3 µM pal-HRQKHFEKRR or pal-HAQKHFEAAA), and/or PIP_2 (50 µM, phosphatidylinositol 4,5-bisphosphate diC8, Echelon Biosciences), a programmable puller (model P-2000, Sutter Instruments, Novato CA) was used to fabricate quartz recording pipettes with a resistance of 3-5 MΩ. These pipettes were filled with an internal solution containing: 120 mM KCl, 10 mM HEPES, 0.1 mM $CaCl_2$, 2 mM $MgCl_2$, 1.1 mM EGTA, 30 mM dextrose, pH 7.35, and 275 mOsm.

Upon gaining access to the cells, the internal solution was allowed to diffuse into the cell for 10 minutes.

Experiments involving perfusion of AMPH or DA (**Fig. 17b** and inward current experiments) utilized double-barrel quartz tubing with an inner diameter of 250 μm (Polymicro Technologies, Phoneix AZ) placed ~80 μm from the cell. DAT-mediated inward currents were recorded at -60 mV.

To record DA efflux, a carbon fiber electrode (ProCFE; fiber diameter of 5 μm; obtained from Dagan Corporation) juxtaposed to the plasma membrane and held at +700 mV (a potential greater than the oxidation potential of DA) was used to measure DA flux through oxidation reactions. Amperometric currents in response to the addition of AMPH were recorded using an Axopatch 200B amplifier (Molecular Devices, Union City, CA) with a low-pass Bessel filter set at 1 kHz; traces were digitally filtered offline at 1 Hz using Clampex9 software (Molecular Devices, Union City, CA). DA efflux was quantified as the peak value of the amperometric current for all experiments except for recordings from *Drosophila* neurons. For *Drosophila* neurons, total DA efflux was quantified as the integral of the trace for a fixed 15 minute window. Dopaminergic neurons were recognized by fluorescence microscopy since the TH-GAL4 drives the expression of mCherry in dopaminergic neurons.

[^{3}H]DA uptake

Cells were plated on poly-D-lysine coated, 24-well plates and grown to ~90% confluence. On the day of the experiment, cells were washed once with 37°C KRH buffer containing 10 mM dextrose, 100 μM pargyline, 1 mM tropolone, and 100 μM ascorbic acid, and equilibrated for 5 minutes at 37°C. Saturation kinetics of DA uptake was determined using a mixture of [^{3}H]DA (PerkinElmer Life Sciences, Waltham, MA) and unlabeled DA diluting to final

DA concentrations of 0.01 μM - 10 μM. Uptake was initiated by bath addition of the dilution row mixture. Uptake was terminated after 10 minutes by washing twice in ice-cold KRH buffer. Scintillation fluid (Optiphase HiSafe 3, PerkinElmer Life Sciences) was added to the wells and the plates were counted in a Wallac Tri-Lux β-scintillation counter (Wallac). Nonspecific binding was determined in the presence of 10 μM cocaine. K_m and V_{max} values were derived by fitting Michaelis-Menten kinetics to the background corrected uptake data, using GraphPad Prism 5.0 (GraphPad Software, San Diego, CA). All determinations were performed in triplicates.

Computational modeling

To evaluate the interactions between PIP_2-enriched membranes and the N-terminal region of the hDAT (residues 1-59), as well as the hDAT K/A and hDAT K/N mutants, molecular models were constructed with the knowledge-based structure-prediction tool Rosetta (Das and Baker, 2008). 1,000 different structures obtained from the structure prediction protocols in Rosetta were filtered through clustering according to a criterion of *maximization of common structure conservation* implemented in the in-house algorithm RMSDTT, which has been introduced into the molecular graphics program, visual molecular dynamics (VMD) (Humphrey *et al.*, 1996). Clusters with the largest numbers of conformations (usually 2−3 top clusters for each construct) were selected for further refinement with atomistic molecular dynamics (MD) simulations, to find the motifs within each cluster that were most frequently found in the Rosetta prediction. Predicted structures of the hDAT N-terminus, incorporating these most frequent motifs, were then subjected to both unbiased MD and replica exchange MD (Earl and Deem, 2005) simulations to assess the stability of the overall fold of the N-terminus, as well as of the individual structural elements identified with Rosetta.

The top structures that underwent the filtering process, described above, were further examined for suitability in the complete model of the hDAT transmembrane bundle (TMB)

(Beuming *et al.*, 2008, Kniazeff *et al.*, 2008, Bisgaard *et al.*, 2011). The structures were embedded into a compositionally-asymmetric lipid membrane model (5:45:50 mixture of PIP_2/POPE (phosphatidylethanolamine) / POPC (phosphatidylcholine) on the intracellular leaflet, and 30:70 mixture of sphingomyelin / POPC on the extracellular leaflet (Kiessling *et al.*, 2009). Docking of the N-terminus (1-59 residues) to the TMB (residues 57-590) was carried out with Modeller (Sali and Blundell, 1993). Specific poses for the N-terminal constructs, relative to the TMB, were selected based on the criterion of positioning the largest positive electrostatic potential isosurfaces (EPIs) towards the membrane surface. As shown before (Khelashvili *et al.*, 2012), such configurations not only result in the strongest electrostatic interactions between the protein and the PIP_2-containing membrane, but also produce the highest levels of concomitant PIP_2 sequestration by the N-terminal peptide. These juxtamembrane poses of the N-terminus served as starting configurations for subsequent studies of the dynamics of PIP_2 lipids near the hDAT N-terminus, as detailed below.

The protocol used to evaluate the interaction of the hDAT N-terminus with PIP_2-containing membranes is based on the application of the self-consistent mean-field model (SCMFM) that evaluates the steady state distributions of charged lipid species (PIP_2, in this case) under the influence of electrostatic forces from a membrane-adsorbing macromolecule (here, the hDAT N-terminus) and quantifies the corresponding adsorption energies. As described in detail (Khelashvili *et al.*, 2008, Khelashvili *et al.*, 2009, Khelashvili *et al.*, 2012), the SCMFM is a mesoscale approach, based on the non-linear Poisson-Boltzmann (NLPB) theory of electrostatics (Sharp and Honig, 1990) and Cahn-Hilliard dynamics, in which the protein is considered in 3-dimensional full atomistic detail, and the lipid membrane is considered as a 2-dimensional, tensionless, incompressible low-dielectric elastic slab in which the equilibrium distribution of different lipid species around adsorbing protein is obtained by self-consistent minimization. The governing free energy function contains contributions from electrostatic

interactions, lipid mixing entropy, and mixing entropy of mobile salt ions in the solution. The SCMFM calculation of the membrane interaction of the hDAT N-terminus constructs (hDAT and the hDAT K/A or hDAT K/N mutants) considered in full atomistic detail (with partial charge and atomic radii taken from the all-atom CHARMM27 force field with CMAP corrections for proteins (Mackerell *et al.*, 2004), was carried out with the N-terminus positioned 2Å away from the lipid surface with average surface charge density of -0.0031*e* (corresponding to a lipid mixture with 5% PIP_2). The NLPB equation was then solved numerically as described (Khelashvili *et al.*, 2008, Khelashvili *et al.*, 2009, Khelashvili *et al.*, 2012), in a 0.1 M ionic solution of monovalent counterions (corresponding to λ=9.65Å Debye length), and using a dielectric constant of 2 for membrane interior and protein, and 80 for the solution.

AMPH uptake

Plated hDAT, hDAT K/N, and hDAT K/A cells, as well as untransfected cells (to account for non-specific AMPH uptake) were washed with KRH assay buffer and incubated for 5 min at 37 °C with 10 nM AMPH. Cells were washed three times with ice-cold KRH and AMPH was extracted with acidic organic solvent. AMPH was quantified by reversed-phase HPLC using the Waters AccQ·Tag® method which uses pre-column derivatized reagents that help separate and easily detect fluorescence adducts (Waters Corporation, Milford, MA). AMPH uptake (with non-specific uptake subtracted) was normalized to hDAT levels and expressed as a percent.

***Drosophila* genetics, molecular biology, and construction of UAS hDAT**

Flies lacking the *Drosophila* dopamine transporter (DAT^{fmn}) (Kume *et al.*, 2005) and flies harboring TH-Gal4(Friggi-Grelin *et al.*, 2003) were outcrossed to a control line (Bloomington Indiana (BI) 6326) and selected by PCR or by eye color. TH-GAL4 (BI 8848) and M{vas-int.Dm}ZH-2A, M{3xP3-RFP.attP'} ZH-22A (BI 24481) were obtained from the BI stock center and outcrossed to flies lacking the *Drosophila* DAT (DAT^{fmn}) and carrying the *white* (w^{1118})

mutation (BI stock number 6236) for 5–10 generations. Transgenes (hDAT or hDAT K/A) were cloned into pBI-UASC(Wang *et al.*, 2012), and constructs were injected into embryos from M{vas-int.Dm}ZH-2A, M{3xP3-RFP.attP'}ZH-22A (BI 24481). Initial potential transformants were isolated by selecting for red eyes and lack of GFP signal in the head. Transformants were also verified by RFP fluorescence and outcrossed 5-8 times to DAT^{fmn} flies. The presence of DAT^{fmn} lesion was verified by PCR. Flies were maintained on a standard cornmeal/molasses/yeast media at 25°C and 65% humidity with a 12 hour/12hour light/dark cycle. Lights came on at 8 AM and off at 8 PM.

Behavioral analysis

Three-day-old males were collected and placed into tubes with food for three days. After three days locomotion was recorded for 32 hours by beam breaks and analyzed using equipment/software from Trikinetics (www.trikinetics.com). For the AMPH-induced locomotion, males were starved for 6 hours and then fed sucrose (10 mM) containing either AMPH (1 mM) or vehicle.

Statistical analysis

Compiled data are expressed as normalized mean values ± standard error. For statistical analysis, we used either a Student's t-test or one-way ANOVA depending on the n of the experimental groups. $P < 0.05$ was considered statistically significant.

CHAPTER 3

PUTATIVE PHOSPHATIDYLINOSITOL (4,5)-BISPHOSPHATE BINDING SITES ON DOPAMINE TRANSPORTER INTRACELLULAR LOOP REGIONS CONTROL TRANSPORTER FUNCTION

Introduction

To date, direct interactions between phosphotidylinositol (4,5)-bisphosphate (PIP_2) and the hDAT have been documented to occur via electrostatic interactions between PIP_2 and Lys residues of the hDAT N-terminus (Hamilton and Belovich *et al.*, 2014). However, studies conducted with the hSERT have shown that PIP_2 also interacts with positive residues in the intracellular loop regions of the transporter, specifically Lys residues K352 and K460 in IL3 and IL4, respectively (Buchmeyer *et al.*, 2013). Mutating both of these residues to Ala (hSERT K352A-K460A) results in an impaired ability of the hSERT to interact with PIP_2 compared to WT hSERT, as demonstrated *in vitro* using PIP_2-coated beads to pull down lysates from HEK 293 cells (Buchmeyer *et al.*, 2013). Additional *in vitro* experiments have shown that the hSERT K352A-K460A has an impaired ability to pass efflux currents induced by *para*-chloroamphetamine (*p*CA), while substrate uptake capability is unaffected (Buchmeyer *et al.*, 2013). Thus, these data suggest that PIP_2 interaction with non-N-terminal residues is important for substrate efflux by the hSERT. Intriguingly, the interactions of PIP_2 with the hSERT appear to have an asymmetric regulation of transporter function (*e.g.,* affecting substrate efflux, but not substrate uptake), similar to what has been reported for the hDAT N-terminal K/A constructs with impaired PIP_2 interactions (Hamilton and Belovich *et al.,* 2014). Thus, the work described in this chapter aims to investigate the hypothesis that PIP_2 also regulates hDAT function (specifically AMPH-induced DA efflux) *via* interactions with hDAT intracellular loops.

The focus of this chapter is to determine whether the homologous hDAT residues of the hSERT/PIP_2 binding sites also have a significant role in transporter function, specifically in DA uptake and AMPH-induced DA efflux. The homologous residues for the hSERT/PIP_2 interaction sites in the hDAT are K337 and R443 (Yamashita *et al.,* 2005). Simultaneous mutation of these putative PIP_2 binding site residues to Ala (hDAT K337A-R443A) results in an impaired ability of the transporter to be expressed at the cell surface in CHO cells, hindering functional investigation of hDAT K337A-R443A (Hamilton and Belovich *et al.*, 2014). However, mutation of each residue individually does not impair surface expression, allowing for *in vitro* investigation of functional properties (discussed below). When expressed in CHO cells, hDAT K337A shows an impairment in AMPH-induced DA efflux, as well as an impairment in DA uptake ability, but with normal total and surface expression levels. CHO cells expressing hDAT R443A, on the other hand, display a reduction in AMPH-induced DA efflux only, with DA uptake comparable to WT hDAT as well as normal total and surface expression. Individual mutation of both of these putative PIP_2 binding sites results in functional deficiencies compared to WT hDAT, although they do not display the same phenotypic profile. These data indicate that K337 and R443 may be essential for hDAT function *via* distinct molecular mechanisms and invites further study into the diverse roles that PIP_2 may play in regulating neurotransmitter transporter function.

Results

hDAT K337A shows impairments in both AMPH-induced DA efflux and DA uptake

To determine the ability of hDAT K337A to respond to AMPH, CHO cells were transiently transfected with either WT hDAT or hDAT K337A and bath loaded with DA (bath concentration: 10 μM DA). AMPH was added to the bath solution and DA efflux was measured as amperometric current detected with a carbon fiber electrode (Hamilton and Belovich *et al.*, 2014). In comparison to WT hDAT cells, K337A hDAT cells show a significant impairment in peak amplitude of the AMPH-induced amperometric current, as seen in both the representative

traces (**Fig. 26a**) and the quantitated average peak amplitudes (**Fig. 26b**). Peak amplitude of WT hDAT is 100.0% ± 19.7% compared to hDAT K337A peak amperometric current of 45.36 % ± 10.7% (**Fig. 26b**).

To rule out decreased surface expression of hDAT K337A as a cause for the impaired AMPH response, biotinylation assays as previously described were conducted with WT hDAT and hDAT K337A cells (Mazei-Robison *et al*., 2008). For each genotype, the surface fraction (**Fig. 26c**, top) was quantitated and normalized to the mature glycosylated total hDAT (**Fig. 26c** middle) and represented as % WT hDAT. There were no significant changes in hDAT K337A surface expression compared to WT hDAT (**Fig. 26d**). Additionally, there was no change in the ratio of mature glycosylated and immature unglycosylated forms of the hDAT K337A compared to WT hDAT (**Fig. 26c**, middle).

In order to assess whether hDAT K337A has an impairment in uptake capacity, hDAT K337A cells (open squares) and WT hDAT cells (filled squares) were incubated with varying concentrations of [^{3}H]DA to assess uptake capacity of the hDAT K337A (**Fig. 26e**). Figure 26e represents an average of all data points (12) gathered across four different trials. hDAT K337A (**Fig. 26e,** open squares) shows a decrease in V_{max} compared to WT hDAT (WT hDAT V_{max} = 1.019 ± 0.07 pmols/min/10^5 cells; hDAT K337A V_{max} = 0.6992 ± 0.04 pmols/min/10^5 cells), but has an unchanged apparent affinity for DA compared to WT hDAT (WT hDAT K_m = 0.6437 ± 0.17 μM; hDAT K337A K_m = 0.6053 ± 0.14 μM) (**Fig. 26f**).

hDAT R443A shows impaired AMPH-induced DA efflux, but normal DA uptake

Similar to hDAT K337A, hDAT R443A shows impaired response to AMPH *in vitro*. CHO cells transiently transfected with either WT hDAT or hDAT R443A were bath-loaded with DA and exposed to a final concentration of 10 μM AMPH. As seen in the representative traces,

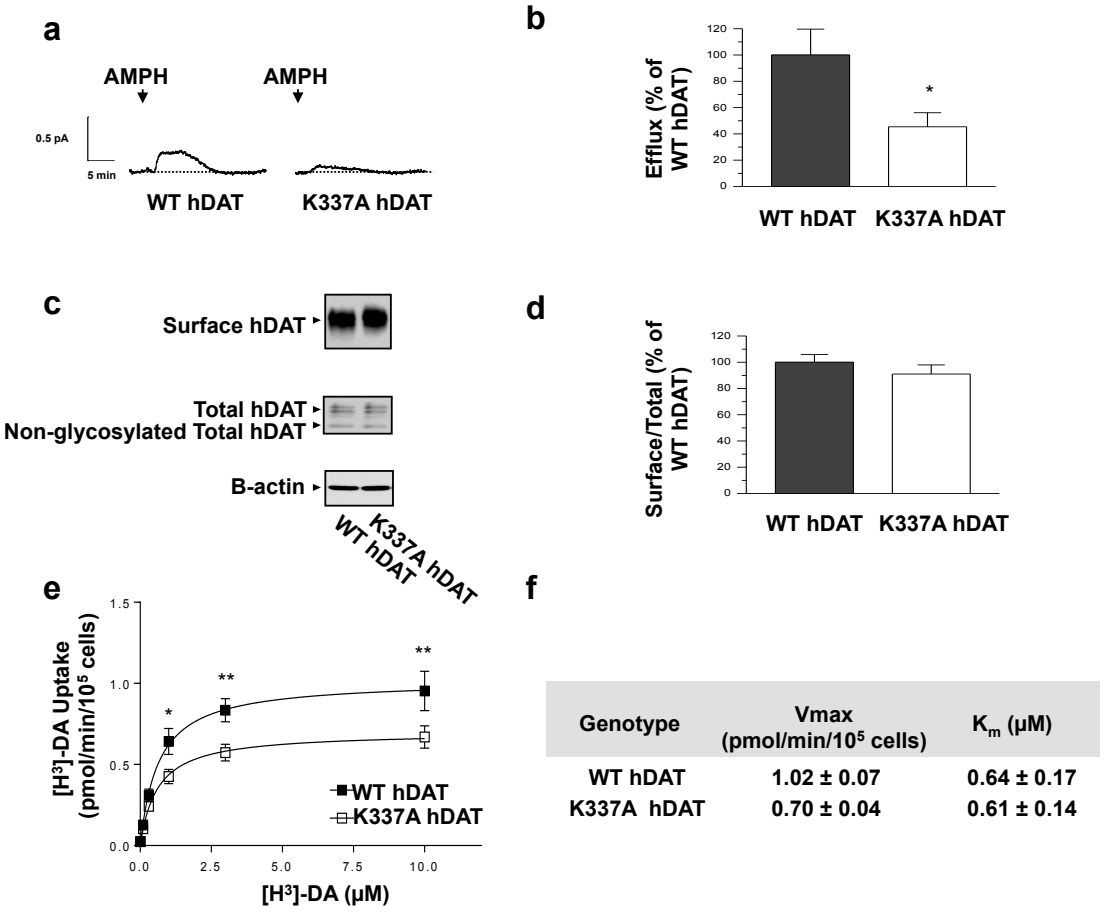

Genotype	Vmax (pmol/min/10^5 cells)	K_m (μM)
WT hDAT	1.02 ± 0.07	0.64 ± 0.17
K337A hDAT	0.70 ± 0.04	0.61 ± 0.14

Figure 26. hDAT K337A shows decreased AMPH-induced DA efflux and DA uptake, but no decrease in trafficking and surface expression ratios compared to WT hDAT. (**a**) Representative traces of amperometric currents from WT hDAT and K337A hDAT cells in response to 10 μM AMPH indicated by arrows. (**b**) Quantitation of peak amplitude of AMPH-induced amperometric current normalized to WT hDAT peak amperometric current. (*p = 0.0269 by Two-tailed Student's T-test; n = 9). (**c**) Representative immunoblots of biotinylated surface fractions of WT hDAT and K337A hDAT (top), total lysates, including mature glycosylated and immature non-glycosylated forms (middle), and actin as loading control (bottom). (**d**) Quantification of surface expression is represented by normalization of surface band to glycosylated total hDAT band and is expressed as a Surface/Total ratio. Data are normalized to WT hDAT Surface/Total ratios, and presented as % WT hDAT Surface/Total. (p = 0.3626 by Two-tailed Student's T-test; n = 10). (**e**) Substrate saturation uptake curve, cumulative results from 4 experiments, each data point collected in triplicate for 12 replicates total. (*p < 0.05, **p <0.01 by Two-way ANOVA with Bonferonni's multiple comparison's test; n = 4, 12 replicates total). (**f**) V_{max} and apparent K_m values were obtained using the Michaelis-Menten equation using all available data points.

AMPH-induced DA efflux is reduced in hDAT R443A compared to WT hDAT (**Fig. 27a**). On average, the peak AMPH-induced amperometric current amplitude of hDAT R443A cells was observed to be 57.5 ± 10% of WT hDAT (100 ± 15.5%) (**Fig. 27b**).

Again, as with hDAT K337A, hDAT R443A's impairment of AMPH-induced DA efflux is not due to alterations in total or surface protein expression (**Fig. 27c-d**). The surface fraction for each genotype (**Fig. 27c**, top) was quantitated and normalized to the mature glycosylated total hDAT (**Fig. 27c** middle) and expressed as a percent of WT hDAT (**Fig. 27d**). hDAT R443A surface expression does not significantly differ from WT hDAT surface expression, nor does R443A hDAT display differences in glycosylation (**Fig. 27c**, middle).

Finally, hDAT R443A's uptake capabilities were tested using [^{3}H]DA. hDAT R443A cells (open squares) and WT hDAT cells (filled squares) were incubated with varying concentrations of [^{3}H]DA (**Fig. 27e**). Figure 27e represents an average of all data points (11-12) gathered across four different trials. hDAT R443A shows no change in V_{max} compared to WT hDAT (WT hDAT V_{max} = 1.39 ± 0.10 pmols/min/10^5 cells; hDAT R443A V_{max} = 1.275 ± 0.12 pmols/min/10^5 cells) and has an unchanged apparent affinity for DA compared to WT hDAT (WT hDAT K_m = 0.938 ± 0.25 μM; hDAT R443A K_m = 1.028 ± 0.34 μM) (**Fig. 27f).**

Discussion

The results in Figure 26 show that hDAT K337A has severe deficiencies in both DA uptake and AMPH-induced DA efflux functions. The K337 residue is located is located two amino acid residues away from Y335, which has previously been shown to be important for the hDAT's ability to change its conformation towards an inward-facing conformation (Norregaard *et al.*, 1998, Loland *et al.,* 2002). As confirmed by the 2013 $dDAT_{cryst}$ structure showing the intracellular gate (**Fig. 28**), the dDAT's homologous residue of hDAT Y335, dDAT Y334

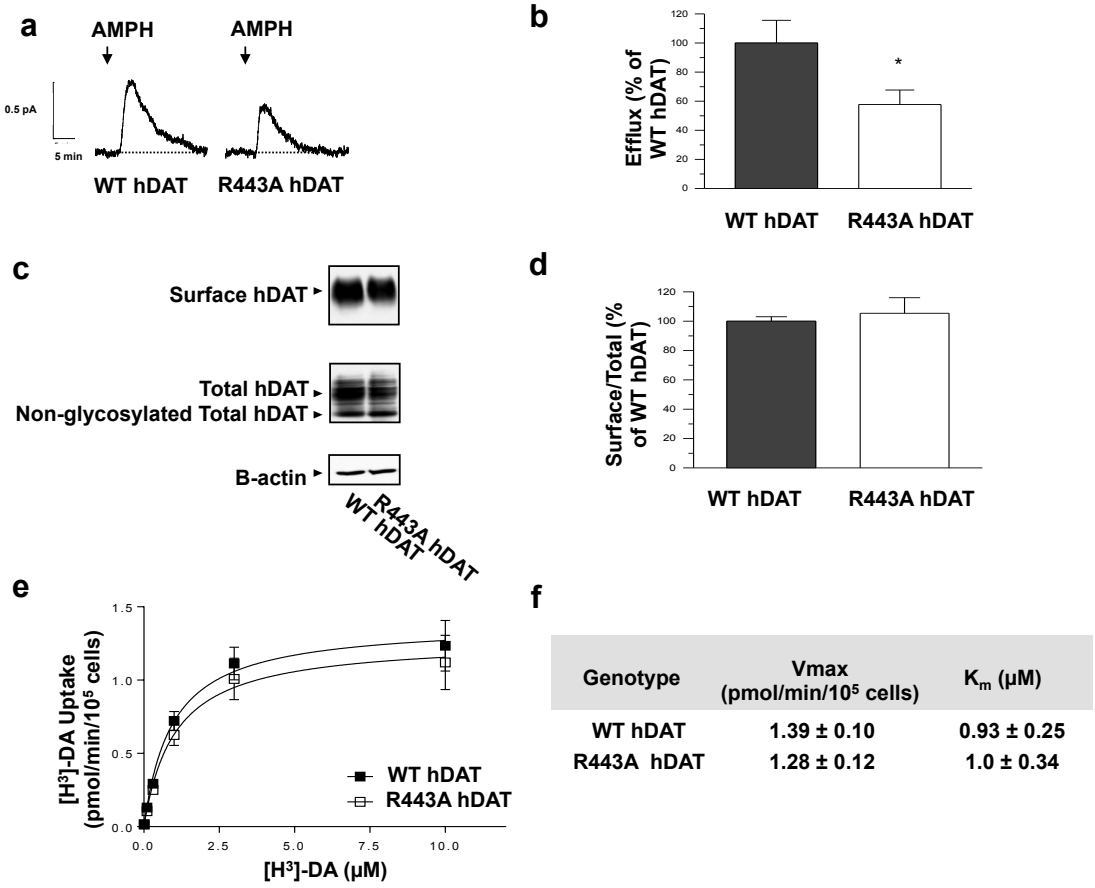

Genotype	Vmax (pmol/min/10^5 cells)	K_m (μM)
WT hDAT	1.39 ± 0.10	0.93 ± 0.25
R443A hDAT	1.28 ± 0.12	1.0 ± 0.34

Figure 27. hDAT R443A shows decreased AMPH-induced DA efflux, but no decrease in trafficking and surface expression ratios and DA uptake compared to WT hDAT. (**a**) Representative traces of amperometric currents, arrows indicate addition of AMPH. (**b**) Quantitation of peak current amplitudes, normalized to peak WT hDAT current amplitudes. (*p < 0.03 by two-tailed paired Student's *t*-test; n = 14). (**c**) Representative immunoblots of biotinylated (surface) hDAT (top), total glycosylated hDAT and total non-glycosylated hDAT (middle), and actin as loading control (bottom). (**d**) Quantification of surface expression is represented by normalization of surface band to glycosylated total hDAT band and is expressed as a Surface/Total ratio. Data are normalized to WT hDAT Surface/Total ratios, and presented as % WT hDAT Surface/Total (p = 0.6232 by two-tailed Student T-test; n = 20). (**e**) Curves represent averaged uptake data from 3 trials in triplicate and 1 trial in duplicate (11 data points total) at 10 minutes at the specified DA concentrations. (No significance by Two-way ANOVA with Bonferonni Post test). (**f**) V_{max} and apparent K_m values were obtained using the Michaelis-Menten equation.

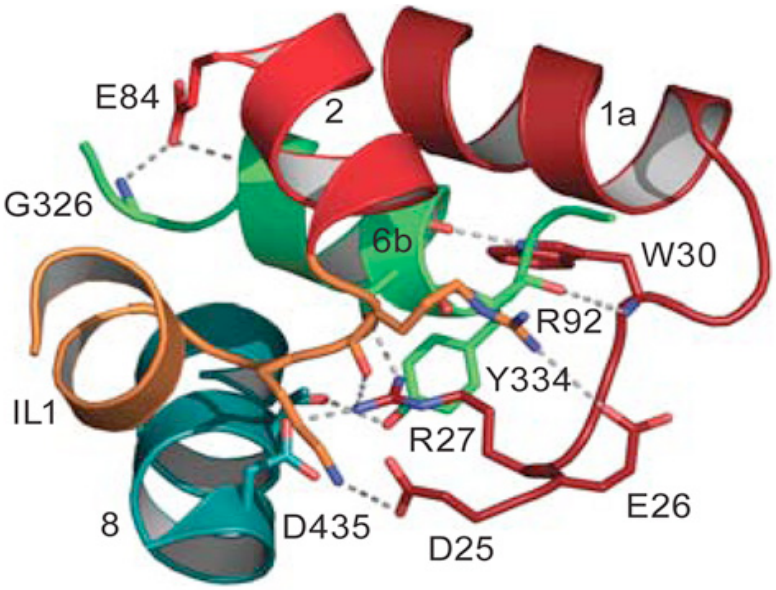

Figure 28. Structure of the dDAT$_{cryst}$ intracellular gate in closed conformation. Structure is viewed from cytoplasm. A network of polar interactions on the cytoplasmic face of the transporter stabilizes the closed conformation of the intracellular gate. Residue Y334 (hDAT Y335) appears positioned to form interactions with IL1 and TM8. IL4 residue D435 (hDAT 436) forms a salt bridge with N-terminus residue R27 (hDAT R60). Figure modified from Penmatsa *et al.,* 2013.

coordinates a salt bridge between dDAT R27 (hDAT R60) and dDAT D435 (hDAT D436) (Penmatsa *et al.*, 2013). Therefore, if PIP_2 does indeed interact with K337, this interaction may help coordinate the hDAT's conformational change towards the inward facing state. Direct interaction between hDAT K337 and PIP_2 has not yet been established, but could possibly be investigated *via* GST-pulldown experiments as previously published (Hamilton and Belovich *et al.*, 2014). Furthermore, as Zn^{2+} has previously been used to rescue the ability of hDAT Y335A to adopt an inward-facing conformation and restore uptake function (Loland *et al.*, 2002), it should be investigated whether Zn^{2+} can also rescue hDAT K337A function.

hDAT K337A also shows an impairment in AMPH-induced DA efflux (**Fig. 26**). One possible explanation for this observation is that K337's proximity to Y335 influences inward vs. outward facing conformation of the transporter. If true, this would suggest the hDAT must adopt specific conformations before AMPH-induced DA efflux can occur. This idea could be experimentally addressed by the application of Zn^{2+} to rescue AMPH-induced DA efflux. This concept has been demonstrated with the ASD-associated variant, hDAT T356M, which prefers an outward facing conformation and has impaired AMPH-induced DA efflux susceptible to Zn^{2+} rescue (Hamilton and Campbell *et al.*, 2013, Hamilton and Shekar *et al.*, 2015, see Chapter 5 of this thesis for detailed discussion). If Zn^{2+} does rescue AMPH-induced DA efflux (along with DA uptake as discussed above), this would support the hypothesis that hDAT K337A's impaired AMPH-induced DA efflux is due to an altered conformational equilibrium. An alternative explanation for hDAT K337A's impaired AMPH-induced DA efflux is that PIP_2 interacts with both K337 and the hDAT N-terminus to coordinate the conformational changes required for efflux. However, since there is limited functional data on the K337 residue, this concept will be discussed in the context of the R443 residue (below).

In contrast to hDAT K337A, hDAT R443A does not show any indication of impaired DA uptake, instead showing only an impairment in AMPH-induced DA efflux (**Fig. 27**). This asymmetric functional profile is the same as that of hDAT constructs with impaired N-terminal PIP_2 interactions (Hamilton and Belovich *et al.*, 2014). Computational modeling studies support the notion that the R443 residue interacts with both PIP_2 and the hDAT N-terminus (Khelashvilli *et al.,* 2015). As represented in **Figure 29a**, PIP_2 is predicted to form close associations with R443 and with other positive residues in the N-terminus, specifically K3, K5, K27, K35, and R51 (Khelashvilli *et al.*, 2015). In turn, R443 is also predicted to form close associations with N-terminal residues K3, K35, and R51 (**Fig. 29b**) (Khelashvilli *et al.*, 2015). Overall, this model suggests that PIP_2 interacts with the positive residues on the hDAT N-terminus and R443, essentially bringing the N-terminus into proximity with R443 and surrounding residues in IL4 and TM9 (Khelashvilli *et al.*, 2015).

In the context of AMPH-induced DA efflux, this model is especially intriguing, as the hDAT N-terminus and its phosphorylation are both essential for this mechanism (Khoshbouei *et al.,* 2003, Khoshbouei *et al.*, 2004), as well as PIP_2 interactions (Hamilton and Belovich *et al.*, 2014). The idea that PIP_2 can simultaneously interact with both the N-terminus and R443 supports the hypothesis that PIP_2 brings the negative charges of the phosphorylated N-terminus into proximity with positively charged R443, possibly triggering the conformational changes required for DA efflux. As Figure 27 shows, removing the positive charge at residue R443 (hDAT R443A) significantly impairs AMPH-induced DA efflux, indicating that R443 does indeed play a vital role in this mechanism. However, more studies will need to be conducted with phosphomimetic mutation of the hDAT N-terminus in an hDAT R443A background to determine whether R443 interaction with the phosphorylated N-terminus is necessary for AMPH-induced DA efflux.

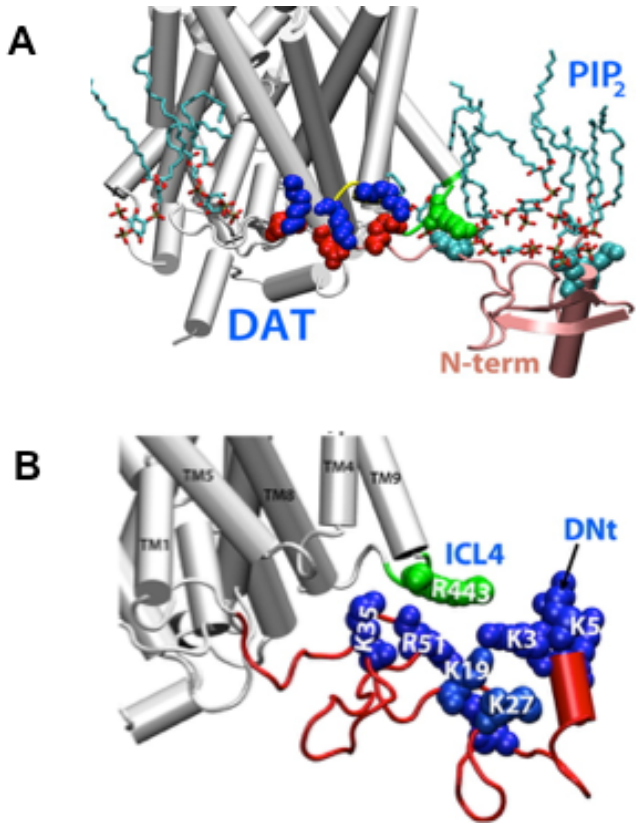

Figure 29. Computational model of DAT IL4 and DAT N-terminus interactions, coordinated by PIP_2. (a) The DAT N-terminus (N-term, mauve) is predicted to be brought into proximity with residue R443 (space-filling model, green) by interactions with PIP_2 (stick models; hydrophobic region is rendered in teal and phospho-head groups are rendered in red). Teal space-filling residues are N-terminus residues predicted to interact with PIP_2. Blue and red space-filling residues represent components of the intracellular gating region. (b) N-terminus residues (blue) and R443 (green) are predicted to be in close proximity. Peptide backbone of N-terminus is rendered in red. DNt indicates distal N-terminus (indicated by black arrow). Images adapted from Khelashvilli *et al.,* 2015.

Of further interest is the fact that R443 is located on the same intracellular loop (IL4) as D460, which forms a salt bridge between R60 and E428, residues that compose part of the intracellular gate (Khleashvilli *et al.,* 2015). R443 is also two amino acids away from R445, which has been predicted to interact with E428 in the $dDAT_{cryst}$ structure and during dynamic molecular simulations (Penmatsa *et al.*, 2013, Khelashvilli *et al.,* 2015). These interactions stabilize the inward-closed state of the transporter, and are predicted to be disrupted by the hDAT N-terminus interacting with IL4 (Khelashvilli *et al.*, 2015). Furthermore, PIP_2 enriched membranes are modeled to induce the transporter to favor an inward facing conformation (Khelashvilli *et al.*, 2015). Using these statements as background, it would be reasonable to assume that hDAT R443A would have impaired ability to adopt an inward-facing conformation, like hDAT Y335A, and would therefore show reduced ability to uptake DA. However, hDAT R443A does not show impairments in DA uptake *in vitro* (**Fig. 27**). This suggests that R443 plays a different role other than that modeled computationally. Instead, it may be more fruitful to examine the role of the phosphorylated N-terminus, PIP_2, and the interactions with R443 during AMPH-induced DA efflux. However, as with K337, R443 remains a putative PIP_2 binding site, and the direct interaction between this residue and PIP_2 must be established in future studies.

CHAPTER 4

DE NOVO MUTATION IN THE DOPAMINE TRANSPORTER GENE ASSOCIATES DOPAMINE DYSFUNCTION WITH AUTISM SPECTRUM DISORDER[2]

Abstract

De novo genetic variation is an important class of risk factors for autism spectrum disorder (ASD). Recently, whole exome sequencing of ASD families has identified a novel *de novo* missense mutation in the human dopamine (DA) transporter (hDAT) gene, which results in a Thr to Met substitution at site 356 (hDAT T356M). The dopamine transporter (DAT) is a presynaptic membrane protein that regulates dopaminergic tone in the central nervous system by mediating the high-affinity re-uptake of synaptically released DA, making it a crucial regulator of DA homeostasis. Here, we report the first functional, structural, and behavioral characterization of an ASD-associated *de novo* mutation in the hDAT. We demonstrate that the hDAT T356M displays anomalous function, characterized as a persistent reverse transport of DA (substrate efflux). Importantly, in the bacterial homolog leucine transporter, substitution of A289 (the homologous site to T356) with a Met promotes an outward-facing conformation upon substrate binding. In the substrate-bound state, an outward-facing transporter conformation is a required for substrate efflux. In *Drosophila melanogaster*, expression of hDAT T356M in DA neurons lacking *Drosophila* DAT leads to hyperlocomotion, a trait associated with DA dysfunction and ASD. Taken together, our findings demonstrate that alterations in DA

[2] The work presented in this chapter is *in press* as Hamilton P. J.[*], N.G. Campbell[*], S. Sharma, K. Erreger, F. H. Hansen, C. Saunders, A. N. Belovich, NIH ARRA Autism Sequencing Consortium, M. Sahai, E. H. Cook, U. Gether, H. S. Mchaourab, H. J. G. Matthies[#], J. S. Sutcliffe[#] and A. Galli[#] (2013). "De novo mutation in the dopamine transporter gene associates dopamine dysfunction with autism spectrum disorder." *Molecular Psychiatry* **18**(12): 1315–23. [*] and [#] denote equal contributions.

homeostasis, mediated by aberrant DAT function, may confer risk for ASD and related neuropsychiatric conditions.

Introduction

Genetic factors have been implicated as important components in the etiology of autism spectrum disorder (ASD). It is now accepted that rare genetic variation affecting single nucleotides of protein-coding DNA, as well as rare genomic copy number variants (CNVs), are significant ASD risk factors (Sebat *et al.*, 2007, Sanders *et al.*, 2011, Devlin and Scherer, 2012, Sanders *et al.*, 2012). In particular, increasing evidence suggests that *de novo* genetic variation is a risk factor in ASD and other neuropsychiatric diseases (Cook and Scherer, 2008, Pinto *et al.*, 2010, Levy *et al.*, 2011, Sanders *et al.*, 2011, Devlin and Scherer, 2012). Several groups have conducted whole exome sequencing (WES) on ASD families, and collectively, these studies indicate that discrete *de novo* mutation (single nucleotide variation (SNV) or small indels) contribute to the overall genetic risk of ASD (Iossifov *et al.*, 2012, Neale *et al.*, 2012, O'Roak *et al.*, 2012, Sanders *et al.*, 2012). Among these variations is the first ASD-associated, *de novo* mutation found in the human dopamine (DA) transporter (hDAT) gene (*SLC6A3*) (Neale *et al.*, 2012). This mutation results in a Thr to Met substitution at position 356 (hDAT T356M). The consequences of this *de novo* mutation and its impact on DA neurotransmission have yet to be elucidated.

The neurotransmitter DA plays an important role in the central nervous system by regulating a variety of functions, including motor activity, motivation, attention, and reward (Carlsson, 1987, Giros and Caron, 1993, Bjorklund and Dunnett, 2007, Palmiter, 2008). Disrupted DA function is implicated in a number of neuropsychiatric disorders, including bipolar disorder, schizophrenia, attention-deficit hyperactivity disorder (ADHD) (Seeman and Niznik, 1990, Volkow *et al.*, 2007, Cousins *et al.*, 2009) and, more recently, ASD (Nieminen-von Wendt

et al., 2004, Anderson *et al.*, 2008, Nakamura *et al.*, 2010, Tassone *et al.*, 2011, Makkonen *et al*., 2011). The dopamine transporter (DAT) is a presynaptic membrane protein that regulates DA neurotransmission via the high-affinity reuptake of synaptically released DA (Kristensen *et al.*, 2011). It is the major molecular target of cocaine, amphetamine (AMPH; Adderall™), and methylphenidate (Ritalin™)(Giros *et al.*, 1996, Jones *et al.*, 1998, Khoshbouei *et al.*, 2004, Kahlig *et al.*, 2005, Sulzer *et al.*, 2005). Due to DAT's role in DA neurotransmission, *SLC6A3* variants have been a focus of genetic association studies linking the etiology of brain disorders to dysregulated DA neurotransmission (Kurian *et al.*, 2009, Kurian *et al.*, 2011). Recent studies have identified a rare, inherited, functional missense *SLC6A3* variant, hDAT A559V (rs28364997) (Grunhage *et al.*, 2000, Mazei-Robison *et al.*, 2005), that has been associated with ADHD, which is commonly comorbid in ASD subjects (Roman *et al.*, 2004, Leyfer *et al.*, 2006, de Bruin *et al.*, 2007, Ronald *et al.*, 2008). These studies point to a contribution of DAT genetic variants in complex brain disorders.

While the role of DA in ADHD has been established (Nemoda *et al.*, 2011), DA's role in ASD is poorly understood (Dichter *et al.*, 2012). Many individuals with ASD exhibit co-occurrence of ADHD symptoms (~20-45%)(Goldstein and Schwebach, 2004, Sturm *et al.*, 2004, Yoshida and Uchiyama, 2004, Gadow *et al.*, 2006). The comorbid nature of ADHD with ASD points to dysregulation of common signaling pathways (e.g. DA) as a mechanism underlying these neuropsychiatric disorders (Di Martino *et al.*, 2013).

Here, we characterized the first ASD-identified, *de novo* mutation in hDAT by presenting structural, functional, and behavioral analysis of this *de novo* variant. These results implicate altered DA homeostasis as a potential liability in ASD risk.

Results

T356M *de novo* DAT variant has impaired function

A recent study assessed the role of *de novo* variation in ASD by using WES in 175 ASD parent-child trios (Neale *et al.*, 2012). In this study, a *de novo SLC6A3* variant was identified, resulting in a Thr to Met substitution at site 356 (Neale *et al.*, 2012). Given the rarity of non-synonymous *de novo* events, it is not surprising that this mutation was absent in the ~1,000 unrelated ASD cases and controls (Neale *et al.*, 2012) and has not been deposited in 1,000 genomes (Genomes Project *et al.*, 2012), dbSNP (build 137) (Sherry *et al.*, 2001), or the NHLBI Exome Sequencing Project. The subject carried no other coding *de novo* mutations. The T356 is completely conserved across several species (**Fig. 30a**). Importantly, the T356 residue is located in the seventh transmembrane domain of hDAT and resides in a highly conserved region implicated in ion binding (Yamashita *et al.*, 2005). The molecular modeling of hDAT and *in silico* mutagenesis of T356 is shown in **Figure 30b**.

The subject harboring this *de novo* mutation is the elder male child of healthy nonconsanguineous Caucasian parents (proband has a healthy younger sibling). There is no immediate family history of ASD or related psychiatric conditions. The subject has a normal IQ (94) and has no history of seizures or other co-morbidities. By the age of 6 years-old, the proband was diagnosed with ASD (see supplemental material for full clinical reports).

To evaluate whether the T356M variant may be a risk factor in the proband's ASD, we compared the activities of hDAT and hDAT T356M in a heterologous expression system. We examined radioactive [^{3}H]DA uptake and affinity. In hDAT T356M cells, the maximal velocity of DA influx (V_{max}) was significantly reduced, whereas the apparent DA affinity (K_m) of hDAT T356M was not significantly different from that of hDAT (**Fig. 31a**, top). A representative plot of DA uptake kinetics for hDAT and hDAT T356M is shown in **Figure 31a** (bottom). The reduced

a

Human	IVTTSINSLTSFSSGFVVFSFL	368
Gorilla	IVTTSINSLTSFSSGFVVFSFL	368
Dog	VITTSVNSLTSFSSGFVVFSFL	365
Mouse	IITTSINSLTSFSSGFVVFSFL	367
Rat	IITTSINSLTSFSSGFVVFSFL	367
Zebrafish	IITSSINSLTSFFSGFVIFSFL	377
Drosophilia	LLTSFINSATSFIAGFVIFSVL	367
C. elegans	LFTSFINCATSFLSGFVIFSVL	361

b

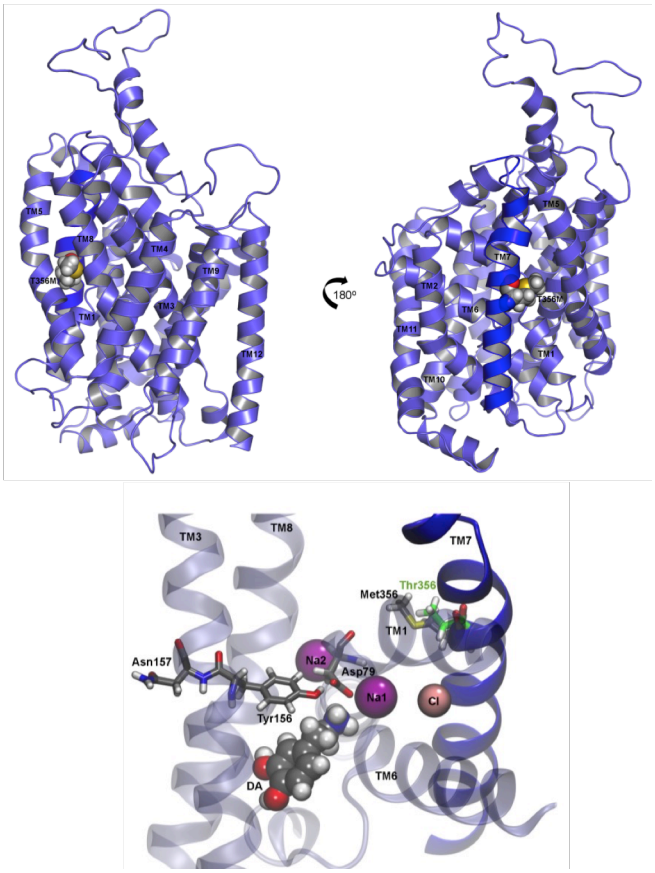

Figure 30. Cross-species conservation and *in silico* mutagenesis of T356. **(a)** Alignment of the DAT amino acid sequence across multiple species. Threonine 356 is represented in red. **(b)** In an equilibrated three-dimensional homology model of hDAT, the T356M mutation is located on transmembrane domain 7 (TM7). Top: Schematic views representing a 180° rotation show T356M with respect to the TM helices. TM7 is shown in dark blue. Bottom: Critical residues that interact with DA{18568020}{20816875} are shown, as well as the bound Na^+ and Cl^- ions. The methionine is rendered together at position 356 with the wild type threonine (green).

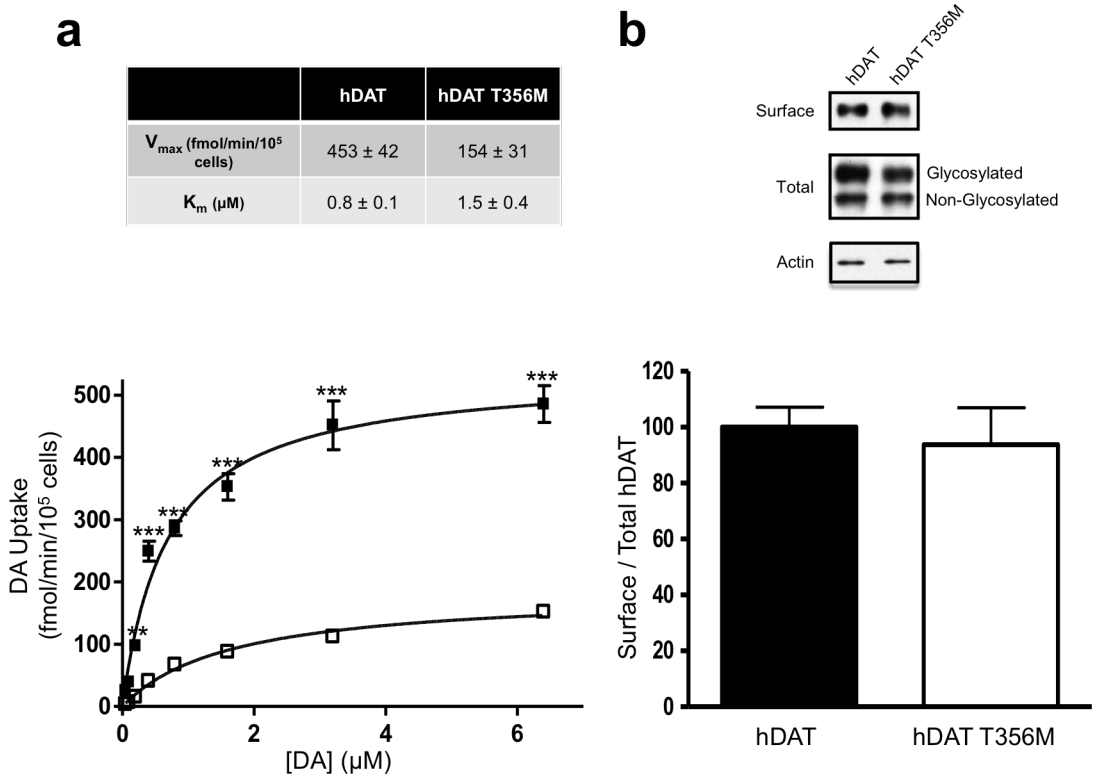

	hDAT	hDAT T356M
V_{max} (fmol/min/10^5 cells)	453 ± 42	154 ± 31
K_m (μM)	0.8 ± 0.1	1.5 ± 0.4

Figure 31. hDAT T356M has impaired function. (a) Top: Kinetic parameters (V_{max} and K_m) for hDAT and hDAT T356M (V_{max}: $p \leq 0.005$; by Student's t-test; n = 3, in triplicate; K_m: $p \geq 0.20$; by Student's t-test; n = 3, in triplicate). Bottom: Representative plot of [^{3}H]DA uptake kinetics in hDAT (filled squares) or hDAT T356M (empty squares) cells (** = $p \leq 0.01$, *** = $p \leq 0.001$; by two-way ANOVA followed by Bonferroni post-test; n = 3, in triplicate). **(b)** Representative immunoblots for biotinylated (surface) and total protein fractions from hDAT and hDAT T356M cells. Surface fractions were quantitated, normalized to total DAT (Glycosylated), and expressed as a percent of hDAT ($p \geq 0.05$; by Student's t-test; n = 8-11).

[^{3}H]DA transport capacity was not associated with a reduction in either total or DAT surface expression (**Fig. 31b**, top), as assessed by measuring changes in DAT proteins in the total and biotinylated fraction, respectively. The total fraction for hDAT and hDAT T356M contained both glycosylated and non-glycosylated forms of the DAT. Surface fractions were quantitated, normalized to total DAT (glycosylated), and expressed as a percent of hDAT (**Fig. 31b**, bottom). Furthermore, normalizing the total DAT fraction (glycosylated) to actin loading control yielded no significant differences between hDAT and hDAT T356M total expression (data are expressed as a percentage of hDAT; hDAT 100 ± 17.6% versus hDAT T356M 96.4 ± 13.7%; $p \geq 0.87$ by Student's t-test; n = 8-11).

hDAT T356M displays ADE

Although hDAT T356M displays similar surface expression to that of hDAT, it demonstrates reduced ability to accumulate intracellular DA. One possibility is that constitutive DA efflux, here referred to as anomalous DA efflux (ADE), contributes to this reduced DA uptake in the hDAT T356M cells. This efflux would impede the intracellular accumulation of DA.

To determine whether hDAT T356M exhibits ADE, cells were whole cell patch clamped and perfused for 10 minutes with an internal solution containing 2 mM DA (Bowton *et al.*, 2010). The electrode, in current clamp configuration, allows the cell to control its membrane voltage. In addition, this technique ensures that cells expressing either hDAT or hDAT T356M were equally loaded with DA. DA efflux was quantified through amperometry (Bowton *et al.*, 2010). We have previously shown that, in the presence of ADE, cocaine decreases the amperometric signal through blockade of DAT (Mazei-Robison *et al.*, 2008). In hDAT cells, amperometric currents were unaffected by application of cocaine (**Fig 32a**, top, hDAT, COC), indicating no ADE. In contrast, amperometric signals from hDAT T356M cells were significantly reduced by the application of cocaine (**Fig. 32a**, top, hDAT T356M, COC), revealing ADE. hDAT T356M-

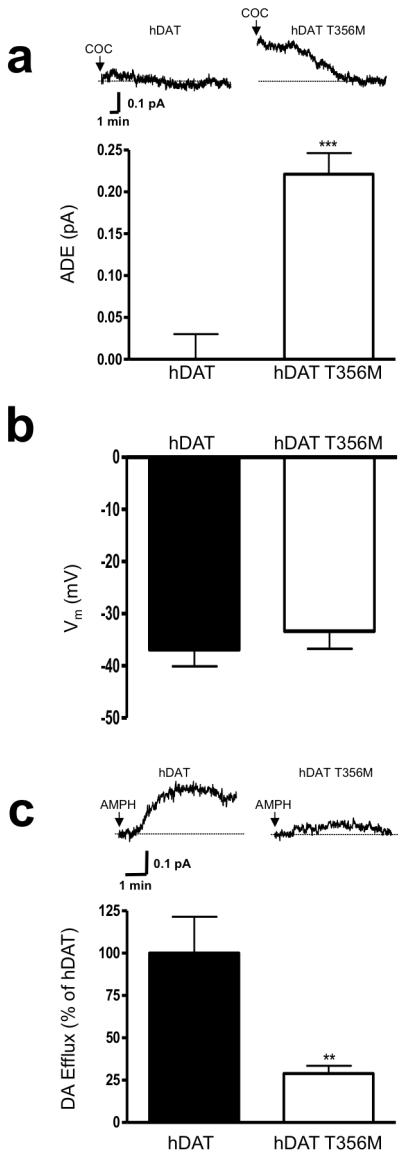

Figure 32. hDAT T356M exhibits robust anomalous DA efflux (ADE). (a) Top: representative amperometric currents recorded from hDAT and hDAT T356M cells. Arrows indicate application of 10 μM cocaine (COC). Bottom: quantitation of the cocaine-induced reduction in the amperometric current (ADE). Data are reported as maximal current (*** = $p \leq 0.001$ by Student's t-test; n = 4-5). **(b)** hDAT T356M cells do not display altered resting membrane potential with respect to hDAT cells ($p \geq 0.05$ by Student's t-test, n = 9-25). **(c)** Representative AMPH-induced amperometric currents recorded from hDAT and hDAT T356M cells. Arrows indicate application of 10 μM AMPH. Bottom: quantitation of AMPH-induced DA efflux. Data are represented as maximal current expressed as percent of the current recorded in hDAT cells (** = $p \leq 0.01$ by Student's t-test; n = 5-7).

expressing cells displayed a significant increase in ADE, compared to hDAT transfected cells (**Fig. 32a**, bottom).

Cell membrane depolarization has been shown to support DA efflux (Khoshbouei *et al.*, 2003). **Figure 32b** reveals that there is not a significant difference in resting membrane potential (measured in current clamp) between cells expressing hDAT or hDAT T356M. This indicates that differences in the function of hDAT and hDAT T356M are not due to resting membrane potential.

Next, we determined possible changes in the ability of AMPH to cause DA efflux by patch delivering DA into hDAT or hDAT T356M cells while recording DA efflux with amperometry. AMPH dose-response assays (measuring the peak of the amperometric current at different AMPH concentrations) revealed that hDAT T356M and hDAT cells have comparable AMPH EC_{50} (EC_{50}; hDAT: 0.15 ± 0.05 μM; hDAT T356M: 0.16 ± 0.07 μM; $n = 4$; $p \geq 0.95$ by Student's t-test). Then, using a saturating AMPH concentration (10 μM) we determined DA efflux in either hDAT or hDAT T356M cells (**Fig. 32c**, top). AMPH-induced DA efflux was significantly reduced in hDAT T356M cells in comparison to hDAT cells (**Fig. 32c**). These results strongly suggest that ADE does not share common mechanisms with AMPH-induced DA efflux.

In LeuT, substitution of Ala289 with a Met promotes an outward-facing conformation

To investigate the structural consequences of the T356M *de novo* mutation in a DAT homolog with a known crystal structure, we analyzed changes in the conformational cycle of the leucine transporter (LeuT). We substituted A289 (the homologous amino acid to T356) with a Met (LeuT A289M). We measured distances between pairs of spin labels (r (Å)) and the distance distribution (P(r), the probability of a given distance between the two labels) monitoring

the intra- and extracellular gates by double electron electron resonance (DEER) (McHaourab *et al.*, 2011). First, we examined the pair 309/480 (**Fig. 33a**, left) that monitors the relative movement of the extracellular loop 4 (EL4) in LeuT. This loop obstructs the permeation pathway in the Apo conformation (Claxton *et al.*, 2010), as indicated by the close proximity of the pair 309/480 (**Fig. 33a**, middle, Apo black line). Upon Na^+ binding, the distance between EL4 and TM12 increases (Claxton *et al.*, 2010), indicating opening of the extracellular vestibule and enabling substrate access (data not shown) (Claxton *et al.*, 2010). Subsequent Leu binding resets the closed EL4 conformation in the occluded conformation of the transporter (Na^+ and Leu bound in the vestibule) (**Fig. 33a**, right; +Na/L black line). The extracellular Apo state (**Fig. 33a**, middle; Apo; compare red and black lines) as well as Na^+ bound state (data not shown) are similar in LeuT and LeuT A289M. Yet, LeuT A289M with Na^+ and Leu bound in the vestibule has a destabilized bound structure with fluctuations on the extracellular side (**Fig. 33a**, right; +Na/L; compare red and black lines). The probability distribution in the Na/Leu bound state contains distinct populations of conformations that indicate fluctuations of LeuT A289M to a permeation pathway that has increased probability to be open to the outside, relative to LeuT (**Fig. 33a**, right; red line, arrows).

We then examined the pair 7/86 (**Fig. 33b**, left), to determine the distance between the N-terminus and intracellular loop 1 (IL1) and to monitor fluctuation dynamics on the intracellular side (McHaourab *et al.*, 2011). This is necessary to describe changes in the population of transporters with an inward facing conformation (McHaourab *et al.*, 2011). In the LeuT background, distance distributions between spin (McHaourab *et al.*, 2012) or fluorescent probes (Zhao *et al.*, 2011) in the Apo state are bimodal, reflecting the equilibrium of this intracellular gate between closed and open conformations (**Fig. 33b**, middle; Apo; black lines). Introduction of the A289M leads to a shift in the equilibrium to favor the closed conformation side (**Fig. 33b**, middle; Apo; compare red and black lines, arrow). Na^+ binding does not alter the equilibrium

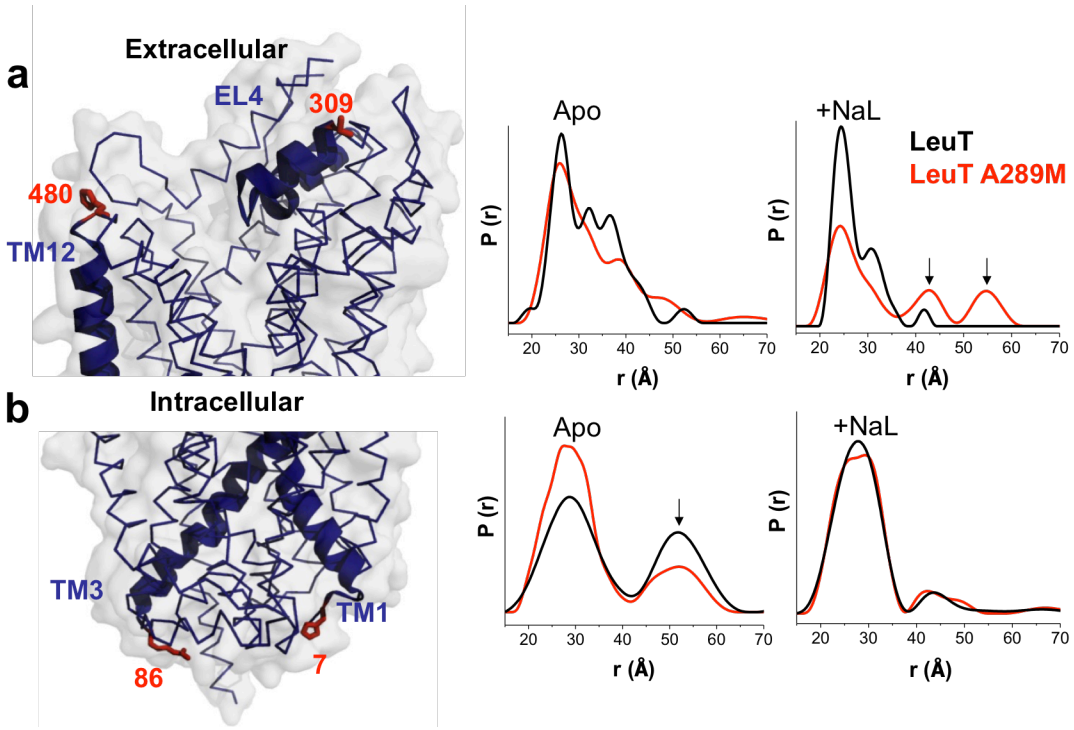

Figure 33. In the leucine transporter (LeuT), substitution of Ala289 with a Met supports an outward-open facing conformation. Distance distributions of extracellular and intracellular spin labeled Cys pairs in LeuT reveal changes in the conformational equilibrium caused by mutating Ala289 to a Met. **(a)** Left: extracellular reporter pairs (309-480) tagged on three-dimensional structure of LeuT. Right: distance of the extracellular reporter pair for LeuT (black) and A289M (red), in the Apo conformation (Apo) and in the presence of Na+ and Leu (+NaL). **(b)** Left: intracellular reporter pairs (7-86) tagged on the three-dimensional structure of LeuT. Right: distance of the intracellular reporter pair for LeuT (black) and A289M (red), in the Apo conformation (Apo) and in the presence of Na+ and Leu (+NaL). The LeuT structure was obtained from PDB 2A65. The structures were generated using PyMOL.

between the two conformations (data not shown), while Na^+ and Leu binding resets this shift to LeuT-like conformations (**Fig. 33b**, middle; +Na/L; compare red and black lines).

Our results demonstrate that, because of the A289M, the presence of substrate and Na^+ fails to completely close the extracellular pathway as in LeuT, inducing fluctuations on the extracellular side. These fluctuations to an open-to-the-outside permeation pathway persist, possibly enabling substrate release. This is in contrast to LeuT, where substrate binding closes the extracellular permeation pathway.

Drosophila expressing hDAT T356M in DA neurons are hyperactive

Locomotion is an elemental behavior regulated across species, including *Drosophila melanogaster*, by DA (Pendleton *et al.*, 2002, Wicker-Thomas and Hamann, 2008, Pizzo *et al.*, 2013). Thus, locomotion in flies offers a powerful model for elucidating the behavioral impact of ADE associated with hDAT T356M.

We expressed hDAT or hDAT T356M in flies homozygous for the *Drosophila* DAT null allele, DAT^{fmn} (dDAT KO)(Kume *et al.*, 2005), by using the Gal4/UAS system to express a single copy of hDAT or hDAT T356M in a $dDAT^{fmn}$ mutant background, selectively in DA neurons (Matthies and Broadie, 2003). To generate the transgenic flies, we used phiC31 based integration, which leads to the expression of comparable levels of mRNA for the relevant transgenes (hDAT or hDAT T356M). Locomotion was quantitated by beam crossing detection over a >24 hour period (data binned in 15 minute intervals) during both the light (horizontal white bar) and dark (horizontal black bar) cycle. While dDAT KO are hyperactive (Kume *et al.*, 2005), flies expressing hDAT in DA neurons have reduced locomotion as compared to dDAT KO, demonstrating the behavioral significance of our approach (**Fig. 34a**, compare hDAT to dDAT KO).

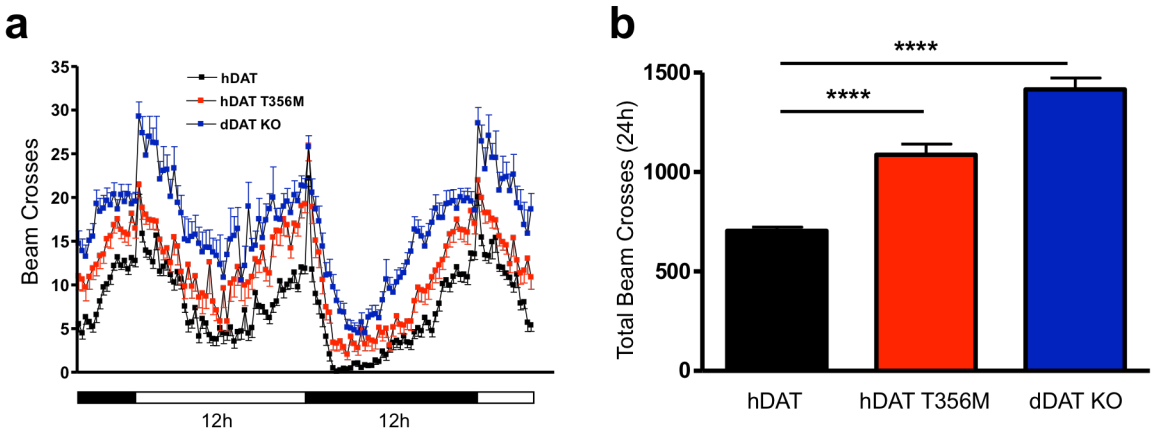

Figure 34. Expression of hDAT T356M in *Drosophila* leads to hyperactivity. hDAT or hDAT T356M was expressed in DA neurons of dDAT KO flies. **(a)** Locomotor activity was assayed over 32 hours during the light (horizontal white bars) or dark (horizontal black bars) cycle. Flies expressing hDAT T356M (red squares), as well as dDAT KO flies (blue squares), were hyperactive throughout the 32 hour period with respect to flies expressing wild type hDAT (black squares) (n = 32; beam breaks binned in 15 minute intervals). **(b)** Quantitation of total beam crosses over 24 hours for hDAT, hDAT T356M, and dDAT KO flies (**** = $p \leq 0.0001$; n = 32).

We hypothesized that flies harboring the hDAT T356M would be hyperactive with respect to hDAT expressing flies due to an increase in extracellular DA promoted by ADE. This is shown in figure 34a. **Figure 34b** shows total (24 hour) locomotor activity in the different fly lines. Total activity (24 hours) of hDAT T356M and dDAT KO flies is significantly higher than hDAT flies (**Fig. 34b**).

hDAT T356M cells display compromised AMPH-induced DA efflux (**Fig. 32c**). This suggests a reduced ability of AMPH to increase locomotion in flies expressing hDAT T356M. Changes in locomotion were determined upon AMPH or vehicle exposure (15 minutes) and calculated as beam crosses. We observed no significant increase in locomotion in hDAT T356M flies when exposed to AMPH as compared to vehicle control (hDAT T356M (vehicle) 9.7 ± 0.7 beam breaks versus hDAT T356M (AMPH) 12.7 ± 1.6 beam breaks; $n = 24$; $p \geq 0.05$). This is in contrast to flies expressing hDAT, where AMPH induced a significant increase in locomotion (hDAT (vehicle) 6.2 ± 0.9 beam breaks versus hDAT (AMPH) 18.2 ± 1.0 beam breaks; $n = 24$; $p \leq 0.001$). Moreover, in the dDAT KO flies, similar to the hDAT T356M flies, AMPH failed to induce a significant increase in locomotion (data not shown).

Discussion

Alterations in DA tone underlie multiple neuropsychiatric disorders, including bipolar disorder, schizophrenia, and ADHD (Seeman and Niznik, 1990, Volkow *et al.*, 2007, Cousins *et al.*, 2009). With respect to ADHD, altered DA signaling, including changes in DAT function, may contribute to the cognitive and hyperactive traits of the disorder (Mazei-Robison *et al.*, 2008, Bowton *et al.*, 2010). ASD, like ADHD, is phenotypically and etiologically complex. However, there is mounting evidence that risk for ASD resides, at least in part, in dopaminergic factors. Variants in DA receptor (DRD) sub-type genes, including *DRD1, DRD3,* and *DRD4*, have been associated with increased risk for ASD (Hettinger *et al.*, 2008) as well as with specific

phenotypic behavior within ASD. These include repetitive or stereotyped behaviors (de Krom *et al.*, 2009, Gadow *et al.*, 2010, Staal *et al.*, 2012), oppositional defiant disorder, and separation anxiety disorder (Gadow *et al.*, 2010). Male children carrying four tandem repeats in the promoter region of the *MAOA* gene (the gene product responsible for degrading amine neurotransmitters, including DA) showed elevated risk for developing ASD (Tassone *et al.*, 2011). It must be noted that none of these genes are significant in genome-wide association studies of ASD. However, in positron emission tomography (PET) studies in adults with ASD, DAT binding was significantly elevated in the orbitofrontal cortex (Nakamura *et al.*, 2010).

Genes harboring *de novo* events are highly significant for understanding the etiology of ASD (Neale *et al.*, 2012). This is not surprising since rate of reproduction is typically low in individuals with autism. Consequently, genetic variants would be subject to negative selection (Devlin and Scherer, 2012). This suggests that the biological networks identified from these *de novo* events, and the broader pathways they function within, are candidate risk factors for ASD. In this study, we examine the functional, structural, and behavioral consequences of the first identified *de novo* hDAT missense variant associated with ASD.

Our amperometric recordings demonstrate that the *de novo* hDAT T356M mutation confers cocaine sensitive ADE. We also show that ADE does not share common mechanisms with AMPH-induced DA efflux since hDAT T356M has an impaired AMPH response. It is intriguing to speculate that anomalous transporter-mediated neurotransmitter efflux may be an unappreciated source of risk for mental illness, especially in disorders associated with altered DA signaling. It is possible that ADE, driven by DAT variants or variants in other genes in the DAT regulatory network (such as DRD subtypes), could impact risk for ASD. A similar point for ADE has been argued previously, in the context of ADHD, for the hDAT variant A559V, in its

functional identification (Mazei-Robison *et al.*, 2008) and original characterization (Bowton *et al.*, 2010).

The question remains as to how the hDAT T356M *de novo* mutation perturbs transporter structure to trigger ADE. Since the crystal structure of hDAT is unavailable, we analyzed changes in the conformational cycle of the hDAT bacterial homolog, LeuT. In LeuT A289M, we measured the distances between pairs of spin labels monitoring the intra- and extracellular gates by DEER. The spin labels monitoring the extracellular gate clearly show that in LeuT A289M, in contrast to LeuT, the presence of Na^+ and leucine promotes a permeation pathway unoccluded to the outside. In terms of transporter function, it is difficult to draw parallels between hDAT T356M and LeuT A289M. Nevertheless, it is compelling to speculate that the mechanism by which the substrate promotes an outward open conformation in LeuT A289M, could also support the ability of hDAT T356M to promote ADE when cytoplasmic DA is available. This would suggest that the mechanism of ADE for hDAT T356M is distinct from that of hDAT A559V, which is a result of a tonic activation of DRD2 and the downstream kinase CaMKII (Bowton *et al.*, 2010). Thus, there may be multiple mechanistic routes to promote hDAT-mediated ADE, and yet ADE might support the comorbid nature of ASD with ADHD.

In an *in vivo* context, hDAT T356M may alter extracellular DA levels and, as a consequence, increase locomotion (Kume *et al.*, 2005). We selectively expressed hDAT T356M specifically in DA neurons of dDAT KO flies. *Drosophila* expressing hDAT T356M exhibited prominent hyperactivity as compared to *Drosophila* expressing hDAT. In addition, AMPH has an impaired ability to increase locomotion in hDAT T356M and dDAT KO flies. This might stem from the decreased ability of AMPH to cause DA efflux in hDAT T356M cells.

Here, we report novel and profound functional abnormalities associated with the hDAT *de novo* mutation T356M, resulting in enhancement of non-vesicular, DAT-dependent DA release, referred to as ADE. Our data raise the possibility that ADE could impact the risk for ASD.

Materials and methods

Subjects and clinical assessment

Subjects from this family included the proband, unaffected sibling, and both parents (AC04-0029-01, AC04-0029-02, AC04-0029-03, AC04-0029-04), who were recruited by the Boston-based Autism Consortium as described previously (Wolfson, 2007, Neale *et al*., 2012). Clinical assessment followed standard research criteria for ASD diagnosis. The proband was classified as having a comparatively "narrow" diagnosis (as opposed to a "broader ASD") based on diagnostic algorithms from the Autism Diagnostic Interview Revised (ADI-R) (Lord *et al.*, 1994) using criteria described by Risi *et al.* (Risi *et al*., 2006), and classification resulting from the diagnostic algorithm of the Autism Diagnostic Observational Session (ADOS) (Lord *et al.*, 2000). Proband IQ was assessed at age 5 years, 9 months using the Wechsler Preschool and Primary Scale of Intelligence (WPPSI; Wechsler, D. (1967)). The Social Responsiveness Scale (SRS; Western Psychological Services) was performed on both parents to index the presence and severity of broader autism phenotype traits, followed by medical and family history provided by the biological mother.

SLC6A3 T356M de novo discovery

Methodological details and validation of the *de novo* mutation are published (Neale *et al.*, 2012). Briefly, DNA derived from whole blood of both parents and the probands was subjected to whole exome sequence analysis. The T356M variant, identified as a heterozygote

in the proband and absent in both parents, was experimentally validated and confirmed to be a *de novo* mutation that does not appear in the unaffected sibling.

Cell culture and transfection

The GFP-hDAT-pCIHygro expression vectors containing either hDAT or hDAT T356M sequence were generated, confirmed and transiently transfected into Chinese hamster ovary cells using FuGENE-6 (Promega). Assays were conducted 24-48 hours post transfection.

Amperometry and patch clamp electrophysiology

hDAT and hDAT T356M cells were plated at a density of ~30,000 per 35-mm culture dish and experiments conducted as previously described (Mazei-Robison *et al.*, 2008, Bowton *et al.*, 2010).

[^{3}H]DA uptake

hDAT and hDAT T356M cells were seeded (50,000 cells/well) into polyornithine coated, 24-well plates, 48 hours before assaying. Uptake kinetic assays were performed as described in the supplementary information of Rickhag *et al*. (Rickhag *et al.*, 2013) and in Rasmussen *et al.* (Rasmussen *et al.*, 2009).

AMPH uptake

Plated hDAT and hDAT T356M cells were washed with KRH buffer and incubated for 5 min at 37°C with 10 nM AMPH. Cells were washed three times with ice-cold KRH. AMPH was quantified using a HPLC system previously described (Siuta *et al.*, 2010).

Cell surface biotinylation and western blot

For cell surface biotinylation assays and Western blots, hDAT and hDAT T356M cells were cultured in 6-well plates and experiments conducted as in Mazei-Robinson *et al*. (Mazei-Robison *et al.*, 2008).

Homology modeling of hDAT and construction of the T356M simulation system

As the template, the homology model uses the known crystal structure for the cognate and homologous structure of the recent outward-open crystal structure of LeuT (Krishnamurthy and Gouaux, 2012). The substrate DA, two Na^+ ions and a Cl^- ion were positioned as described in Shan *et al*. (Shan *et al.*, 2011). To model the mutant hDAT construct with T356M, the mutation was introduced using the free energy perturbation (FEP) method (Guptaroy *et al.*, 2009).

Double Electron Electron Resonance

Cysteine residues were introduced using site directed mutagenesis into LeuT and LeuT A289M constructs (Claxton *et al.*, 2010). Experiments were conducted as in Claxton *et al.* (Claxton *et al.*, 2010). In Figure 33, Apo refers to ion Na^+ and leucine-free transporter while the +NaL state was obtained by addition of 200 mM NaCl and 4-fold molar excess of Leu relative to LeuT. Double Electron Electron Resonance (DEER) (Jeschke and Polyhach, 2007) was performed at 83K on a Bruker 580 pulsed EPR spectrometer operating at Q-band frequency using a standard 4-pulse sequence (Zou and McHaourab, 2010). DEER echo decays were analyzed to obtain distance distributions (Jeschke *et al.*, 2002).

***Drosophila* genetics**

Drosophila homozygotes for the DAT null allele DAT^{fmn} (dDAT KO)(Kume *et al.*, 2005) and flies harboring TH-Gal4 (Friggi-Grelin *et al.*, 2003) were outcrossed to a control line

(Bloomington Indiana (BI) 6326) and selected by PCR or eye color. TH-GAL4 (BI 8848) and M{vas-int.Dm}ZH-2A, M{3xP3-RFP.attP'} ZH-22A (BI 24481) were obtained from the BI stock center and outcrossed to dDAT KO flies carrying the *white* (w^{1118}) mutation (BI stock number 6236) for 5–10 generations. Transgenes (hDAT or hDAT T356M) were cloned into pBI-UASC (Wang *et al.*, 2012) and constructs were injected into embryos from M{vas-int.Dm}ZH-2A, M{3xP3-RFP.attP'}ZH-22A (BI 24481). Initial potential transformants were isolated and selected.

Behavioral analysis

Three-day-old males were collected and placed into tubes with food for 72 hours. Locomotion was recorded by beam breaks and analyzed using equipment/software from Trikinetics (www.trikinetics.com). For the AMPH-induced locomotion, males were starved for six hours and then fed sucrose (5 mM) containing either AMPH (10 mM) or vehicle. Data were analyzed by One-way ANOVA followed by a Newman-Keuls Multiple Comparison Post-test.

Clinical information

Proband (male) is the eldest of two children and heterozygous for the mutation described herein.

Patient ID: AC04-0029-01 (proband)

Event: *SLC6A3 de novo* missense (T356M) mutation

At the time of testing, patient was a 66-69-month-old non-Hispanic male Caucasian diagnosed with autism (on both ADOS and ADIR). Maternal interview on pregnancy provided the following details: Mother experienced anemia during pregnancy (gestational age = 39 weeks). Labor was induced (use of Pitocin) because of failure to progress (Note: no C-section was done). Child was born 8 lbs 6 oz (134 ounces), with no other delivery issues.

Subset and composite scores on the Wechsler Preschool and Primary Scale of Intelligence (WPPSI) indicate normal intelligence. Full Scale IQ was Average (94), and the subsets of Verbal-IQ and Performance-IQ was scored as Average (101) and Low Average (86) respectively, indicating normal intelligence.

ADIR revealed deficits across all four subsets: (1) Reciprocal Social Interaction (score=13; cutoff=10); (2) Abnormalities in Communication (score=13; cutoff=8); (3) Restricted, Repetitive and Stereotyped Patterns of Behavior (score=4; cutoff=3); (4) Development Evident at or before 36 Months (score=1; cutoff=1).

Patient experienced a delay in speech requiring therapy. No history of seizures, gastrointestinal conditions, sleep deficits, and no diet restrictions. Currently taking multivitamins, with no use of other medications (besides amoxicillin, Tylenol, and Benadryl).

No family history for psychiatric illness requiring hospitalization. Known history of Asperger's Disorder (Mother's cousin's son), and depression (Father's paternal uncle).

Patient ID: AC04-0029-02 (father)

Father is an adult non-Hispanic Caucasian male. Age at conception of proband is 36. Slightly above normative range of intelligence (IQ=118; Wechsler Adult Intelligence Scale). No presence of broader autism phenotype, and no psychiatric medication use current or past. No co-morbid diagnoses. He holds a postgraduate degree and reports an annual household income of $81-101k.

Patient ID: AC04-0029-03 (mother)

Mother is an adult non-Hispanic Caucasian female. Age at conception of proband is 32. Above normative range of intelligence (IQ=131; Wechsler Adult Intelligence Scale); no presence of broader autism phenotype, and no psychiatric medication use current or past. No co-morbid diagnoses. She holds a postgraduate degree and reports an annual household income of $81-101k. No medication use reported for mother before, during, or after pregnancy except for epidural during labor.

Patient ID: AC04-0029-04 (sibling)

Sibling is a non-Hispanic Caucasian 3 year old (37 months) of unspecified sex. Normative intelligence (IQ=118; WPPSI). No behavioral problems reported. No medication use endorsed for current or past. No comorbid diagnoses.

CHAPTER 5

ZN^{2+} REVERSES FUNCTIONAL DEFECITS IN A *DE NOVO* DOPAMINE TRANSPORTER VARIANT ASSOCIATED WITH AUTISM SPECTRUM DISORDER[3]

Abstract

Our laboratory recently characterized a novel autism spectrum disorder (ASD)-associated *de novo* missense mutation in the human dopamine transporter (hDAT) gene SLC6A3 (hDAT T356M). This hDAT variant exhibits dysfunctional forward and reverse transport properties that may contribute to DA dysfunction in ASD. Here, we report that Zn^{2+} reverses, at least in part, the functional deficits of ASD-associated hDAT variant T356M. These data suggest that the molecular mechanism targeted by Zn^{2+} to restore partial function in hDAT T356M may be a novel therapeutic target to rescue functional deficits in hDAT variants associated with ASD.

Introduction

The dopamine (DA) transporter (DAT) tunes DA neurotransmission by active re-uptake of DA from the synapse (Kristensen *et al.*, 2011). Our laboratory has recently characterized the first *de novo* mutation in the human dopamine transporter (hDAT) reported in a patient diagnosed with autism spectrum disorder (ASD), which results in a Thr to Met substitution at site 356 (hDAT T356M). We reported novel and profound functional abnormalities associated with the hDAT *de novo* mutation T356M, resulting in enhancement of non-vesicular, DAT-dependent DA release, referred to as anomalous DA efflux. Our data raise the possibility that anomalous DA efflux (or other disturbances in DA neurotransmission) may represent a complication

[3] The work presented in this chapter is *in press* as Hamilton, P. J.[*], A. Shekar[*], A. N. Belovich, N. Bibus Christianson, N. G. Campbell, J. S. Sutcliffe, A. Galli, H. J.G. Matthies[*] and K. Erreger[*] (2015). "Zn^{2+} reverses functional deficits in a de novo dopamine transporter variant associated with autism spectrum disorder." *Molecular Autism* **6**:8 [*] denotes equal contributions.

relevant for behavioral abnormalities in ASD. Extracellular zinc (Zn^{2+}) inhibits DA uptake (Norregaard *et al.*, 1998). Three amino acid side chains have been identified in DAT which coordinate zinc: H193 in extracellular loop 2 (EL2), H375 in the first helical part of extracellular loop 4 (EL4A), and E396 in the second helix of extracellular loop 4 (EL4B) (Norregaard *et al.*, 1998, Loland *et al.*, 1999). Structural data from the DAT-homolog LeuT in the inward- and outward-facing conformation suggest that the relative orientation of H375 and E396 shifts during the transport cycle (Krishnamurthy *et al.*, 2012).

hDAT T356M displays decreased forward and reverse-transport function compared with wild-type hDAT (Hamilton and Campbell *et al.*, 2013). The reduced transport capacity of the mutant was not associated with a reduction in hDAT surface expression. Amphetamine (AMPH) is a psychostimulant that targets the hDAT causing reverse transport of DA (DA efflux) (Sulzer *et al.*, 2005). hDAT T356M exhibits impaired AMPH-induced DA efflux. Here, we show that the presence of Zn^{2+} partially rescues both DA uptake and the AMPH-induced DA efflux impairments of hDAT T356M. Zn^{2+} diminishes the anomalous DA efflux property of the hDAT T356M, which might account for its ability to partially rescue transporter functions. Rescue of hDAT function by Zn^{2+} might reveal a new molecular mechanism to target for pharmacological intervention in patients with ASD.

Results

Zn^{2+} enhances [^{3}H]DA uptake in hDAT T356M

CHO cells were transiently transfected with either wild-type hDAT or hDAT T356M. Cells were incubated with 50 nM [^{3}H]DA at 37 °C for 5 min in the presence of varying concentrations of Zn^{2+}. Consistent with previous reports (Norregaard *et al.*, 1998, Loland *et al.*, 1999), Zn^{2+} decreases the DA uptake rate for wild-type hDAT (**Fig. 35A**, filled squares). In contrast, for

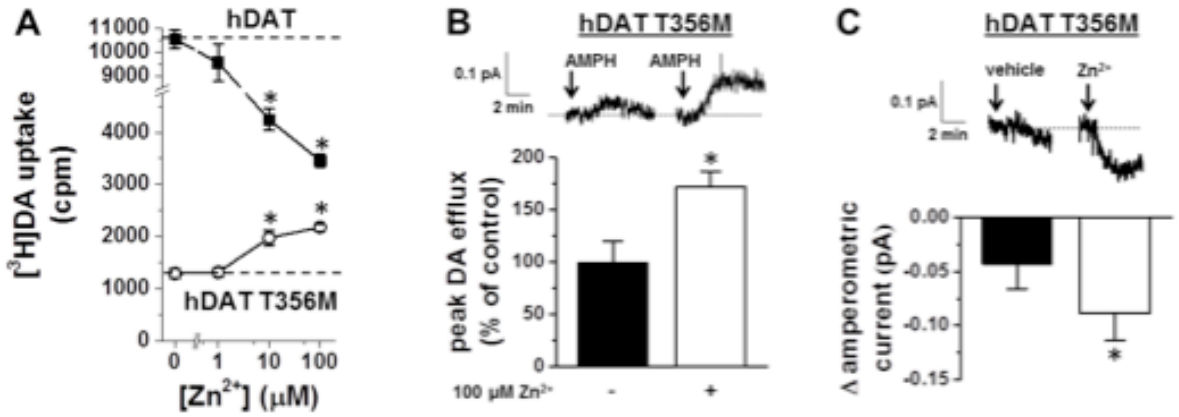

Figure 35. Zn^{2+} partially reverses the hDAT T356M deficits in [^{3}H]DA uptake and AMPH-mediated efflux. Methods were as previously described in Hamilton and Campbell *et al.,* 2013. **(a)** [^{3}H]DA uptake counts (cpm) are plotted for hDAT and hDAT T356M over a range of Zn^{2+} concentrations. While Zn^{2+} inhibits hDAT [^{3}H]DA uptake, Zn^{2+} instead increases hDAT T356M [^{3}H]DA uptake (* = $p < 0.05$ by one-way ANOVA followed by Dunnett's test compared to 0 Zn^{2+} control; n = 4). **(b)** (*Top*) Representative AMPH-induced amperometric currents (reflecting DA efflux) are displayed in the presence or absence of 100 μM Zn^{2+}. Arrows indicate application of 10 μM AMPH. Bottom: maximal DA efflux amperometric current recorded in the presence of Zn^{2+} normalized to maximal current recorded in the presence of vehicle. (* = $p < 0.05$ by Student's t-test; n = 5).

hDAT T356M cells, Zn^{2+} increases DA uptake, partially reversing the functional deficit of this variant (**Fig. 35A**, open circles).

Zn^{2+} enhances AMPH-induced DA efflux in hDAT T356M

To specifically measure reverse transport, DA was loaded into the cytoplasm of hDAT T356M cells by a whole-cell patch clamp pipette held in current-clamp mode. This configuration supplies intracellular DA directly to the cell independent of forward transport by hDAT and allows the cell to control its membrane voltage. The whole-cell patch pipette was filled with an internal solution containing 2 mM DA as described previously (Hamilton and Campbell *et al.*, 2013). DA efflux in response to 10 μM AMPH was measured by amperometry in the presence of 100 μM Zn^{2+} or vehicle control (Hamilton and Campbell *et al.*, 2013). Representative amperometric traces are shown in **Figure 35B** (top). The peak of DA efflux normalized to vehicle control is shown in **Figure 35B** (bottom). Zn^{2+} increases AMPH-induced DA efflux in hDAT T356M compared to vehicle control (**Fig. 35B**), indicating an enhancement of reverse transport DA in the presence of Zn^{2+}. For comparison, Zn^{2+} partially rescues AMPH-induced DA efflux for hDAT T356M to a level of 48% ± 12% of wild-type hDAT AMPH-induced DA efflux (Hamilton and Campbell *et al.*, 2013).

Zn^{2+} decreases baseline anomalous DA efflux in hDAT T356M

Using the whole-cell patch clamp technique coupled to amperometry, the effect of 100 μM Zn^{2+} on the baseline (anomalous) DA efflux of hDAT T356M was studied. The whole-cell patch pipette delivered intracellular DA into the cell in current-clamp mode. To determine the effect of Zn^{2+} on baseline DA efflux, the change in amperometric current was compared following the application of 100 μM Zn^{2+} or vehicle control. Baseline DA efflux decreased significantly in the presence of Zn^{2+} in comparison with that of vehicle, indicating that Zn^{2+}

inhibits the constitutive DA efflux by hDAT T356M. Representative amperometric traces are shown in **Figure 35C** (top), and mean values are plotted in **Figure 35C** (bottom).

Discussion

Here, we explore the potential for Zn^{2+} in rescuing the biophysical abnormalities in the hDAT variant T356M, which we recently reported in Hamilton et al. (Hamilton and Campbell *et al.*, 2013). These functional deficits in hDAT T356M may contribute to the dysfunction in DA neurotransmission associated with ASD. Zn^{2+} was previously shown to partially restore DA uptake function in DAT mutant Y335A, which exhibits low uptake under basal conditions (Kahlig *et al.*, 2006). Here, we demonstrate that Zn^{2+} reverses deficits in both forward and reverse transport in the T356M variant. Additionally, Zn^{2+} decreases baseline anomalous DA efflux of the hDAT T356M *de novo* mutation, possibly providing an explanation for the positive effects of Zn^{2+} on the uptake and efflux properties of this mutant transporter. This is a novel and intriguing finding in terms of ameliorating irregularities in DAT function in a *de novo* ASD-associated mutation.

T356 is located in transmembrane domain 7, and the hDAT Zn^{2+} binding site spans the spatial micro-environment between the transmembrane helices 7 and 8 and extracellular loop 2 (EL2) (Loland *et al.*, 2002, Stockner *et al.*, 2013). Binding of Zn^{2+} to DAT alters the conformational equilibrium between the inward- and outward-facing state of the DAT (Loland *et al.*, 2002, Stockner *et al.*, 2013). However, mutation of an intracellular tyrosine to alanine (Y335A) converts the inhibitory Zn^{2+} switch into an activating Zn^{2+} switch, whereby Zn^{2+} rescues functions of the Y335A mutant transporter (Kahlig *et al.,* 2006, Loland *et al.*, 2002). Therefore, the functional impact of Zn^{2+} binding to mutant transporters can be different than for wild-type hDAT as we observe here for T356M (**Fig. 35A**). Whereas Zn^{2+} has been suggested to promote

the outward facing conformation of wild-type hDAT, the structural effect of Zn^{2+} binding to hDAT T356M is unknown and remains an interesting topic for future investigation.

Clinical data have previously established that mean serum Zn^{2+} levels are significantly lower in children diagnosed with ASD compared to unaffected children and that there exist disturbances in Zn^{2+} metabolism in patients diagnosed with ASD (Jackson *et al.*, 1978, Faber *et al.,* 2009, Li *et al.*, 2014). hDAT T356M is the first *de novo* DAT mutation found in a patient with ASD, and hDAT T356M functional deficits can partially be rescued by Zn^{2+}. Whether or not Zn^{2+} regulation of hDAT may be directly relevant for the etiology of ASD is presently unknown. However, our work suggests that the molecular mechanism engaged by Zn^{2+} to partially restore function in hDAT T356M may be a novel therapeutic target to rescue, at least in part, functional deficits in hDAT variants associated with ASD.

CHAPTER 6

RARE AUTISM-ASSOCIATED VARIANTS IMPLICATE SYNTAXIN 1 (STX1 R26Q) PHOSPHORYLATION AND THE DOPAMINE TRANSPORTER (HDAT R51W) IN DOPAMINE NEUROTRANSMISSION AND BEHAVIORS[4]

Abstract

Syntaxin 1 (STX1) is a presynaptic plasma membrane protein that coordinates synaptic vesicle fusion. STX1 also regulates the function of neurotransmitter transporters, including the dopamine (DA) transporter (DAT). The DAT is a membrane protein that controls DA homeostasis through the high-affinity re-uptake of synaptically released DA. We adopt newly developed animal models and state-of-the-art biophysical techniques to determine the contribution of the identified gene variants to impairments in DA neurotransmission observed in autism spectrum disorder (ASD). Here, we characterize two independent autism-associated variants in the genes that encode STX1 and the DAT. We demonstrate that each variant dramatically alters DAT function. We identify molecular mechanisms that converge to inhibit reverse transport of DA and DA-associated behaviors. These mechanisms involve decreased phosphorylation of STX1 at Ser14 mediated by casein kinase 2 as well as a reduction in STX1/DAT interaction. These findings point to STX1/DAT interactions and STX1 phosphorylation as key regulators of DA homeostasis. We determine the molecular identity and the impact of these variants with the intent of defining DA dysfunction and associated behaviors as possible complications of ASD.

[4] The work presented in this chapter is *in press* as Cartier E.[*], P. J. Hamilton[*], A. N. Belovich, A. Shekar, N. G. Campbell, C. Saunders, T. F. Andreassen, U. Gether, J. Veenstra-Vanderweele, J. S. Sutcliffe, P. G. Ulery-Reynolds, K. Erreger[#], H. J.G. Matthies[#] and A. Galli[#] (2014). "Rare Autism-Associated Variants Implicate Syntaxin 1 (STX1 R26Q) Phosphorylation and the Dopamine Transporter (hDAT R51W) in Dopamine Neurotransmission and Behaviors. *EBioMedicine (Lancet*) **2**(2): 135-146. [*] and [#] denote equal contributions.

Introduction

Autism spectrum disorder (ASD) is defined by deficits in social communication and by the presence of restricted and repetitive behaviors, which are often the first signs of ASD (Rowberry *et al.,* 2014, Wolff *et al*., 2014). Increased striatal size is among the most consistent neuroimaging findings in ASD, and increased size and growth of the striatum, a dopamine (DA) enriched brain region, have been associated with severity of repetitive behaviors (Langen *et al*., 2007, Langen *et al*., 2009, Langen *et al.,* 2014, Hollander *et al*, 2015). Consistent with the involvement of striatal dysfunction in ASD, recent studies have found that individuals with ASD display diminished response to reward (Dichter *et al*., 2012, Damiano *et al*., 2012, Lin *et al*., 2012) which stems from striatal hypofunction (Kohls *et al.,* 2013, Kohls *et al.,* 2014). Striatal DA input has important roles in reward, movement, and habit (Zald *et al.,* 2004, Howe *et al.,* 2011, Howe *et al.,* 2013). Importantly, excessive striatal dopaminergic signaling results in repetitive behavior (Fasano and Petrovic, 2010).

The DA transporter (DAT) shapes striatal DA signaling via re-uptake of synaptically released DA (Kristensen *et al*., 2011). In addition to its role in vesicular fusion, the plasma membrane protein syntaxin 1 (STX1) plays a pivotal role in regulating DAT functions (Binda *et al*., 2008), and it has been observed to regulate other neurotransmitters: sodium symporters (NSS) (Quick, 2002, Quick, 2003, Quick, 2006, Dipace *et al.,* 2007). Therefore, at the dopaminergic synapse, in addition to synaptic release, the actions of STX1 may regulate DAT functions and, as a consequence, DA neurotransmission and associated behaviors.

ASD is associated with variants in several genes of the DA network, including those encoding STX1 (Nakamura *et al*., 2008, Nakamura *et al*., 2011, Durdiakova *et al*., 2014), the DAT (Hamilton *et al.,* 2013, Bowton *et al*., 2014), DA receptors, as well as enzymes involved in DA metabolism (Hettinger *et al*., 2012, Qian *et al*., 2013, Reiersen and Todorov, 2011, Yoo *et*

al., 2013, Nguyen *et al*., 2014). Altered gene expression of *STX1A* has also been described in post-mortem brain and in lymphocytes from people with ASD (Nakamura *et al*., 2008, Nakamura *et al*., 2011). These data point to DA dysfunction as a potential complication and possible risk factor for ASD, but without a clear understanding of the underlying mechanisms.

Here, we have identified rare, inherited, functional missense variants in the gene that encodes STX1 (*STX1A*; resulting in an Arg to Gln substitution at site 26) and in the gene that encodes DAT (*SLC6A3*; resulting in an Arg to Trp substitution at site 51) in separate individuals with ASD. Among the different DAT functions, reverse transport of DA has emerged as a contributing factor in DA neurotransmission and remains incompletely understood (Leviel, 2011). Both of these variants disrupt the molecular mechanisms of reverse transport of DA, resulting in DA dysfunction and associated behavioral abnormalities. To mechanistically characterize these variants, we identify novel molecular events involved in the STX1 regulation of DAT. Our results suggest a coordinated molecular network, including STX1 and DAT that might contribute to disruption of dopaminergic signaling in individual with ASD.

Results

Autism-related hDAT and STX1 variants alter DA transport

Exome capture and sequencing analysis identified two families harboring separate rare and inherited SNPs. One family harbors a single nucleotide variant (SNV) in the gene that encodes hDAT (*SLC6A3*; resulting in an Arg to Trp substitution at site 51; hDAT R/W) (**Fig. 36a**, left panel). The other family harbors a SNV in the gene that encodes STX1A (*STX1A*; resulting in an Arg to Gln substitution at site 26; STX1 R/Q) (**Fig. 36a**, right panel). Neither of these SNVs were found in control samples (n = 1463) and were not deposited in the NHLBI Exome Sequencing Project (URL: http://evs.gs.washington.edu/EVS/) [3 (November, 2014) accessed].

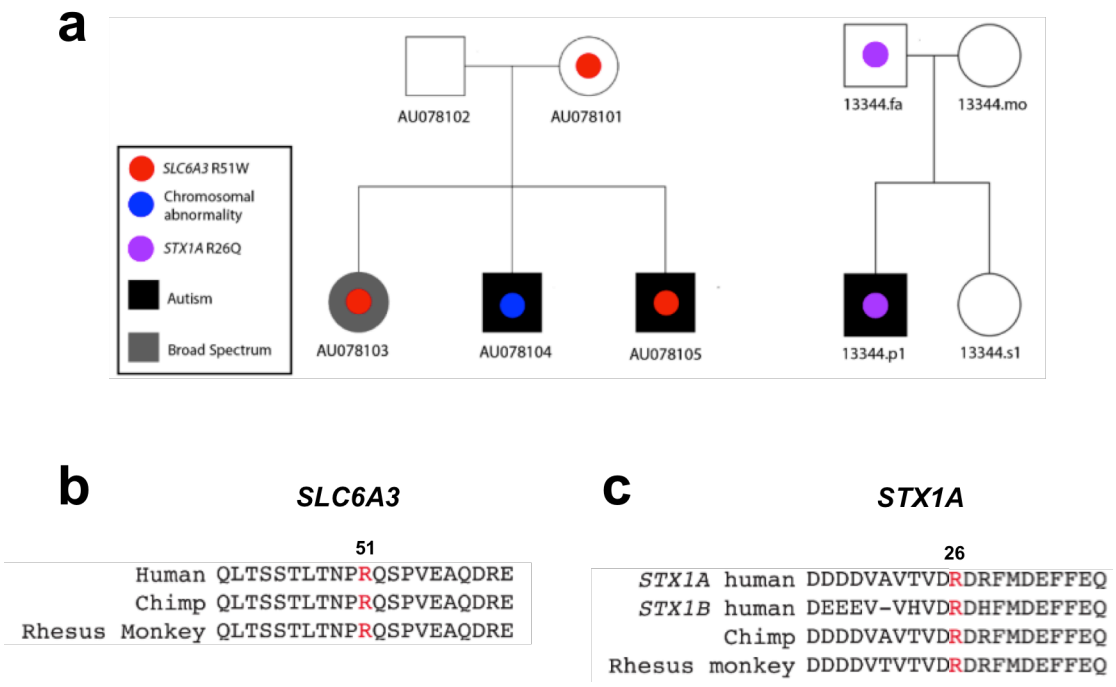

Figure 36. Pedigree and cross-species conservation of hDAT R/W and STX1 R/Q. **(a)** Variant inheritance is shown for the families harboring the hDAT R/W and the STX1 R/Q genotypes. Filled symbols indicate individuals with an ASD diagnosis, while open symbols reflect individuals without an ASD diagnosis. **(b)** Alignment of the DAT amino acid sequence across multiple species. Arginine 51 is represented in red. **(c)** Alignment of the STX1 amino acid sequence across isoforms and multiple species. Arginine 25 is represented in red.

The family harboring the *STX1A* R/Q variant is in a cohort of families belonging to the Simons Simplex Collection (SSC), a well-characterized ASD collection. The family harboring the *SLC6A3* R/W variant is in the cohort of families studied by the Autism Sequencing Consortium (ASC). Details on ASC samples and characteristics have been previously published (Neale *et al*, 2012). The ADIR scores are presented in table format in **Table 3**. Thus, we are classifying these variants as ASD-specific. The hDAT Arg51 is located at the N-terminus in a region highly conserved across multiple species (**Fig. 36b**). STX1A Arg26 is located at the N-terminus and is also conserved across several species as well as in other STX1 isoforms, including STX1B (**Fig. 36c**). The two redundant neuronaThil STX1 isoforms (STX1A and STX1B) are 84% identical. Both isoforms are present in DA neurons and striatal DA terminals and colocalize with DAT (**Fig. 37**). In this study we utilize STX1B, here simply referred as STX1.

To evaluate whether the STX1 R/Q variant promotes DA dysfunction, we determined the impact of this variant on a key STX1 regulatory site (Ser14) implicated in neuropsychiatric disorders (Castillo *et al.,* 2010) and hDAT function. hDAT cells (see Methods) expressing STX1 R/Q show reduced STX1 phosphorylation at Ser14 (**Fig. 38a**). One function of STX1 is to regulate the DAT-mediated reverse transport of DA in response to AMPH (Binda *et al.,* 2008) Therefore, we used AMPH as a tool to probe whether STX1 R/Q has an altered ability to regulate DA efflux, measured by amperometry in hDAT cells. The amperometric probe, a carbon fiber electrode juxtaposed to the cell membrane, measures DA efflux by oxidation/reduction reactions, with DA efflux represented as a positive current. hDAT cells expressing STX1 R/Q display a significantly reduced AMPH-induced DA efflux as compared to hDAT cells expressing STX1 (**Fig. 38b**). It is important to point out that in hDAT cells expressing STX1 R/Q, the V_{max} of DA uptake was significantly increased, whereas the K_m of DA was not significantly different from that of hDAT cells expressing STX1 (**Fig. 38c,** top). A representative

ASD collection	Identifier	Sex	Diagnosis	Y.O.B.	Social (cutoff=10)	Communication (cutoff=8)	Repetitive (cutoff=3)	Evident before 36 months	Verbal
Autism Sequencing Consortium	AU078103	Female	Spectrum	1993	9	6	6	yes	yes
Autism Sequencing Consortium	AU078104	Male	Autism	1995	20	22	8	yes	yes
Autism Sequencing Consortium	AU078105	Male	Autism	1997	21	15	7	yes	yes
Simons Simplex Collection	13344.p1	Male	Autism	1998	24	14	11	yes	yes
Simons Simplex Collection	13344.s1	Female	Designated sibling	2000	N/A	N/A	N/A	N/A	N/A

Table 3. Autism Diagnostic Interview-Revised (ADI-R) algorithm domain scores. Trained clinicians conducted the ADI-R and algorithm scores were calculated. ADIR subdomain scores with diagnostic cutoffs are shown along with the autism cohort, subject identifier, sex, year of birth and verbal capabilities of the individuals. Individuals received a diagnosis of “autism” or “spectrum” based on measures from the ADIR and Autism Diagnostic Observation Schedule (ADOS).

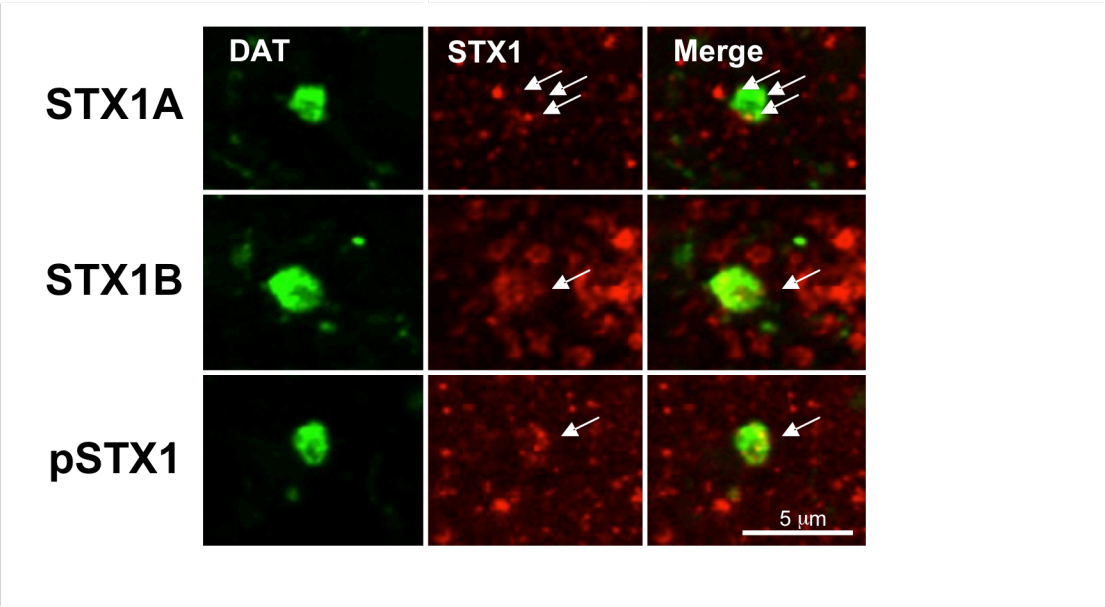

Figure 37. STX1A, STX1B and p-STX1 colocalize with DAT in the striatum. Striatal slices were reacted with anti-DAT antibodies (green) and the appropriate anti-STX1 antibodies (red) as indicated, processed, and imaged by confocal microscopy.

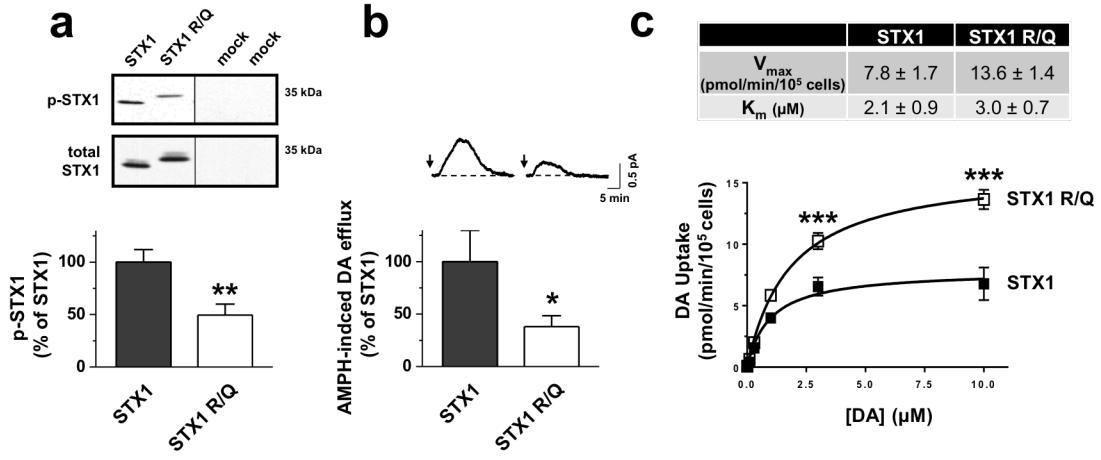

Figure 38. STX1 R to Q missense mutation decreases STX1 phosphorylation and reverse transport of DA without decreasing DA uptake. (a) Top: stably transfected hDAT cells expressing either STX1 or STX1 R/Q were immunoblotted with a phospho-specific antibody directed against STX1 at Ser14 (top lane). The mock transfection of GFP alone (mock) supports absence of non-specific binding. Bottom lane shows total STX1 proteins. Bottom: quantitation of band intensities of phospho-STX1 (p-STX1) normalized to the respective total STX1 and expressed as a percentage STX1 (** = $p < 0.01$ by Student's t-test; n = 5, in triplicate). **(b)** Top: representative AMPH-induced DA efflux recorded from stably transfected hDAT cells expressing either STX1 or STX1 R/Q. Arrows indicate application of 10 μM AMPH. Bottom: quantitation of AMPH-induced DA efflux. Data are represented as maximal current expressed as percent of the current recorded in hDAT cells expressing STX1 (* = $p < 0.05$ by Student's t-test; n = 7). **(c)** STX1 R/Q enhances DAT-mediated DA uptake. Top: kinetic parameters (V_{max} and K_m) for stably transfected hDAT cells expressing either STX1 or STX1 R/Q (V_{max}: $p < 0.05$ by Student's t-test; n = 3, in triplicate; K_m: $p > 0.46$ by Student's t-test; n = 3, in triplicate). Bottom: representative plot of [^{3}H]DA uptake kinetics in stably transfected hDAT cells expressing STX1 (filled squares) and STX1 R/Q (empty squares) cells (*** = $p < 0.001$, by two-way ANOVA followed by Bonferroni post-test; in triplicate).

plot of DA uptake kinetics is shown in **Figure 38c** (bottom). These data indicate that the STX1 R/Q variant asymmetrically regulates hDAT function by selectively impairing DA efflux.

In order to determine whether other ASD-associated variants can disrupt DAT function by parallel mechanisms to those of STX1, we explored changes in hDAT function in cells expressing hDAT R/W. The AMPH-induced reverse transport of DA was reduced in hDAT R/W cells with respect to hDAT cells (**Fig. 39a**). These data parallel the reduction in DA efflux observed in hDAT cells expressing the STX1 R/Q variant (**Fig. 38b**). This reduction in AMPH-induced DA efflux in the hDAT R/W is not mirrored by a significant reduction in DA uptake or DA apparent affinity (**Fig. 39b**), indicating the hDAT R/W variant also asymmetrically regulates hDAT function by selectively impairing DA efflux.

Previously, we determined that reverse transport of DA induced by AMPH is tightly regulated by the interaction of STX1 at the DAT N-terminus (Binda *et al.,* 2008). Therefore, we explored whether the reduced reverse transport of DA in hDAT R/W cells stemmed from a decreased association of STX1 to hDAT R/W. We immunoprecipitated hDAT and immunoblotted the immunoprecipitates for STX1 (**Fig. 39c**). The amount of STX1 recovered in the DAT immunoprecipitates was reduced in the hDAT R/W cells compared to the hDAT cells (**Fig. 39c**, IB: STX1). In the absence of antibody against DAT, no signal was detected for STX1 in the immunoprecipitates (**Fig. 39c**, beads). The total STX1 and hDAT in the hDAT R/W cells was not decreased with respect to hDAT cells (**Fig. 39c**, total STX1 and total hDAT). These data demonstrate that the hDAT R/W variant has a reduced STX1/DAT interaction. Quantitation of multiple experiments is shown in the bar graph of **Figure 39c**. These data highlight that the ASD-associated hDAT and STX1 variants both impair reverse transport of DA without inhibiting DAT-mediated DA uptake functions.

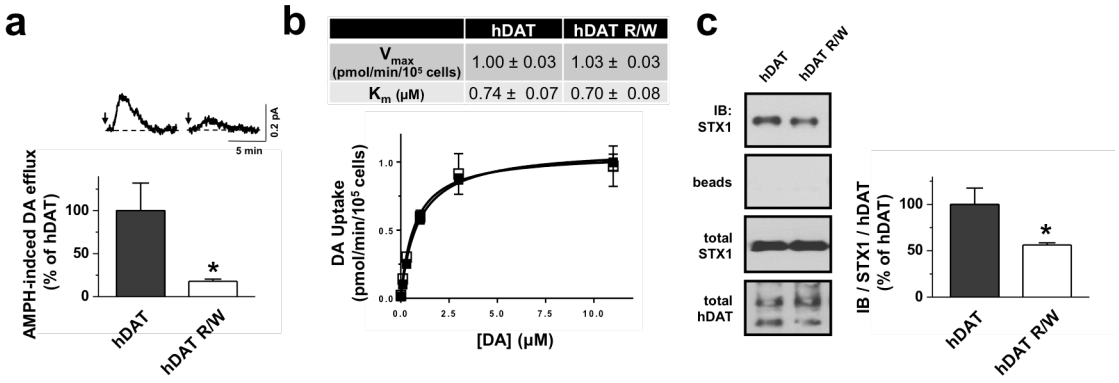

Figure 39. hDAT R to W missense mutation has decreased STX1 association, reduced reverse transport of DA, but normal DA uptake. (a) Top: representative AMPH-induced DA efflux recorded from hDAT or hDAT R/W cells expressing STX1. Arrows indicate application of 10 μM AMPH. Bottom: quantitation of AMPH-induced DA efflux. Data are represented as maximal current expressed as percent of the current recorded in hDAT cells (* = $p < 0.05$ by Student's t-test; n = 5). **(b)** hDAT R/W exhibits normal DA uptake function. Top: kinetic parameters (V_{max} and K_m) for hDAT and hDAT R/W (V_{max}: $p > 0.92$ by Student's t-test; n = 3, in triplicate; K_m: $p > 0.62$ by Student's t-test; n = 3, in triplicate). Bottom: representative plot of [^{3}H]DA uptake kinetics in hDAT (filled squares) and hDAT R/W (empty squares) cells ($p > 0.05$, by two-way ANOVA followed by Bonferroni post-test; in triplicate). **(c)** Top: hDAT immunoprecipitates from either hDAT or hDAT R/W cells expressing STX1 were immunoblotted for STX1 (top lane). The beads fraction supports the absence of non-specific binding. Third lane shows an immunoblot for total STX1 proteins. Bottom lane shows an immunoblot for total hDAT proteins. Bottom: quantitation of hDAT pull down band intensities normalized to the respective total STX1 and total hDAT; expressed as a percentage hDAT cells (* = $p < 0.05$ by Student's t-test; n = 5).

STX1 phosphorylation regulates STX1/DAT interaction

STX1 is phosphorylated at Ser14 by the kinase CK2 (Hirling and Scheller, 1996, Foletti *et al.,* 2000), a posttranslational modification involved in the functional regulation of STX1 (Khelashvili *et al.,* 2012, Dubois *et al.,* 2002). Figure 38a shows that the STX1 R/Q variant has reduced phosphorylation at Ser14. Therefore, we sought to determine the functional consequences of impaired Ser14 phosphorylation. First, we demonstrated that the highly selective ATP/GTP-competitive inhibitor of CK2, 4,5,6,7-tetrabromobenzotriazole (TBB, 10 μM), effectively reduces p-STX1 in hDAT cells. p-STX1 levels were determined either upon TBB treatment or control conditions with a phospho-specific antibody that recognizes phosphorylation of Ser14 (Castillo *et al.,* 2010) (**Fig. 40a**). TBB significantly decreases basal levels of p-STX1, demonstrating that CK2 regulates the phosphorylation state of STX1 at Ser14. Next, we investigated whether STX1 phosphorylation at Ser14 regulates the association of STX1 with the DAT. hDAT cells were treated with either TBB (10 μM for 20 min) or vehicle control, and the cell lysates were immunoprecipitated for DAT and subsequently immunoblotted for STX1. Inhibition of STX1 phosphorylation with TBB reduces STX1/DAT association (**Fig. 40b**), demonstrating that phosphorylation promotes the STX1/DAT interaction. TBB (10 μM for 20 min) did not change the level of DAT available at the cell surface (hDAT surface expression for TBB exposure was 89.0 ± 12.9% of vehicle control; $p > 0.40$ by Student's t-test; $n = 4$), indicating that the reduced STX1/DAT interaction following CK2 inhibition is not due to DAT trafficking away from the plasma membrane. Collectively, these results are consistent with a coordinated signaling complex whereby phosphorylation of STX1 at Ser14 promotes its association with DAT.

STX1 can be phosphorylated at residues other than Ser14. For example, casein kinase 1 can promote STX1 phosphorylation at Thr21 (Dubois *et al.,* 2002). Therefore, we validated whether the level of phosphorylation of Ser14 alone supports STX1/DAT interactions. We

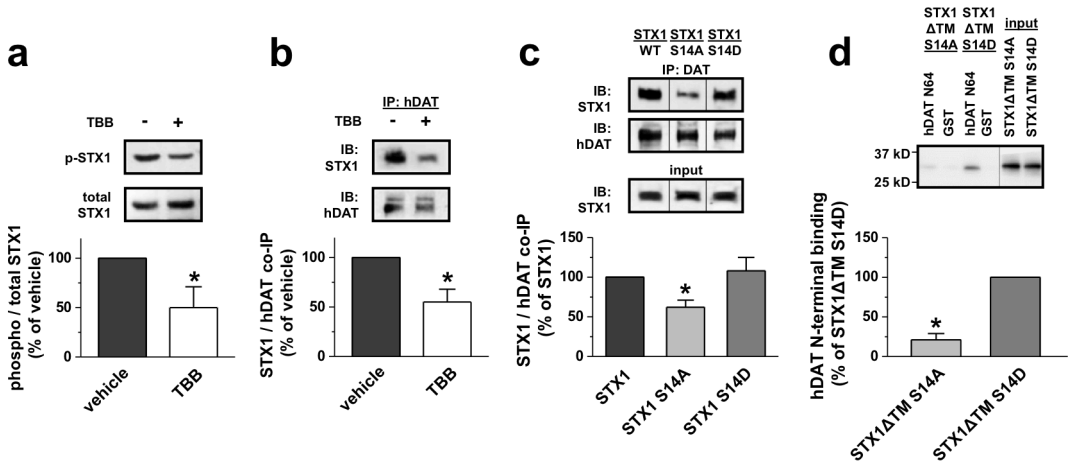

Figure 40. CK2-mediated phosphorylation of STX1 at S14 promotes STX1/DAT interaction. (a) Stably transfected hDAT cells transfected with STX1 were treated with either vehicle or 10 μM TBB for 20 minutes. STX1 proteins were immunoblotted for p-STX1 (with a phospho-specific antibody directed against Ser14) and STX1. p-STX1 band densities were normalized to the corresponding total STX1 band densities and expressed as a percentage of vehicle control. CK2 inhibition with TBB significantly decreased the levels of p-STX1 (* = $p < 0.05$ by Student's t-test; n = 4). **(b)** Stably transfected hDAT cells transfected with STX1 were treated with either vehicle or 10 μM TBB for 20 minutes. hDAT proteins were immunoprecipitated and immunoblotted for STX1 and DAT. STX1 band densities were normalized to DAT and expressed as a percentage of vehicle control. CK2 inhibition significantly decreased STX1/DAT interaction (* = $p < 0.05$ by Student's t-test; n = 4). **(c)** Stably transfected hDAT cells were transfected with either STX1, STX1 S14A, or STX1 S14D. hDAT immunoprecipitates were immunoblotted for either STX1 (top band) or hDAT (middle band). Input (bottom band) serves as loading control. All STX1 isoform band densities were normalized to hDAT and expressed as a percentage of STX1. STX1 S14A displays a significantly decreased association with DAT (* = $p < 0.05$ by one-way ANOVA followed by Newman-Keuls Multiple Comparison Test; n = 6). **(d)** Purified STX1ΔTM peptides (S14A or S14D) were incubated with a GST fusion protein of the first 64 amino acids of the hDAT N-terminus (N64) or with GST alone. The samples were then immunoblotted for STX1. STX1 band densities were expressed as a percentage of STX1ΔTM S14D. STX1ΔTM S14A displays reduced binding to the hDAT N-terminus (* = $p < 0.05$ by Student's t-test; n = 5).

generated STX1 constructs that either prevent Ser14 phosphorylation, by mutating Ser14 to Ala (STX1 S14A), or mimic Ser14 phosphorylation, by mutating Ser14 to Asp (STX1 S14D). We performed immunoprecipitation experiments in hDAT cells transfected with the different STX1 constructs. We observed that the STX1/DAT association is blunted in hDAT cells expressing STX1 S14A as compared to hDAT cells expressing STX1 (**Fig. 40c**). Furthermore, the pseudo-phosphorylated STX1 S14D exhibits increased interaction with hDAT with respect to STX1 S14A. Thus, phosphorylation of STX1 at Ser14 supports STX1/DAT association. Plasma membrane levels of hDAT, as measured by biotinylation, were not altered by the expression of either STX1 S14A or STX1 S14D when compared to STX1 (STX1 S14A: hDAT surface expression was 101 ± 39% and STX1 S14D: hDAT surface expression was 88 ± 16% relative to hDAT cells expressing STX1; $p > 0.89$ by one-way ANOVA; $n = 5–6$).

To determine whether Ser14 phosphorylation regulates the direct association between STX1 and DAT, we used an in vitro GST pull-down assay modified from Binda *et al.* (2008). which previously demonstrated that the hDAT N-terminus directly interacts with STX1 (Binda *et al.,* 2008). GST hDAT N-terminal fusion proteins (hDAT N64, see the Materials and Methods section) were used to pull down recombinant soluble constructs of STX1 lacking the transmembrane domain (STX1ΔTM) with Ser14 mutated to Ala (STX1ΔTM S14A) or Asp (STX1ΔTM S14D) (**Fig. 40d**). hDAT N64 robustly pulled down STX1ΔTM S14D. However, hDAT N64 pull down of STX1ΔTM S14A was dramatically blunted. GST alone did not pull down either STX1ΔTM construct. Quantitative analysis of band densities in **Figure 40d** demonstrates that the STX1ΔTM S14A peptide exhibits a significantly reduced direct association with the DAT N-terminus relative to the STX1ΔTM S14D peptide. Input bands show that the STX1ΔTM constructs were of expected size and exhibited minimal degradation. These data further support the notion that STX1 phosphorylation at Ser14 is a key regulator of the dynamic, direct interaction between STX1 and DAT.

STX1 phosphorylation supports reverse transport of DA

Figure 38b shows that the STX1 R/Q variant promotes a reduction in DA efflux. Therefore, it is possible that the CK2-mediated phosphorylation of STX1 at Ser14 support reverse transport of DA. We first determined whether AMPH causes an increase in STX1 phosphorylation. To test this, p-STX1 levels were measured in hDAT cells transfected with STX1 and treated either with vehicle, AMPH, or AMPH in the presence of TBB (**Fig. 41a**). AMPH treatment increased the level of p-STX1 with respect to vehicle control. Pre-treatment of cells with TBB (10 μM for 20 min) prevented the AMPH-induced phosphorylation of STX1 at Ser14, demonstrating that AMPH induces phosphorylation of STX1 in a CK2-dependent manner. Quantitation of the band density of p-STX1, normalized to total STX1 and expressed as a percent of control is shown in **Figure 41a** (bottom).

These findings implicate CK2 and phosphorylation of STX1 at Ser14 as possible novel molecular mediators of reverse transport of DA. Thus, we investigated the role of CK2 function and STX1 phosphorylation at Ser14 in AMPH-induced DA efflux. DA efflux was quantified by amperometry in hDAT cells expressing STX1 under control conditions or pharmacological inhibition of CK2 with TBB (10 μM for 20 min). TBB reduced AMPH-induced DA efflux as compared to vehicle control treated cells (**Fig. 41b**). These data support our hypothesis that STX1 phosphorylation at Ser14 regulates reverse transport of DA. To further test this hypothesis, we determined if the ability of TBB to regulate DA efflux is altered by preventing or mimicking phosphorylation of STX1. We expressed STX1 S14A or STX1 S14D constructs in hDAT cells and measured AMPH-induced DA efflux in the presence or absence of TBB. In hDAT cells expressing STX1 S14A, AMPH-induced DA efflux was not sensitive to pharmacological inhibition of CK2, and the absolute DA efflux in vehicle control was comparable to hDAT cells expressing STX1 that were TBB treated (**Fig. 41c**, compare to **Fig. 41b** TBB treated). Further, in hDAT cells expressing STX1 S14D, AMPH-induced DA efflux was also not

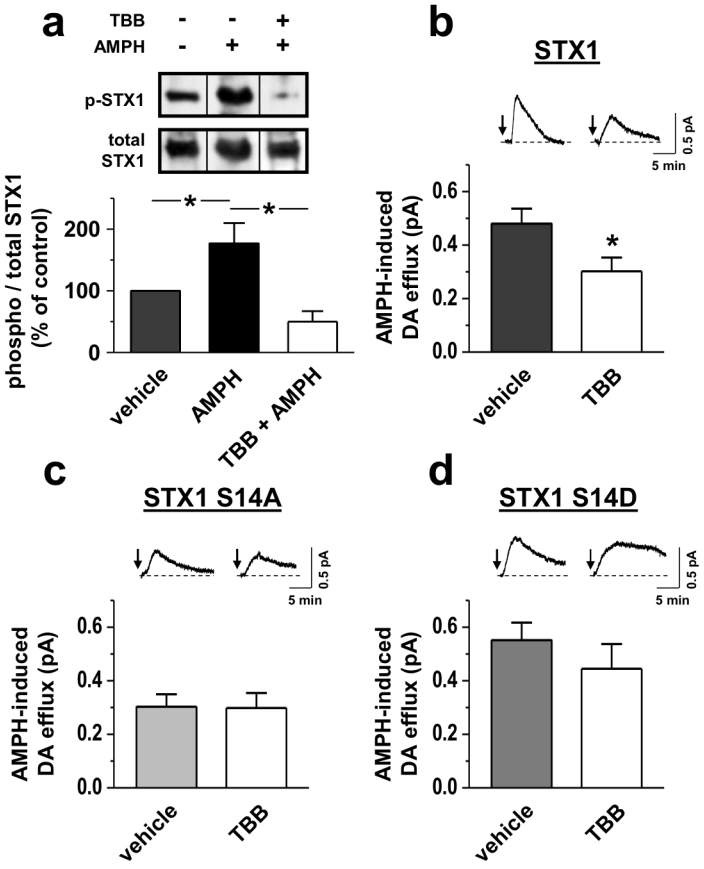

Figure 41. STX1 phosphorylation promotes reverse transport of DA. (a) Top: stably transfected hDAT cells expressing STX1 were treated with either vehicle or 10 μM TBB for 20 minutes. This was followed by an additional treatment with vehicle or 10 μM AMPH for 15 minutes. STX1 immunoprecipitates were immunoblotted for either p-STX1 (Ser14) or STX1. Bottom: the immunoprecipitated band densities were quantified, normalized to the corresponding density of total precipitated STX1, and expressed as a percentage of vehicle control (* = $p < 0.05$ by one-way ANOVA followed by Newman-Keuls Multiple Comparison Test; n = 3). **(b)** Representative AMPH-induced DA efflux recorded from stably transfected hDAT cells expressing STX1 treated with either vehicle or 10 μM TBB for 20 minutes just before the amperometric recordings. Arrows indicate application of 10 μM AMPH. Bottom: quantitation of AMPH-induced DA efflux. Data are represented as maximal oxidative current (* = $p < 0.05$ by Student's t-test; n = 5). **(c)** Representative AMPH-induced amperometric currents recorded from stably transfected hDAT cells expressing STX1 S14A treated with either vehicle or 10 μM TBB for 20 minutes. Arrows indicate application of 10 μM AMPH. Bottom: quantitation of maximal oxidative current ($p > 0.05$ by Student's t-test; n = 4-7). **(d)** Representative AMPH-induced amperometric currents recorded from stably transfected hDAT cells expressing STX1 S14D treated with either vehicle or 10 μM TBB for 20 minutes. Arrows indicate application of 10 μM AMPH. Bottom: quantitation of AMPH-induced DA efflux. Data are represented as maximal oxidative current ($p > 0.05$ by Student's t-test; n = 6).

sensitive to TBB. However, the absolute DA efflux in the presence of TBB was comparable to vehicle treated hDAT cells expressing STX1 (**Fig. 41d**, compare to **Fig. 41b** vehicle treated). These results demonstrate that preventing STX1 phosphorylation (STX1 S14A) parallels pharmacological inhibition of CK2, and mimicking STX1 phosphorylation (STX1 S14D) obscures the ability of TBB to inhibit DA efflux. It also points to the phosphorylation state of STX1 at Ser14 as a determining factor in the magnitude of reverse transport of DA, further supporting our hypothesis that the STX1 R/Q variant alters DA neurotransmission via reduced phosphorylation.

Cultured catecholamine neurons from the superior cervical ganglion (SCG) have large presynaptic boutons that are amenable to imaging approaches, allowing us to determine whether AMPH drives STX1 phosphorylation at these release sites. SCG neurons natively express the NET, which has 66% amino acid sequence homology with the DAT, as well as the accompanying catecholamine presynaptic machinery (Matthies *et al.,* 2009). Here, we utilized confocal imaging of SCG presynaptic boutons coupled with immunofluorescence to reveal the presence of endogenous p-STX1, closely localized to the NET (**Fig. 42a**). Consistent with our findings in hDAT cells (see **Fig. 41a**), AMPH treatment (10 μM for 20 min) enhances STX1 phosphorylation at Ser14 in SCG presynaptic terminals (**Fig. 42b**). SCG cultured neurons also express endogenous CK2α (**Fig. 42c**). Lastly and notably, in mouse striatal slices, there is a similar profile of endogenous STX1 and p-STX1 expression. (**Fig. 42d**). These data present SCG neurons as a biologically relevant preparation in which to observe the functional role of STX1 in reverse transport of DA.

STX1 phosphorylation regulates reverse transport of DA at neuronal release sites

Next, we explored the role of STX1 phosphorylation in DAT-mediated reverse transport of DA at the level of the SCG presynaptic boutons. Since SCG neurons do not natively express

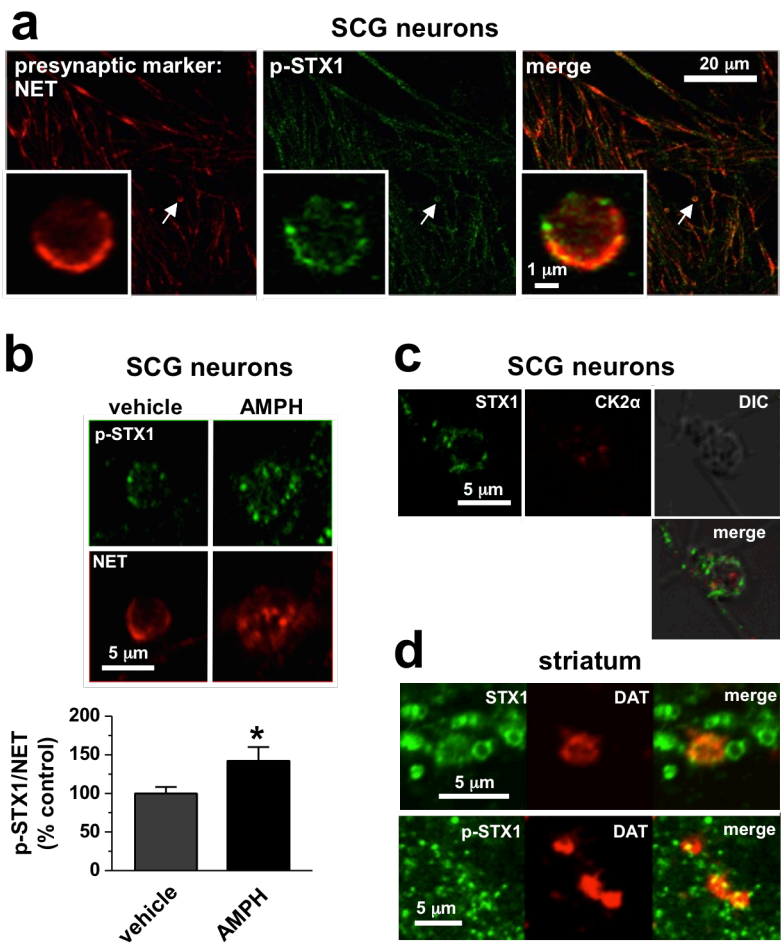

Figure 42. AMPH treatment increases p-STX1 levels in boutons. (a) Mouse superior cervical ganglion (SCG) neurons were fixed and p-STX1 (green) was visualized by immunoflourescence. The norepinephrine transporter (NET, red) was used as a marker of presynaptic boutons. The merge shows that p-STX1 is present in presynaptic boutons of cultured catecholamine neurons. *Inset*: Confocal section of a single presynaptic bouton (arrow). **(b)** Top: SCG neurons were treated with either vehicle or 10 µM AMPH for 20 minutes. Cells were fixed and immunostained for p-STX1 (green) and for the NET (red). AMPH increases the intensity of p-STX1 in presynaptic boutons. Bottom: p-STX1 levels were quantified by the ratio of p-STX1 pixel intensity normalized to NET pixel intensity. AMPH significantly increases the intensity of p-STX1 in presynaptic boutons (* = $p < 0.05$ by Student's t-test; n = 5-6). **(c)** In SCG neurons cultured from NET KO mice, p-Stx1 colocalizes with CK2. **(d)** In mouse striatal slices, DAT co-localizes with STX1 and p-STX1.

DAT, we used neurons cultured from NET knockout mice and transiently transfected with hDAT labeled with a GFP tag (**Fig. 43a**, inset). GFP fluorescence was used to identify neurons positive for hDAT expression. AMPH-induced DA efflux was recorded with amperometry from individual synaptic boutons (**Fig. 43a**). This DA efflux was cocaine sensitive, indicating its DAT dependence (data not shown). TBB (10 μM for 20 min) reduced AMPH-induced DA release as compared to vehicle control (**Fig. 43a**). These data demonstrate, at the level of a single bouton, that CK2 function and STX1 phosphorylation are critical mediators of AMPH-induced DAT-mediated DA release.

We then determined the importance of STX1 for reverse transport of DA in ex vivo preparations. In mouse striatal slices, pre-incubation in botulinum toxin serotype C (BoNT/C, 100 nM for 60 min), a protein known to cleave STX1, inhibits AMPH-induced DA efflux as measured by high speed chronoamperometry (**Fig. 43b**). Importantly, this BoNT/C pre-incubation paradigm was not effective in significantly altering DA uptake (**Fig. 43c**). These data demonstrate the pivotal role of STX1 in supporting DA efflux without altering forward transport of DA in brain tissues.

STX1 phosphorylation and STX1/DAT association regulates dopaminergic behaviors

In adult *Drosophila* males, we developed locomotor assays for an in vivo examination of DAT-mediated reverse transport of DA and the impact of ASD variants on this transport process. First, we explored how impairments in STX1 phosphorylation, which affects STX1/DAT associations, regulate DA-associated behaviors. In *Drosophila*, locomotion requires functional DA neurotransmission (Hamilton and Campbell *et al.,* 2013, Hamilton and Belovich *et al*., 2014, Pizzo *et al.,* 2013). To probe for changes in locomotion, adult males were fed a sucrose solution containing either AMPH (1 mM) or vehicle. We observed that AMPH significantly stimulated locomotion in wild-type (WT) *Drosophila* (**Fig. 44a**). However, AMPH did not significantly

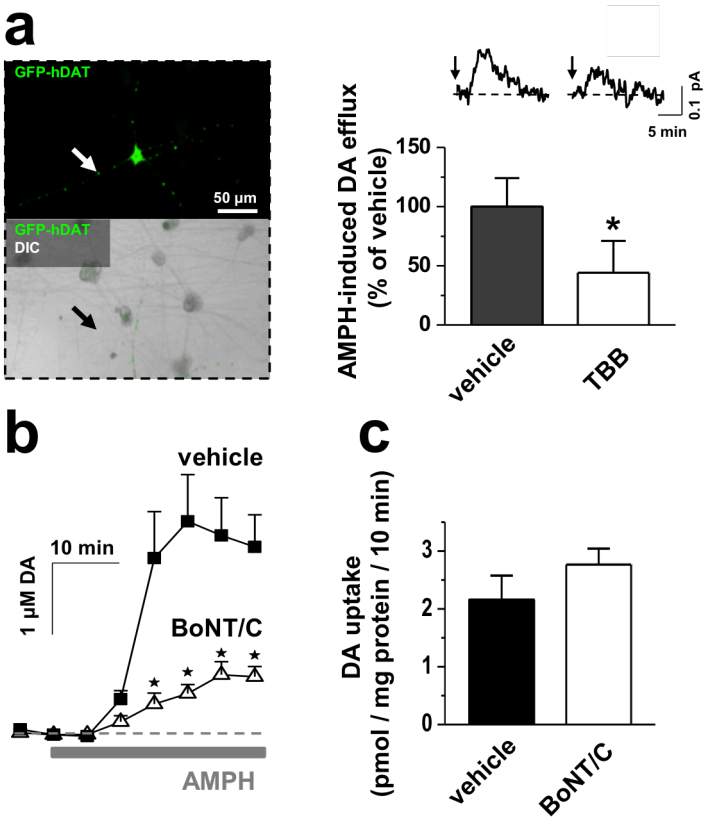

Figure 43. Inhibition of either STX1 phosphorylation or cleavage of STX1 inhibits DA efflux but not uptake. (a) *Inset*: Image of a single GFP-hDAT transfected SCG neuron; arrows indicate the site of amperometric recording (i.e. the presynaptic bouton). Top: representative AMPH-induced amperometric currents recorded from a single presynaptic bouton of SCG neurons expressing GFP-hDAT after treatment with either vehicle or 10 µM TBB for 20 minutes. Bottom: quantitation of the maximal oxidative current normalized to vehicle treatment (* = $p < 0.05$ by Student t-test; n = 5). **(b)** AMPH (10 µM)-induced DA efflux recorded in mouse striatal slices preincubated (1 hr) either with vehicle or BoNT/C (100 nM) (* = $p < 0.05$ by two-way ANOVA; n = 6). **(c)** [3H]DA uptake measure in striatal slices receiving identical treatment as in panel (c) ($p > 0.05$ by Student's t-test; n = 4).

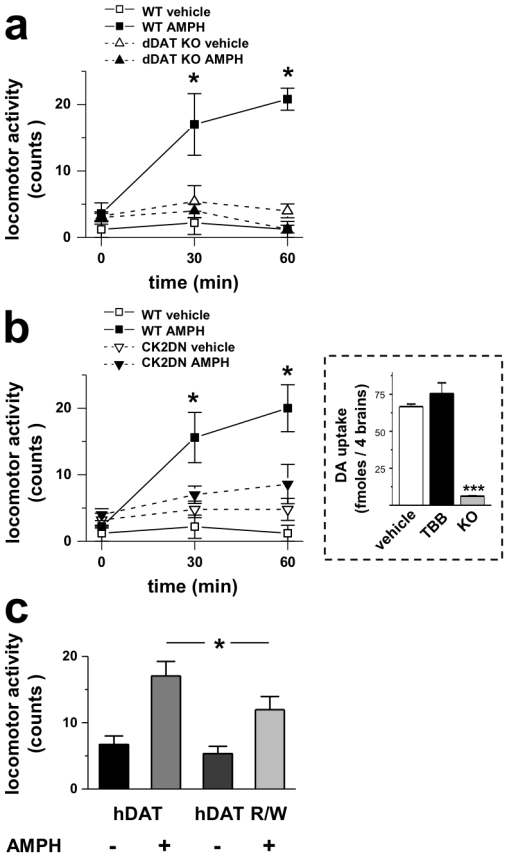

Figure 44. STX1 phosphorylation regulates AMPH-induced behaviors. (a) DAT knockout (KO) flies demonstrate that AMPH-induced locomotor behavior is DAT-dependent. Locomotor activity in response to vehicle (open symbols) or (1mM) AMPH (filled symbols) in either wild-type (WT) (squares) or in DAT KO flies (triangles). WT flies exhibit a significant AMPH-induced increase in locomotion while DAT KO flies do not exhibit this significant increase (* = $p < 0.05$ for vehicle vs AMPH, two-way ANOVA followed by Bonferroni post-test; n = 5). **(b)** *Drosophila* were generated expressing a dominant-negative (DN) version of CK2α expressed specifically in dopaminergic neurons. Locomotor activity in response to vehicle (open symbols) or AMPH (filled symbols) in either wild-type (WT) (squares) or in CK2 dominant negative flies (CK2DN) (triangles). WT flies exhibit a significant increase in AMPH-induced locomotion while CK2DN flies do not (* = $p < 0.05$ for vehicle vs AMPH, two-way ANOVA followed by Bonferroni post-test; n = 5). *Inset:* DA uptake in intact fly brains in the presence of 10 μM TBB or vehicle. The absence of uptake in the dDAT KO fly brains shows the dependence of DA uptake on the dDAT (*** = $p < 0.0001$ by one-way ANOVA followed by Newman-Keuls Multiple Comparison Test; n = 3). **(c)** hDAT R/W expressing flies have blunted locomotor responses to AMPH. Changes in locomotion were determined upon AMPH or vehicle exposure over 30 minutes and calculated as beam crosses (counts). AMPH (1 mM) caused a significant increase in locomotion in both hDAT flies ($p < 0.001$ by one-way ANOVA followed by Newman-Keuls Multiple Comparison Test; n = 24) and hDAT R/W flies ($p < 0.05$ by one-way ANOVA followed by Newman-Keuls Multiple Comparison Test; n = 24). However, in hDAT R/W flies, AMPH exposure led to a reduced increase in locomotion than in hDAT flies (* = $p < 0.05$ by one-way ANOVA followed by Newman-Keuls Multiple Comparison Test; n = 24).

increase locomotion in flies lacking dDAT (DAT KO) (Kume *et al.,* 2005), indicating that AMPH-induced locomotion is a DAT-dependent behavior (**Fig. 44a**). These data strongly support this assay as a model to test the multiple functions of DAT in vivo.

CK2 function promotes STX1 phosphorylation at Ser14, STX1/DAT interaction, and reverse transport of DA. Thus, to probe the behavioral significance of impaired STX1 phosphorylation at Ser14 and STX1/DAT interaction, we evaluated whether inhibited CK2 function alters AMPH-induced locomotion. We expressed a dominant negative form of CK2 (CK2DN) in flies by using the Gal4/UAS system to express a single copy CK2DN in a WT background, selectively in DA neurons. We compared the AMPH-induced behavioral responses of flies expressing CK2DN to WT flies. AMPH did not significantly increase locomotor activity in flies expressing dominant negative CK2 mutant (**Fig. 44b**). Furthermore, vehicle treatment did not modify locomotion of flies expressing CK2DN with respect to WT flies, suggesting that extracellular DA level did not change under basal conditions. Consistent with this, CK2 inhibition by TBB treatment (10 μM for 15 min) did not alter DA uptake in intact *Drosophila* brains (**Fig. 44b**, inset). Importantly, brains obtained from dDAT KO flies show robustly reduced DA uptake, demonstrating the DAT dependence of DA uptake in our newly developed uptake assay. Collectively, these data point to CK2 activity, STX1 phosphorylation at Ser14, and STX1/DAT association as critical mediators of reverse transport of DA and associated behaviors.

Next, we explored how the ASD-associated hDAT R/W variant that impairs STX1/DAT association affects DA-dependent behaviors in our *Drosophila* model system. We expressed hDAT or hDAT R/W in DA neurons of dDAT KO flies as described above. We fed male *Drosophila* a sucrose solution containing either AMPH (1 mM) or vehicle and quantified locomotion in 30-minute intervals. AMPH exposure induced a significantly smaller increase in locomotion in hDAT R/W expressing flies as compared to hDAT expressing flies (**Fig. 44c**,

compare hDAT + AMPH versus hDAT R/W + AMPH). These data are consistent with the reduced ability of AMPH to cause DA efflux in hDAT R/W expressing cells. Basal locomotion of flies expressing hDAT R/W did not significantly differ from hDAT expressing flies.

Discussion

Alterations in DA neurotransmission have been identified in several neuropsychiatric disorders, including ASD (Seeman *et al.,* 1990, Volkow *et al.,* 2007, Cousins *et al.,* 2009, Nguyen *et al.,* 2014). Recently, we demonstrated that an ASD-associated hDAT de novo variant displays dramatically altered DAT function, including constitutive reverse transport of DA, which leads to hyperlocomotion (Hamilton and Campbell *et al*., 2013). Thus, we hypothesized that novel DAT variants (or variant in the genes known to regulate the DAT) that affect DA neurotransmission might contribute to the pathology and/or complications of ASD. We identify and describe two independent gene variants that converge mechanistically to disrupt DAT function and associated behaviors, with distinct mechanisms regulating either STX1 phosphorylation or STX1/DAT interaction.

We found that the STX1 R/Q variant has decreased phosphorylation of Ser14, a key residue involved in the functional regulation of STX1 (Dubois *et al.,* 2002, Khelashvili *et al.,* 2012). STX1 in this hypo-phosphorylated state fails to support DAT-mediated reverse transport of DA without inhibiting DA uptake function. Interestingly, in hDAT cells expressing STX1 R/Q, we observe a significantly increased V_{max} of DA uptake. In parallel experiments in mouse striatal slices, cleaving STX1 with BoNT/C promotes a decrease in reverse transport of DA with a trend towards increased DA uptake. These data suggest that STX1 function asymmetrically regulates reverse transport of DA and DA uptake. Therefore, to define how hypo-phosphorylation of STX1 R/Q impairs DA reverse transport, we studied the regulatory effects of CK2 function on DA efflux.

CK2 phosphorylates STX1 at Ser14 to regulate STX1 function and protein interactions (Hirling and Scheler, 1996, Foletti *et al.,* 2000, Dubois *et al.,* 2002). Here, we discovered that CK2-mediated phosphorylation of STX1 at Ser14 increases the direct association between STX1 and the hDAT N-terminus. Consistently, pharmacological inhibition of CK2 strongly reduces reverse transport of DA without altering DA uptake. Thus, CK2 is a key player involved in DA efflux. It is possible that this mechanism is important in a broader array of DA-associated neuropsychiatric disorders, since the expression of CK2, as well as the phosphorylation state of STX1 at Ser14, is decreased in post-mortem brain tissue from patients with schizophrenia (Aksenova *et al.,* 1991, Castillo *et al.,* 2010). To have a more complete understanding of how genetic variants within the DA network discovered in ASD patients alter behaviors, we translated our molecular discoveries in vivo. First, we inhibited CK2 function by selectively expressing CK2DN specifically in DA neurons of WT flies. *Drosophila* expressing CK2DN exhibited a robust reduction in AMPH-induced hyperlocomotion as compared to WT flies. These data underscore the importance of CK2 function and STX1 phosphorylation in regulating behaviors sustained by reverse transport of DA. Interestingly, inhibiting CK2 function did not regulate basal locomotion or DA uptake in intact *Drosophila* brains.

Parallel to STX1 R/Q, we found that the hDAT R/W variant displays inhibited reverse transport of DA without impairments in uptake function. It is important to note that CK2 function, in addition to phosphorylating STX1 at Ser14, also promotes STX1/DAT interactions. Here, we show that hDAT R/W has reduced association with STX1, resulting in reduced reverse transport of DA and DA-related behaviors. *Drosophila* expressing hDAT R/W selectively in DA neurons demonstrate reduced sensitivity to the psychomotor effects of AMPH. Interestingly, basal locomotion remained unaltered in hDAT R/W flies, indicating normal DAT-mediated DA clearance as supported by our uptake data. These data suggest that the phosphorylation state

of STX1 at Ser14 and STX1/DAT interaction asymmetrically regulate reverse transport of DA and DAT-mediated uptake.

Mounting evidence demonstrates that reverse transport of DA and associated behaviors can be promoted by changes in the association between the N-terminus of DAT and STX1 (Binda *et al.,* 2008). Additionally, it has been suggested that reverse transport of DA might participate in shaping DA neurotransmission (Leviel, 2011). Here, we used AMPH as a tool to induce reverse transport of DA to determine whether ASD-associated variants disrupt this event. We show that AMPH promotes phosphorylation of STX1 at Ser14 and, as a consequence, STX1/DAT interaction to cause reverse transport of DA. Therefore, we felt that it was important to demonstrate these discoveries at the level of a single active site, the SCG bouton.

Several ASD-associated hDAT variants have now been found to impact reverse transport of DA. The STX1 R/Q variant reported here ablates AMPH-induced efflux similarly to hDAT R/W. Interestingly, two other variants were previously found to cause dysregulation of DA efflux, including a de novo DAT T356M variant and the recurrent DAT A559V variant seen in two boys with ASD, as well as in individuals with bipolar disorder and ADHD. These findings demonstrate diverging mechanisms by which reverse transport of DA can be disrupted. They align with other examples of neurodevelopmental risk emerging from genetic variants causing opposite effects on gene expression or signaling cascades (Cook *et al.,* 1997, Sanders *et al.,* 2011).

Here, we characterize two independent autism-associated variants in the genes that encode STX1 and the DAT. We demonstrate that each variant dramatically alters DAT function. We identify molecular mechanisms that converge to inhibit reverse transport of DA and DA-

associated behaviors. The physiological importance of reverse transport of DA has only recently emerged and remains incompletely understood. However, defining the molecular identity and the impact of these variants on DA efflux may further shape our understanding of the etiology of ASD. Therefore, large genotyping studies aimed at uncovering other variants of the hDAT and STX1A genes in ASD cases and matched controls would be worthwhile.

Materials and methods

All human subjects provided informed consent and the research was approved by institutional human subjects boards. All experiments, procedures, and surgeries involving mice were performed in compliance with and were approved by the Institutional Animal Care and Use Committee of Vanderbilt University.

Subjects and clinical assessment

All ASD cases were ascertained using the Autism Diagnostic Interview—Revised (ADIR), the Autism Diagnostic Observation Schedule—Generic (ADOS), and the DSM-IV diagnosis of pervasive developmental disorder (Neale *et al*., 2012, Lim *et al*., 2013, Liu *et al*., 2013). Clinical assessment of families harboring either variant is dependent on which collection they belong to. In brief, families that contain the *SLC6A3* R/W or *STX1A* R/Q variant belong to the Autism Sequencing Consortium (ASC) and the Simons Simplex Collection (SSC) respectively, and have been previously reported (Neale *et al*., 2012, De Rubeis *et al*., 2014, Iossifov *et al*., 2014).

ADIR is an extensive, semi-structured parent/guardian interview that queries both historical and current information on the development, behavior, and skills of a child. The ADOS is a structured observational assessment administered directly to participants. It is employed to

confirm behaviors reported on the ADIR and consists of modules adapted for differing language abilities. When used together, the ADIR and ADOS are deemed the “gold-standard” instruments for validating and ASD diagnosis.

SLC6A3 R/W and *STX1A R/Q* discovery and validation

Methodological details on *SLC6A3* R/W and *STX1A* R/Q discovery are published (Neale *et al*., 2012, De Rubeis *et al*., 2014, Iossifov *et al*., 2014) and validation of the variant was performed as described in Bowton *et al*. (2014). DNA derived from both parents, the probands, and siblings were subjected to sequence analysis. In all instances, each variant was predicted to be heterozygous at their respective site and experimentally validated and confirmed via Sanger sequencing.

Cell culture and transfection

STX1 constructs in the pcDNA3.1(−) expression vector and the GFP-hDAT-pCIHygro expression vectors containing hDAT or hDAT R/W (Arg51 to Trp) sequence were generated, confirmed and transiently transfected into Chinese hamster ovary (CHO) cells. In some experiments (noted in figure legend), stably transfected hDAT CHO cells were used. These cells were generated as described in Bowton *et al*. (2010). Cells were maintained in a 5% CO_2 incubator at 37 °C and maintained in Ham's F-12 medium supplemented with 10% fetal bovine serum (FBS), 1 mM l-glutamine, 100 U/mL penicillin, and 100 µg/mL streptomycin. Stably transfected hDAT CHO cells were kept under selection with 250 µg/mL hygromycin B (Corning Cellgro). Fugene-6 (Roche Molecular Biochemicals) in serum-free media was used to transfect cells using a 6:1 transfection reagent:DNA ratio. Assays were conducted 24–48 h post-transfection.

Superior cervical ganglion neuron culture and transfection

SCG neurons were cultured from 1 to 3 day old male mouse pups. SCGs were dissected in complete Ultraculture medium (Lonza) supplemented with 20 ng/mL nerve growth factor (NGF). SCGs were washed with PBS and incubated for 20 min in collagenase (3%) and trypsin (2.5%) at 37 °C. They were washed in complete Ultraculture medium with NGF. Dissociated cells were obtained by SCG trituration in medium. Cells were plated on poly-d-lysine coated MatTek® dish treated with collagen (type IV). 24 h post-plating, the media was replaced with Ultraculture medium with NGF and 10 μM 5-fluoro-2-deoxyuridine (FDU). SCGs were transfected via intranuclear microinjection of DNA.

Cell surface biotinylation and protein immunoblot

Cells were cultured in 6-well plates. For cell surface biotinylation assays, cells were labeled with sulfo-NHS-SS-biotin (1.0 mg/mL; Pierce) before purification and analysis via SDS-PAGE/immunoblots. hDAT was detected using a rat monoclonal primary antibody to the N-terminus of hDAT (1:1000) (Millipore Bioscience Research Reagents, catalog number MAB369) and a goat-anti-rat-HRP-conjugated secondary antibody (1:5000) (Jackson ImmunoResearch, catalog number sc-2006). The phosphorylation level of STX1 at Ser14 was detected using a rabbit polyclonal antibody against phospho-S14 either from Castillo *et al*. (2010) or with a commercially available antibody (1:2500) (Abcam, catalog number ab63571) and with a goat-anti-rabbit-HRP-conjugated secondary antibody (1:5000) (Jackson ImmunoResearch, catalog number sc-3837). Total STX1 was detected using a mouse monoclonal antibody (1:5000) (Sigma, catalog number S 0664) and a goat-anti-mouse-HRP-conjugated secondary antibody (1:5000) (Jackson ImmunoResearch, catalog number sc-2005).

Immunostaining

SCG neurons (at least 14 days in culture) were serum starved for 1 h in DMEM:F12 and treated with vehicle or AMPH for 20 min. Neurons were subsequently fixed with PBS plus Ca^{2+}/Mg^{2+} and 4% paraformaldehyde, washed three times with PBS plus Ca^{2+}/Mg^{2+}, permeabilized and blocked with PBS with 4% bovine serum albumin (BSA)/0.15% Tween 20, and immunostained with the appropriate antibody dissolved in PBS plus 4% BSA and 0.05% Tween 20. NET was detected using a mouse monoclonal antibody (1:5000) (Mab Technologies; NET05-2) and p-STX1 with an affinity purified rabbit polyclonal (1:1000), anti-pSTX at Ser14 (Castillo *et al*., 2010). Primary antibodies were visualized with the appropriate Alexa-labeled secondary antibody from Invitrogen.

Mouse brain slices were prepared as outlined in the High Speed Chronoamperometry section, except recovery was in aCSF for 1 h at 37 °C. Slices were fixed, permeabilized, washed, and blocked as outlined above. DAT was visualized using rat monoclonal against DAT and STX1A and STX1B were detected using rabbit polyclonal antiserum from SYSY. p-STX at Ser14 was detected using an affinity purified rabbit polyclonal(1:1000) (Castillo *et al*., 2010). Primary antibodies were visualized with the appropriate covalently Alexa-labeled secondary antibody from Invitrogen.

Immunofluorescence was imaged by capturing Z-series using a Zeiss using a 63 × Plan-APOCHROMAT oil lens (Vanderbilt University Medical Center Cell Imaging Shared Resource). All images shown are from single confocal sections, and image processing was performed using ImageJ and Adobe Photoshop.

Co-immunoprecipitations

Cells were grown to confluence in 25 cm^2 culture flasks and serum deprived for 1 h prior to assay. Cells were washed three times with 4 °C phosphate-buffered saline (Gibco) containing 1 mM EGTA and 1 mM EDTA, and then lysed in RIPA buffer (100 mM NaCl, 1.0% IGEPAL CA-630 (NP-40), 0.5% sodium deoxycholate, 0.1% SDS, 50 mM Tris, pH = 7.4, supplemented with a protease inhibitor cocktail (Sigma)). Lysates were passed twice through a 27.5 gauge needle, and centrifuged at 15,000 ×*g* for 30 min. With a portion of the total cell lysate (TCL) collected to run as the totals, 1 mL of the remaining supernatant was incubated at 4 °C for 4 h with Sepharose-G beads (Fisher Scientific), previously washed with 1% BSA in RIPA buffer, and then preincubated with 2.5 µg DAT antibody (rat monoclonal, #MAB369, Millipore). For the control, supernatant was incubated with BSA-blocked Sepharose-G beads alone (no DAT antibody). After the 4-hour incubation, beads were spun down, washed with cold RIPA buffer, and eluted with Laemmli sample buffer at 37 °C for 30 min. TCL and bead eluates were analyzed by SDS-PAGE (10%) and immunoblotted for total STX1 and DAT. Band intensity was quantified using ImageJ software (National Institutes of Health).

Expression and purification of STX1

The cDNAs encoding STX, STX S14D and STX S14A lacking the transmembrane domain (STXΔTM, STX1ΔTM S14A and STX1ΔTM S14D) were inserted into the bacterial expression vector pGEX, thereby adding an N-terminal GST-tag followed by a thrombin cleavage site. The resulting fusion proteins were produced in *Escherichia coli* BL21 DE3 LysS. The culture was grown at 30 °C to OD 0.8 and expression was induced with 1 mM isopropylβ-d-1-thiogalactopyranoside at 30 °C, and the culture was harvested 4 h after induction. The frozen pelleted bacteria were lyzed in buffer (PBS, 0.1% TX-100, 20 µg/mL DNAse I, 1 mM DTT, mix protease inhibitor (GE Healthcare)). The lysate was cleared by centrifugation followed by incubation with 100 µL glutathione sepharose beads (GE Healthcare, Uppsala, Sweden) at 4 °C

for 1.5 h. The beads were pelleted at 3000 rpm for 5 min and washed 3 times in buffer (PBS, 0.1% TX-100, 1 mM DTT) before elution by cleavage with 1 µL thrombin (GE Healthcare, Uppsala, Sweden) O/N at 4 °C. PMSF (1 mM) was added, and the beads were filtered through a P200 tip. The concentration of the purified STX1B was measured by BCA assay (Thermo Fisher Scientific, Waltham, MA).

GST pull-down assay

A DAT GST fusion protein containing the 64 N-terminal residues of the transporter (GST hDAT 1–64) was expressed and bound to glutathione sepharose beads as described (Binda *et al*., 2008). For the pull-down, 20 µL beads with either GST or GST hDAT 1–64 bound were incubated with 2 µg of purified STXΔTM, STX1ΔTM S14A or STX1ΔTM S14D in 500 µL buffer (PBS, 0.1% TX-100, 0.1% BSA) for 30 min at 4 °C and washed three times in buffer without BSA. Bound protein was eluted by incubation of beads for 1 h at room temperature with 1 µL thrombin in 15 µL buffer (PBS, 0.1% TX-100) followed by addition of SDS loading buffer + 100 mM DTT and incubation for 25 min at 70 °C. Each sample was split in two and loaded in two different Any-kD precast gels (BioRad, Hercules, CA). One gel was used as a Coomassie loading control and the other was transfered to a PDVF membrane and immunoblotted with primary mouse STX1 antibody (Sigma Aldrich. St. Louis, MO) 1:1000 and anti-mouse HRP-conjugated secondary antibody (Thermo Fisher Scientific, Waltham, MA) 1:5000.

Amperometry

Cells were plated at a density of ~ 20,000 per 35-mm culture dish. To load cells with DA, dishes were washed with KRH assay buffer (130 mM NaCl, 1.3 mM KCl, 1.2 mM KH_2PO_4, 10 mM HEPES, and 2.2 mM $CaCl_2$, pH 7.4) containing 10 mM dextrose, 100 µM pargyline, 1 mM tropolone, and 100 µM ascorbic acid, and incubated with 1 µM DA in KRH assay buffer

for 20 min at 37 °C. To preload SCG neurons, dishes were washed with KRH assay buffer (as above) containing 100 nM raclopride. Dishes were washed three times with the external bath solution (130 mM NaCl, 10 mM HEPES, 34 mM dextrose, 1.5 mM $CaCl_2$, 0.5 mM $MgSO_4$, 1.3 mM KH_2PO_4, adjusted pH to 7.35, and 300 mOsm). A carbon fiber electrode (ProCFE; fiber diameter of 5 μm; obtained from Dagan Corporation) juxtaposed to the plasma membrane and held at + 700 mV (a potential greater than the oxidation potential of DA) was used to measure DA flux through oxidation reactions. Amperometric currents in response to the addition of 10 μM AMPH were recorded using an Axopatch 200B amplifier (Molecular Devices, Union City, CA) with a low-pass Bessel filter set at 1 kHz; traces were digitally filtered offline at 1 Hz using Clampex9 software (Molecular Devices, Union City, CA). DA efflux was quantified as the peak value of the amperometric current for all experiments except for recordings from SCG neurons. For SCG neurons, total DA efflux was quantified as the integral of the trace for a fixed 15-minute window.

High speed chronoamperometry

Striatal hemislices (300 μm) from 6 to 10 week old C57BL/6 mice were prepared with a vibratome (Leica VT1000S) in an ice cold oxygenated (95% O2/5% CO_2) sucrose cutting solution consisting of (in mM): 210 sucrose, 20 NaCl, 2.5 KCl, 1 $MgCl_2$, 1.2 NaH_2PO_4, 10 glucose, 26 $NaHCO_3$. Slices were then transferred to oxygenated artificial cerebrospinal fluid (aCSF) at 28 °C for a minimum of 1 h. The aCSF consisted of (in mM): 125 NaCl, 2.5 KCl, 1 $MgCl_2$, 2 $CaCl_2$, 1.2 NaH_2PO_4, 10 glucose, 26 $NaHCO_3$, 0.25 ascorbic acid. Striatal slices were treated at 37 °C for 1 h with either 100 nM BONT/C or vehicle control. DA concentration was measured by chronoamperometry in striatal slices. Briefly, carbon fiber electrodes (100 μm length × 30 μm O.D.) coated with nafion for DA selectivity were lowered into the desired recording site or sites so that the tip of the recording electrode was positioned at a depth of 75–100 μm. The voltage was stepped from 0 mV to 550 mV for 100 ms and then back to 0 mV and

the charging current of the carbon fiber electrode was allowed to decay for 20 msec before the signals were integrated. Data were collected at a frequency of 1 Hz with an Axopatch 200B amplifier. The integrated charge was converted to DA concentration based on in vitro calibration with DA.

[^{3}H]DA uptake

For DA uptake in a heterologous expression system: cells were plated on poly-d-lysine coated, 24-well plates and grown to ~ 90% confluence. On the day of the experiment, cells were washed with 37 °C KRH buffer containing 10 mM dextrose, 100 µM pargyline, 1 mM tropolone, and 100 µM ascorbic acid, and equilibrated for 5 min at 37 °C. Saturation kinetics of DA uptake was determined using a mixture of [^{3}H]DA (PerkinElmer Life Sciences, Waltham, MA) and unlabeled DA (Sigma Aldrich) diluting to final DA concentrations of 0.05 µM–10 µM. Uptake was initiated by bath addition of the dilution row mixture. Uptake was terminated after 10 min by washing twice in ice-cold KRH buffer. Scintillation fluid (Optiphase HiSafe 3, PerkinElmer Life Sciences) was added to the wells and the plates were counted in a Wallac Tri-Lux β-scintillation counter (Wallac). Nonspecific binding was determined in the presence of 10 µM cocaine. K_m and V_{max} values were derived by fitting Michaelis–Menten kinetics to the background corrected uptake data, using GraphPad Prism 5.0 (GraphPad Software, San Diego, CA). All determinations were performed in triplicates.

For DA uptake in striatal slices: striatal hemislices (prepared as previously mentioned) were treated at 37 °C for 1 h with either 100 nM BONT/C or vehicle control. Slices were then exposed to 50 nM [^{3}H]DA for 10 min. DAT-specific DA uptake was determined by subtracting the non-specific signal in the presence of 3 µM GBR12909. At the end of the [^{3}H]DA treatment, the slices were washed with cold aCSF and the striatum dissected. Tissue samples were then homogenized in 200 µL of lysis buffer consisting of 150 mM NaCl, 25 mM HEPES, 2 mM

sodium orthovanadate, 2 mM sodium fluoride, 1% Triton-100. The homogenate was centrifuged at 13,000 ×*g* at 4 °C for 30 min and the supernatant added to 500 µL of buffer 150 mM NaCl, 25 mM HEPES, 2 mM sodium orthovanadate, 2 mM sodium fluoride, 0.1% Triton-100. The protein concentration of each sample was measured and 500 µL of each sample was added to scintillation vials to count [^{3}H]DA. Counts were expressed as a ratio to protein content and normalized to the mean value for the control condition within each experiment.

For DA uptake in dissected *Drosophila* brains: 2–5 day old males were collected, anesthetized with CO_2, and brains were dissected in Schneider's medium (GIBCO) with 1.5% BSA. The retina was removed, and four brains per condition were pooled in Millipore Millicell inserts in 24 well plates. Brains were washed with Schneider's medium, then washed in a standard fly saline solution (HL3) plus 1.5% BSA and 10 mM $MgSO_4$. For 15 min at room temperature, brains were exposed to 200 nM [^{3}H]DA in HL3 plus 1.5% BSA and 115 µM ascorbic acid. Brains were then washed six times with 1.4 mL HL3 plus 1.5% BSA at 4 °C. Brains were placed into scintillation vials in 100 µL 0.1% SDS. Scintillation fluid was added to count [^{3}H]DA.

Drosophila genetics, molecular biology, and construction of UAS hDAT

Flies lacking the *Drosophila* dopamine transporter (*DAT*^{fmn}) (Kume *et al*., 2005) and flies harboring TH-Gal4 were outcrossed to a control line (Bloomington Indiana (BI) 6326) and selected by PCR or by eye color. TH-GAL4 (BI 8848) and M{vas-int.Dm}ZH-2A, M{3xP3-RFP.attP'} ZH-22A (BI 24481) were obtained from the BI stock center and outcrossed to flies lacking the *Drosophila* DAT (*DAT*^{fmn}) and carrying the *white* (*w*^{1118}) mutation (BI stock number 6236) for 5–10 generations. Transgenes (hDAT or hDAT R/W) were cloned into pBI-UASC, and constructs were injected into embryos from M{vas-int.Dm}ZH-2A, M{3xP3-RFP.attP'}ZH-22A (BI 24481). Initial potential transformants were isolated by selecting for red eyes and lack of GFP

signal in the head. Transformants were also verified by RFP fluorescence and outcrossed 5–8 times to DAT^{fmn} flies. The presence of DAT^{fmn} lesion was verified by PCR. To generate CK2-DN flies, we drove the expression of a severely functionally compromised dominant negative version of CK2α (UAS-*Tik*) (Bose *et al*., 2006) in dopaminergic neurons by using TH-Gal4. UAS-*Tik* is based on a CK2α allele (*Tik*) that in a heterozygous condition, causes no obvious neural abnormalities (Lin *et al*., 2002). *Tik* has two substitutions, M161K and E165D. M161K is in the ATP-binding pocket preventing nucleotide-binding thereby eliminating catalytic activity (Lin *et al.,* 2002, Rasmussen *et al.,* 2005). Overexpression from the UAS-*Tik* construct to dominantly blocks CK2 function (Bose *et al*., 2006). Therefore, UAS-*Tik* can be used as a CK2-DN construct. Flies were maintained on a standard cornmeal/molasses/yeast media at 25 °C and 65% humidity with a 12 hour/12 hour light/dark cycle. Lights came on at 8 AM and off at 8 PM.

Behavioral analysis

Three day old males were collected and placed into tubes with food for three days. After three days locomotion was recorded for 32 h by beam breaks and analyzed using equipment/software from Trikinetics (www.trikinetics.com). For the AMPH-induced locomotion, males were starved for 6 h and then fed sucrose (10 mM) containing either AMPH (1 mM) or vehicle.

Statistical analysis

Compiled data are expressed as normalized mean ± s.e.m. For statistical analysis, we used either a Student's t-test or ANOVA depending on the n of the experimental groups. $p < 0.05$ was considered statistically significant.

CHAPTER 7

FUTURE DIRECTIONS

The work presented in this dissertation lays the foundation for investigating the mechanism of AMPH-induced reverse transport of DA in two contexts: 1) structure-function studies of determining the conformational changes necessary for the transporter to enter an efflux-willing state, and 2) studies of the endogenous physiological role of the AMPH-induced DA efflux mechanism in behavioral models. Both of these directions represent valuable avenues of exploration: the mechanistic studies may reveal future molecular targets for pharmacological therapies for AMPH abuse, while the behavioral studies may shed light on poorly understood modes of dopaminergic neurotransmission.

The work in Chapter 2 established the electrostatic interaction between PIP_2 and Lys residues 3 and 5 of the hDAT N-terminus hDAT as an important part of the AMPH-induced DA efflux mechanism. Previous work has shown that the N-terminus is phosphorylated as a result of AMPH exposure, and that this phosphorylation event is necessary for AMPH-induced DA efflux to occur (Khoshbouei *et al.,* 2004, Fog *et al.*, 2006). What remains unclear at this point is whether PIP_2 interaction is required for phosphorylation, and/or whether PIP_2 plays a more complex role in coordinating the conformations of the N-terminus with other regions of the transporter.

Chapter 3 explores the possibility that other suspected PIP_2 binding sites of the hDAT may be involved in the AMPH-induced DA efflux mechanism, such as R443 and K337. Recent computational work has generated a visual model to show how PIP_2 might coordinate the interaction between the N-terminus and residues involved in the intracellular gating mechanism

of the transporter (Khelashvilli *et al.*, 2015). However, the simulation does not address the conformation of the N-terminus when phosphorylated, although it is tempting to speculate that PIP_2 coordination would bring a phospho-group into direct contact with positive charges near the intracellular gating region.

Additionally, Chapters 4 and 5 not only placed ADE in the context of autism spectrum disorder, but also provided valuable insights into some of the steps that must occur for AMPH-induced DA efflux to occur. In Chapter 4, hDAT T356M was shown to have a preference for an outward-facing conformation (**Fig. 33**), which accounts for the inability to uptake DA and the constitutive "leak" of intracellular DA by this variant. As established in Loland *et al.*, 2002, a mutant hDAT construct, hDAT Y335A, with an impaired ability to change conformation towards an inward-facing state, was rescued by the addition of Zn^{2+}. Incidentally, Zn^{2+} impairs the ability of the WT hDAT to uptake DA, further suggesting that Zn^{2+} stabilizes an inward facing conformation. The data from the hDAT T356M and Zn^{2+} studies (Chapter 5), shows that the addition of Zn^{2+} partially restores DA uptake function in the hDAT T356M, as well as diminishes ADE (**Fig. 35**), indicating that Zn^{2+} enables hDAT T356M to adopt an inward-facing conformation with greater frequency than without Zn^{2+}. Importantly, the hDAT T356M also shows an impaired ability to respond to AMPH, even when using whole-cell patch clamp pipette to establish intracellular DA concentrations sufficient for AMPH-induced DA efflux. In the presence of Zn^{2+}, however, hDAT T356M regains partial ability to respond to AMPH (**Fig. 35**), suggesting that the hDAT must be in an inward facing conformation in order to efflux DA. Although these chapters do not directly address the role of PIP_2, they do underscore the importance of the intracellular conformational state of the transporter in the AMPH-induced DA efflux mechanism, lending credence to the idea that the intracellular gating region must be particularly aligned for efflux to occur. However, future studies with hDAT K337A to assess (1)

direct PIP_2 binding and (2) Zn^{2+} rescue of AMPH-induced DA efflux may provide a link between PIP_2 binding and proper alignment of the intracellular gate as requirements for DA efflux.

I propose two hypotheses to explain why PIP_2 is necessary for AMPH-induced DA efflux: (1) PIP_2 interaction with the N-terminus of the hDAT may be necessary to coordinate phosphorylation of the N-terminus, or (2) PIP_2 may use the electrostatic interactions between positive residues of the N-terminus and positive residues near the intracellular gate to bring the phosphorylated N-terminus into proximity of the intracellular gate. These hypotheses are not mutually exclusive, as PIP_2 has been known to coordinate up to 5 positive charges (Rosenhouse-Dantsker and Logothetis, 2007), and data from proposed experiments might support the combined hypothesis that PIP_2 both coordinates N-terminal phosphorylation and coordinating the phosphorylated N-terminus with the intracellular gating region.

To begin addressing hypothesis (1), I propose P^{32} labeling experiments to be conducted on cells expressing the PIP_2-impaired hDAT constructs (hDAT K/A). If interaction with PIP_2 is necessary for coordinating phosphorylation of the N-terminus, then I would expect hDAT K/A to show reduced P^{32} levels in response to AMPH treatment. If hDAT K/A does not show reduced P^{32} levels in response to AMPH, then the N-terminus/PIP_2 interaction may be necessary for coordinating interaction with intracellular gate, in support of hypothesis (2). Furthermore, I propose to utilize the pseudophosphorylated hDAT construct, wherein all five Ser residues on the N-terminus are mutated to Asp (S/D hDAT), and examine whether the addition of the PIP_2-sequestering peptide, through a patch pipette, will prevent AMPH-induced DA efflux. If the S/D hDAT AMPH response is impervious to PIP_2 depletion, then it is likely that PIP_2 does not play a role beyond coordinating phosphorylation of the N-terminus. If, on the other hand, the S/D hDAT AMPH response is affected by PIP_2 depletion, then it is likely that PIP_2 may play a more

complex role in coordinating the phosphorylated N-terminus with other regions of the transporter.

To address hypothesis (2), that PIP_2 brings the phosphorylated N-terminus into proximity of the intracellular gate, evidence exists to show that a pseudophosphorylated, PIP_2-impaired hDAT variant, K/A hDAT with N-terminal Ser residues mutated to Asp, has a reduced ability to respond to AMPH (Hamilton and Belovich *et al.*, 2014). This indicates that phosphorylation of the hDAT N-terminus alone is insufficient for the transporter to respond to AMPH-induced DA efflux mechanism and that PIP_2 interactions with the phosphorylated hDAT N-terminus are also necessary for efflux to occur. Since putative PIP_2 binding sites are located near the hDAT intracellular gate (predicted residues K337 and R443), I propose to examine whether PIP_2 directly interacts with R443 or K337 to coordinate the phosphorylated N-terminus with other regions of the transporter. Since mutation of K337 or R443 to Ala results in decreased AMPH-induced DA efflux (**Figures 26**-**27**; **Chapter 3**), it is possible that disrupting the electrostatic interactions between PIP_2 and these regions perturbs the ability of the N-terminus to come into proximity with the intracellular gate.

I propose to first establish the direct interaction with R443 and K337. As performed by Buchmayer *et al.*, PIP_2-coated beads can be incubated with lysate from hDAT R443A or hDAT K337A expressing heterologous cells (Buchmayer *et al.,* 2013). If no difference in PIP_2 binding is observed, then perhaps the impairments in R443A and K337A are due to an impairment in interaction between the phosphorylated N-terminus. In this case, I would test whether R443A or K337A in a S/D hDAT background responds to AMPH. If S/D hDAT-R443A or S/D hDAT-K337A show impaired AMPH response compared to S/D hDAT, then phosphorylated N-terminus interactions with R443 and/or K337 are important for this process. If they do not show impaired AMPH response compared to S/D hDAT, then it is possible that the phosphorylated N-

terminus may interact with other residues in the intracellular gating regions, or interfere with salt bridges.

Finally, Chapter 6 represents an important insight into the role of the AMPH-induced DA efflux mechanism in ASD and in behaviors in general. Chapter 6 presents the first known examples of neuropsychiatric disease-associated hDAT variants possessing impaired AMPH-induced DA efflux without concomitant impairments in uptake and/or a DA leak (ADE). Although hDAT R51W was untested for ADE, the unchanged ability of the transporter to uptake substrate indicated that it was not a likely candidate for ADE (**Fig. 39**). Similarly, WT hDAT cells co-expressing STX1 R26Q showed an increase in DA uptake, making ADE further unlikely for that variant as well (**Fig. 38**). Taken together, the only impaired transporter function in both of these ASD-associated variants was an impairment in AMPH-induced DA efflux. As outlined in Chapter 1 (**Table 1**), there have been several instances of neuropsychiatric disease-associated hDAT variants with impaired ability to respond to AMPH. However, more focus was given to the ADE phenotype present in these variants, which as seen in the hDAT T356M *Drosophila* and hDAT A559V mouse models, readily translates to the behavior of hyperlocomotion. Until hDAT R51W and STX1 R26Q, there was no evidence that the AMPH-induced DA efflux mechanism carried any non-AMPH related behavioral importance. Indeed, the hDAT R51W *Drosophila* do not express hyperlocomotion (**Fig. 44**), although they do show an expected impaired AMPH-induced locomotion response, like hDAT T356M *Drosophila*. This suggests that the ability of the hDAT to respond to a coordinated intracellular signal (like that provided by AMPH) may have a discernable role in neurotransmission and neurological pathologies.

The behavioral models generated during this dissertation represent an opportunity to begin addressing the role of the AMPH-induced DA efflux mechanism in physiology. If the AMPH-induced DA efflux mechanism does represent an ability of the transporter to respond in a

coordinated manner to an endogenous signal (elevated Ca^{2+} and CaMKII activation in the presence of high intracellular DA levels, for example), then it is possible that examining more sophisticated behaviors in these efflux-impaired organisms may reveal previously unknown deficits. Again, it has been shown that the amount of DA released by an AMPH-triggered efflux event is enough to approach a DA quantum, similar to the amount of DA released by vesicular secretion (Kahlig *et al.,* 2005).

One of the greatest challenges facing this research question has been how to selectively manipulate the AMPH-induced efflux function of the hDAT without disrupting the essential DA uptake function of the hDAT. Previously available tools, such as genetic knockouts and pharmacological inhibition of the hDAT, are currently not sophisticated enough to target only the efflux mechanism of the hDAT. However, since the variants generated here (K/A hDAT, hDAT R51W) show a selective impairment in AMPH-induced DA efflux function, we can now begin to address questions regarding the endogenous role of this mechanism in a more precise manner.

To begin narrowing the field of behavioral tests, examining known behavioral symptoms in human individuals with ASD may provide more focus. For example, the reward circuitry in ASD patients shows alteration, as well as the striatal regions (which controls implicit learning and habits) (Dichter *et al.*, 2012). Therefore, I propose to examine reward-related behaviors of efflux-impaired organisms, and whether these animals respond to natural rewards (food, sucrose) in a manner consistent with WT. Furthermore, if mouse models of efflux-impaired variants are made, exploration of ASD-associated repetitive behaviors or anxiety behaviors may be examined as well.

REFERENCES

Abramson, J., I. Smirnova, V. Kasho, G. Verner, S. Iwata and H. R. Kaback (2003). "The lactose permease of Escherichia coli: overall structure, the sugar-binding site and the alternating access model for transport." *FEBS Lett* **555**(1): 96-101.

Aksenova, M. V., G. S. Burbaeva, K. V. Kandror, D. V. Kapkov and A. S. Stepanov (1991). "The decreased level of casein kinase 2 in brain cortex of schizophrenic and Alzheimer's disease patients." *FEBS letters* **279**(1) 55-57.

Anderson, B. M., N. Schnetz-Boutaud, J. Bartlett, H. H. Wright, R. K. Abramson, M. L. Cuccaro, J. R. Gilbert, M. A. Pericak-Vance and J. L. Haines (2008). "Examination of association to autism of common genetic variationin genes related to dopamine." *Autism Res* **1**(6): 364-369.

Balla, T., Z. Szentpetery and Y. J. Kim (2009). "Phosphoinositide signaling: new tools and insights." *Physiology (Bethesda)* **24**: 231-244.

Bear, M. F., B. Connor and M. F. Paradiso (2006). "Neuroscience: Exploring the Brain." Lippincott Williams & Wilkins, 3rd Edition.

Ben-Aissa, K., G. Patino-Lopez, N. V. Belkina, O. Maniti, T. Rosales, J. J. Hao, M. J. Kruhlak, J. R. Knutson, C. Picart and S. Shaw (2012). "Activation of moesin, a protein that links actin cytoskeleton to the plasma membrane, occurs by phosphatidylinositol 4,5-bisphosphate (PIP2) binding sequentially to two sites and releasing an autoinhibitory linker." *J Biol Chem* **287**(20): 16311-16323.

Berry-Kravis, E. and K. Potanos (2004). "Psychopharmacology in fragile X syndrome--present and future." *Ment Retard Dev Disabil Res Rev* **10**(1): 42-48.

Beuming, T., J. Kniazeff, M. L. Bergmann, L. Shi, L. Gracia, K. Raniszewska, A. H. Newman, J. A. Javitch, H. Weinstein, U. Gether and C. J. Loland (2008). "The binding sites for cocaine and dopamine in the dopamine transporter overlap. *Nat Neurosci* **11**(7): 780-789.

Binda, F., C. Dipace, E. Bowton, S. D. Robertson, B. J. Lute, J. U. Fog, M. Zhang, N. Sen, R. J. Colbran, M. E. Gnegy, U. Gether, J. A. Javitch, K. Erreger and A. Galli (2008). "Syntaxin 1A interaction with the dopamine transporter promotes amphetamine-induced dopamine efflux." *Mol Pharmacol* **74**(4): 1101-1108.

Bisgaard, H., M. A. Larsen, S. Mazier, T. Beuming, A. H. Newman, H. Weinstein, L. Shi, C. J. Loland and U. Gether (2011). "The binding sites for benztropines and dopamine in the dopamine transporter overlap." *Neuropharmacology* **60**(1): 182-190.

Bjorklund, A. and S. B. Dunnett (2007). "Fifty years of dopamine research." *Trends Neurosci* **30**(5): 185-187.

Bose A., B. Kahali, S. Zhange, J. M. Lin, R. Allada, U. Karandikar and P. Bidwai (2006). "Drosophila CK2 regulates lateral-inhibition during eye and bristle development." *Mech Dev* **123**(9): 649–664.

Boudanova, E., D. M. Navaroli and H. E. Melikian (2008). "Amphetamine-induced decreases in dopamine transporter surface expression are protein kinase C-independent." *Neuropharmacology* **54**(3): 605-612.

Bowton, E., C. Saunders, K. Erreger, D. Sakrikar, H. J. Matthies, N. Sen, T. Jessen, R. J. Colbran, M. G. Caron, J. A. Javitch, R. D. Blakely and A. Galli (2010). "Dysregulation of dopamine transporters via dopamine D2 autoreceptors triggers anomalous dopamine efflux associated with attention-deficit hyperactivity disorder." *J Neurosci* **30**(17): 6048-6057.

Bowton, E., C. Saunders, I. A. Reddy, N. G. Campbell, P. J. Hamilton, L. K. Henry, H. Coon, D. Sakrikar, J. M. Veenstra-VanderWeele, R. D. Blakely, J. Sutcliffe, H. J. Matthies, K.

Erreger and A. Galli (2014). "SLC6A3 coding variant Ala559Val found in two autism probands alters dopamine transporter function and trafficking." *Transl Psychiatry* **4**: e464.

Brozoski, T. J., R. M. Brown, H. E. Rosvold and P. S. Goldman (1979). "Cognitive deficit caused by regional depletion of dopamine in prefrontal cortex of rhesus monkey." *Science* **205**(4409): 929-932.

Buchmayer, F., K. Shicker, T. Steinkellner, P. Geier, G. Stubiger, P. J. Hamilton, A. Jurik, T. Stockner, J. W. Yang, T. Montgomery, M. Holy, T. Hofmaier, O. Kudlacek, H. J. Matthies, G. F. Ecker, V. Bochkov, A. Galli, S. Boehm, and H. H. Sitte (2013). "Amphetamine actions at the serotonin transporter rely on the availability of phosphatidylinositol-4,5-bisphosphate." *Proc Natl Acad Sci U S A* **110**(28): 11642-11647.

Carboni, E., A. Imperato, L. Perezzani and G. Di Chiara (1989). "Amphetamine, cocaine, phencyclidine and nomifesine increase extracellular dopamine concentrations preferentially in the nucleus accumbens of freely moving rats." *Neuroscience* **28**(3): 653-661.

Carlsson, A. (1987). "Perspectives on the discovery of central monoaminergic neurotransmission." *Annu Rev Neurosci* **10**: 19-40.

Cartier, E., P. J. Hamilton, A. N. Belovich, A. Shekar, N. G. Campbell, C. Saunders, T. F. Andreassen, U. Gether, J. Veenstra-Vanderweele, J. S. Sutcliffe, P. G. Ulery-Reynolds, K. Erreger, H. J. Matthies and A. Galli (2015). "Rare autism-associated variants implicate syntaxin 1 (STX1 R26Q) phosphorylation and the dopamine transporter (hDAT R51W) in dopamine neurotransmission and behaviors." *EBioMedicine* **2**(2): 135-146.

Carvelli, L., R. D. Blakely and L. J. DeFelice (2008). "Dopamine transporter/syntaxin 1A interactions regulate transporter channel activity and dopaminergic synaptic transmission." *Proc Natl Acad Sci U S A* **105**(37): 14192-14197.

Carvelli, L., P. W. McDonald, R. D. Blakely and L. J. DeFelice (2004). "Dopamine transporters depolarize neurons by a channel mechanism." *Proc Natl Acad Sci U S A* **101**(45): 16046-16051.

Castillo, M. A., S. Ghose, C. A. Tamminga, and P. G. Ulery-Reynolds (2010). "Deficits in syntaxin 1 phosphorylation in schizophrenia prefrontal cortex." *Biol psychiatry* **67**(3): 208-216.

Cervinski, M.A., J.D. Foster, and R. A. Vaughan (2005). "Psychoactive substrates stimulate dopamine transporter phosphorylation and down-regulation by cocaine-sensitive and protein kinase C-dependent mechanisms." *J Biol Chem* **280**(49): 40442-40449.

Chen, N. and M. E. Reith (2008). "Substrates dissociate dopamine transporter oligomers." *J Neurochem* **105**(3): 910-920.

Choe, E. S. and J. Q. Wang (2002). "CaMKII regulates amphetamine-induced ERK1/2 phosphorylation in striatal neurons." *Neuroreport* **13**(8): 1013-1016.

Claxton, D. P., M. Quick, L. Shi, F. D. de Carvalho, H. Weinstein, J. A. Javitch and H. S. McHaourab (2010). "Ion/substrate-dependent conformational dynamics of a bacterial homolog of neurotransmitter:sodium symporters." *Nat Struct Mol Biol* **17**(7): 822-829.

Cook, E. H., Jr., V. Lindgren, B. L. Leventhal, R. Courchesne, A. Lincoln, C. Shulman, C. Lord and E. Courchesne (1997). "Autism or atypical autism in maternally but not paternally derived proximal 15q duplication." *Am J Hum Genet* **60**(4): 928-934.

Cook, E. H., Jr. and S. W. Scherer (2008). "Copy-number variations associated with neuropsychiatric conditions." *Nature* **455**(7215): 919-923.

Cousins, D. A., K. Butts and A. H. Young (2009). "The role of dopamine in bipolar disorder." *Bipolar Disord* **11**(8): 787-806

Cragg, S. J. and M. E. Rice (2004). "DAncing past the DAT at a DA synapse." *Trends Neurosci* **27**(5): 270-277.

Cremona, M.L., H. J. Matthies, K. Pau, E. Bowton, N. Speed, B. J. Lute, M. Anderson, N. Sen, S. D. Robertson, R. A. Vaughan, J. E. Rothman, A. Galli, J. A. Javitch and A. Yamamoto (2011). "Flotillin-1 is essential for PKC-triggered endocytosis and membrane microdomain localization of DAT." *Nat Neurosci* **14**(4): 469-477.

Czech, M.P. (2000). "PIP2 and PIP3: complex roles at the cell surface." *Cell* **100**(6): 603-606.

Damiano, C.R., J., Aloi, M. Treadway, J. W. Bodfish and G. S. Dichter (2012). "Adults with autism spectrum disorders exhibit decreased sensitivity to reward parameters when making effort-based decisions." *J Neurodev Disord* **4**(1): 13.

Darnell, J. C., S. J. Van Driesche, C. Zhang, K. Y. Hung, A. Mele, C. E. Fraser, E. F. Stone, C. Chen, J. J. Fak, S. W. Chi, D. D. Licatalosi, J. D. Richter and R. B. Darnell (2011). "FMRP stalls ribosomal translocation on mRNAs linked to synaptic function and autism." *Cell* **146**(2): 247-261.

Das, R. and D. Baker (2008). "Macromolecular modeling with rosetta." *Annu Rev Biochem* **77**: 363-382.

de Bruin, E. I., P. F. de Nijs, F. Verheij, C. A. Hartman and R. F. Ferdinand (2007). "Multiple complex developmental disorder delineated from PDD-NOS." *J Autism Dev Disord* **37**(6): 1181-1191.

De Rubeis, S., X. He, A. P. Goldberg, C. S. Poultney, K. Samocha, A. E. Cicek, Y. Kou, L. Liu, M. Fromer, S. Walker, T. Singh, L. Klei, J. Kosmicki, F. Shih-Chen, B. Aleksic, M. Biscaldi, P. F. Bolton, J. M. Brownfeld, J. Cai, N. G. Campbell, A. Carracedo, M. H. Chahrour, A. G. Chiocchetti, H. Coon, E. L. Crawford, S. R. Curran, G. Dawson, E. Duketis, B. A. Fernandez, L. Gallagher, E. Geller, S. J. Guterm R. S. Hill, J. Ionita-Laza, P. Jimenz Gonzalez, H. Kilpinen, S. M. Klauck, A. Kolevzon, I. Lee, I. Lei, J. Lei, T. Lehtimaki, C. F. Lin, A. Ma'ayan, C. R. Marshall, A. L. McInnes, B. Neale, M. J. Owen, M. Parellada, J. R. Parr, S. Purcell, K. Puura, D. Rajagopalan, K. Rehnstrom, A. Reichenberg, A. Sabo, M Sachse, S. J. Sanders, C. Schafer, M. Schutle-Ruther, D. Skuse, C. Stevens, P. Szatmari, K. Tammimies, O. Valladares, A. Voran, W. Li-San, L. A. Weiss, A. J. Willsey, T. W. Yu, R. K. Yuen, DDD Study, Homozygosity Mapping Collaborative for Autism; UK10K Consortium, E. H. Cook, C. M. Freitag, M. Gill, C. M. Hultman, T. Lehner, A. Palotie, G. D. Schellenberg, P. Sklar, M. W. State, J. S. Sutcliffe, C. A. Walsh, S. W. Scherer, M. E. Zwick, J. C. Barett, D. J. Cutler, K. Roeder, B. Devlin, M. J. Daly and J. D. Buxbaum (2014). "Synaptic, transcriptional and chromatin genes disrupted in autism." *Nature* **515**(7526), 209-215.

Deken, S. L., M. L. Beckman, L. Boos and M. W. Quick (2000). "Transport rates of GABA transporters: regulation by the N-terminal domain and syntaxin 1A." *Nat Neurosci* **3**(10): 998-1003.

de Krom, M., W. G. Staal, R. A. Ophoff, J. Hendriks, J. Buitelaar, B. Franke, M. V. de Jonge, P. Bolton, D. Collier, S. Curran, H. van Engeland and J. M. van Ree (2009). "A common variant in DRD3 receptor is associated with autism spectrum disorder." *Biol Psychiatry* **65**(7): 625-630.

Devlin, B. and S. W. Scherer (2012). "Genetic architecture in autism spectrum disorder." *Curr Opin Genet Dev* **22**(3): 229-237.

Di Martino, A., X. N. Zuo, C. Kelly, R. Grzadzinski, M. Mennes, A. Schvarcz, J. Rodman, C. Lord, F. X. Castellanos and M. P. Milham (2013). "Shared and distinct intrinsic functional network centrality in autism and attention-deficit/hyperactivity disorder." *Biol Psychiatry* **74**(8): 623-632.

Dichter, G. S., C. A. Damiano and J. A. Allen (2012). "Reward circuitry dysfunction in psychiatric and neurodevelopmental disorders and genetic syndromes: animal models and clinical findings." *J Neurodev Disord* **4**(1): 19.

Dichter, G. S., J. A. Richey, A. M. Rittenberg, A. Sabatino and J. W. Bodfish (2012). "Reward circuitry function in autism during face anticipation and outcomes." *J Autism Dev Disord* **42**(2): 147-160.

Dipace, C., U. Sung, F. Binda, R. D. Blakely and A. Galli (2007). "Amphetamine induces a calcium/calmodulin-dependent protein kinase II-dependent reduction in norepinephrine transporter surface expression linked to changes in syntaxin 1A/transporter complexes." *Mol Pharmacol* **71**(1): 230-239.

Dubois, T., P. Kerai, M. Learmonth, A. Cronshaw and A. Aitken (2002). "Identification of syntaxin-1A sites of phosphorylation by casein kinase I and casein kinase II." *Eur J Biochem* **269**(3): 909-914.

Durdiakova, J., V. Warrier, S. Banerjee-Basu, S. Baron-Cohen and B. Chakrabarti (2014). "STX1A and Asperger syndrome: a replication study." *Mol Autism* **5**(1): 14.

Earl, D. J. and M. W. Deem (2005). "Parallel tempering: theory, applications, and new perspectives." *Phys Chem Chem Phys* **7**(23): 3910-3916.

Faber, S., G. M. Zinn, J. C. Kern, 2nd and H. M. Kingston (2009). "The plasma zinc/serum copper ratio as a biomarker in children with autism spectrum disorders." *Biomarkers* **14**(3): 171-180.

Faraone, S. V. and M. T. Tsuang (2003). "Heterogeneity and the genetics of bipolar disorder." *Am J Med Genet C Semin Med Genet* **123C**(1): 1-9.

Fasano A. and I. Petrovic (2010). "Insights into pathophysiology of punding reveal possible treatment strategies." *Mol Psychiatry* **15**(6): 560–573

Fischer, J. F. and A. K. Cho (1979). "Chemical release of dopamine from striatal homogenates: evidence for an exchange diffusion model." *J Pharmacol Exp Ther* **208**(2): 203-209.

Fitzgerald, P. and T. G. Dinan (2008). "Prolactin and dopamine: what is the connection? A review article." *J Psychopharmacol* **22**(2 Suppl): 12-19.

Fog, J. U., H. Khoshbouei, M. Holy, W. A. Owens, C. B. Vaegter, N. Sen, Y. Nikandrova, E. Bowton, D. G. McMahon, R. J. Colbran, L. C. Daws, H. H. Sitte, J. A. Javitch, A. Galli and U. Gether (2006). "Calmodulin kinase II interacts with the dopamine transporter C terminus to regulate amphetamine-induced reverse transport." *Neuron* **51**(4): 417-429.

Foletti, D. L., R. Lin, M. A. Finley and R. H. Scheller (2000). "Phosphorylated syntaxin 1 is localized to discrete domains along a subset of axons." *J Neurosci* **20**(12): 4535-4544.

Forrest, L. R. and G. Rudnick (2009). "The rocking bundle: a mechanism for ion-coupled solute flux by symmetrical transporters." *Physiology* (Bethesda) **24**: 377-386.

Foster, J. D., B. Pananusorn and R. A. Vaughan (2002). "Dopamine transporters are phosphorylated on N-terminal serines in rat striatum." *J Biol Chem* **277**(28): 25178-25186.

Friggi-Grelin, F., H. Coulom, M. Meller, D. Gomez, J. Hirsh and S. Birman (2003). "Targeted gene expression in Drosophila dopaminergic cells using regulatory sequences from tyrosine hydroxylase." *J Neurobiol* **54**(4): 618-627.

Fulks, J. L., B. E. O'Bryhim, S. K. Wenzel, S. C. Fowler, E. Vorontsova, J. W. Pinkston, A. N. Ortiz and M. A. Johnson (2010). "Dopamine Release and Uptake Impairments and Behavioral Alterations Observed in Mice that Model Fragile X Mental Retardation Syndrome." *ACS Chem Neurosci* **1**(10): 679-690.

Gabriel, L. R., S. Wu, P. Kearney, K. D. Bellve, C. Standley, K. E. Fogarty and H. E. Melikian (2013). "Dopamine transporter endocytic trafficking in striatal dopaminergic neurons: differential dependence on dynamin and the actin cytoskeleton." *J Neurosci* **33**(45): 17836-17846.

Gadow, K. D., C. J. Devincent, D. M. Olvet, V. Pisarevskaya and E. Hatchwell (2010). "Association of DRD4 polymorphism with severity of oppositional defiant disorder, separation anxiety disorder and repetitive behaviors in children with autism spectrum disorder." *Eur J Neurosci* **32**(6): 1058-1065.

Gadow, K. D., C. J. DeVincent and J. Pomeroy (2006). "ADHD symptom subtypes in children with pervasive developmental disorder." *J Autism Dev Disord* **36**(2): 271-283.

Gadow, K. D., J. Roohi, C. J. DeVincent and E. Hatchwell (2008). "Association of ADHD, tics, and anxiety with dopamine transporter (DAT1) genotype in autism spectrum disorder." *J Child Psychol Psychiatry* **49**(12): 1331-1338.

Geller, B., B. Zimerman, M. Williams, M. P. Delbello, K. Bolhofner, J. L. Craney, J. Frazier, L. Beringer and M. J. Nickelsburg (2002). "DSM-IV mania symptoms in a prepubertal and early adolescent bipolar disorder phenotype compared to attention-deficit hyperactive and normal controls." *J Child Adolesc Psychopharmacol* **12**(1): 11-25.

Genomes Project, Consortium, G. R. Abecasis, A. Auton, L. D. Brooks, M. A. DePristo, R. M. Durbin, R. E. Handsaker, H. M. Kang, G. T. Marth and G. A. McVean (2012). "An integrated map of genetic variation from 1,092 human genomes." *Nature* **491**(7422): 56-65.

Giambalvo, C. T. (1992). "Protein kinase C and dopamine transport--1. Effects of amphetamine in vivo." *Neuropharmacology* **31**(12): 1201-1210.

Giambalvo, C.T. (2004). "Mechanisms underlying the effects of amphetamine on particulate PKC activity." *Synapse* **51**(2): 128-139.

Giros, B. and M. G. Caron (1993). "Molecular characterization of the dopamine transporter." *Trends Pharmacol Sci* **14**(2): 43-49.

Giros, B., S. el Mestikawy, N. Godinot, K. Zheng, H. Han, T. Yang-Feng and M. G. Caron (1992). "Cloning, pharmacological characterization, and chromosome assignment of the human dopamine transporter." *Mol Pharmacol* **42**(3): 383-390.

Giros, B., M. Jaber, S. R. Jones, R. M. Wightman and M. G. Caron (1996). "Hyperlocomotion and indifference to cocaine and amphetamine in mice lacking the dopamine transporter." *Nature* **379**(6566): 606-612.

Gnegy, M. E., H. Khoshbouei, K. A. Berg, J. A. Javitch, W. P. Clarke, M. Zhang and A. Galli (2004). "Intracellular Ca2+ regulates amphetamine-induced dopamine efflux and currents mediated by the human dopamine transporter." *Mol Pharmacol* **66**(1): 137-143.

Goldstein, S. and A. J. Schwebach (2004). "The comorbidity of Pervasive Developmental Disorder and Attention Deficit Hyperactivity Disorder: results of a retrospective chart review." *J Autism Dev Disord* **34**(3): 329-339.

Grunhage, F., T. G. Schulze, D. J. Muller, M. Lanczik, E. Franzek, M. Albus, M. Borrmann-Hassenbach, M. Knapp, S. Cichon, W. Maier, M. Rietschel, P. Propping and M. M. Nothen (2000). "Systematic screening for DNA sequence variation in the coding region of the human dopamine transporter gene (DAT1)." *Mol Psychiatry* **5**(3): 275-282.

Guptaroy, B., M. Zhang, E. Bowton, F. Binda, L. Shi, H. Weinstein, A. Galli, J. A. Javitch, R. R. Neubig and M. E. Gnegy (2009). "A Juxtamembrane Mutation in the N-Terminus of the Dopamine Transporter Induces Preference for an Inward-Facing Conformation." *Mol Pharmacol* **75**(3): 514-524 (2009).

Hamilton, P. J., A. N. Belovich, G. Khelashvili, C. Saunders, K. Erreger, J. A. Javitch, H. H. Sitte, H. Weinstein, H. J. Matthies and A. Galli (2014). "PIP2 regulates psychostimulant behaviors through its interaction with a membrane protein." *Nat Chem Biol* **10**(7): 582-589.

Hamilton, P. J., N. G. Campbell, S. Sharma, K. Erreger, F. Herborg Hansen, C. Saunders, A. N. Belovich, N. A. A. S. Consortium, M. A. Sahai, E. H. Cook, U. Gether, H. S. McHaourab, H. J. Matthies, J. S. Sutcliffe and A. Galli (2013). "De novo mutation in the dopamine transporter gene associates dopamine dysfunction with autism spectrum disorder." *Mol Psychiatry* **18**(12): 1315-1323.

Hamilton, P. J., A. Shekar, A. N. Belovich, N. B. Christianson, N. G. Campbell, J. S. Sutcliffe, A. Galli, H. J. Matthies and K. Erreger (2015). "Zn(2+) reverses functional deficits in a de

novo dopamine transporter variant associated with autism spectrum disorder." *Mol Autism* **6**: 8.

Hansen, F. H., T. Skjorringe, S. Yasmeen, N. V. Arends, M. A. Sahai, K. Erreger, T. F. Andreassen, M. Holy, P. J. Hamilton, V. Neergheen, M. Karlsborg, A. H. Newman, S. Pope, S. J. Heales, L. Friberg, I. Law, L. H. Pinborg, H. H. Sitte, C. Loland, L. Shi, H. Weinstein, A. Galli, L. E. Hjermind, L. B. Moller and U. Gether (2014). "Missense dopamine transporter mutations associate with adult parkinsonism and ADHD." *J Clin Invest* **124**(7): 3107-3120.

Hastrup, H., A. Karlin and J. A. Javitch (2001). "Symmetrical dimer of the human dopamine transporter revealed by cross-linking Cys-306 at the extracellular end of the sixth transmembrane segment." *Proc Natl Acad Sci U S A* **98**(18): 10055-10060.

Hastrup, H., N. Sen and J. A. Javitch (2003). "The human dopamine transporter forms a tetramer in the plasma membrane: cross-linking of a cysteine in the fourth transmembrane segment is sensitive to cocaine analogs." *J Biol Chem* **278**(46): 45045-45048.

Hettinger, J. A., X. Liu, C. E. Schwartz, R. C. Michaelis and J. J. Holden (2008). "A DRD1 haplotype is associated with risk for autism spectrum disorders in male-only affected sib-pair families." *Am J Med Genet B Neuropsychiatr Genet* **147B**(5): 628-636.

Hettinger, J. A., X. Liu, M. L. Hudson, A. Lee, I. L. Cohen, R. C. Michaelis, C. E. Schwartz, S. M. Lewis and J. J. Holden (2012). "DRD2 and PPP1R1B (DARPP-32) polymorphisms independently confer increased risk for autism spectrum disorders and additively predict affected status in male-only affected sib-pair families." *Behav Brain Funct* **8**: 19.

Hilgemann, D.W. and R. Ball (1996). "Regulation of cardiac Na+,Ca2+ exchange and KATP potassium channels by PIP2." *Science* **273**(5277): 956-959.

Hirling, H. and R. H. Scheller (1996). "Phosphorylation of synaptic vesicle proteins: modulation of the alpha SNAP interaction with the core complex." *Proc Natl Acad Sci U S A* **93**(21): 11945-11949.

Hollander, E., E. Anagnostou, W. Chaplin, K. Esposito, M. M. Haznedar, E. Licalzi, S. Wasserman, L. Soorya and M. Buchsbaum (2005). "Striatal volume on magnetic resonance imaging and repetitive behaviors in autism." *Biol Psychiatry* **58**(3): 226-232.

Holton, K. L., M. K. Loder and H. E. Melikian (2005). "Nonclassical, distinct endocytic signals dictate constitutive and PKC-regulated neurotransmitter transporter internalization." *Nat Neurosci* **8**(7): 881-888.

Hope, H.R. and L. J. Pike (1996). "Phosphoinositides and phosphoinositide-utilizing enzymes in detergent-insoluble lipid domains." *Mol Biol Cell* **7**(6): 843-851.

Hong, W. C. and S. G. Amara (2013). "Differential targeting of the dopamine transporter to recycling or degradative pathways during amphetamine- or PKC-regulated endocytosis in dopamine neurons." *FASEB* J **27**(8): 2995-3007.

Howe, M. W., H. E. Atallah, A. McCool, D. J. Gibson and A. M. Graybiel (2011). "Habit learning is associated with major shifts in frequencies of oscillatory activity and synchronized spike firing in striatum." *Proc Natl Acad Sci U S A* **108**(40): 16801-16806.

Howe, M. W., P. L. Tierney, S. G. Sandberg, P. E. Phillips, and A. M. Graybiel (2013). "Prolonged dopamine signalling in striatum signals proximity and value of distant rewards." *Nature* **500**(7464): 575-579.

Humphrey, W., A. Dalke and K. Schulten (1996). "VMD: visual molecular dynamics." *J Mol Graph* **14**(1): 33-38, 27-38.

Ingram, S. L., B. M. Prasad and S. G. Amara (2002). "Dopamine transporter-mediated conductances increase excitability of midbrain dopamine neurons." *Nat Neurosci* **5**(10): 971-978.

Iossifov, I., M. Ronemus, D. Levy, Z. Wang, I. Hakker, J. Rosenbaum, B. Yamrom, Y. H. Lee, G. Narzisi, A. Leotta, J. Kendall, E. Grabowska, B. Ma, S. Marks, L. Rodgers, A. Stepansky,

J. Troge, P. Andrews, M. Bekritsky, K. Pradhan, E. Ghiban, M. Kramer, J. Parla, R. Demeter, L. L. Fulton, R. S. Fulton, V. J. Magrini, K. Ye, J. C. Darnell, R. B. Darnell, E. R. Mardis, R. K. Wilson, M. C. Schatz, W. R. McCombie and M. Wigler (2012). "De novo gene disruptions in children on the autistic spectrum." *Neuron* **74**(2): 285-299.

Iwata, S., G. H. Hewlett and M. E. Gnegy (1997). "Amphetamine increases the phosphorylation of neuromodulin and synapsin I in rat striatal synaptosomes." *Synapse* **26**(3): 281-291.

Jardetzky, O. (1966). "Simple allosteric model for membrane pumps." *Nature* **211**(5052): 969-970.

Jackson, M. J. and P. J. Garrod (1978). "Plasma zinc, copper, and amino acid levels in the blood of autistic children." *J Autism Child Schizophr* **8**(2): 203-208.

Jeschke, G., A. Koch, U. Jonas and A. Godt (2002). "Direct conversion of EPR dipolar time evolution data to distance distributions." *J Magn Reson* **155**(1): 72-82.

Jeschke, G. and Y. Polyhach (2007). "Distance measurements on spin-labelled biomacromolecules by pulsed electron paramagnetic resonance." *Phys Chem Chem Phys* **9**(16): 1895-1910.

Johnson, L. A., B. Guptaroy, D. Lund, S. Shamban and M. E. Gnegy (2005). "Regulation of amphetamine-stimulated dopamine efflux by protein kinase C beta." *J Biol Chem* **280**(12): 10914-10919.

Jones, S. R., R. R. Gainetdinov, R. M. Wightman and M. G. Caron (1998). "Mechanisms of amphetamine action revealed in mice lacking the dopamine transporter." *J Neurosci* **18**(6): 1979-1986.

Kadamur, G. and E.M. Ross (2013). "Mammalian phospholipase C." *Annu Rev Physiol* **75**: 127-154.

Kahlig, K. M., F. Binda, H. Khoshbouei, R. D. Blakely, D. G. McMahon, J. A. Javitch and A. Galli (2005). "Amphetamine induces dopamine efflux through a dopamine transporter channel." *Proc Natl Acad Sci U S A* **102**(9): 3495-3500.

Kahlig, K. M., J. A. Javitch and A. Galli (2004). "Amphetamine regulation of dopamine transport. Combined measurements of transporter currents and transporter imaging support the endocytosis of an active carrier." *J Biol Chem* **279**(10): 8966-8975.

Kahlig, K. M., B. J. Lute, Y. Wei, C. J. Loland, U. Gether, J. A. Javitch and A. Galli (2006). "Regulation of dopamine transporter trafficking by intracellular amphetamine." Mol Pharmacol **70**(2): 542-548.

Kantcheva, A. K., M. Quick, L. Shi, A. M. Winther, S. Stolzenberg, H. Weinstein, J. A. Javitch and P. Nissen (2013). "Chloride binding site of neurotransmitter sodium symporters." *Proc Natl Acad Sci U S A* **110**(21): 8489-8494.

Kantor, L. and M. E. Gnegy (1998). "Protein kinase C inhibitors block amphetamine-mediated dopamine release in rat striatal slices." *J Pharmacol Exp Ther* **284**(2): 592-598.

Kantor, L., M. Zhang, B. Guptaroy, Y. H. Park and M. E. Gnegy (2004). "Repeated amphetamine couples norepinephrine transporter and calcium channel activities in PC12 cells." *J Pharmacol Exp Ther* **311**(3): 1044-1051.

Katzung B.G., S. B. Masters and A. J. Trevor AJ (2009). "Basic & Clinical Pharmacology." McGraw-Hill Companies, Inc., 11th Edition.

Khelashvili, G., A. Galli and H. Weinstein (2012). "Phosphatidylinositol 4,5-biphosphate (PIP(2)) lipids regulate the phosphorylation of syntaxin N-terminus by modulating both its position and local structure." *Biochemistry* **51**(39): 7685-7698.

Khelashvili, G., D. Harries and H. Weinstein (2009). "Modeling membrane deformations and lipid demixing upon protein-membrane interaction: the BAR dimer adsorption." *Biophys J* **97**(6): 1626-1635.

Khelashvili, G., H. Weinstein and D. Harries (2008). "Protein diffusion on charged membranes: a dynamic mean-field model describes time evolution and lipid reorganization." *Biophys J* **94**(7): 2580-2597.

Khelashvili, G., N. Stanley, M. A. Sahai, J. Medina, M. V. LeVine, L. Shi, G. De Fabritiis and H. Weinstein (2015). "Spontaneous inward opening of the dopamine transporter is triggered by PIP2-regulated dynamics of the N-terminus." *ACS Chem Neurosci* **6**(11): 1825-1837.

Khoshbouei, H., N. Sen, B. Guptaroy, L. Johnson, D. Lund, M. E. Gnegy, A. Galli and J. A. Javitch (2004). "N-terminal phosphorylation of the dopamine transporter is required for amphetamine-induced efflux." *PLoS Biol* **2**(3): E78.

Khoshbouei, H., H. Wang, J. D. Lechleiter, J. A. Javitch and A. Galli (2003). "Amphetamine-induced dopamine efflux. A voltage-sensitive and intracellular Na+-dependent mechanism." *J Biol Chem* **278**(14): 12070-12077.

Kiessling, V., C. Wan and L. K. Tamm (2009). "Domain coupling in asymmetric lipid bilayers." *Biochim Biophys Acta* **1788**(1): 64-71.

Kohls, G., M. T. Perino, J. M. Taylor, E. N. Madva, S. J. Cayless, V. Troiani, E. Price, S. Faja, J. D. Herrington and R. T. Schultz (2013). "The nucleus accumbens is involved in both the pursuit of social reward and the avoidance of social punishment." *Neuropsychologia* **51**(11): 2062-2069.

Kohls, G., H. Thonessen, G. K. Bartley, N. Grossheinrich, G. R. Fink, B. Herpertz-Dahlmann and K. Konrad (2014). "Differentiating neural reward responsiveness in autism versus ADHD." *Dev Cogn Neurosci* **10C**: 104-116.

Kniazeff, J., L. Shi, C. J. Loland, J. A. Javitch, H. Weinstein and U. Gether (2008). "An intracellular interaction network regulates conformational transitions in the dopamine transporter." *J Biol Chem* **283**(25): 17691-17701.

Krishnamurthy, H. and E. Gouaux (2012). "X-ray structures of LeuT in substrate-free outward-open and apo inward-open states." *Nature* **481**(7382): 469-474.

Kristensen, A. S., J. Andersen, T. N. Jorgensen, L. Sorensen, J. Eriksen, C. J. Loland, K. Stromgaard and U. Gether (2011). "SLC6 neurotransmitter transporters: structure, function, and regulation." *Pharmacol Rev* **63**(3): 585-640.

Kume, K., S. Kume, S. K. Park, J. Hirsh and F. R. Jackson (2005). "Dopamine is a regulator of arousal in the fruit fly." *J Neurosci* **25**(32): 7377-7384.

Kurian, M. A., Y. Li, J. Zhen, E. Meyer, N. Hai, H. J. Christen, G. F. Hoffmann, P. Jardine, A. von Moers, S. R. Mordekar, F. O'Callaghan, E. Wassmer, E. Wraige, C. Dietrich, T. Lewis, K. Hyland, S. Heales, Jr., T. Sanger, P. Gissen, B. E. Assmann, M. E. Reith and E. R. Maher (2011). "Clinical and molecular characterisation of hereditary dopamine transporter deficiency syndrome: an observational cohort and experimental study." *Lancet Neurol* **10**(1): 54-62.

Kurian, M. A., J. Zhen, S. Y. Cheng, Y. Li, S. R. Mordekar, P. Jardine, N. V. Morgan, E. Meyer, L. Tee, S. Pasha, E. Wassmer, S. J. Heales, P. Gissen, M. E. Reith and E. R. Maher (2009). "Homozygous loss-of-function mutations in the gene encoding the dopamine transporter are associated with infantile parkinsonism-dystonia." *J Clin Invest* **119**(6): 1595-1603.

Langen, M., D. Bos, S. D. Noordermeer, H. Nederveen, H. van Engeland and S. Durston (2014). "Changes in the development of striatum are involved in repetitive behavior in autism." *Biol Psychiatry* **76**(5): 405-411.

Langen, M., H. G. Schnack and H. Nederveen, D. Bos, B. E. Lahuis, M. V. de Jonge, H. van Engelhand and S. Durston (2009). "Changes in the developmental trajectories of striatum in autism." *Biol Psychiatry* **66**(4): 327-333.

Langen, M., S. Durston, W. G. Staal, S. J. Palmen and H. van Engeland (2007). "Caudate nucleus is enlarged in high-functioning medication-naive subjects with autism." *Biol Psychiatry* **62**(3): 262-266.

Lee, K. H., M. Y. Kim, D. H. Kim and Y. S. Lee (2004). "Syntaxin 1A and receptor for activated C kinase interact with the N-terminal region of human dopamine transporter." *Neurochem Res* **29**(7): 1405-1409.

Leviel, V. (2011). "Dopamine release mediated by the dopamine transporter, facts and consequences." *J Neurochem* **118**(4): 475-489.

Levy, D., M. Ronemus, B. Yamrom, Y. H. Lee, A. Leotta, J. Kendall, S. Marks, B. Lakshmi, D. Pai, K. Ye, A. Buja, A. Krieger, S. Yoon, J. Troge, L. Rodgers, I. Iossifov and M. Wigler (2011). "Rare de novo and transmitted copy-number variation in autistic spectrum disorders." *Neuron* **70**(5): 886-897.

Leyfer, O. T., S. E. Folstein, S. Bacalman, N. O. Davis, E. Dinh, J. Morgan, H. Tager-Flusberg and J. E. Lainhart (2006). "Comorbid psychiatric disorders in children with autism: interview development and rates of disorders." *J Autism Dev Disord* **36**(7): 849-861.

Li, S. O., J. L. Wang, G. Bjorklund, W. N. Zhao and C. H. Yin (2014). "Serum copper and zinc levels in individuals with autism spectrum disorders." *Neuroreport* **25**(15): 1216-1220.

Lim, E. T., S. Raychaudhuri, S. J. Sanders, C. Stevens, A. Sabo, D. G. MacArthur, B. M. Neale, A. Kirby, D. M. Ruderfer, M. Fromer, M. Lek, L. Liu, J. Flannick, S. Ripke, U. Nagaswamy, D. Muzny, J. G. Reid, A. Hawes, I. Newsham, Y. Wu, L. Lewis, H. Dinh, S. Gross, L. S. Wang, C. F. Lin, O. Valladares, S. B. Gabriel, M. dePristo, D. M. Altshuler, S. M. Purcell, Nhlbi Exome Sequencing Project, M. W. State, E. Boerwinkle, J. D. Buxbaum, E. H. Cook, R. A. Gibbs, G. D. Schellenberg, J. S. Sutcliffe, B. Devlin, K. Roeder and M. J. Daly (2013). "Rare complete knockouts in humans: population distribution and significant role in autism spectrum disorders." *Neuron* **77**(2): 235-242.

Lin, A., A. Rangel and R. Adolphs (2012). "Impaired learning of social compared to monetary rewards in autism." *Front Neurosci* **6**: 143.

Lin, J. M., V. L. Kilman, K. A. Keegan, B. Paddock, M. Emery-Le, M. Rosbash and R. Allada (2002). "A role for casein kinase 2alpha in the Drosophila circadian clock." *Nature* **420**(6917): 816-820.

Liu, L., A. Sabo, B. M. Neale, U. Nagaswamy, C. Stevens, E. Lim, C. A. Bodea, D. Muzny, J. G. Reid, E. Banks, H. Coon, M. Depristo, H. Dinh, T. Fennel, J. Flannick, S. Gabriel, K. Garimella, S. Gross, A. Hawes, L. Lewis, V. Makarov, J. Maguire, I. Newsham, R. Poplin, S. Ripke, K. Shakir, K. E. Samocha, Y. Wu, E. Boerwinkle, J. D. Buxbaum, E. H. Cook, Jr., B. Devlin, G. D. Schellenberg, J. S. Sutcliffe, M. J. Daly, R. A. Gibbs and K. Roeder (2013). "Analysis of rare, exonic variation amongst subjects with autism spectrum disorders and population controls." *PLoS Genet* **9**(4): e1003443.

Loland, C. J., L. Norregaard, T. Litman and U. Gether (2002). "Generation of an activating Zn(2+) switch in the dopamine transporter: mutation of an intracellular tyrosine constitutively alters the conformational equilibrium of the transport cycle." *Proc Natl Acad Sci U S A* **99**(3): 1683-1688.

Loland, C. J., L. Norregaard and U. Gether (1999). "Defining proximity relationships in the tertiary structure of the dopamine transporter. Identification of a conserved glutamic acid as a third coordinate in the endogenous Zn(2+)-binding site." *J Biol Chem* **274**(52): 36928-36934.

Lord, C., S. Risi, L. Lambrecht, E. H. Cook, Jr., B. L. Leventhal, P. C. DiLavore, A. Pickles and M. Rutter (2000). "The autism diagnostic observation schedule-generic: a standard measure of social and communication deficits associated with the spectrum of autism." *J Autism Dev Disord* **30**(3): 205-223.

Lord, C., M. Rutter and A. Le Couteur (1994). "Autism Diagnostic Interview-Revised: a revised version of a diagnostic interview for caregivers of individuals with possible pervasive developmental disorders." *J Autism Dev Disord* **24**(5): 659-685.

Lyons, D. J., A. Hellysaz and C. Broberger (2012). "Prolactin regulates tuberoinfundibular dopamine neuron discharge pattern: novel feedback control mechanisms in the lactotrophic axis." *J Neurosci* **32**(23): 8074-8083.

Mabb, A. M., M. C. Judson, M. J. Zylka and B. D. Philpot (2011). "Angelman syndrome: insights into genomic imprinting and neurodevelopmental phenotypes." *Trends Neurosci* **34**(6): 293-303.

Mackerell, A. D., Jr., M. Feig and C. L. Brooks, 3rd (2004). "Extending the treatment of backbone energetics in protein force fields: limitations of gas-phase quantum mechanics in reproducing protein conformational distributions in molecular dynamics simulations." *J Comput Chem* **25**(11): 1400-1415.

Makkonen I., H. Kokki, J. Kuikka, U. Turpeinen and R. Riikonen (2011). " Effects of fluoxetine treatment on striatal dopamine transporter binding and cerebrospinal fluid insulin-like growth factor-1 in children with autism." *Neuropediatrics* **42**(5): 207-209.

Matthies, H. J. and K. Broadie (2003). "Techniques to dissect cellular and subcellular function in the Drosophila nervous system." *Methods Cell Biol* **71**: 195-265.

Matthies, H. J., Q. Han, A. Shields, J. Wright, J. L. Moore, D. G. Winder, A. Galli and R. D. Blakely (2009). "Subcellular localization of the antidepressant-sensitive norepinephrine transporter." *BMC Neurosci* **10**: 65.

Mazei-Robison, M. S. and R. D. Blakely (2005). "Expression studies of naturally occurring human dopamine transporter variants identifies a novel state of transporter inactivation associated with Val382Ala." *Neuropharmacology* **49**(6): 737-749.

Mazei-Robison, M. S., E. Bowton, M. Holy, M. Schmudermaier, M. Freissmuth, H. H. Sitte, A. Galli and R. D. Blakely (2008). "Anomalous dopamine release associated with a human dopamine transporter coding variant." *J Neurosci* **28**(28): 7040-7046.

McHaourab, H. S., P. R. Steed and K. Kazmier (2011). "Toward the fourth dimension of membrane protein structure: insight into dynamics from spin-labeling EPR spectroscopy." *Structure* **19**(11): 1549-1561.

McHaourab, H. S., Y. L. Lin and B. W. Spiller (2012). "Crystal structure of an activated variant of small heat shock protein Hsp16.5." *Biochemistry* **51**(25): 5105-5112.

McLaughlin, S. and D. Murray (2005). "Plasma membrane phosphoinositide organization by protein electrostatics." *Nature* **438**(7068): 605-611.

McLaughlin, S., J. Wang, A. Gambhir, and D. Murray (2002). "PIP(2) and proteins: interactions, organization, and information flow." *Annu Rev Biophys Biomol Struct* **31**: 151-175.

Mergy, M. A., R. Gowrishankar, G. L. Davis, T. N. Jessen, J. Wright, G. D. Stanwood, M. K. Hahn and R. D. Blakely (2014). "Genetic targeting of the amphetamine and methylphenidate-sensitive dopamine transporter: on the path to an animal model of attention-deficit hyperactivity disorder." *Neurochem Int* **73**: 56-70.

Nakamura, K., A. Anitha, K. Yamada, M. Tsujii, Y. Iwayama, E. Hattori, T. Toyota, S. Suda, N. Takei, Y. Iwata, K. Suzuki, H. Matsuzaki, M. Kawai, Y. Sekine, K. J. Tsuchiya, G. Sugihara, Y. Ouchi, T. Sugiyama, T. Yoshikawa and N. Mori (2008). "Genetic and expression analyses reveal elevated expression of syntaxin 1A (STX1A) in high functioning autism." *Int J Neuropsychopharmacol* **11**(8): 1073-1084.

Nakamura, K., Y. Iwata, A. Anitha, T. Miyachi, T. Toyota, S. Yamada, M. Tsujii, K. J. Tsuchiya, Y. Iwayama, K. Yamada, E. Hattori, H. Matsuzaki, K. Matsumoto, K. Suzuki, S. Suda, K. Takebayashi, N. Takei, H. Ichikawa, T. Sugiyama, T. Yoshikawa and N. Mori (2011). "Replication study of Japanese cohorts supports the role of STX1A in autism susceptibility." *Prog Neuropsychopharmacol Biol Psychiatry* **35**(2): 454-458.

Nakamura, K., Y. Sekine, Y. Ouchi, M. Tsujii, E. Yoshikawa, M. Futatsubashi, K. J. Tsuchiya, G. Sugihara, Y. Iwata, K. Suzuki, H. Matsuzaki, S. Suda, T. Sugiyama, N. Takei and N. Mori (2010). "Brain serotonin and dopamine transporter bindings in adults with high-functioning autism." *Arch Gen Psychiatry* **67**(1): 59-68.

Neale, B. M., Y. Kou, L. Liu, A. Ma'ayan, K. E. Samocha, A. Sabo, C. F. Lin, C. Stevens, L. S. Wang, V. Makarov, P. Polak, S. Yoon, J. Maguire, E. L. Crawford, N. G. Campbell, E. T. Geller, O. Valladares, C. Schafer, H. Liu, T. Zhao, G. Cai, J. Lihm, R. Dannenfelser, O.

Jabado, Z. Peralta, U. Nagaswamy, D. Muzny, J. G. Reid, I. Newsham, Y. Wu, L. Lewis, Y. Han, B. F. Voight, E. Lim, E. Rossin, A. Kirby, J. Flannick, M. Fromer, K. Shakir, T. Fennell, K. Garimella, E. Banks, R. Poplin, S. Gabriel, M. DePristo, J. R. Wimbish, B. E. Boone, S. E. Levy, C. Betancur, S. Sunyaev, E. Boerwinkle, J. D. Buxbaum, E. H. Cook, Jr., B. Devlin, R. A. Gibbs, K. Roeder, G. D. Schellenberg, J. S. Sutcliffe and M. J. Daly (2012). "Patterns and rates of exonic de novo mutations in autism spectrum disorders." *Nature* **485**(7397): 242-245.

Nemoda, Z., A. Szekely and M. Sasvari-Szekely (2011). "Psychopathological aspects of dopaminergic gene polymorphisms in adolescence and young adulthood." *Neurosci Biobehav Rev* **35**(8): 1665-1686.

Nieminen-von Wendt, T. S., L. Metsahonkala, T. A. Kulomaki, S. Aalto, T. H. Autti, R. Vanhala, O. Eskola, J. Bergman, J. A. Hietala and L. O. von Wendt (2004). "Increased presynaptic dopamine function in Asperger syndrome." *Neuroreport* **15**(5): 757-760.

Ng, J., J. Zhen, E. Meyer, K. Erreger, Y. Li, N. Kakar, J. Ahmad, H. Thiele, C. Kubisch, N. L. Rider, D. H. Morton, K. A. Strauss, E. G. Puffenberger, D. D'Agnano, Y. Anikster, C. Carducci, K. Hyland, M. Rotstein, V. Leuzzi, G. Borck, M. E. Reith and M. A. Kurian (2014). "Dopamine transporter deficiency syndrome: phenotypic spectrum from infancy to adulthood." *Brain* **137**(Pt 4): 1107-1119.

Nguyen, M., A. Roth, E. J. Kyzar, M. K. Poudel, K. Wong, A. M. Stewart and A. V. Kalueff (2014). "Decoding the contribution of dopaminergic genes and pathways to autism spectrum disorder (ASD)." *Neurochem Int* **66**: 15-26.

Norregaard, L., D. Frederiksen, E. O. Nielsen and U. Gether (1998). "Delineation of an endogenous zinc-binding site in the human dopamine transporter." *EMBO J* **17**(15): 4266-4273.

O'Roak, B. J., L. Vives, S. Girirajan, E. Karakoc, N. Krumm, B. P. Coe, R. Levy, A. Ko, C. Lee, J. D. Smith, E. H. Turner, I. B. Stanaway, B. Vernot, M. Malig, C. Baker, B. Reilly, J. M. Akey, E. Borenstein, M. J. Rieder, D. A. Nickerson, R. Bernier, J. Shendure and E. E. Eichler (2012). "Sporadic autism exomes reveal a highly interconnected protein network of de novo mutations." *Nature* **485**(7397): 246-250.

Palmiter, R. D. (2008). "Dopamine signaling in the dorsal striatum is essential for motivated behaviors: lessons from dopamine-deficient mice." *Ann N Y Acad Sci* **1129**: 35-46.

Patlak, C. S. (1957). "Contributions to the theory of active transport. II. The gate type non-carrier mechanism and generalizations concerning tracer flow, efficiency, and measurement of energy expenditure." *Bull Math Biophys* **19**: 209-235.

Pendleton, R. G., A. Rasheed, T. Sardina, T. Tully and R. Hillman (2002). "Effects of tyrosine hydroxylase mutants on locomotor activity in Drosophila: a study in functional genomics." *Behav Genet* **32**(2): 89-94.

Penmatsa, A., K. H. Wang and E. Gouaux (2013). "X-ray structure of dopamine transporter elucidates antidepressant mechanism." *Nature* **503**(7474): 85-90.

Pinto, D., A. T. Pagnamenta, L. Klei, R. Anney, D. Merico, R. Regan, J. Conroy, T. R. Magalhaes, C. Correia, B. S. Abrahams, J. Almeida, E. Bacchelli, G. D. Bader, A. J. Bailey, G. Baird, A. Battaglia, T. Berney, N. Bolshakova, S. Bolte, P. F. Bolton, T. Bourgeron, S. Brennan, J. Brian, S. E. Bryson, A. R. Carson, G. Casallo, J. Casey, B. H. Chung, L. Cochrane, C. Corsello, E. L. Crawford, A. Crossett, C. Cytrynbaum, G. Dawson, M. de Jonge, R. Delorme, I. Drmic, E. Duketis, F. Duque, A. Estes, P. Farrar, B. A. Fernandez, S. E. Folstein, E. Fombonne, C. M. Freitag, J. Gilbert, C. Gillberg, J. T. Glessner, J. Goldberg, A. Green, J. Green, S. J. Guter, H. Hakonarson, E. A. Heron, M. Hill, R. Holt, J. L. Howe, G. Hughes, V. Hus, R. Igliozzi, C. Kim, S. M. Klauck, A. Kolevzon, O. Korvatska, V. Kustanovich, C. M. Lajonchere, J. A. Lamb, M. Laskawiec, M. Leboyer, A. Le Couteur, B. L. Leventhal, A. C. Lionel, X. Q. Liu, C. Lord, L. Lotspeich, S. C. Lund, E. Maestrini, W. Mahoney, C. Mantoulan, C. R. Marshall, H. McConachie, C.

J. McDougle, J. McGrath, W. M. McMahon, A. Merikangas, O. Migita, N. J. Minshew, G. K. Mirza, J. Munson, S. F. Nelson, C. Noakes, A. Noor, G. Nygren, G. Oliveira, K. Papanikolaou, J. R. Parr, B. Parrini, T. Paton, A. Pickles, M. Pilorge, J. Piven, C. P. Ponting, D. J. Posey, A. Poustka, F. Poustka, A. Prasad, J. Ragoussis, K. Renshaw, J. Rickaby, W. Roberts, K. Roeder, B. Roge, M. L. Rutter, L. J. Bierut, J. P. Rice, J. Salt, K. Sansom, D. Sato, R. Segurado, A. F. Sequeira, L. Senman, N. Shah, V. C. Sheffield, L. Soorya, I. Sousa, O. Stein, N. Sykes, V. Stoppioni, C. Strawbridge, R. Tancredi, K. Tansey, B. Thiruvahindrapduram, A. P. Thompson, S. Thomson, A. Tryfon, J. Tsiantis, H. Van Engeland, J. B. Vincent, F. Volkmar, S. Wallace, K. Wang, Z. Wang, T. H. Wassink, C. Webber, R. Weksberg, K. Wing, K. Wittemeyer, S. Wood, J. Wu, B. L. Yaspan, D. Zurawiecki, L. Zwaigenbaum, J. D. Buxbaum, R. M. Cantor, E. H. Cook, H. Coon, M. L. Cuccaro, B. Devlin, S. Ennis, L. Gallagher, D. H. Geschwind, M. Gill, J. L. Haines, J. Hallmayer, J. Miller, A. P. Monaco, J. I. Nurnberger, Jr., A. D. Paterson, M. A. Pericak-Vance, G. D. Schellenberg, P. Szatmari, A. M. Vicente, V. J. Vieland, E. M. Wijsman, S. W. Scherer, J. S. Sutcliffe and C. Betancur (2010). "Functional impact of global rare copy number variation in autism spectrum disorders." *Nature* **466**(7304): 368-372.

Pizzo, A. B., C. S. Karam, Y. Zhang, H. Yano, R. J. Freyberg, D. S. Karam, Z. Freyberg, A. Yamamoto, B. D. McCabe and J. A. Javitch (2013). "The membrane raft protein Flotillin-1 is essential in dopamine neurons for amphetamine-induced behavior in Drosophila." *Mol Psychiatry* **18**(7): 824-833.

Qian, Y., M. Chen, H. Forssberg and R. Diaz Heijtz (2013). "Genetic variation in dopamine-related gene expression influences motor skill learning in mice." *Genes Brain Behav* **12**(6): 604-614.

Quick, M. W. (2002). "Role of syntaxin 1A on serotonin transporter expression in developing thalamocortical neurons." *Int J Dev Neurosci* **20**(3-5): 219-224.

Quick, M. W. (2003). "Regulating the conducting states of a mammalian serotonin transporter." *Neuron* **40**(3): 537-549.

Quick, M. W. (2006). "The role of SNARE proteins in trafficking and function of neurotransmitter transporters." *Handb Exp Pharmaco*l **175**: 181-196.

Rasmussen T., I. H. Skjoth, H. H. Jensen, K. Niefind, B. Boldyreff and O. G. Issinger (2005). "Biochemical characterization of the recombinant human Drosophila homologues Timekeeper and Andante involved in the Drosophila circadian oscillator." *Mol Cell Biochem* **274**(1–2): 151–161.

Rasmussen, T. N., P. Plenge, T. Bay, J. Egebjerg and U. Gether (2009). "A single nucleotide polymorphism in the human serotonin transporter introduces a new site for N-linked glycosylation." *Neuropharmacology* **57**(3): 287-294.

Reiersen, A. M. and A. A. Todorov (2011). "Association between DRD4 genotype and Autistic Symptoms in DSM-IV ADHD." *J Can Acad Child Adolesc Psychiatry* **20**(1): 15-21.

Rickhag, M., F. H. Hansen, G. Sorensen, K. N. Strandfelt, B. Andresen, K. Gotfryd, K. L. Madsen, I. Vestergaard-Klewe, I. Ammendrup-Johnsen, J. Eriksen, A. H. Newman, E. M. Fuchtbauer, J. Gomeza, D. P. Woldbye, G. Wortwein and U. Gether (2013). "A C-terminal PDZ domain-binding sequence is required for striatal distribution of the dopamine transporter." *Nat Commun* **4**: 1580.

Risi, S., C. Lord, K. Gotham, C. Corsello, C. Chrysler, P. Szatmari, E. H. Cook, Jr., B. L. Leventhal and A. Pickles (2006). "Combining information from multiple sources in the diagnosis of autism spectrum disorders." *J Am Acad Child Adolesc Psychiatry* **45**(9): 1094-1103.

Robbins, J., S. J. Marsh, and D. A. Brown (2006). "Probing the regulation of M (Kv7) potassium channels in intact neurons with membrane-targeted peptides." *J Neurosci* **26**(30): 7950-7961.

Robertson, S. D., H. J. Matthies and A. Galli (2009). "A closer look at amphetamine-induced reverse transport and trafficking of the dopamine and norepinephrine transporters." *Mol Neurobiol* **39**(2): 73-80.

Roman, T., L. A. Rohde and M. H. Hutz (2004). "Polymorphisms of the dopamine transporter gene: influence on response to methylphenidate in attention deficit-hyperactivity disorder." *Am J Pharmacogenomics* **4**(2): 83-92.

Ronald, A., E. Simonoff, J. Kuntsi, P. Asherson and R. Plomin (2008). "Evidence for overlapping genetic influences on autistic and ADHD behaviours in a community twin sample." *J Child Psychol Psychiatry* **49**(5): 535-542.

Rosenhouse-Dantsker, A. and D. E. Logothetis (2007). "Molecular characteristics of phosphoinosited binding." *Pflugers Arch* **455**(1): 45.53.

Rowberry, J., S. Macari, G. Chen, D. Campbell, J. M. Leventhal, C. Weitzman and K. Chawarska (2015). "Screening for autism spectrum disorders in 12-month-old high-risk siblings by parental report." *J Autism Dev Disord* **45**(1): 221-229.

Sakrikar, D., M. S. Mazei-Robison, M. A. Mergy, N. W. Richtand, Q. Han, P. J. Hamilton, E. Bowton, A. Galli, J. Veenstra-Vanderweele, M. Gill and R. D. Blakely (2012). "Attention deficit/hyperactivity disorder-derived coding variation in the dopamine transporter disrupts microdomain targeting and trafficking regulation." *J Neurosci* **32**(16): 5385-5397.

Sali, A. and T. L. Blundell (1993). "Comparative protein modelling by satisfaction of spatial restraints." *J Mol Biol* **234**(3): 779-815.

Sanders, S. J., A. G. Ercan-Sencicek, V. Hus, R. Luo, M. T. Murtha, D. Moreno-De-Luca, S. H. Chu, M. P. Moreau, A. R. Gupta, S. A. Thomson, C. E. Mason, K. Bilguvar, P. B. Celestino-Soper, M. Choi, E. L. Crawford, L. Davis, N. R. Wright, R. M. Dhodapkar, M. DiCola, N. M. DiLullo, T. V. Fernandez, V. Fielding-Singh, D. O. Fishman, S. Frahm, R. Garagaloyan, G. S. Goh, S. Kammela, L. Klei, J. K. Lowe, S. C. Lund, A. D. McGrew, K. A. Meyer, W. J. Moffat, J. D. Murdoch, B. J. O'Roak, G. T. Ober, R. S. Pottenger, M. J. Raubeson, Y. Song, Q. Wang, B. L. Yaspan, T. W. Yu, I. R. Yurkiewicz, A. L. Beaudet, R. M. Cantor, M. Curland, D. E. Grice, M. Gunel, R. P. Lifton, S. M. Mane, D. M. Martin, C. A. Shaw, M. Sheldon, J. A. Tischfield, C. A. Walsh, E. M. Morrow, D. H. Ledbetter, E. Fombonne, C. Lord, C. L. Martin, A. I. Brooks, J. S. Sutcliffe, E. H. Cook, Jr., D. Geschwind, K. Roeder, B. Devlin and M. W. State (2011). "Multiple recurrent de novo CNVs, including duplications of the 7q11.23 Williams syndrome region, are strongly associated with autism." *Neuron* **70**(5): 863-885.

Sanders, S. J., M. T. Murtha, A. R. Gupta, J. D. Murdoch, M. J. Raubeson, A. J. Willsey, A. G. Ercan-Sencicek, N. M. DiLullo, N. N. Parikshak, J. L. Stein, M. F. Walker, G. T. Ober, N. A. Teran, Y. Song, P. El-Fishawy, R. C. Murtha, M. Choi, J. D. Overton, R. D. Bjornson, N. J. Carriero, K. A. Meyer, K. Bilguvar, S. M. Mane, N. Sestan, R. P. Lifton, M. Gunel, K. Roeder, D. H. Geschwind, B. Devlin and M. W. State (2012). "De novo mutations revealed by whole-exome sequencing are strongly associated with autism." *Nature* **485**(7397): 237-241.

Saunders, C., J. V. Ferrer, L. Shi, J. Chen, G. Merrill, M. E. Lamb, L. M. Leeb-Lundberg, L. Carvelli, J. A. Javitch and A. Galli (2000). "Amphetamine-induced loss of human dopamine transporter activity: an internalization-dependent and cocaine-sensitive mechanism." *Proc Natl Acad Sci U S A* **97**(12): 6850-6855.

Sebat, J., B. Lakshmi, D. Malhotra, J. Troge, C. Lese-Martin, T. Walsh, B. Yamrom, S. Yoon, A. Krasnitz, J. Kendall, A. Leotta, D. Pai, R. Zhang, Y. H. Lee, J. Hicks, S. J. Spence, A. T. Lee, K. Puura, T. Lehtimaki, D. Ledbetter, P. K. Gregersen, J. Bregman, J. S. Sutcliffe, V. Jobanputra, W. Chung, D. Warburton, M. C. King, D. Skuse, D. H. Geschwind, T. C. Gilliam, K. Ye and M. Wigler (2007). "Strong association of de novo copy number mutations with autism." *Science* **316**(5823): 445-449.

Seeman, P. and H. B. Niznik (1990). "Dopamine receptors and transporters in Parkinson's disease and schizophrenia." *FASEB J* **4**(10): 2737-2744.
Shan, J., J. A. Javitch, L. Shi and H. Weinstein (2011). "The substrate-driven transition to an inward-facing conformation in the functional mechanism of the dopamine transporter." *PLoS One* **6**(1): e16350.
Sharp, K. A. and B. Honig (1990). "Electrostatic interactions in macromolecules: theory and applications." *Annu Rev Biophys Biophys Chem* **19**: 301-332.
Sherry, S. T., M. H. Ward, M. Kholodov, J. Baker, L. Phan, E. M. Smigielski and K. Sirotkin (2001). "dbSNP: the NCBI database of genetic variation." *Nucleic Acids Res* **29**(1): 308-311.
Sitte, H. H., S. Huck, H. Reither, S. Boehm, E. A. Singer and C. Pifl (1998). "Carrier-mediated release, transport rates, and charge transfer induced by amphetamine, tyramine, and dopamine in mammalian cells transfected with the human dopamine transporter." *J Neurochem* **71**(3): 1289-1297.
Siuta, M. A., S. D. Robertson, H. Kocalis, C. Saunders, P. J. Gresch, V. Khatri, C. Shiota, J. P. Kennedy, C. W. Lindsley, L. C. Daws, D. B. Polley, J. Veenstra-Vanderweele, G. D. Stanwood, M. A. Magnuson, K. D. Niswender and A. Galli (2010). "Dysregulation of the norepinephrine transporter sustains cortical hypodopaminergia and schizophrenia-like behaviors in neuronal rictor null mice." *PLoS Biol* **8**(6): e1000393.
Smith, M. A., M. M. Pennock, E. G. Pitts, K. L. Walker and K. C. Lang (2014). "The effects of amphetamine, butorphanol, and their combination on cocaine self-administration." *Behav Brain Res* **274**: 158-163.
Sonders, M. S. and S. G. Amara (1996). "Channels in transporters." *Curr Opin Neurobio*l **6**(3): 294-302.
Sonders, M. S., S. J. Zhu, N. R. Zahniser, M. P. Kavanaugh and S. G. Amara (1997). "Multiple ionic conductances of the human dopamine transporter: the actions of dopamine and psychostimulants." *J Neurosci* **17**(3): 960-974.
Sorkina, T., S. Doolen, E. Galperin, N. R. Zahniser and A. Sorkin (2003). "Oligomerization of dopamine transporters visualized in living cells by fluorescence resonance energy transfer microscopy." *J Biol Chem* **278**(30): 28274-28283.
Staal, R. G., E. V. Mosharov and D. Sulzer (2004). "Dopamine neurons release transmitter via a flickering fusion pore." *Nat Neurosc*i **7**(4): 341-346.
Staal, W. G., M. de Krom and M. V. de Jonge (2012). "Brief report: the dopamine-3-receptor gene (DRD3) is associated with specific repetitive behavior in autism spectrum disorder (ASD)." *J Autism Dev Disord* **42**(5): 885-888.
Steinkellner, T., J. W. Yang, T. R. Montgomery, W. Q. Chen, M. T. Winkler, S. Sucic, G. Lubec, M. Freissmuth, Y. Elgersma, H. H. Sitte and O. Kudlacek (2012). "Ca(2+)/calmodulin-dependent protein kinase IIalpha (alphaCaMKII) controls the activity of the dopamine transporter: implications for Angelman syndrome." *J Biol Chem* **287**(35): 29627-29635.
Stockner, T., T. R. Montgomery, O. Kudlacek, R. Weissensteiner, G. F. Ecker, M. Freissmuth and H. H. Sitte (2013). "Mutational analysis of the high-affinity zinc binding site validates a refined human dopamine transporter homology model." *PLoS Comput Biol* **9**(2): e1002909.
Sturm, H., E. Fernell and C. Gillberg (2004). "Autism spectrum disorders in children with normal intellectual levels: associated impairments and subgroups." *Dev Med Child Neurol* **46**(7): 444-447.
Sudhof, T. C. (2004). "The synaptic vesicle cycle." *Annu Rev Neurosci* **27**: 509-547.
Suh, B.C. and B. Hille (2008). "PIP2 is a necessary cofactor for ion channel function: how and why?" *Annu Rev Biophys* **37**: 175-195.
Sulzer, D. and E. N. Pothos (2000). "Regulation of quantal size by presynaptic mechanisms." *Rev Neurosci* **11**(2-3): 159-212.

Sulzer, D., M. S. Sonders, N. W. Poulsen and A. Galli (2005). "Mechanisms of neurotransmitter release by amphetamines: a review." *Prog Neurobiol* **75**(6): 406-433.
Surmeier, D. J. (2007). "Dopamine and working memory mechanisms in prefrontal cortex." *J Physiol* **581**(Pt 3): 885.
Surmeier, D. J., J. Ding, M. Day, Z. Wang and W. Shen (2007). "D1 and D2 dopamine-receptor modulation of striatal glutamatergic signaling in striatal medium spiny neurons." *Trends Neurosci* **30**(5): 228-235.
Tassone, F., L. Qi, W. Zhang, R. L. Hansen, I. N. Pessah and I. Hertz-Picciotto (2011). "MAOA, DBH, and SLC6A4 variants in CHARGE: a case-control study of autism spectrum disorders." *Autism Res* **4**(4): 250-261.
Torres, G. E., A. Carneiro, K. Seamans, C. Fiorentini, A. Sweeney, W. D. Yao and M. G. Caron (2003). "Oligomerization and trafficking of the human dopamine transporter. Mutational analysis identifies critical domains important for the functional expression of the transporter." *J Biol Chem* **278**(4): 2731-2739.
Torres, G. E., R. R. Gainetdinov and M. G. Caron (2003). "Plasma membrane monoamine transporters: structure, regulation and function." *Nat Rev Neurosci* **4**(1): 13-25.
van Rheenen, J., E. M. Achame, H. Janssen, J. Calafat and K. Jalink (2005). "PIP2 signaling in lipid domains: a critical re-evaluation." *EMBO J* **24**(9): 1664-1673.
Varnai, P., X. Lin, S. B. Lee, G. Tuymetova, T. Bondeva, A. Spat, S. G. Rhee, G. Hajnoczky, and T. Balla (2002). "Inositol lipid binding and membrane localization of isolated pleckstrin homology (PH) domains. Studies on the PH domains of phospholipase C delta 1 and p130." *J Biol Chem* **277**(30): 27412-27422.
Ventura, R., T. Pascucci, M. V. Catania, S. A. Musumeci and S. Puglisi-Allegra (2004). "Object recognition impairment in Fmr1 knockout mice is reversed by amphetamine: involvement of dopamine in the medial prefrontal cortex." *Behav Pharmacol* **15**(5-6): 433-442.
Volkow, N. D., G. J. Wang, J. Newcorn, F. Telang, M. V. Solanto, J. S. Fowler, J. Logan, Y. Ma, K. Schulz, K. Pradhan, C. Wong and J. M. Swanson (2007). "Depressed dopamine activity in caudate and preliminary evidence of limbic involvement in adults with attention-deficit/hyperactivity disorder." *Arch Gen Psychiatry* **64**(8): 932-940.
Wang, D., S. L. Deken, T. L. Whitworth and M. W. Quick (2003). "Syntaxin 1A inhibits GABA flux, efflux, and exchange mediated by the rat brain GABA transporter GAT1." *Mol Pharmacol* **64**(4): 905-913.
Wang, J. and D. A. Richards (2012). "Segregation of PIP2 and PIP3 into distinct nanoscale regions within the plasma membrane." *Biol open* **1**(9): 857-862.
Wang, J. W., E. S. Beck and B. D. McCabe (2012). "A modular toolset for recombination transgenesis and neurogenetic analysis of Drosophila." *PLoS One* **7**(7): e42102.
Weeber, E. J., Y. H. Jiang, Y. Elgersma, A. W. Varga, Y. Carrasquillo, S. E. Brown, J. M. Christian, B. Mirnikjoo, A. Silva, A. L. Beaudet and J. D. Sweatt (2003). "Derangements of hippocampal calcium/calmodulin-dependent protein kinase II in a mouse model for Angelman mental retardation syndrome." *J Neurosci* **23**(7): 2634-2644.
Wei, Y., J. M. Williams, C. Dipace, U. Sung, J. A. Javitch, A. Galli and C. Saunders (2007). "Dopamine transporter activity mediates amphetamine-induced inhibition of Akt through a Ca2+/calmodulin-dependent kinase II-dependent mechanism." *Mol Pharmacol* **71**(3): 835-842.
Whorton, M.R. and R. MacKinnon (2011). "Crystal structure of the mammalian GIRK2 K+ channel and gating regulation by G proteins, PIP2, and sodium." *Cell* **147**(1): 199-208.
Wicker-Thomas, C. and M. Hamann (2008). "Interaction of dopamine, female pheromones, locomotion and sex behavior in Drosophila melanogaster." *J Insect Physiol* **54**(10-11): 1423-1431.
Wise, R. A. (1998). "Drug-activation of brain reward pathways." *Drug Alcohol Depend* **55**(1-2): 13-22.

Wolff, J. J., K. N. Botteron, S. R. Dager, J. T. Elison, A. M. Estes, H. Gu, H. C. Hazlett, J. Pandey, S. J. Paterson, R. T. Schultz, L. Zwaigenbaum, J. Piven and IBIS Network (2014). "Longitudinal patterns of repetitive behavior in toddlers with autism." *J Child Psychol Psych* **55**(8), 945-953.

Wolfson, W. (2007). "Boston Autism Consortium searches for genetic clues to autism's puzzle." *Chem Biol* **14**(2): 117-118.

Yamashita, A., S. K. Singh, T. Kawate, Y. Jin and E. Gouaux (2005). "Crystal structure of a bacterial homologue of Na+/Cl--dependent neurotransmitter transporters." *Nature* **437**(7056): 215-223.

Yoshida, Y. and T. Uchiyama (2004). "The clinical necessity for assessing Attention Deficit/Hyperactivity Disorder (AD/HD) symptoms in children with high-functioning Pervasive Developmental Disorder (PDD)." *Eur Child Adolesc Psychiatry* **13**(5): 307-314.

Yoo, H. J., I. H. Cho, M. Park, S. Y. Yang, and S. A. Kim (2013). "Association of the catechol-o-methyltransferase gene polymorphisms with Korean autism spectrum disorders." *J Kor. Med Sci* **28**(9): 1403-1406.

Zald, D. H., I. Boileau, W. El-Dearedy, R. Gunn, F. McGlone, G. S. Dichter and A. Dagher (2004). "Dopamine transmission in the human striatum during monetary reward tasks." *J Neurosci* **24**(17): 4105-4112.

Zhao, Y., D. S. Terry, L. Shi, M. Quick, H. Weinstein, S. C. Blanchard and J. A. Javitch (2011). "Substrate-modulated gating dynamics in a Na+-coupled neurotransmitter transporter homologue." *Nature* **474**(7349): 109-113.

Zhu, S. J., M. P. Kavanaugh, M. S. Sonders, S. G. Amara and N. R. Zahniser (1997). "Activation of protein kinase C inhibits uptake, currents and binding associated with the human dopamine transporter expressed in Xenopus oocytes." *J Pharmacol Exp Ther* **282**(3): 1358-1365.

Zou, P. and H. S. McHaourab (2010). "Increased sensitivity and extended range of distance measurements in spin-labeled membrane proteins: Q-band double electron-electron resonance and nanoscale bilayers." *Biophys J* **98**(6): L18-20.